ISSN print: 1224-5984
ISSN online: 2248-3942

Rom Biotechnol Lett. 2022; 27(1): 3167-3183
doi: 10.25083/rbl/27.1/3167-3183

Received for publication, October, 11, 2021
Accepted, January, 01, 2022

Original paper

Review of Heart Sound Analyses from Phonocardiogram Records

ALI FATIH GUNDUZ
Malatya Turgut Özal University, Akçadağ Vocational Highschool, 44600 Malatya, Turkey

Abstract Cardiovascular diseases are considered as one of the most common causes of death worldwide. Well-beings of people in the risk groups are monitored by various state-of-the-art tools in clinics and home-care units. Phonocardiograph is one of the them which captures sounds coming from the heart and gives high-quality graphical records (i.e., Phonocardiogram, PCG) of them for examination of pathologies. PCG records have been studied and interpreted in order to localize heart sound segments and classify abnormalities for decades. Moreover, there have been competitions for heart sound classification and researchers have developed successful solutions based on signal processing and machine learning approaches. Main steps of those studies are grouped as preprocessing, segmentation, feature extraction and classification. In this study we present a survey of proposed methods and used datasets. The features used in the literature are listed as time, frequency and time-frequency domains. Performances of different studies are presented and compared. From this perspective, it is concluded that there is still room for automated heart sound analysis. Larger open access PCG databases are required for testing state-of-the-art machine learning methods.

Keywords Phonocardiogram classification, heart sound databases, heart sound analysis, segmentation, feature extraction, cardiovascular monitoring

To cite this article: GUNDUZ AF. Review of Heart Sound Analyses from Phonocardiogram Records. *Rom Biotechnol Lett*. 2022; 27(1): 3167-3183. DOI: 10.25083/rbl/27.1/3167-3183.

*Corresponding author: ALI FATIH GUNDUZ, Malatya Turgut Özal University, Akçadağ Vocational Highschool, 44600 Malatya, Turkey.
E-mail: fatih.gunduz@ozal.edu.tr; fatih.gunduz.ali@gmail.com

Introduction

Heart, blood vessels and blood together form the cardiovascular system. Heart is located in the left of the middle chest surrounded with two lungs and diaphragm muscle. Blood vessels include veins (carrying blood from body to heart), arteries (carrying blood from heart to body) and capillaries (smallest vessels that enable material exchange between body cells and blood). Different sized vessels form a vascular network of approximately 96500 kilometers (60000 miles) [1] in which blood is consistently transported to supply vital elements to body cells. During this circulation process, body cells receive oxygen, nutrients, hormones and get rid of carbon dioxide and cellular waste products.

According to World Health Organization (WHO), diseases of cardiovascular system are the most prominent factors of death globally being the cause of an estimated 31% of all deaths worldwide [2]. In addition to having a high morbidity, they also deteriorate life quality of patients. Most common cardiovascular diseases are myocardial infarction, stroke, Kawasaki disease, high blood pressure (hypertension), high cholesterol, coronary artery disease, cardiomyopathy, rhythm disorders (arrhythmia) and heart structure related congenital defects. Hypertension, diabetes, obesity, smoking, use of alcohol, inadequate physical activity and family history of having CVDs are counted as risk factors. Controlling the risk factors and following a healthy lifestyle are very important for coping with CVDs.

Heart is the core organ of the cardiovascular system pumping and propelling the blood through vessels. Under normal conditions, it usually beats from 60 to 100 times per minute to achieve this task. Depending on the condition of the individual, heart receives messages through hormones, sympathetic and parasympathetic nervous system. According to the needs indicated by those messages, the heart can pump less or more blood than usual. During rest or sleep heart rate decreases while during periods of physical exercise heart rate increase.

Heart is made up of four chambers which are entitled according to their locational properties like left/right and upper/lower. The two upper chambers are called as atria and the two lower chambers are called as ventricles. A muscular wall (septum) divides the heart into left and right parts. In a healthy heart, blood of left side cannot be mixed with the blood of right side. The left atrium is separated from left ventricle by mitral valve and the right atrium is separated from the right ventricle by tricuspid valve. Those two valves are called as atrioventricular valves. Similarly, two valves separate ventricles from blood vessels that carry the leaving blood. Pulmonic valve is placed between right ventricle and pulmonary artery while aortic valve is located between left ventricle and aorta.

Having a specific type of muscle kind (cardiac muscle) heart is under involuntary control. Functioning of the heart is rhythmic and regular but non-stationary. The period from one heart beat to another heart beat is called as cardiac cycle. Heart beats are controlled by a system of electrical signals generated in the heart. Sinoatrial node (SA, a small tissue in the wall of right atrium) is called as the pacemaker of the heart. The electrical signals generated by SA sets the rate of heartbeats and triggers the heart to contract in rhythm. Contraction of the heart starts from atria and then ventricles follow them.

One complete cardiac cycle is divided into two phases: pumping phase (namely systole) and filling phase (namely diastole). In the systole phase, the ventricles contract in order to pump the blood through the vessels to the body. Backward blood flow into atria is prevented by atrioventricular valves. Those valves close creating the first heart sound (S1). When the contraction of the ventricles end, this time backward blood flow into ventricles is stopped by the pulmonic and aortic valves. Those valves close immediately creating the second heart sound (S2). Then the ventricles relax and they are refilled with blood coming from the atria. This phase is called as diastole during which the heart gets ready for the following heartbeat. Generally, one cardiac cycle lasts 0.8 seconds at a normal heart rate but some factors like gender and age can change cardiac cycle period smoothly [3].

Each heartbeat consists of characteristic electrical and mechanical events. Those events occur in accordance with each other during the cardiac cycle. This relation between those mechanical and electrical events is defined as the dynamics of the heartbeat. Basic concepts of this topic have been defined by Wiggers (1923), Lewis (1925) and their colleagues [4]. Changes at aortic pressure, heart chambers' volume, arterial flow and heart sounds are some of the recurrent attributes of cardiac cycle. Carefully observing those events help clinicians to understand and diagnose various CVDs.

Healthcare professionals use many modalities for recognizing CVDs such as Electrocardiography (ECG or EKG), Echocardiography (echo), Phonocardiography (PCG), Magnetic Resonance Imaging (MRI), Ballistocardiography (BCG), Impedance Cardiography (ICG) and etc. Those medical monitoring tools works with different kind of signals such as electrical, acoustic, seismic, optical and radio-frequency [5]. Hospitals, clinics, treatment centers and home-care units have many medical devices and equipment. Thanks to advances in the technology of communication and information, today patients can access many forms of body sensors as well. With increasing access to monitoring devices, healthcare information about blood pressure, heart rhythm, heart rate variability, respiration rate and many other features can be followed regularly.

Although there are plenty of alternatives, many clinicians' first choice for examining circulatory and respiratory systems would be auscultation (i.e listening to the body sounds by using a stethoscope). Stethoscope was invented by Rene Laennec in 1816 but it is still a valid

method for diagnosis. Auscultation is cost-effective, simple, noninvasive, practical and fast therefore stethoscopes have been the very symbol of medical profession for two centuries. Being consisted of a diaphragm, two earpieces and rubber tubing, stethoscopes basically convert vibration signal into acoustic signal.

Internal body sounds can be heard from lungs, abdomen, heart and major blood vessels. For cardiac examination, there are four main regions to put the diaphragm of the stethoscope from which the valves can be best heard. Those regions are aortic region (centered at the second right intercostal space), pulmonic region (in the second intercostal space along the left sternal border), tricuspid region (between the 3rd, 4th, 5th, and 6th intercostal spaces at the left sternal border) and mitral region (near the apex of the heard between the 5th and 6th intercostal spaces in the mid-clavicular line) [6].

Auscultation evidences can be interpreted successfully as long as clinicians have good listening skills and experience. When abnormal sounds are heard, they are graded on a 6-point level scale (Levine scale) by physicians [7]. This process can be hard for intern doctors and inexperienced physicians. Moreover, same sounds can be subjectively categorized and graded by distinct listeners since human ear has physical limitations [8, 9]. Permanent records are not kept by traditional stethoscopes which makes consultation for same hearing impossible. Those drawbacks of conventional stethoscopes paved the way of modern phonocardiography. A phonocardiogram (PCG) is a high-quality graphical record of heart sounds which are captured and stored in electronic environment with the help of the machine called phonocardiograph [10]. Digitalization of heart sounds allowed the transmission of recordings to computers, automated analysis, long-term storage and graphic visualization [11].

Computer aided auscultation improves recognition of pathological signs and it is preferred for many reasons. On one hand, temporal rate of various sound components can be seen better in PCG records by time-scaling. Medical interns find it useful to study internal structure of the heart sound signals. On the other hand, it can be supported by concurrently collected ECG signals. ECG signals are especially useful when they are used for segmentation of cardiac cycles since there is observable correlation between ECG and PCG [12].

Computerized heart sound analysis has been focused widely and many studies have been conducted with different datasets and state-of-the-art methods. Those studies have been reviewed, compared and discussed in the literature by researchers. In this study, we present a novel review study in which major steps of heart sound analysis is discussed comprehensively. Additionally, feature engineering and important heart sound features are looked through systematically. As a contribution to the literature, recent datasets are presented in detail. Finally, heart sound classification methods are evaluated in a consistent manner.

Acoustic properties of the heart

In essence, computer aided auscultation is similar to acoustic signal processing since the sounds heard from cardiovascular system have the same spectrum as that of audio signals [12]. PCG records are examined for abnormality detection, heart sound localization and classification. The most common challenges of automated heart sound analysis are poor recording quality and environmental noises such as breathing of patients and rustlings of the microphone [5]. Additionally, like other biologic signals, heart sounds are non-stationery and they show sudden frequency changes. Moreover, frequency bands of their internal components are very close.

Under normal conditions of cardiac cycle, heart generates a dominant pair of sounds namely S1 and S2. They are also known as fundamental heart sounds (FHS) and basically described as lub-dub sounds of the heart [13]. Both S1 and S2 consist of two components. Closure of mitral and tricuspid valves produces the M1 and T1 sounds which form the S1 together. Similarly, closure of aortic valve produces A2 sound and pulmonic valve produces P2 sound. A2 and P2 are the components of S2. In normal cases, the time interval between M1-T1 and A2-P2 is not to exceed 30 ms [14]. Having a larger time interval between FHS components is an anomaly and, in such cases, those split sounds can be heard separately. Frequency ranges of S1 and S2 are 10-140 Hz and 10-200 respectively [15].

In addition to FHS, gallop rhythms (namely S3 and S4) and heart murmurs can be detected in PCG records as well [16]. S3 and S4 are known as extra heart sounds and they do not exist in most adults. Even when they are occasionally found, they are difficult to be distinguished by auscultation [14]. S3 occurs at early diastole while S4 takes place at late diastole just before the onset of S1. Frequency ranges of both S3 and S4 are 20-70 Hz [15]. On the other hand, heart murmurs have a larger frequency range of 200-600 Hz [16]. In medicine literature, a heart murmur is a rustling sound made by abnormal turbulent blood. Common causes of heart murmurs can be grouped as septal defects, valve abnormalities and heart muscle disorders (cardiomyopathy). Regurgitation through valves, stenosis of valves, septal/valvular defects and perforations can make a whistling sound indicating abnormality in blood circulation. Intensity, frequency, location and duration of those sounds are carefully examined in PCG records for cardiovascular diagnosis.

Heart murmurs are categorized according to their occurrence during cardiac cycle. Firstly, systolic murmurs are seen at the beginning of S1 and ends before S2. Secondly, diastolic murmurs take place during diastole such as aortic and pulmonary valve regurgitations. Finally, continuous murmurs are seen through all cardiac cycle [14]. In Figure 1 various PCG records are shown.

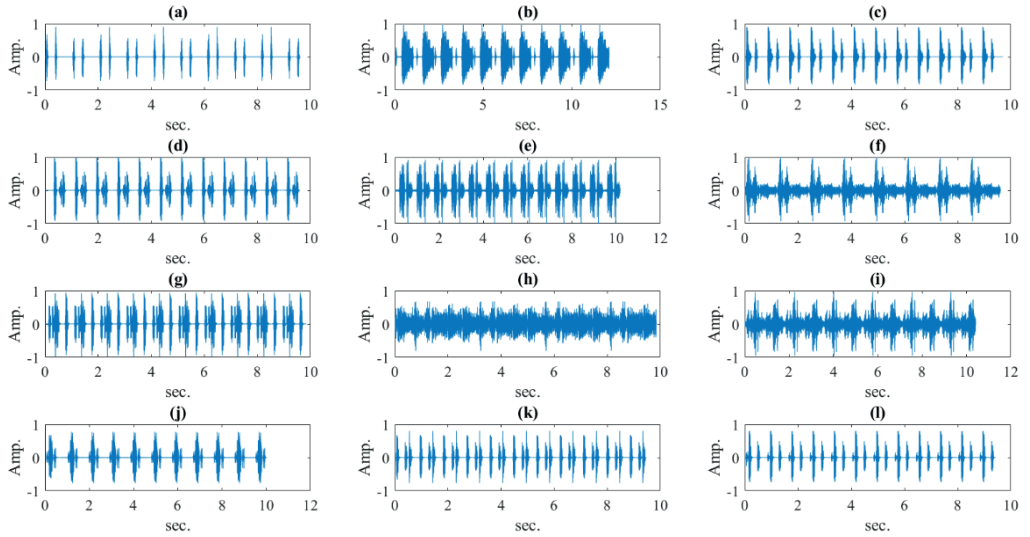

Figure 1. Pathologic and normal PCG records are exhibited. a: normal, b: aortic-insufficiency, c: aortic-stenosis-early, d: aortic-stenosis-late, e: atrial-septal-defect, f: mitral-regurgitation, g: mitral-stenosis, h: patent-ductus-arteriosus, i: pericardial rub, j: pulmonic-stenosis, k: s3 exists, l: s4 exists. Data obtained from University of Washington Heart Sound database in wav format and plotted as figure in MATLAB environment by us.

Heart sound localization

During auscultation, a clinician focuses on hearing the lubs and dubs of the heart to follow cardiac cycles. Determination of cardiac cycles and then localization of temporal positions of S1 and S2 is also known as segmentation. PCG records are divided into four segments: S1, systole, S2 and diastole [5, 12, 15, 17]. The time interval between ending of S1 to beginning of S2 is defined as systole and the time interval between the ending of S2 to onset of S1 is named as diastole. Temporal ratios of segments to each other and overall cardiac cycle is considered as an important feature in machine learning based studies. Moreover, envelopes, morphological and statistical properties of each segment can be examined separately. Expected temporal durations of those segments according to Schmidt et al. [18] is given in Table 1.

Table 1. Cardiac cycle segments and their durations

Segment	Mean (ms)	± Difference in 95% confidence interval (ms)
S1	122	32
Systole	208	80
S2	92	28
Diastole	523	311

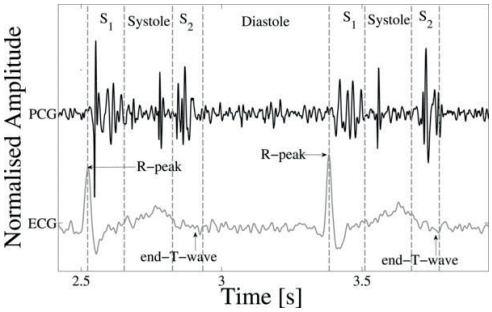

Figure 2. Synchronously collected ECG and PCG records example. Four states of PCG (S1, systole, S2 and diastole) are shown. Adapted from [17].

Heart sound datasets

In this section, we presented the datasets used in several studies. Those datasets are grouped into two categories: individual and public. Individual datasets belong to researchers, hospitals or small communities. They have been used in limited number of studies. On the other hand, public datasets are generally shared with larger communities and they have been used in researches world-wide. Some of them were used in contests and participants

developed state-of-art methods and tested them by using those PCG records.

PCG based computer aided diagnosis has been studied for decades. Early studies based on individual datasets and involved relatively small number of samples by which CNN based methods can be poorly trained. Another problem of working with PCG datasets is dissonance among the age range of the subjects. Datasets composed of children and teenagers is expected to show high heart rhythm variability [19]. Also, structural similarities between normal and abnormal PCG records make the classification task more challenging and hand-crafted studies based on selected features from small datasets are prone to overtraining [20]. Many studies present high accuracies but a direct comparison between those studies is not possible due to use of uncommon datasets. To overcome those constraints, larger public PCG datasets were prepared and made available for computation challenges like PhysioNet CinC/2016.

Researchers used different sampling frequencies during data acquisition for different datasets. 2 kHz can be accepted as the minimum limit of sampling frequency since there is not heart sound components with frequency higher than 1000 Hz [8, 21, 22].

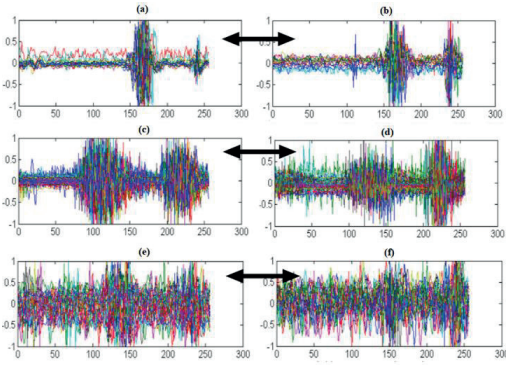

Figure 3. Structural similarities between normal and abnormal PCG records make heart sound classification more challenging. Normal PCG records: a, c and e. Abnormal PCG records: b, d and f. Similar records are shown by arrows. Adapted from [20]. Data from PhysioNet/CinC dataset.

Individual datasets

Bhatikar et al. [23] collected a total of 241 PCG records with murmurs (pathologic or innocent) from pediatric patients of cardiology clinic of The Children's Hospital, Denver, Colorado. Durations of the data were in the range of 10-15 seconds and sampling frequency was 44.1 kHz. Cardiac cycles were segmented manually by clinicians. Ahlstrom et al. [24] used a database recorded at the Department of Internal Medicine at Ryhov County Hospital, Jönköping, Sweden and at the Department of Clinical Physiology, University Hospital, Örebro, Sweden. Tang et al. [22] collected concurrent ECG and PCG data in their laboratory and used sampling frequency as 2 kHz accepting dominant frequency of heart sounds do not exceed 600 Hz. Zhang et al. [25] studied heart sounds after medical heart valve replacement operation. They used a database of 150 heart sounds which are generated by artificial (mechanical prosthetic) heart valves. Dataset was separated into five classes and sampling frequency was used as 8000 Hz. Moukadem et al. [26] used a database of 80 records and half of them were pathological. Gharehbaghi et al. [27] tried to separate innocent murmurs from pathological ones by using four data sets consisting of 10 second duration concurrent ECG and PCG. Those data sets were collected from volunteered patients at Linköping University hospital and Tehran Children Medical Center. Springer et al. [17] used 405 synchronous PCG and ECG records of 30-40 seconds which are collected from 123 adult patients at Massachusetts General Hospital. Karar et al. [28] used a database provided by CliniSurf, Faculty of Medicine, University of Bern, Switzerland. The database consists of 19 abnormal and 3 normal heart sounds. Each record has got about 15 cycles and sampling frequency is 44.1 kHz. Othman and Khaleel [29] used a database of 9 PCG records consisting of 3 normal, 3 abnormal with mitral regurgitation and 3 abnormal with mitral stenosis. Bozkurt et al. [30] used UoC-Murmur database (466 records) belonging to University of Crete, Greece. The concurrent PCG and ECG records were collected from children of 8-years-old age and classified by pediatric cardiology experts either as normal or as pathologic. Durations of them change in the range of 4-10 seconds and sampling frequency is 44.1 kHz. Aziz et al. [31] built their own PCG dataset by using their own data acquisition system at Rawalpindi Institute of Cardiology, Rawalpindi, Pakistan. From 56 subjects, they collected 140 normal and 140 pathologic (85 arterial septal defect, 55 ventricular septal defect) PCG records which were labeled by expert cardiologists into three classes (Normal, ASD, VSD). Sampling frequency was 44100 Hz and the duration of each record is 5 seconds. Yaseen et al. [32] build a database from public premade sources. They randomly selected 1000 PCG records from five different classes (200 records per each class). Those records were labeled by experts as normal, aortic stenosis, mitral regurgitation, mitral valve prolapse and mitral stenosis heart sounds. PCG records were resampled to 8000 Hz and stored in wav format. Safara et al. [33] used a dataset consists of 59 heart sounds (16 normal, 43 pathological).

Publicly available datasets

Texas Heart Institute Heart Sound Series

The database produced by the Robert J. Hall Heart Sounds Laboratory of Texas Heart Institute at St. Luke's Episcopal Hospital in 2009. The database includes 44 types of heart sounds [34] but it is not available now.

E-General Medical

A cardiac auscultation database of size 64 records was provided by eGeneral Medical Inc. It used to require payment for all database [15] but a part of it was free [12]. Database consisted of normal sounds, S3, S4 and different

pathologic cases. It has been used in several studies [16] and today it is not available online.

Frontiers in Bioscience

A total of 25 records available from int-prop.lf2.cuni.cz/heart_sounds/h14/sound.htm. Records are in wav format and their durations change in the range of 1.50 to 4.26 seconds.

Thinklabs Heart Sound Library

105 heart sounds in the range of 10-50 seconds. Available from Thinklabs' youtube channel https://www.youtube.com/c/Thinklabs1.

University of Washington

Different kinds of murmurs, split heart sounds and normal records present in wav format. Available from https://depts.washington.edu/physdx/heart/tech1.html.

3M Littmann Heart and Lung Sounds Database

PCG files are divided according to auscultation area. Records can be listened from browser. A total of 51 records available from http://www.3m.com/healthcare/littmann/mmm-library.html.

Heart Sound & Murmur Library Open Michigan

University of Michigan Health Systems provided an online database to educate undergraduate medical students and teach them clinical auscultation skills. The Michigan heart sound and murmur database (MHSDB) includes 23 records in mp3 format. It is available from www.med.umich.edu/lrc/psb_open/html/repo/primer_heartsound/primer_heartsound.html.

Cardiac Auscultatory Recording Database (CARD)

John Hopkins Outpatient Center Pediatric Cardiology Clinic digitized their clinic examinations in 1997. CARD is built from simultaneous PCG and ECG records of volunteered patients. CARD also includes clinical data for each case described by responsible cardiologist. 20 second duration recordings obtained from more than 1200 patient forms the CARD [35]. Audio files are stored in wav format and sampled at 4 KHz. It is available from http://murmurlab.com/card6/ after registration.

PASCAL (Pattern Analysis, Statistical modelling and ComputAtional Learning)

PASCAL [36] heart sound database was shared publicly in 2011 for two challenges. First competition was for heart sound segmentation and the second competition was for heart sound classification. The data were gathered from two sources and grouped into two (A and B). Group A was gathered by patients using iStethoscope Pro iPhone app. On the other hand, samples of group B were collected in hospital environment by physicians [37, 38]. The first group consists of four categories while the second group has only three categories of heart sounds. Sampling rate is 44100 Hz and the samples are stored in wav format. Durations of the samples vary in the range of 1 to 30 seconds [15] [36]. It has been used in several researches and it is still available online [39]. Details of it is given in the Table 2.

Table 2. PASCAL heart sound dataset details. Categories and number of samples in them are shown. Resource [36]

	Train				Test
Group	**Normal**	**Murmur**	**Extra heart sound**	**Artifact**	**Unlabeled**
A	31	34	19	40	52
B	319	93	46	-	195

Physionet CinC/2016

Similar to PASCAL dataset, PhysioNet heart sound dataset was built for a challenge in 2016. It was assembled from nine independent heart sound databases which were collected by seven distinct groups. Therefore, data acquisition hardware, data quality, labeling details and sampling frequencies were slightly different. In order to overcome this heterogeneity problem, all samples were resampled to 2 KHz and provided as wav files after anti-aliasing filtering [15]. Avoiding from specific diagnosis details, only three labels were assigned to PCG records: normal, abnormal and unsure.

The dataset is divided into train and test sets. While there is open access to train set, the test set is kept private. Submissions of the 2016/CinC challenge participants were ranked according to their performance on the test set. Moreover, poor signal quality and good signal quality were weighted differently during competition. Signal quality information is not available for train set. Details of the samples are given in the Table 3.

Table 3. PhysioNet database details. Resource [15]

Set	**Patients**	**PCGs**	**Abnormal**	**Normal**	**Unsure**
Train-A	121	409	276	116	17
Train-B	106	490	73	295	122
Train-C	31	31	20	7	4
Train-D	38	55	26	26	3
Train-E	356	2054	146	1781	127
Train-F	112	114	31	78	5
Total	764	3240	572	2303	365
Test-B	45	205	32	100	73
Test-C	14	14	9	4	1
Test-D	17	24	11	11	2
Test-E	153	883	59	763	61
Test-G	44	116	21	95	0
Test-I	35	35	21	12	2
Total	308	1277	153	985	139

Currently, the PCG dataset of PhysioNet is the largest one among other publicly available databases [40]. PCG records have different durations in the range of 5-120 seconds. Records are mono channel with 16-bit resolution in little-endian format. In addition to PCG, there is also simultaneously recorded ECG data for each sample of Train-A set. Train part of the database is available from https://physionet.org/content/challenge-2016/1.0.0/.

Materials and Methods

Research area of heart sound examination is an intersection of pattern recognition and signal analysis. Computer aided auscultation studies generally focus on either heart sound segmentation or on classification of heart sounds for detecting abnormalities [41]. But many classification studies [42] involve segmentation as a sub-step even though their main target is classification of heart sounds. Segmentation is not a fundamental prerequisite and, in the literature, there are classification studies which do not involve segmentation at all such as [43, 44]. On the other hand, localization of heart sounds and segmentation is the main purpose of many studies [17]. The general structure of the proposed methods in the literature is as follows: preprocessing, segmentation, feature extraction and classification.

Preprocessing

The main processes applied on the signal during preprocessing phase include filtering, resampling, baseline removal, denoising, decimation and normalization. Filtering is generally the first step of preprocessing. It can be done by amplitude or frequency-based filters. Potes et al. [45] used a band-pass filter of 25-400 Hz. In several studies [46, 47] Butterworth bandpass filter of 25-400 Hz was applied to remove high frequency noise and low frequency artifacts. In [48] fourth order Butterworth high-pass and low-pass filters were used with 600 and 25 Hz cutoffs while in [49] 57th order Butterworth lowpass filter with 900 Hz was used. In [50] 3th order median filter and 10th order Butterworth low-pass filter with 150 Hz cutoff were applied. In another study [51] a model was proposed for separating breathing sounds from heart sounds based on Kalman filter. They used synthetic data which were prepared by adding Gaussian noise (representing the respiratory sounds) to real acquired heart sound signal. In order to obtain segments from pathological records, Atbi and Debbal [52] used a low-pass FIR filter with 100 Hz cutoff frequency eliminating all high frequency components.

Many researchers normalized the signal into the [-1, 1] range by dividing with absolute maximum of the signal [16, 34, 53]. Some choose to normalize according to Equation 1 to obtain more visible peaks while weaking the noise [52, 54]. Another widely used normalization method [17, 39, 48] is z-score normalization. Safara et al. [33] normalized the signal according to Equation 2. Several studies [55, 56] involve baseline removal in this phase.

$$x_{norm} = \left(\frac{x}{\max(|x|)}\right)^2 \quad (1)$$

$$x_{norm} = \frac{x}{\sqrt{\sum x^2}} \quad (2)$$

In many studies, the classifier models need a uniform input shape. For example, inputs of CNN models and spectrograms of signals should have same dimensions to be processed. However, the datasets contain PCG records with variable length and/or different sampling frequencies. Features such as MFCC extracted from those signals differ in dimensions. Resampling and decimation are used to build a uniform input shape. Those steps beyond providing a uniform input shape also reduces computational cost. In studies [20, 45, 46, 48] PCG signals were down sampled from 2 kHz to 1000 Hz. Rubin et al. [57] decimated the PCG records to 3 second duration instances. In another study [58], first 5 seconds of the records were clipped and the remaining parts were discarded. Potes et al. [45] used 2.5 seconds decimation while shorter records were zero padded.

Another preprocessing step is denoising. Aziz et al. [31] used EMD for denoising. Gradolewski et al. [59] used Wavelet Packet Decomposition (WPD) to denoise PCG signals contaminated by white and pink noise. Similarly, Discrete Wavelet Transform was used in several studies [8] for denoising purposes by using thresholds. Threshold based denoising is either done by removing all samples below the threshold (hard thresholding) or it is done by producing a smoother transition over deleted values by subtracting threshold value from samples (soft thresholding) which are given in Equations (3-4).

$$y_{thr(T)}(t) = \begin{cases} y(t), & |y(t)| \geq T \\ 0, & otherwise \end{cases} \quad (3)$$

$$y_{thr(T)}(t) = \begin{cases} y(t) + T, & y(t) < -T \\ 0, & -T \leq y(t) \leq T \\ y(t) - T, & T < y(t) \end{cases} \quad (4)$$

Segmentation

Segmentation can be done by using simultaneously recorded ECG data [8, 24, 27]. Temporal segmentation of cardiac cycle is relatively easy by using ECG because its (PQRST) structure can clearly show the beginning and ending points of cycles. Moreover, it is more noise-free unlike PCG records. While interpreting ECG records, S1 is expected shortly after R peaks and S2 occurs at the end of the T wave [17]. However, the main disadvantages of this approach are needing auxiliary data and synchronizing it exactly with the PCG signal's timing.

Another segmentation approach depends solely on PCG. ECG-independent approach consists of various methods. Generally, envelope of the signal is extracted and used in this process. Envelope extracting approaches can be conducted with different mathematical properties of signals such as Shannon energy [37, 60, 61], Shannon entropy [62], variance fractal dimension [63], Hilbert-Huang transform [64] and autocorrelation [34]. Equations (5-9) can be used to map the original signal to non-negative domain for envelope extraction [29, 53].

Absolute value: $E = |S_i|$ (5)

Energy: $E = S_i^2$ (6)

Shannon entropy: $E = -|S_i| \log |S_i|$ (7)

Shannon energy: $E = -S_i^2 \log (S_i^2)$ (8)

Average Shannon energy: $E_{avg} = -\frac{1}{N}\sum_i^N S_i^2 \log (S_i^2)$ (9)

In the literature, there are methods based on amplitude thresholding such as [53, 65] and [66]. Similarly, peaks within predefined intervals are considered as S1 and S2 [9]. In an alternative approach, Ghosh et al. [61] segmented PCG records based on systolic and diastolic time intervals.

In several studies Hidden Markov Models (HMMs) are used for segmentation such as [67-69]. Schmidt et al. [18] proposed a hidden semi–Markov Model (HSMM) modeling the expected durations of the segments. Springer et al. [17] improved HSMM based approach of [18] by novel contributions such as adding probability of staying in a state for a defined duration, modifying Viterbi algorithm, applying Logistic Regression and then used a combination of homomorphic, Hilbert, PSD and Wavelet envelopes. In their study, the gold standard of the FHS positions in the PCG is derived from synchronously gathered ECG records. Abdollahpur et al. [48] proposed a novel method for cycle quality assessment build upon the work of [17]. After segmentation, original PCG signal is split into four distinct signals whose features are extracted and interpreted individually.

Feature engineering

PCG signals contain large number of samples and success of signal processing methods depend on extracting meaningful features from the signal. Features can be extracted from signals in time, frequency and time-frequency domains. In many studies, different features collected from distinct features are combined. However, when the number of extracted features increase dramatically, computational cost increases as well. In such cases dimension reduction methods Principal Component Analysis (PCA), Singular Value Decomposition (SVD) or Independent Component Analysis (ICA) are applied in several studies [70-72]. Another solution of this problem is to choose the most meaningful features and not to increase feature set sizes by using rest of the features.

Alternatively, deep learning-based classification methods do not need manual feature engineering. Those models can be applied directly on either PCG signals or on envelograms obtained from those signals without feature extraction [73]. The researchers can use those models as is or they can just take the generated features by those models to use with conventional classifiers [74].

Time Domain Features

Time domain features of a signal present the statistical attributes changing over time. PCG signals have various morphological characteristics which can be observed from time domain perspective. Most commonly used time domain features such as mean, standard deviation, median, signal energy, maxima, minima and zero-crossing rate are calculated directly from the signal itself. Moreover, signals can be converted into probability density functions and their entropies can be calculated by different methods. Some of the time domain features widely used in the researches are given in the Table 4.

Table 4. Time domain features

Feature	Formula	Ref
mean	$\bar{x} = \frac{1}{N}\sum_i^N x(i)$	[75-77]
Standard deviation	$s = \sqrt{\frac{1}{N}\sum_i^N (x(i) - \bar{x})^2}$	[75-77]
Skewness	$\left[\frac{1}{N}\sum_i^N (x(i) - \bar{x})^3\right] / s^3$	[75-77]
Kurtosis	$\left[\frac{1}{N}\sum_i^N (x(i) - \bar{x})^4\right] / s^4$	[75-77]
Median	Middle value or average of two middle values for arrays with even number of samples	[77]
Maxima, minima		[76]
Zero crossing rate	$\frac{1}{2N}\sum_{i=1}^{N} \lvert sgn[x(i)] - sgn[x(i-1)]\rvert$	[13, 76]
Shannon entropy	$-\sum_i^n \lvert p_i * \log (p_i)\rvert$	[76]
Avg Shannon enrgy	$-\frac{1}{N_{seg}}\sum_i^{N_{seg}} S_i^2 \log (S_i^2)$	[24]
Karcı entropy	$\sum_i^n \lvert(-p_i)^{\alpha} * \ln(p_i)\rvert$	[13]

Percentile rate	$\frac{25^{th} percentile}{75^{th}\ percentile}$	[77]
RMS	$\sqrt{\frac{1}{N}\sum_i^N x(i)^2}$	[76]
Zero cross rate	Rate of sign changes at signal	[76]
Total original signal power	$\sum_i^N \frac{x(i)^2}{N}$	[38]
Avg widths of segments		[71]
Ratios of segments' avg widths to each other		[78]

Frequency Domain Features

When a sinusoid signal is added with another one the result is another sinusoid signal but may be shifted in amplitude, phase and frequency. Assuming the general formula given in Equation 10 is valid for the signals of interest, amplitudes of different frequency components provide meaningful features. In the Equation 10, A is amplitude, f is frequency, t is time and θ is phase offset in radians.

$$y(t) = \sum_i A_i \sin(2\pi f_i t + \theta_i) \quad (10)$$

But frequency domain features lack the ability of indicating temporal positions of abnormalities. Moreover, suitability of them is often criticized due to the non-stationary structure of PCG signals. They are generally considered insufficient alone however they are used together or within other methods. Those features are used for band-pass filter banks and zero crossing analysis [40].

Fourier Transform (FT)

FT provides frequencies and their magnitudes of a signal and it is very useful for stationary signals. FT technique is used to examine harmonic components of a signal by transforming the signal from time domain to frequency domain. FT provides valuable information about frequency bands but it lacks the capacity of locating the frequency regions in time. Another major disadvantage of FT is that it cannot be applied on multi-channel signals. Debbal et al. [79] applied Fast Fourier Transform (FFT) on PCG data and detected FHS frequencies in the spectrum (gathered around 40-200 Hz) however they concluded that duration and transient variations cannot be detected by FFT. Bhatikar et al. [23] used 0-300 Hz energy spectrum obtained by Fast Fourier Transform.

$$e^{ix} = \cos(x) + isin(x) \quad (11)$$

$$F(f) = \int_{t=-\infty}^{\infty} f(t)\, e^{-i2\pi f t} dt \quad (12)$$

Direct Cosine Transform (DCT)

DCT can be used for audio and image signal compression. Discrete time domain signal is firstly converted into a sum of cosine functions with different frequencies. Their amplitudes are interpreted as the features. In essence, DCT is similar to FT but DCT uses only cosine functions for transformation and output values are real numbers.

Time-Frequency Domain Features

Short Term Fourier Transform (STFT)

STFT was developed to overcome time resolution problem of FT. STFT assumes that some portion of an input signal is stationary. Each stationary-accepted sub-region is applied FT and then all parts are added up. STFT formula is given in Equation 13 where w(t) is window function.

$$\mathrm{H(t,f)} = \int h(t) w(t-\tau) e^{-2\pi f \tau} d\tau \quad (13)$$

In STFT, there is a trade of between time and frequency resolution. Fixed size windows of STFT affect the time-frequency representation. As window size increases, frequency capturing performance rises but time resolution decreases. Conversely, if window size is kept small then time domain gets more accurate while losing frequency information.

Wavelet Transform (WT)

Being a better alternative than FT and STFT, WT was originally developed to optimize frequency dependent temporary resolutions [80]. WT can be defined as a short wave that has an average value approaching zero. The energy carried by the wave is condensed in time. WT provides good resolution both in time and frequency domains.

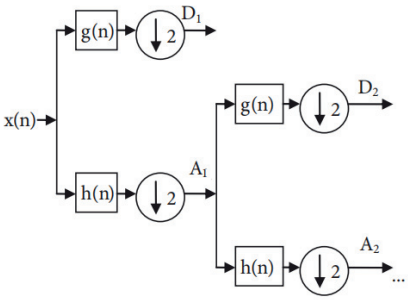

Figure 4. DWT decomposition scheme. D: detail, A: approximation, h: low-pass filter, g: high-pass filter

When an orthogonal basis function is used as wavelet, the WT is named as discrete wavelet transform (DWT). If a non-orthogonal basis function is used as wavelet, then the transform is called as continuous wavelet transform (CWT). Another effective wavelet-based feature extraction method is wavelet packet decomposition (WPT). Similar to STFT, its top level is good in time resolution and as level decomposition goes on temporal resolution decreases in the favor of frequency resolution. WT is used for denoising, data compression, obtaining sub-band features and visualizing spectral components as well. The general formula is given in Equation 14 where ψ(t) is wavelet function, ϕ(t) is scaling function, h(t) is low-pass impulse response and g(t) is high-pass impulse response, c_i and $d_{i,j}$ are coefficients [12].

$$y(t) = \sum_{j=-\infty}^{\infty} c_i \varphi_j(t) + \sum_{i=-\infty}^{\infty} \sum_{j=-\infty}^{\infty} d_{i,j} \psi_{i,j}(t) \quad (14)$$

Empirical Mode Decomposition (EMD)

EMD is proposed as a part of Hilbert-Huang Transform [72] and it has been used for many purposes such as denoising [31], detection of heart sounds [81] and segmentation [50].

EMD iteratively reduces the input signal into intrinsic mode functions (IMFs) and a residual. The process of extracting IMFs from the raw signal is known as sifting. The original signal can be expressed in terms of IMFs and residual signal as given Equation 15. An IMF must satisfy two requirements. First, in the whole dataset, the number of extrema and the number of zero-crossings must either be equal or differ at most by one. Second, at any point, the mean value of the envelope defined by the local maxima and the envelope defined by the local minima is zero.

$$y(t) = \sum_{k=1}^{N} h_k(t) + r(t) \quad (15)$$

After IMFs are obtained, they can be examined individually. Generally, the first IMF is discarded since it contains high frequency components. Time and frequency domain features can be extracted from IMFs.

The main steps of sifting are:

1. Calculating all of the local minima and maxima from the signal y(t)
2. Cubic spline interpolation is applied on local minima and maxima in order to obtain envelopes $e_{min}(t)$ and $e_{max}(t)$
3. Mean of upper and lower envelopes are calculated according to Equation 16.

$$a(t) = (e_{max}(t) + e_{min}(t)) / 2 \quad (16)$$

4. Mean envelope is subtracted from the original signal y(t) to obtain ith IMF $h_i(t)$ according to Equations 17, 18.

$$h_i(t) = y(t) - a(t) \quad (17)$$

$$r_i(t) = y(t) - h_i(t) \quad (18)$$

5. Treat $r_i(t)$ as the new signal and repeat steps 1-4 until residual signal contains no more IMF

Mel-Frequency Cepstral Coefficients (MFCC)

MFCC is a well-known technique used in speech recognition and speaker identification. It has also found usage in PCG analysis as well [45]. Human ears do not perceive pitch linearly. Mel scaling aims to mimic human auditory systems by mapping the frequencies below 1000 Hz linearly and by mapping the frequencies above 1000 Hz logarithmically [12].

To obtain MFCC features, pre-emphasizing is the first step in which high frequencies are amplified. Then the quasi-stationary signal is divided into short frames across which the signal is assumed to be stationary. Generally consecutive frames overlap a pre-defined amount of time. Then a window (such as Hamming, Hanning or etc.) is applied on the frames to reduce edge effects and smooth the edges. Then Discrete Fourier Transform is applied on the windowed frames to compute the periodogram. Then the Fourier transformed signal is passed through Mel-filter bank (a set of bandpass filters). This phase results in non-linear frequency resolution. It is given in Equations (19-20) where f is physical frequency and f_{MEL} is its Mel-frequency representation.

$$X(k) = \sum_{n=0}^{N-1} x(n)\, e^{\frac{-j2\pi nk}{N}};\ 0 \le k \le N-1 \quad (19)$$

$$f_{MEL} = 2595 \log_{10}\left(1 + \frac{f}{700}\right) \quad (20)$$

Now Mel spectrum is fit into log format in which most of the signal information is represented by the first few coefficients. M is total number of Mel weighting filters and $H_m(k)$ is the weight given to kth energy spectrum bin according to Equation 21.

$$P_{filt} = \sum_{k=0}^{N-1} [|X(k)|^2 H_m(k)];\ 0 \le m \le M-1 \quad (21)$$

Finally, MFCCs are obtained by taking a discrete cosine transform. This process converts the Mel spectrum to finite sequence of cosine functions oscillating at different frequencies. In Equation 22, *MFCC(t,k)* is kth cepstral feature of tth time frame and $P_{filt}(t,n)$ is filtered power at time frame t for nth filter bank. The number of MFCCs for each frame is C and zeroth coefficient can be excluded since it represents the average log energy of the input signal.

$$MFCC(t,k) = \sum_{n=0}^{N-1} \log\left(P_{filt}(t,n)\right) \cos\left(\frac{k\pi}{N}(n - 0.5)\right);\ k = 0,1,2 \ldots, C-1 \quad (22)$$

Classification

In this section we present a list of proposed solutions with year, dataset and performance results. It is not an exhaustive list and involves results from previous challenges.

Classification is done with many machine learning methods including support vector machine, k nearest neighbor, multilayer perceptron, decision trees, convolutional neural networks and their ensembles. Ensemble classifiers reduces the error rate significantly and usually their performances are better than their base classifiers [37]. Performance comparisons of PhysioNet challenge are done according to Equations (28-30) where w_{a1}, w_{a2}, w_{n1} *and* w_{n2} are weights of good signal quality of abnormal, poor signal quality of abnormal, good signal quality of normal and poor signal quality of normal records. Rules for determining the overall classification result of the challenge are given in Table 5. On the other hand, the rest of the comparisons are done according to well-known formulas given in the Equations 23-27.

Table 5. Rules of PhysioNet CinC/2016 scoring

Label	Quality	Weight	Predicted Abnnormal	Predicted Unsure	Predicted Normal
Abnormal	Clean	w_{a1}	A_{a1}	A_{q1}	A_{n1}
	Noisy	w_{a2}	A_{a2}	A_{q2}	A_{n2}
Normal	Clean	w_{n1}	N_{a1}	N_{q1}	N_{n1}
	Noisy	w_{n2}	N_{a2}	N_{q2}	N_{n2}

Classification performance is highly dependent on the preprocessing, segmentation and feature extraction phases. Several studies are shown in Table 6 with details about used dataset, deployed method, extracted features and performance results. Comparing them, it is seen that classification accuracies change in the range of 75 to 99 percent. Especially on private datasets, accuracies above 90 percent are reported generally. On the other hand, challenge datasets such as PhsyioNet evaluated performance results over hidden test sets avoiding overfitting. Diversity of those datasets prevent us from direct comparison between them but general trends and validation methods give insight about the success of the proposed methods and usefulness of the selected features.

In studies [45, 70, 90, 91], distinct frequency subbands of the signal were decomposed and used to extract features or envelopes. S1 and S2 intervals are searched for in low frequency subbands in [90]. In [45], more features were obtained from decomposed subbands. Koçyiğit [70] used discrete wavelet transform to get signal subband and then applied PCA and ICA dimension reduction methods on it to extract features. The extracted features were given to Naïve Bayes classifier and 99.8% accuracy was obtained.

The HSMM-based segmentation method proposed by Springer [17] was used by many Physionet 2016/CinC contestants in their studies [42, 45, 57, 74-76, 87]. Features were extracted from four segments of the detected cardiac cycle and variations in the durations of them were interpreted as the signs of anomalies. On the other hand, some studies [13, 43, 58, 70] processed the PCG signal as a whole without using any segmentation method on them. When PCG analysis approaches with segmentation-based and without segmentation methods are compared, it is seen that there is not much difference. For example, in PhysioNet 2016 CinC, Potes et al. [45] took the first place with a segmentation-based approach by obtaining a score of 86.02. However, Zabihi et al. [43] took the second place by obtaining 85.90 without applying segmentation. In [45] features were extracted from four states in time domain and frequency domain while in [43] desired features were extracted from whole signal alone. The small difference between those studies indicates that selection of features is more important for PCG classification than applying state-of-the-art segmentation methods.

In earlier studies, different types of Artificial Neural Networks (ANN) have been applied [43, 48, 87] to solve heart sound classification problem. Features from time, frequency and time-frequency domains formed feature vectors of sizes 40 to 675. ANN models are trained with those feature vectors after applying dimension reduction. Accuracies higher than 80% percent are obtained by former ANN based approaches. It is also used for segmentation of heart sounds. Ghaemmaghami et al. [93] extracted and used 6 mel-frequency filterbank features to categorize temporal frames of audio recordings as S1, systole, S2, diastole and noise by using time-delay neural networks (TDNN). TDNN is good for detecting local correlations between segments and it is able to capture long term temporal correlations between cycles frames. Temporal events in heart sounds can be detected by TDNN as well.

Currently researchers' interest focused more on different types of Deep Neural Networks (DNN). For instance, Recurrent Neural Networks (RNN) have been used in recognizing sequential data for decades and it is also applicable on heart sounds since they have strong temporal correlation. Vanishing gradient problem of RNN is handled by structures like Long-Short Term Memory (LSTM) and Gated Recurrent Unit (GRU). Khan et al. [94] used LSTM with MFCC features of unsegmented PCG data obtaining an AUC score of 91.4% and accuracy above 80%. Among the DNN based methods, LSTM models have relatively high complexity but they are capable of modeling temporal structures and dependencies.

An alternative of using DNN is to generate 2D images or image-like inputs from time series data by applying time-frequency spectrograms, MFCC or heat maps and then training Convolutional Neural Networks (CNN) [57, 82, 92]. There are also solutions [20, 46, 95] based on 1D CNN models which only perform simpler one-dimensional convolutions (scalar addition and multiplication) on PCG signals.

Both DNN and CNN methods require large datasets and long training time for better classification accuracies. To train those models in reasonable time periods, researchers generally take the advantage of using modern GPU hardware.

$$Accuracy = \frac{TP+TN}{All} \tag{23}$$

$$Recall = Sensitivity = \frac{TP}{TP+FN} \tag{24}$$

$$Specificity = \frac{TN}{TN+FP} \tag{25}$$

$$Precision = Positive\ Predictive\ Value = \frac{TP}{TP+FP} \quad (26)$$

$$F1\ Score = \frac{2*Presicion*Recall}{Presicion+Recall} \quad (27)$$

$$Modified\ Sensitivity(Msn) = \frac{w_{a1}\ A_{a1}}{A_{a1}+A_{q1}+A_{n1}} + \frac{w_{a2}\ (A_{a2}+A_{q2})}{A_{a2}+A_{q2}+A_{n2}} \quad (28)$$

$$Modified\ Specificity(Msp) = \frac{w_{n1}\ N_{n1}}{N_{a1}+N_{q1}+N_{n1}} + \frac{w_{n2}\ (N_{a2}+N_{q2})}{N_{a2}+N_{q2}+N_{n2}} \quad (29)$$

$$Modified\ accuracy(Macc) = \frac{Sensitivity+Specificity}{2} \quad (30)$$

Table 6. Performance results of studies in the literature

Ref	Year	Data	Classes	Features	Methods	Results (%)	
[47]	2020	PhysioNet	2	MFCC based features	Convolutional recurrent neural network	Acc: 98.34 Sen: 98.66 Spe: 98.01	
[31]	2020	private	3	MFCC 1D Local ternary patterns	SVM	Acc: 95.24	
[82]	2020	Dataset of Yaseen et al. [32]	5	Bispectrum images (full-image and contour)	CNN	**Full-img** Acc:98.70 Sen:98.70 Spe:99.67	**Contour** Acc:97.10 Sen:97.10 Spe:99.28
[61]	2020	Dataset of Yaseen et al. [32]	5	Time-frequency domain energy and entropy features	Multi class composite classifier	Acc: 98.33	
[20]	2020	PhysioNet	2	-	1D CNN	Sen: 89.67 Spe: 86.89 Ppr: 69.70	
[83]	2020	PASCAL	4 & 5	Time domain MFCC	SVM kNN	Acc: 99.25 Acc: 98.50	
[13]	2020	PhysioNet	2	Time domain Time-frequency domain MFCC	Ensemble of kNN, SVM, neural networks	Acc: 90.93 Sen: 98.00 Spe: 64.00	
[92]	2019	PhysioNet	2	STFT spectrogram Mel Spectrogram MFCC	CNN (VGGNet) Majority voting ensemble	Acc: 86.04 Sen: 86.46 Spe: 85.63	
[46]	2019	PhysioNet	2	Time-frequency MFCC based feature maps	Ensemble of 1D CNN and 2D CNN	Acc: 89.22 Sen: 89.94 Spe: 86.35	
[84]	2019	187 PCG records from PhysioNet	2	Cochleagram	Multilayer perceptron	Acc: 93.70 Sen: 84.50 Spe: 95.20 F1: 83.50	
[85]	2018	private	2	Time and frequency domains	ANFIS HMM	Acc: 98.70	
[86]	2018	Open Michigan Library PASCAL PhysioNet	2	Time-frequency MFCC STFT	Recurrent neural network CNN Bidirectional long short-term memory	Sen: 96.00 Spe: 100.00 F1: 98	
[30]	2018	UoC proprietary	2	Sub-band envelopes of segmented PCG	CNN	Acc: 81.50 Sen: 84.50 Spe: 78.50	
[32]	2018	individual	5	MFCC DWT	kNN SVM DNN	**kNN** Acc: 97.40 Sen: 97.60 Spe: 98.80 F1: 99.20 **SVM** Acc: 97.90 Sen: 98.20 Spe: 99.40 F1: 99.70	**DNN** Acc: 92.10 Sen: 94.50 Spe: 98.20 F1: 98.30

[78]	2017	PhysioNet	2	Time, frequency, sparse coding	SVM	Macc: 80.70 Sen: 84.30 Spe: 77.20
[49]	2017	Private	2	Time-frequency	kNN	Acc: 93.20
[48]	2017	PhysioNet	2	Time, time-frequency	Neural networks	Macc: 82.63 Mse: 76.96 Msp: 88.31
[42]	2017	PhysioNet	2	Time, frequency, time-frequency	Ensemble classifiers	Macc: 80.10 Mse: 79.60 Msp: 80.60
[93]	2017	Self-collected 128 records of 20 seconds duration	5	MFCC	Time Delay Neural Network	Acc: 95.80 Sen: 83.20 Spe: 99.20
[45]	2016	PhysioNet	2	Time, frequency	Adaboost & CNN ensemble	Macc: 86.02 Mse: 94.24 Msp: 77.81
[43]	2016	PhysioNet	2	Time, frequency and time-frequency	Ensemble of neural networks	Macc: 85.90 Mse: 86.91 Msp: 84.90
[87]	2016	PhysioNet	2	Time, frequency domain features, CWT features, MFCC	Neural networks	Macc: 85.20 Mse: 87.43 Msp: 82.97
[88]	2016	PhysioNet	2	Time-frequency	LR SVM kNN	Macc: 84.54 Mse: 86.39 Msp: 82.69
[76]	2016	PhysioNet	2	Time, frequency and time-frequency domain features	Random Forest LogitBoost	Macc: 84.48 Mse: 88.48 Msp: 80.48
[57]	2016	PhysioNet	2	MFCC heat map images	CNN	Macc: 83.99 Mse: 72.78 Msp: 95.21
[89]	2016	private	2	MFCC based features	kNN GMM LR SVM DNN	Acc: 78.11 Acc: 86.98 Acc: 87.57 Acc: 90.53 Acc: 91.12
[75]	2016	PhysioNet	2	Statistical features of WT applied data	SVM	Acc: 74.60 Sen: 64.40 Spe: 84.90
[90]	2016	PhysioNet	2	Statistical features Frequency domain	Fuzzy logic (PROBAfind)	Acc: 95.00 Sen: 93.00 Spe: 97.00
[33]	2013	private	4	Time-frequency	SVM	Acc: 97.56
[21]	2009	Students' training CD	15	Time-frequency	Divergence analysis	Acc: 99.00
[91]	2009	Littman and Frontiers in Bioscience datasets	5	Time-frequency	SVM with several kernel functions (Best results obtained with Gaussian Radial Basis Function kernel)	Acc: 91.43 Sen: 87.50 Spe: 94.74

Conclusion and suggestions

In this study we reviewed PCG analysis methods and existing databases. Feature extraction techniques and methodological approaches are presented and compared. Heart sound analysis is an interesting topic and it is still challenging. The fundamental heart sounds corrupted with various pathological factors. Mitral stenosis, mitral regurgitation, aortic insufficiency, aortic regurgitation, valve disorders, septal defects and gallop rhythms cause heart murmurs that differ from each other with respect to frequency and location. Main tasks of heart sound analysis focus on detecting murmurs and segmentation. Besides, classifying distinct types of murmurs has been targeted by several studies. On the other hand, heart sound segmentations are done by detecting peak values, using

systolic/diastolic temporal assumptions, threshold-based methods and using external signals (commonly ECG). Environmental and digital noises are tried to be remove from heart sounds. For this purpose, signal denoising is applied as the first step of automated PCG analysis. It is followed by feature engineering in conventional approaches but CNN-based methods do not involve feature extraction. Those features are grouped in time, frequency and time-frequency domains. Wavelet based features are most preferred time-frequency domain features and as it is seen in Table 6, the most commonly used features belong to time-frequency domain. Similar to Wavelet transform, EMD is also good at representing the sound signal in time-frequency domain. After this step, PCG records are classified by several algorithms such as HMM, SVM, decision trees and neural networks.

Although the current studies make a good sum, there is still room for improvements. Firstly, there is need for a universally standardized and open access database. In the past, the lack of data was a problem for researchers. Researchers generally used private databases decades ago but today there are databases like PASCAL, CARD, PhysioNet and etc. Among those PCG databases, the largest one is PhysioNet with 665 abnormal and 2575 normal records having an imbalance ratio of 2575/665 = 3.87. Although it is the largest one, state-of-the-art CNN-based methods require larger databases with smaller imbalance ratio. Secondly, more information on data acquisition and auscultation locations should be given in those standardized databases. Heart sounds generally recorded from aortic area, pulmonic area, tricuspid area and mitral area. Depending on the position of the auscultation sensor, loudness of first and second heart sounds could be captured differently. Finally, data acquisition should be improved by avoiding from noise. Additionally, an extra classifier can be added to the systems in order to detect signal quality. Excluding records with significant environmental noise increases methods' accuracy and results in more meaningful conclusions about pathologies.

Performance of automated heart sound analysis is promising and it has many possible benefits. Development of computationally efficient methods paves the way of intelligent biomedical devices. Smart phones, wearable systems and other portable gadgets empower home health care systems. Moreover, those equipments could play crucial role in monitoring and diagnosis of CHDs in rural areas where it is hard to access expert clinicians' consultation.

References

1. Yang, Lucy, et al. "The role of epoxyeicosatrienoic acids in the cardiovascular system." British journal of clinical pharmacology 80.1 (2015): 28-44.
2. WHO. *Cardiovascular Diseases*. Accessed: January 2021. [Online]. Available: https://www.who.int/health-topics
3. Al Ahmad, Mahmoud, and Soha Ahmed. "Heart-rate and pressure-rate determination using piezoelectric sensor from the neck." 2017 4th IEEE international conference on engineering technologies and applied sciences (ICETAS). IEEE, 2017.
4. Coblentz, B., et al. "The relationship between electrical and mechanical events in the cardiac cycle of man. "British heart journal 11.1 (1949): 1.
5. Jain, Puneet Kumar, and Anil Kumar Tiwari. "Heart monitoring systems—A review." Computers in biology and medicine 54 (2014): 1-13.
6. "Auscultation Assistant". http://www.med.ucla.edu/wilkes/intro.html. Accessed 14 January 2021.
7. Silverman, Mark E., and Charles F. Wooley. "Samuel A. Levine and the history of grading systolic murmurs." The American journal of cardiology 102.8 (2008): 1107-1110.
8. Delgado-Trejos, Edilson, et al. "Digital auscultation analysis for heart murmur detection." Annals of biomedical engineering 37.2 (2009): 337-353.
9. El-Segaier, Milad, et al. "Computer-based detection and analysis of heart sound and murmur." Annals of Biomedical Engineering 33.7 (2005): 937-942.
10. Leng, S., San Tan, R., Chai, K. T. C., Wang, C., Ghista, D., & Zhong, L. (2015). The electronic stethoscope. Biomedical engineering online, 14(1), 1-37.
11. Montinari, Maria Rosa, and Sergio Minelli. "The first 200 years of cardiac auscultation and future perspectives." Journal of multidisciplinary healthcare vol. 12 183-189. 6 Mar. 2019, doi:10.2147/JMDH.S193904
12. Ismail, Shahid, Imran Siddiqi, and Usman Akram. "Localization and classification of heart beats in phonocardiography signals—A comprehensive review. "EURASIP Journal on Advances in Signal Processing 2018.1 (2018): 26.
13. Gündüz, Ali Fatih, and Ali KARCİ. "Heart Sound Classification for Murmur Abnormality Detection Using an Ensemble Approach Based on Traditional Classifiers and Feature Sets. "Bilgisayar Bilimleri 5.1: 1-13.
14. Felner JM. The First Heart Sound. In: Walker HK, Hall WD, Hurst JW, editors. Clinical Methods: The History, Physical, and Laboratory Examinations. 3rd edition. Boston: Butterworths; 1990. Chapter 22. Available from: https://www.ncbi.nlm.nih.gov/books/NBK333/
15. Liu C, Springer D, Li Q, Moody B, Juan RA, Chorro FJ, Castells F, Roig JM, Silva I, Johnson AE, Syed Z, Schmidt SE, Papadaniil CD, Hadjileontiadis L, Naseri H, Moukadem A, Dieterlen A, Brandt C, Tang H, Samieinasab M, Samieinasab MR, Sameni R, Mark RG, Clifford GD. An open access database for the evaluation of heart sound algorithms. Physiological Measurement 2016;37(9).
16. Varghees, V. Nivitha, and K. I. Ramachandran. "A novel heart sound activity detection framework for automated heart sound analysis." Biomedical Signal Processing and Control 13 (2014): 174-188.
17. Springer DB, Tarassenko L, Clifford GD. Logistic regression-HSMM-based heart sound segmentation. IEEE Transactions on Biomedical Engineering 2016;63(4):822-832.

18. Schmidt, Samuel E., et al. "Segmentation of heart sound recordings by a duration-dependent hidden Markov model." Physiological measurement 31.4 (2010): 513.
19. Oliveira, Jorge, et al. "Adaptive sojourn time HSMM for heart sound segmentation." IEEE journal of biomedical and health informatics 23.2 (2018): 642-649.
20. Kiranyaz, Serkan, et al. "Real-time phonocardiogram anomaly detection by adaptive 1D convolutional neural networks." Neurocomputing 411 (2020): 291-301.
21. Dokur, Zümray, and Tamer Olmez. "Feature determination for heart sounds based on divergence analysis." Digital Signal Processing 19.3 (2009): 521-531.
22. Tang, Hong, et al. "Segmentation of heart sounds based on dynamic clustering." Biomedical Signal Processing and Control 7.5 (2012): 509-516.
23. Bhatikar, Sanjay R., Curt DeGroff, and Roop L. Mahajan. "A classifier based on the artificial neural network approach for cardiologic auscultation in pediatrics." Artificial intelligence in medicine 33.3 (2005): 251-260.
24. Ahlstrom, Christer, et al. "Feature extraction for systolic heart murmur classification." Annals of biomedical engineering 34.11 (2006): 1666-1677.
25. Zhang, Di, et al. "Noninvasive detection of mechanical prosthetic heart valve disorder." Computers in biology and medicine 42.8 (2012): 785-792.
26. Moukadem, Ali, et al. "A robust heart sounds segmentation module based on S-transform." Biomedical Signal Processing and Control 8.3 (2013): 273-281.
27. Gharehbaghi, Arash, et al. "A novel method for discrimination between innocent and pathological heart murmurs. "Medical engineering & physics 37.7 (2015): 674-682.
28. Karar, Mohamed Esmail, Sahar H. El-Khafif, and Mohamed A. El-Brawany. "Automated diagnosis of heart sounds using rule-based classification tree." Journal of medical systems 41.4 (2017): 60.
29. Othman, Mazin Z., and Asmaa N. Khaleel. "Phonocardiogram signal analysis for murmur diagnosing using Shannon energy envelop and sequenced DWT decomposition." Journal of Engineering Science and Technology 12.9 (2017): 2393-2402.
30. Bozkurt, Baris, Ioannis Germanakis, and Yannis Stylianou. "A study of time-frequency features for CNN-based automatic heart sound classification for pathology detection." Computers in biology and medicine 100 (2018): 132-143.
31. Aziz, Sumair, et al. "Phonocardiogram signal processing for automatic diagnosis of congenital heart disorders through fusion of temporal and cepstral features." Sensors 20.13 (2020): 3790.
32. Yaseen, G. Y. Son, and S. Kwon. "Classification of heart sound signal using multiple features." *Applied Sciences-Basel* vol. 8, no. 12, p. 2344, 2018.
33. Safara, Fatemeh, et al. "Multi-level basis selection of wavelet packet decomposition tree for heart sound classification." Computers in biology and medicine 43.10 (2013): 1407-1414.
34. Kao, Wen-Chung, and Chih-Chao Wei. "Automatic phonocardiograph signal analysis for detecting heart valve disorders. "Expert Systems with Applications 38.6 (2011): 6458-6468.
35. Thompson, W. Reid, et al. "Artificial intelligence-assisted auscultation of heart murmurs: validation by virtual clinical trial." Pediatric cardiology 40.3 (2019): 623-629.
36. Bentley, P.J., Nordehn, G., Coimbra, M., Mannor, S.: The PASCAL classifying heart sounds challenge 2011 (CHSC2011) Results. www.peterjbentley.com/heartchallenge/
37. Balili, Christine C., Ma Caryssa C. Sobrepena, and Prospero C. Naval. "Classification of heart sounds using discrete and continuous wavelet transform and random forests." 2015 3rd IAPR Asian Conference on Pattern Recognition (ACPR). IEEE, 2015.
38. Chakir, Fatima, et al. "Phonocardiogram signals processing approach for PASCAL classifying heart sounds challenge." Signal, Image and Video Processing 12.6 (2018): 1149-1155.
39. Vrbancic, Grega, and Vili Podgorelec. "Automatic detection of heartbeats in heart sound signals using deep convolutional neural networks." Elektronika ir Elektrotechnika 25.3 (2019): 71-76.
40. Dwivedi, Amit Krishna, Syed Anas Imtiaz, and Esther Rodriguez-Villegas. "Algorithms for automatic analysis and classification of heart sounds–a systematic review. "IEEE Access 7 (2018): 8316-8345.
41. Liu, Qingshu, Xiaomei Wu, and Xiaojing Ma. "An automatic segmentation method for heart sounds. "Biomedical engineering online 17.1 (2018): 1-22.
42. Homsi, Masun Nabhan, and Philip Warrick. "Ensemble methods with outliers for phonocardiogram classification. "Physiological measurement 38.8 (2017): 1631.
43. Zabihi, Morteza, et al. "Heart sound anomaly and quality detection using ensemble of neural networks without segmentation." 2016 Computing in Cardiology Conference (CinC). IEEE, 2016.
44. Deng, Shi-Wen, and Ji-Qing Han. "Towards heart sound classification without segmentation via autocorrelation feature and diffusion maps." Future Generation Computer Systems 60 (2016): 13-21.
45. Potes, Cristhian, et al. "Ensemble of feature-based and deep learning-based classifiers for detection of abnormal heart sounds." 2016 computing in cardiology conference (CinC). IEEE, 2016.
46. Noman, Fuad, et al. "Short-segment heart sound classification using an ensemble of deep convolutional neural networks." ICASSP 2019-2019 IEEE International Conference on Acoustics, Speech and Signal Processing (ICASSP). IEEE, 2019.
47. Deng, Muqing, et al. "Heart sound classification based on improved MFCC features and convolutional recurrent neural networks." Neural Networks 130 (2020): 22-32.

48. Abdollahpur, Mostafa, et al. "Detection of pathological heart sounds." Physiological measurement 38.8 (2017): 1616.
49. Ghaffari, Milad, et al. "Phonocardiography signal processing for automatic diagnosis of ventricular septal defect in newborns and children." 2017 9th International Conference on Computational Intelligence and Communication Networks (CICN). IEEE, 2017.
50. Papadaniil, Chrysa D., and Leontios J. Hadjileontiadis. "Efficient heart sound segmentation and extraction using ensemble empirical mode decomposition and kurtosis features." IEEE journal of biomedical and health informatics 18.4 (2013): 1138-1152.
51. Charleston, S., and Mahmood R. Azimi-Sadjadi. "Reduced order Kalman filtering for the enhancement of respiratory sounds." IEEE Transactions on Biomedical Engineering 43.4 (1996): 421-424.
52. Atbi, A., and S. M. Debbal. "Segmentation of pathological signals phonocardiogram by using the Shannon energy envelogram." Aditi Journal of Computational Mathematics 2.1-2 (2013): 1-14.
53. H. Liang et al., "Heart sound segmentation algorithm based on heart sound envelogram," in Proc. Comput. Cardiol., Lund, Sweden, 1997, vol. 24, pp. 105–108.
54. Sharma, Praveen Kumar, Sourav Saha, and Saraswati Kumari. "Study and design of a Shannon-energy-envelope based phonocardiogram peak spacing analysis for estimating arrhythmic heart-beat." International Journal of Scientific and Research Publications 4.9 (2014): 1-5.
55. Naseri, Hosein, and M. R. Homaeinezhad. "Detection and boundary identification of phonocardiogram sounds using an expert frequency-energy based metric." Annals of biomedical engineering 41.2 (2013): 279-292.
56. Mondéjar-Guerra, V., et al. "Heartbeat classification fusing temporal and morphological information of ECGs via ensemble of classifiers." Biomedical Signal Processing and Control 47 (2019): 41-48.
57. Rubin, Jonathan, et al. "Classifying heart sound recordings using deep convolutional neural networks and mel-frequency cepstral coefficients." 2016 Computing in cardiology conference (CinC). IEEE, 2016.
58. Langley, Philip, and Alan Murray. "Heart sound classification from unsegmented phonocardiograms." Physiological Measurement 38.8 (2017): 1658.
59. Gradolewski, Dawid, et al. "A wavelet transform-based neural network denoising algorithm for mobile phonocardiography." Sensors 19.4 (2019): 957.
60. Moukadem, A., et al. "Comparative study of heart sounds localization. "Bioelectronics, Biomedical and Bio-inspired Systems SPIE N8068A-27, Prague (2011).
61. Ghosh, Samit Kumar, et al. "Automated detection of heart valve diseases using chirplet transform and multiclass composite classifier with PCG signals." Computers in biology and medicine 118 (2020): 103632.
62. Yadollahi, Azadeh, and Zahra MK Moussavi. "A robust method for heart sounds localization using lung sounds entropy. "IEEE transactions on biomedical engineering 53.3 (2006): 497-502.
63. Hasfjord, F. "Heart sound analysis with time dependent fractal dimensions. "Department of Biomedical Engineering at Linköpings university (2004).
64. Zhang, Di, et al. "Analysis and classification of heart sounds with mechanical prosthetic heart valves based on Hilbert-Huang transform." International journal of cardiology 151.1 (2011): 126-127.
65. D. Kumar et al., Detection of S1 and S2 heart sounds by high frequency signatures. in Proc. 28th Annu. Int. Conf. IEEE Eng. Med. Biol. Soc., New York, NY, USA, 2006, vol. 1, pp. 1410–1416.
66. S. Ari et al., A robust heart sound segmentation algorithm for commonly occurring heart valve diseases. J. Med. Eng. Technol., vol. 32, no. 6, pp. 456–65, Jan. 2008.
67. Gamero, L. G., and R. Watrous. "Detection of the first and second heart sound using probabilistic models." Proceedings of the 25th annual international conference of the ieee engineering in medicine and biology society (ieee cat. no. 03ch37439). Vol. 3. IEEE, 2003.
68. Ricke, Anthony D., Richard J. Povinelli, and Michael T. Johnson. "Automatic segmentation of heart sound signals using hidden Markov models." Computers in Cardiology, 2005. IEEE, 2005.
69. Gill, Daniel, Noam Gavrieli, and Nathan Intrator. "Detection and identification of heart sounds using homomorphic envelogram and self-organizing probabilistic model." Computers in Cardiology, 2005. IEEE, 2005.
70. Koçyiğit, Yücel. "Heart sound signal classification using fast independent component analysis." Turkish journal of electrical engineering & computer sciences 24.4 (2016): 2949-2960.
71. Goda, Márton Aron, and Péter Hajas. "Morphological determination of pathological PCG signals by time and frequency domain analysis." 2016 Computing in Cardiology Conference (CinC). IEEE, 2016.
72. Krishnan, Sridhar, and Yashodhan Athavale. "Trends in biomedical signal feature extraction." Biomedical Signal Processing and Control 43 (2018): 41-63.
73. Renna, Francesco, Jorge Oliveira, and Miguel T. Coimbra. "Deep convolutional neural networks for heart sound segmentation." IEEE journal of biomedical and health informatics 23.6 (2019): 2435-2445.
74. Tschannen, Michael, et al. "Heart sound classification using deep structured features." 2016 Computing in Cardiology Conference (CinC). IEEE, 2016.
75. Munia, Tamanna TK, et al. "Heart sound classification from wavelet decomposed signal using morphological and statistical features." 2016 Computing in Cardiology Conference (CinC). IEEE, 2016.

76. Homsi, Masun Nabhan, et al. "Automatic heart sound recording classification using a nested set of ensemble algorithms." 2016 Computing in Cardiology Conference (CinC). IEEE, 2016.
77. Khaled, Sara, Mahmoud Fakhry, and Ahmed S. Mubarak. "Classification of PCG Signals Using A Nonlinear Autoregressive Network with Exogenous Inputs (NARX)." 2020 International Conference on Innovative Trends in Communication and Computer Engineering (ITCE). IEEE, 2020.
78. Whitaker, Bradley M., et al. "Combining sparse coding and time-domain features for heart sound classification." Physiological measurement 38.8 (2017): 1701.
79. Debbal, S. M., and Fethi Bereksi-Reguig. "Computerized heart sounds analysis." Computers in biology and medicine 38.2 (2008): 263-280.
80. Hanbay, Kazım, Muhammed Fatih Talu, and Ömer Faruk Özgüven. "Fabric defect detection systems and methods—A systematic literature review. "Optik 127.24 (2016): 11960-11973.
81. Mishra, Madhusudhan, et al. "Detection of third heart sound using variational mode decomposition." IEEE Transactions on Instrumentation and Measurement 67.7 (2018): 1713-1721.
82. Alqudah, Ali Mohammad, Hiam Alquran, and Isam Abu Qasmieh. "Classification of heart sound short records using bispectrum analysis approach images and deep learning." Network Modeling Analysis in Health Informatics and Bioinformatics 9.1 (2020): 1-16.
83. El Badlaoui, O., A. Benba, and A. Hammouch. "Novel PCG analysis method for discriminating between abnormal and normal heart sounds." IRBM 41.4 (2020): 223-228.
84. Das, Sangita, Saurabh Pal, and Madhuchhanda Mitra. "Supervised model for Cochleagram feature based fundamental heart sound identification." Biomedical Signal Processing and Control 52 (2019): 32-40.
85. Fahad, H. M., et al. "Microscopic abnormality classification of cardiac murmurs using ANFIS and HMM." Microscopy research and technique 81.5 (2018): 449-457.
86. Alam, Shahnawaz, Rohan Banerjee, and Soma Bandyopadhyay. "Murmur detection using parallel recurrent & convolutional neural networks." arXiv preprint arXiv:1808.04411 (2018).
87. Kay, Edmund, and Anurag Agarwal. "Dropconnected neural network trained with diverse features for classifying heart sounds." 2016 Computing in Cardiology Conference (CinC). IEEE, 2016.
88. Bobillo, Ignacio J. Diaz. "A tensor approach to heart sound classification." 2016 Computing in Cardiology Conference (CinC). IEEE, 2016.
89. Chen2016: Chen, Tien-En, et al. "S1 and S2 heart sound recognition using deep neural networks." IEEE Transactions on Biomedical Engineering 64.2 (2016): 372-380.
90. Plesinger, Filip, et al. "Discrimination of normal and abnormal heart sounds using probability assessment." 2016 Computing in Cardiology Conference (CinC). IEEE, 2016.
91. Maglogiannis, Ilias, et al. "Support vectors machine-based identification of heart valve diseases using heart sounds." Computer methods and programs in biomedicine 95.1 (2009): 47-61.
92. Wu, Jimmy Ming-Tai, et al. "Applying an ensemble convolutional neural network with Savitzky–Golay filter to construct a phonocardiogram prediction model." Applied Soft Computing 78 (2019): 29-40.
93. Ghaemmaghami, Houman, et al. "Automatic segmentation and classification of cardiac cycles using deep learning and a wireless electronic stethoscope." 2017 IEEE Life Sciences Conference (LSC). IEEE, 2017.
94. Khan, Faiq Ahmad, Anam Abid, and Muhammad Salman Khan. "Automatic heart sound classification from segmented/unsegmented phonocardiogram signals using time and frequency features. "Physiological measurement 41.5 (2020): 055006.
95. Krishnan, Palani Thanaraj, Parvathavarthini Balasubramanian, and Snekhalatha Umapathy. "Automated heart sound classification system from unsegmented phonocardiogram (PCG) using deep neural network." Physical and Engineering Sciences in Medicine (2020): 1-11

ISSN print: 1224-5984
ISSN online: 2248-3942

Rom Biotechnol Lett. 2022; 27(1): 3184-3190
doi: 10.25083/rbl/27.1/3184-3190

Received for publication, October, 11, 2021
Accepted, January, 15, 2022

Original paper

Fennel and turmeric powders' effectiveness as natural preservatives in beef burgers

SALEH S.M. [1], KASSAB H. A.[1], MARIAM A. RAMADAN [2], EL-BANA M. A.[2]

[1] Food Technology Department, Faculty of Agriculture, Kaferelsheikh University, Egypt.
[2] Food Tech. Res. Institute, Agricultural Research Center, Giza, Egypt.

Abstract This investigation was performed to study the possibility of the utilization of fennel seed powder (FSP) and turmeric seed powder (TSP) at levels of (1.5, 3.0, and 4.5%) as natural preservatives during the preparation of burgers stored at a refrigeration temperature (4 ± 1oC). The obtained results revealed that, FP and TP significantly reduced the total count of bacteria, pH, and thiobarbituric acid (TBA). Furthermore, the results showed that by increasing the concentration of tested powders, the bacterial counts, pH, and TBA values were dropped, with the concentration of 4.5% providing the highest effectiveness. Comparatively, the antioxidant and antibacterial activities of Turmeric ether extract (TEE) were higher than of Fennel ether extract (FEE). In conclusion, fennel and turmeric can play an important role as antioxidants and antibacterial agents in refrigerated burgers.

Keywords fennel, turmeric, refrigerated storage, burger

To cite this article: SALEH SM, KASSAB HA, MARIAM AR, EL-BANA MA. Fennel and turmeric powders' effectiveness as natural preservatives in beef burgers. *Rom Biotechnol Lett*. 2022; 27(1): 3184-3190. DOI: 10.25083/rbl/27.1/3184-3190.

*Corresponding author: EL-BANA MA, Food Tech. Res. Institute, Agricultural Research Center, Giza, Egypt.
E-mail: dr.elbana@yahoo.com

Introduction

The progress experienced in meat industrialization and the rise in the social and economic status of the population in the last years concurred to an increase in the exhaustion of meat products well as in its quality requirement **(Ramos and Gomide, 2007).** Synthetic additives are intentionally added to food during production or processing to improve organoleptic quality and/or to prevent deterioration **(**Sedlacek-bassani ***et al.*, 2020).** Despite the fact that food additives provide technological benefits to food, there is still concern about the dangers associated with their use, such as allergic reactions, carcinogenicity, and behavior problems including hyperactivity (Honorato et al., 2013). Today's consumers look for healthier and more practical meat products, preferably with no synthetic chemical additives but still with pleasant and attractive color and taste, and it rests with the food technologists' challenge to develop new products to meet that demand **(Sales et al., 2015).** The burger has attracted great consumer interest as it is composed from fresh and tasty ingredients and maintains the nutritional value and convenience in the preparation **(Baugreet et al., 2017).** However, burgers are subject to deterioration, mostly due to the action of microorganisms and to lipid oxidation, which may happen through processing and/or storage. The use of natural sources bioactive components seems to be preferred to prevent these undesirable effects like deterioration in foods **(Garcia et al., 2012).** Fennel seeds (*Foeniculum vulgare*) have been known as aromatic and therapeutic herbs, widely used in the flavoring of fish, bread, cheese, and salads **(Kaur and Arora, 2010).** These herbs are good source of bioactive components like phenolic acids, flavonoids, coumarin, tannin, and hydroxycinnamic acids **(Rahimi and Ardekani, 2013).** Turmeric is a spice that comes from the root of Curcuma longa, and followed ginger family, Zingiberaceae **(Gupta *et al*., 2015).** It is bright yellow and has been used as a coloring and flavoring agent in foods. The curcuminoids are the principal phenolic compounds that involved in all bioprotective characteristics of Tumeric **(Braga *et al.*, 2018).** Fennel and turmeric extracts are exploited to inhibit *Staphylococcus aureus* through methicillin-resistant **(Mashareq *et al*., 2016).** Thus, the aim of this study was to investigate the antimicrobial properties of FP and TP as active additives to raise the shelf life of burgers. Also, their effect on microbiological and chemical attributes of the product under refrigeration (4±1˚C) storage was evaluated.

Materials and Methods

Materials

A. Fennel (*Foeniculum vulgare*) seeds and turmeric rhizomes were obtained from the Agricultural Seed, Spices, and Medicinal Plants Co. (Harras), Cairo, Egypt. Season 2020 and stored in a deep freeze at-20°C until further use.

B. Microbial strains: Four standard microbial strains were used in the experiments; *Escherichia coli (ATCC 25922), Salmonella Typhimurium (ATCC 14028), Staphylococcus aureus (ATCC 25923) and Pseudomonas aeruginosa (ATCC 27853).* were kindly provided by the Plant Pathology Department, Faculty of Agriculture, Kafr El-sheikh University.

C**.** Merck Co. Ltd. (Darmstadt, Germany) provided the C-Trypticase soy agar (TSA), Trypticase soy Broth (TSB), nutrient agar medium (NAM), and potato dextrose agar (PDA) used in the microbiological examination.

D. The meat of beef and other components to prepare it were procured from local market.

E. Chemicals: All chemicals and reagents were procured from El-Gomhoria Company Tanta, Egypt.

Methods

The gross chemical composition of samples

Fennel seed powder (FSP) and turmeric seed powder (TSP) were analyzed for moisture, crude protein, ether extract, ash, and crude fiber content according to **A.O.A.C. (2005).** Total carbohydrates were calculated by difference.

Preparation of ethanolic extracts

The prepared ground materials (10 g) of each sample were soaked in 100 ml of ethanol (80%) overnight in a shaker at room temperature according to protocol of Mohdaly et al. (2010). The extracts were filtrated through Whatman No.1 filter paper. The process of re-extraction was typically repeated three times for residues. The combined filtrates were evaporated under vacuum in a rotary evaporator below 40ºC. The extracts obtained after evaporation of organic solvents called fennel ethanolic extract (FEE) and turmeric ethanol extract (TEE) were stored -18±2oC until further analysis.

Determination of total phenolic compounds

Total phenolic compounds of the FEE and TEE were calculated according to the method given by **(*Salem et al*., *2018*)** using Folin-ciocalteau reagent and used to estimate the phenolics-acid content using a standard curve prepared using gallic acid.

Determination of total flavonoids

Total flavonoids of FEE and TEE were determined by the method of **Ordonez *et al.* (2006)** by using standard curve prepared by catechol acid.

FEE and TEE DPPH radical scavenging assay

The 1,1-Diphenyl-2-picrylhydrazyl (DPPH) free radical scavenging activity of sample extracts was determined by spectrophotometer according to a modified method described by **Lee *et al.* (2003)** at 517 nm (HITACI, U-1900). The total antioxidant activity (TAA) is expressed as a % reduction of DPPH.

The potential antibacterial capabilities

The potential antibacterial capabilities of FEE and TEE against examined bacteria were screened qualitatively using agar/disc diffusion as described by **Shihabudeen *et al.* (2010).** The appropriate media were poured into sterile

plates (12 cm diameter), left to solidify, at room temperature. The organisms were inoculated on the surface of the prepared media. A sterile disc, 6 mm in diameter, of Whatman No. 1 filter paper, was dipped in the appropriate solutions, blotted, and then stabilized on the surface of the inoculated petri plates. The inhibitory effect of the ethanol was 80% and ampicillin (25 µg/ml) positive control. The plates of bacteria were preserved for incubation at 37° C for 48 hrs. At the end of the incubation period, the generated inhibition zones were measured with a ruler. All tests were completed in triplicate with four discs per plate. The bacteria were cultured on nutrient agar.

Preparation of beef burgers and their formulae

The method of **Sorour *et al.* (2021)** was used to prepare the beef burger samples. Blends containing 1.5, 3.0, and 4.5 grams of FSP and TSP were used as additions to beef burgers. The formulas for beef burgers were prepared using 65g of the beef meat, 15g of fat, 10.50g of ice water, 1.5 g of spice mixture, 3g of dried onion, 3g of dried garlic, and 2g of NaCL. After that, the petri dishes were exploited to form rounded discs of burger with 9 cm diameter and 1 cm thickness. The burger discs were transferred inside polyethylene films prior to freeze at -18 °C.

Cooking of Beef Burger

The prepared beef burger samples were cooked using an electrical grill (Arcelik Mini Firin, Turkey) at 300 °C (the distance between heat source and the sample was 4 cm) for a total of 10 min, 6 min one side and 4 min in the other side **(Turhan *et al*., 2005).**

Antimicrobial activity

Antimicrobial activity in burgers was supplemented with FSP and TSP at levels of 1.5%, 3.0%, and 4.5%. Reference with TBHQ and a control product were prepared. The tested products and control were packed in a polyethylene bag and stored at (4 ±1°C) for 12 days after preparation. The samples were analyzed chemically and examined microbiologically every three days during the storage period **(Najeeb et al., 2014).**

pH values

A digital pH meter (HAANA, HI902 meter, Germany) was exploited to determine pH values by recording two readings from each of beef samples (**Yassin, 2003**).

Thiobarbituric acid (TBA)

(TBA) was performed according to the method recommended by **Vyncke(1970).**

Statistical analysis

Data was analyzed according to **Steel and Torrie (1980)** procedures (Duncan's multiple range test DMRT).

Results and discussion

Chemical composition of FSP and TSP

The approximate chemical composition of FSP and TSP is given in Table (1). The obtained results found that FSP had higher contents of crude protein and ash (23.22, and 10.10%, respectively) than TSP (11.47, and 8.99%, respectively). Meanwhile, TSP had a higher concentration of ether extract, crude fiber, and total carbohydrates (8.45, 11.77, and 71.09%) than FSP (6.24, 6.75, and 60.44%). The obtained results partially agree with those of **Hegazi et al. (2009) and Al-Nazawi and El-Bahr (2012).** The results showed that TSP had a higher total phenolic content, total flavonoid content, and DPPH (820.90 mg gallic acid/100 g extracts, 411.20 mg catechin/100 g extracts, and 89.13 %, respectively) than FSP (760.35 mg gallic acid/100 g extracts, 330.75 mg catechin/100 g extracts, and 84.65 %, respectively). These results are in the same trend of those found by **Liu et al. (2008), Ghasemzadeh et al. (2012), and Salama et al. (2015).**

Table 1. Chemical composition (%) and bioactive compounds of fennel seeds and turmeric rhizome powder (on a dry weight basis).

Compounds	fennel seeds	Turmeric rhizomes powder
Moisture %	11.23±0.19	11.50±0.13
Ether extract %	6.24±0.31	8.45±0.25
Crude protein %	23.22±0.25	11.47±0.17
Ash %	10.10±0.16	8.99±0.14
Crude fiber %	6.75±0.37	11.77±0.35
*Total carbohydrate %	60.44±0.42	71.09±0.52
Total phenolic contents (mg gallic acid /100 g extracts)	760.35 ± 1.4	820.90 ± 1.70
Total flavonoid contents(mg catechin /100 g extracts)	330.75 ± 2.35	411.20 ± 1.66
DPPH(%)	84.65 ± 0.93	89.13 ± 0.87

Each value is an average of three determinations ± SD.
Total carbohydrate*

Antimicrobial activity of TEE and FEE

To inhibit food-borne pathogens and to extend shelf life, synthetic chemicals with antimicrobial properties are often used as preservatives in food processing and storage. Concerns over the potential risks of synthetic food additives to human health and consumer awareness have directed interest in using naturally occurring alternatives. The market of health and herbal nutraceuticals is addressing its attention to rich plant sources offering functional efficacy. Al-Saiqali et al. (2016).

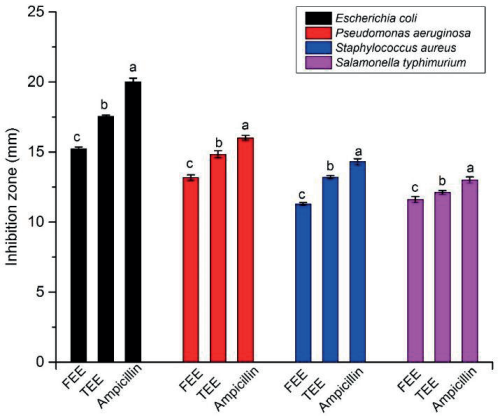

Figure 1: Anti-bacterial activity of fennel seeds and turmeric rhizomes plant extracts against foodborne pathogens, measured as the diameter of inhibition zones (ZOI, mm).

The antimicrobial potential of the TEE and FEE compared with Ampicillin as a reference material or positive control for the antibacterial activity is shown in Fig 1. The results indicated that, TEE and FEE have antibacterial activity against Gram-negative and Gram-positive bacteria. The most effective extract against Gram-negative bacteria was the TEE, which was less effective than ampicillin, while the most effective extract against Gram-positive bacteria was the FEE, which gave a larger inhibition zone than ampicillin. The ethanolic extract gave the highest wide inhibition zones (17.55mm) with *Escherichia coli*, (14.83mm) with *Pseudomonas aeruginosa*, (13.20mm) with *Staphylococcus aureus*, and (12.11mm) with *Salmonella Typhimurium*. These data coincide with those of Gul et al. (2015); Maharjan et al. (2019) and Tayel et al (2021) . They reported that fennel and turmeric displayed significant antibacterial activity, as determined by the agar diffusion method. Overall, the effectiveness of FEE and TEE is higher in Gram-positive than in Gram-negative bacteria. Furthermore, Grace et al. (2017) mentioned that the outer membrane of Gram-negative bacteria could work as selective permeability barrier that restrict larger molecules to penetrate cells and admit of small hydrophilic molecules like phenolic components to pass causing its antibacterial effect.

Besides these, they also possess multidrug-resistant pumps which exclude some of the antibacterial compounds. Furthermore, Floridi et al. (2003) showed that the presence of phenolics in food is particularly important for their oxidative stability and antimicrobial protection. From clinical point of view, there is numerous evidence of sweet fennel to alleviate diseases.

Chemical and microbiological quality assessment of burgers supplemented with FSP and TSP during 12 days of storage at 4 ± 1°C

pH changes

The results in Table (2) showed that there was a significant (at $P \leq 0.05$) increase in pH mean values for different treatments during storage by using different rates of the FSP and TSP, and the highest incremental rates (pH values) were found in the untreated (control). The samples treated with 4.5% FSP and 2.5% TSP had the most significant (at $P \leq 0.05$) effect on pH, with lower values than those of the control samples, followed by samples treated with 3.0% lowering the pH values of treated burgers can enhance microbial inhibition. Finally, the samples were treated with 1.5% FSP and TSP, respectively, till reaching the end of the storage period. There was a significant (at $P \leq 0.05$) increase in pH mean values of all untreated and treated samples with fennel or turmeric at all concentrations for the 12 days of the storage period. Similar findings were found in burgers containing ginger powder during frozen storage, as reported by **(Awad, 2018).** Furthermore**,** the increase in pH could be attributed to the activation effect of microbial load, which may cause protein hydrolysis with the appearance of alkyl groups (**Yassin, 2003**).

Table 2. pH values of burger supplemented by fennel and turmeric powder during storage at 4 ± 1°C for 12 days

Storage period (days)		PH values			
Treatment		0	4	8	12
Control		5.28 ± 0.17^{Da}	6.11 ± 0.10^{Ca}	6.69 ± 0.25^{Ba}	7.09 ± 0.12^{Aa}
TBHQ		5.27 ± 0.21^{Ba}	5.34 ± 0.13^{ABa}	5.77 ± 0.18^{Abc}	5.93 ± 0.11^{Ab}
Fennel	1.5	5.28 ± 0.23^{Ba}	6.05 ± 0.17^{ABa}	6.10 ± 0.19^{Ab}	6.29 ± 0.10^{Ab}
	3.0	5.27 ± 0.16^{Ba}	5.87 ± 0.19^{ABa}	5.93 ± 0.22^{ABa}	6.17 ± 0.17^{Ab}
	4.5	5.26 ± 0.11^{Ba}	5.59 ± 0.24^{ABa}	5.83 ± 0.23^{ABb}	6.03 ± 0.31^{Ab}
Tumeric	1.5	5.29 ± 0.19^{Ba}	6.01 ± 0.31^{ABa}	6.09 ± 0.29^{Ab}	6.26 ± 0.34^{Ab}
	3.0	5.27±0.18Ba	5.83 ± 0.10^{ABa}	5.89 ± 0.20^{ABb}	6.15 ± 0.10^{Ab}
	4.5	5.26±0.23Ba	5.56 ± 0.30^{ABa}	5.81 ± 0.22^{ABbc}	6.00 ± 0.19^{Ab}

Data are means ± SD for 3 replicates. Means with different superscript capital letters(within group at different storage period "row") and small letters (between groups at the same storage period "column") are significantly different at $p<0.05$.

TBA changes

According to the data in Table (3). There were significant differences ($P<0.05$) between the beef burger control and all the low-fat beef burger formulas prepared with different levels of FSP and TSP during storage at 4 ± 1°C for 12 days for TBA values. The amount of thiobarbituric acid in the

prepared beef burger decreased as the level of FSP and TSP increased. TBA values ranged between 0.15 and 0.81. These results may be due to the fact that FSP and TSP have antioxidants that inhibit lipid oxidation throughout storage time. These results are in agreement with those mentioned by **Awad (2018) and Bassano *et al.*(2019).**

Table 3. Thiobarbituric Acid (T.B.A) levels in burgers supplemented with FSP and TSP during 12 days of storage at 4 ± 1°C.

Storage period (days) Treatment		TBA values (mg of malonaldehyde /kg) 0	4	8	12
Control		0.17±0.019^{Da}	0.36±0.033^{Ca}	0.54±0.041^{Ba}	0.81±0.017^{Aa}
TBHQ		0.15±0.034^{Ba}	0.17±0.028^{Bb}	0.21±0.013^{ABb}	0.30±0.023^{Ab}
FSP	1.5	0.16±0.017^{Ca}	0.22±0.017^{BCb}	0.27±0.011^{Bb}	0.36±0.034^{Ab}
	3.0	0.16±0.035^{Ca}	0.21±0.020^{BCb}	0.25±0.024^{Bb}	0.34±0.018^{Ab}
	4.5	0.15±0.027^{Ca}	0.19±0.014^{BCb}	0.23±0.029^{Bb}	0.33±0.054^{Ab}
TSP	1.5	0.16±0.045^{Ca}	0.21±0.018^{BCb}	0.24±0.0337^{Bb}	0.36±0.036^{Ab}
	3.0	0.15±0.064^{Ca}	0.20±0.026^{BCb}	0.23±0.042^{Bb}	0.33±0.047^{Ab}
	4.5	0.15±0.011^{Ca}	0.18±0.026^{BCb}	0.22±0.010^{Bb}	0.31±0.043^{Ab}

Data are means ± SD for 3 replicates. Means with different superscript capital letters(within group at different storage period "row") and small letters (between groups at the same storage period "column") are significantly different at p<0.05.

Total bacterial counts values

According to the data in Table (4). There were significant differences (P<0.05) between beef burger control and all low-fat beef burger formulas prepared with different levels of FSP and TSP during storage at 4 ± 1°C for 12 days for Total count values. The results show that the control samples showed the highest total bacterial counts compared to the other samples. Furthermore. The total bacterial counts of prepared beef burgers supplemented with FSP and TSP in different ratios of 1.5, 3.0, and 4.5 % were 7.10 to 8.31 cfu/g. It is worthy to mention that total bacterial counts were decreased as the level of FSP and TSP increased. These results are in agreement with those found by **Wakoli et al., (2014) and Mancini et al. (2017)** discovered a delay in the TBC of pork burgers with powdered ginger at 1% and 2% during 7 days of storage at 4 °C. During the storage period, the total bacterial count was gradually reduced as the storage time proceeded, until it reached between 7.23 and 9.88 cfu/g. This conclusion was in agreement with Igbinosa et al. (2009). This result is due to the effect of cold storage on microbial load.

Table 4. Total bacterial counts (log CFU */g) of burger supplemented with FSP and TSP during 12 days of storage at 4 ± 1°C.

Storage period (days) Treatment		Total bacterial counts (log CFU */g) 0	4	8	12
Control		7.23±0.22^{Da}	8.17±0.28^{Ca}	9.21±0.15^{Ba}	9.88±0.017^{Aa}
TBHQ		7.09±0.25^{BCa}	7.23±0.15^{Bb}	7.28±0.27^{Bb}	7.91±0.20^{Aa}
FSP	1.5	7.19±0.16^{BCa}	7.44±0.12^{Bb}	7.56±0.18^{Bb}	8.31±0.13^{Aa}
	3.0	7.17±0.18^{BCa}	7.35±0.34^{Bb}	7.42±0.18^{Bb}	8.25±0.19^{Aa}
	4.5	7.12±0.15^{BCa}	7.30±0.19^{Bb}	7.38±0.34^{Bb}	8.17±0.23^{Aa}
TSP	1.5	7.16±0.30^{BCa}	7.39±0.17^{Bb}	7.50±0.11^{Bb}	8.29±0.22^{Aa}
	3.0	7.15±0.37^{BCa}	7.33±0.26^{Bb}	7.39±0.14^{Bb}	8.19±0.28^{Aa}
	4.5	7.10±0.11^{BCa}	7.22±0.23^{Bb}	7.30±0.17^{Bb}	8.11±0.20^{Aa}

Data are means ± SD for 3 replicates. Means with different superscript capital letters(within group at different storage period "row") and small letters (between groups at the same storage period "column") are significantly different at *p<0.05*.

Conclusion

Based on the mentioned results, it could be concluded that fennel and turmeric powders can play an important role as antioxidants and antibacterial agents and can be used to extend the shelf life of beef burgers, especially when kept under refrigeration.

References

1. A.O.A.C. (2005). Association of Official of Analytical Chemists, Official Methods of Analysis. 18th Ed., Pub. By the A.O.A.C., Arlington, Virginia, 2220 USA.
2. Al-Nazawi, M.H. and El-Bahr, S.M. (2012). Hypolipidemic and Hypocholesterolemia effect of medicinal plant combination in the diet of rats: black cumin seed (Nigella sativa) and Turmeric (Curcumin). J. of Animal and Veterinary Advance, 11(12):2013-2019.
3. Alsaiqali, M., El-Shibiny, A.A. ; Adel, M. , Abdel-Samie, M.A.S. and Ghoneim, S. (2016). Use of Some Essential Oils as Antimicrobial Agents to Control Pathogenic Bacteria in Beef Burger. World Journal of Dairy and Food Sciences 11 (1): 109-120.
4. Awad, S. M.S. (2018) Utilization of Ginger powder (Zingiber Officinale Roscoe) in functional food

production. Australian J. of Basic and Applied Sci., 12(12): 121-130.

5. Bassano, J. S., GRASSO, T. L.M.; Juliana, C. P. D.and Elisa, H. G. P. (2019). Spices as natural additives for beef burger production. Food Sci. and Tech.,1:1-5.
6. Baugreet, S., Kerry, J. P., Allen, P. and Hamill, R. M. (2017). Dptimisation of protein-fortified beef patties targeted to the needs of older adultsI: a mixture design approach. Meat Sci., 134, 111-118.
7. Braga, M.C., Vieira, E.C.S. and de Oliveira, T.F. (2018). Curcuma longa L. leaves: characterization (bioactive and antinutritional compounds) for use in human food in Brazil. Food Chem., 265:308–315.
8. Floridi, S., Montanari, L., Marconi, O. and Fantozzi, P. (2003). Determination of free phenolic acids in wort and beer by coulometric array detection. Journal of agricultural and food chemistry, 51(6), 1548-1554.
9. Garcia, C. E. R., Bolognesi, V. J., Dias, J. F. G., Miguel, O. G., and Costa, C. K. (2012). Carotenóides bixina e norbixina extraídos do urucum (Bixa orellana L.) como antioxidantes em produtos carneos. Ciência Rural, 42 (8), 1510-1517.
10. Ghasemzadeh, A., Azarifar, M., Soroodi, O. and Jaafar, H.Z.E. (2012). Flavonoid compounds and their antioxidant activity in extract of some tropical plants. J. Med.Plants Res., 6(13):2639-2643.
11. Grace, U.S., Sankari, M. and Gopi, B. (2017). Antimicrobial activity of ethanolic extract of Zingiber Offi cinal- An invitro study. J. Pharm. Sci. and Re., 9: 1417-1419.
12. Gul S., Whalen J. K., Thomas B.W., Sachdeva V., Deng H.Y. (2015). Physico-chemical properties and microbial responses in biochar-amended soils: Mechanisms and future directions. Agriculture, Ecosystems and Environment, 206: 46–59.
13. Gupta, A. , Mahajan, S. and Sharma, R. (2015) . Evaluation of antimicrobial activity of Curcuma longa rhizome extract against Staphylococcus aureus. Biotechnology Reports, vol. 6, pp. 51– 55.
14. Hegazi, M. A., Osman, M. F. and El-Bana, M.A. (2009). Production and evaluation of fennel (Foeniculum vulgare,mill.) grown with natural fertilizers. J. Agric., Res. , Kaferelsheikh Univ., 35 (2):660-684.
15. Honorato, T.C., Batista, E., Nascimento, K.O., Pires, T. (2013). Food additives: applications and toxicology. Rev. Verde Agroec. Desenv. Sustáv. 8(5):01-11.
16. Igbinosa, O.O., Igbinosa, E.O. and Aiyegoro, O.A. (2009). Antimicrobial activity and phytochemical screening of stem bark extracts from Jatropha curcas (Linn). Afr. J. Pharm. Pharmacol. 3:58-62.
17. Kaur, G.U. and Arora, D.S. (2010). Bioactive potential of Anethum graveolens, Foeniculum vulgare and Trachys-permum ammi belonging to the family Umbelliferae-Current status. J. of Medic. Plant. Res., 4 (2): 087-094.
18. Lee, S.C., Kim, J.H., Nam, K.C.and Ahn, D.U. (2003). Antioxidant properties of far infrared-treated rice hull extract in irradiated raw and cooked turkey breast. J. Food Sci. 68: 1904-1909.
19. Liu, H., Qiu, N., Ding, H. and Yao, R., (2008). Polyphenols content andantioxidant capacity of 68 Chinese herbals suitable for medical or food uses. Food Research International 41, 363–370.
20. Maharjan, R., Thapa, S. and Acharya, A. (2019). Evaluation of antimicrobial activity and synergistic effect of spices against few selected pathogens. TUJM 6, (1) :10-18.
21. Mancini, S., Paci, G., Fratini, F., Torracca, B., Nuvoloni, R., Dal Bosco, A., Roscini, V. and Preziuso, G. (2017). Improving pork burgers quality using Zingiber officinale Roscoe powder (ginger). Meat Science, 129, 161-168.
22. Mashareq, M. K., Amira, M. E., Zenab, A.A., Ali, I. A., and Fathy I. R.(2016). Evaluating Antimicrobial and antioxidant activities of volatile oils extracted from anise, fennel and spearmint plants. J. Agric. Res. Kafr El-Sheikh Univ., 42(2): 196-209.
23. Mohdaly, A., Sarhan, M.A. , Smetanska, I. and Mahmoud, A. (2010). Antioxidant properties of various solvent extracts of potato peels, sugar beet pulp, and sesame cake. J. of the Sci. of Food and Agric., 90: 218-226.
24. Najeeb, A. P., Mandal, P. K. and Pal, U. K. (2014). Efficacy of fruits (red grapes, gooseberry and tomato) powder as natural preservatives in restructured chicken slices. International Food Res. J. 21(6): 2431-2436.
25. Ordonez, J. D., Gomez, M. A. and Vattuone, M. I. (2006). Antioxidant activities of Sechium edule (Jacq.) Swartz extracts. Food Chem ., 97: 452–458.
26. Rahimi, R. and Ardekani, M.R.S. (2013) Medicinal properties of Foeniculum vulgare Mill. in traditional Iranian medicine and modern phytotherapy. Chinese Journal of Integrative Medicine 19 (1):73-9.
27. Ramos, E. M. and Gomide, L. A. M. (2007). Avaliação da qualidade de carnes: fundamentos e metodologias. Viçosa: UFV.
28. Salama, Z. A., El Baz, F. K., Gaafar , A.A. and Zaki, M. F. (2015). Antioxidant activities of phenolics, flavonoids and vitamin C in two cultivars of fennel (Foeniculum vulgare Mill.) in responses to organic and bio-organic fertilizers. J. of the Saudi Society of Agricultural Sci.,14, 91–99.
29. Salem, M. A., Sorour A. M. and El-Bana, M.A. (2018). potential antioxidative . activity of rice milling by-products. Menoufia J. Food and Dairy Sci., 3: 1 - 13.
30. Sales, P. V. G., Sales, V. H. G. and liveira, E. M. (2015). Avaliação sensorial de duas formulações de hambúrguer de peixe. Revista Brasileira de Produtos Agroindustriais, 17(1), 17-23.
31. Sedlacek-bassani, J., Grassi,T. , Diniz, J. and Ponsano, E. (2020). Spices as natural additives for beef burger production. Food Sci. Tech. Campinas, 40 (4): 817-821.
32. Shihabudeen, M. S., Priscilla, H. H. and Thirumurugan, D. K. (2010). Antimicrobial activity and phytochemical analysis of selected Indian folk

medicinal plants. International J. of Pharma Sci. and Res., 1(10):430-434.
33. Sorour, A. M. , Salem , M. A. , Arafa, S.G. and El-Bana, M.A. (2021). Chemical, physical and Sensory evaluation of low fat beef burger with Carboxymethyl cellulose produced from rice and wheat bran. International J. of Environment, 9(1);33-46.
34. Steell, R.G. and Torrie, J.H. (1980). Principles and procedures ofstatistics.2nd Ed. pp 120. McGraw-Hill, New York, USA.
35. Tayel, A.A.; Bahnasy, A.G.; Mazrou, K.E.; Alasmari, A, El Rabey, H.A.; Elboghashy, S.A. and Diab, A.M. (2021). Biopreservation and quality enhancement of fish surimi using colorant plant extracts**.** J. of Food Quality.1:1-8
36. Turhan, S.; Sagir, I. and Ustun, N.S. (2005). Utilization of hazelnut pellicle in low-fat beef burgers. Meat Scie., 71, 312–316.
37. Vyncke, W. (1970). Direct determination of the thiobarbituric acid value in trichloroacetic acid extracts of fish as a measure of oxidative rancidity. Fette Seifen Anstrichmittel, 2: 1084- 1094.
38. Wakoli, A. B., Onyango, D. A. and Rotich, P.J. (2014).Effect of selected spice on food spoilage rate. Global journal of boil, 3(4): 160-162.
39. Yassin, M. N. (2003). Effect of Storage Conditions on the Quality Parameters of Differently Treated Fish. Ph. D. Thesis, Fac. Agric. Ain Shams Univ. Cairo.Egypt.

ISSN print: 1224-5984
ISSN online: 2248-3942

Rom Biotechnol Lett. 2022; 27(1): 3191-3199
doi: 10.25083/rbl/27.1/3191-3199

Received for publication, January, 06, 2021
Accepted, February, 19, 2022

Original paper

Quality characteristics of biscuits supplemented with mango kernel and sugar beet molasses ingredients

BARAKAT AHMED BARAKAT[1], ESSAM MOHAMED ELSEBAIE[2], ELSAYED ABDELRASOUL[1], SAHAR RAMADAN ABDELHADY[2]

[1] Food Technology Research Institute, Agricultural Research Center, Giza, 12611, Egypt
[2] Food Technology Department, Faculty of Agriculture, Kafrelsheikh University, Kafrelsheikh, 33511, Egypt

Abstract Mango kernel is largely treated as a waste material, but its flour can be used in many foods as a potential replace of wheat flour (WF). Sugar beet molasses (SBM) is a raw material with high possibility to be a functional ingredient in baked commodities. The aims of this research were to process mango kernel flour (MAKF) and sugar beet molasses (SBM) to comparison its chemical composition and minerals content and really to evaluate the quality of MAKF and SBM substituted composite biscuits by investigating chemical composition, minerals content, physical and textural characteristics and sensory evaluation of produced biscuits. The composition of MAKF and SBM showed higher concentration of ash (6.97 and 10.62%, respectively) compared to WF. MAKF showed higher amounts of fat and fiber than WF (3.22 and 2.34%, respectively). Moisture and ash contents of the developed biscuits increased with increasing of MAKF and SBM contents. MAKF increased all minerals content in the all prepared biscuits, while SBM caused an increase only in Na and Fe. Sensory evaluation indicated that 5% SBM and 10% MAKF containing biscuit were the most acceptable to the panelists among composite biscuits.

Keywords Mango kernel flour, Sugar beet molasses, Composite biscuit, Textural characteristics, Physical properties

To cite this article: BARAKAT BA, ELSEBAIE EM, ABDELRASOUL E, ABDELHADY SR. Quality characteristics of biscuits supplemented with mango kernel atablend sugar beet molasses ingredients. *Rom Biotechnol Lett*. 2022; 27(1): 3191-3199. DOI: 10.25083/rbl/27.1/3191-3199.

✉ *Corresponding author: ESSAM MOHAMED ELSEBAIE, Food Technology Department, Faculty of Agriculture, Kafrelsheikh University, Kafrelsheikh, 33511, Egypt.
E-mail: essam.ahmed@agr.kfs.edu.eg

Introduction

Mango (*Mangifera indica* L.) is known as the type of fruits because of its delicious taste, attractive appearance and superior nutrients additionally huge production. Despite being a major part of mango, it is a matter to be regretful that the mango seeds are mostly thrown away as a waste material after consuming or processing of pulp while few amounts goes for plantation.

Several million tons of mango seeds and peels are omitted annually from food processing industries because thousand tons of mango fruits are manufactured in products such as puree, nectar, pickles and canned slices etc. which have worldwide popularity (Loelillet, 1994). By breaking the hard coat of mango seed, kernel is obtained. Mango seed kernel is nearly 20 per cent of total fruit weight.

This kernel is a great source of nutrients and natural bioactive compounds as well as has potentiality to use as anticancer, antibacterial and antioxidant compounds (Jahurul et al., 2015; Khammuang, & Sarnthima, 2011). Therefore, addition of MAKF in food products is regarded a good substitute for nutritional enhancement. Das, Sattar, Jony, & Islam (2018) found around 66.10-72.40% pulp, 8.40-12.4% kernel, 9.80-14.30% peel, and 7.50-9.30% seed coat. Also, Nzikou et al. (2010) illustrates that mango kernel contained about 42.50% moisture, 6.36% crude protein, 13.00% oils, 2.02% crude fiber, 3.20% ash and 32.24% total carbohydrate in dry weight basis whereas 50.98% moisture, 5.25% protein, 6.98% fat, 1.65% fiber and 2.47% ash in wet weight basis was reported by Elegbede, Achoba, & Richard (1995).

Beside the nutritional and bioactive attributes, mango kernel also possesses significant functional properties (Menon, Majumder, & Ravi, 2014). Demand of processed foods is increasing significantly throughout the world. Bakery products are also getting notable preference in the global food sector (Kotsianis, Giannou, & Tzia, 2002).

Biscuits are the most popularly consumed bakery items in the world. Some of the reasons for such wide popularity are their ready to eat nature, affordable cost, good nutritional quality, availability in different tastes and longer shelf-life (Bandyopadhyay, Chakraborty, & Bhattacharyya, 2014). Noticeable studies were executed by several researchers about utilization of MAKF in different bakery products. Bandyopadhyay et al. (2014) worked with MAKF and mango peel powder (MPP) to substitute wheat flour in cookies. They estimated that cookies can be produced by incorporating MAKF in WF up to 20% to get suitable color, flavor, texture and overall acceptability. Menon et al. (2014) revealed that bread can be formulated with enriched nutrient content by using mango seed kernel. Ajila, Aalami, & Leelavathi (2010) utilized mango peel powder as potential source of antioxidant in macaroni preparation. Molasses is the final syrup spun off after repeated crystallization in the extraction of sucrose (Douglas, & Glenn, 1982). SBM is abundant in antioxidants and has a clear industrial potential for preparation of extracts rich in antioxidants (Chen, Zhao, & Yu, 2015) and functional foods enriched with antioxidants (Chou, 2003). Molasses has a bitterly sweet taste. Extensive research has shown that it is possible to include beet molasses into formulations of various bakery, confectionery and meat products without negatively impacting their palatability and acceptance.

SBM can be used as a supplement in wheat-based bread and cookies: at 5-10% level flour basis in bread (Filipčev, Lević, Bodroža-Solarov, Mišljenović, & Koprivica, 2010) at 25% levels (flour basis) in semi-sweet cookies (Šimurina, Filipčev, Lević, Pribiš & Pajin, 2006) and as a replacer of half of the amount of honey in ginger nut biscuit formulations (Filipčev, Bodroža-Solarov, Šimurina, & Cvetković, 2012).

Against these backdrops, the main objective of this study is to characterize and analyze MAKF and SBM and to use them in biscuits preparation when substituted with WF in different proportions which may help for the treatment of iron deficiency.

Materials and Methods

Materials

Mango seeds, commercial soft WF (72% extraction), bakery fat, powdered sugar, skimmed milk powder, sodium chloride, sodium bicarbonate, ammonium bicarbonate and vanilla were purchased from the local market of Kafrelsheikh, Egypt. SBM was purchased from factory of sugar beet, Kafrelsheikh, Egypt.

Methods

Preparing of MAKF and SBM

Mango seeds were cleaned and washed twice with tap water, then left to dry in the air. After the stones were individually hammered to obtain the kernels of which the outer cover was removed by hand after kernels were soaked in sulphited tap water at 50 °C for 48 h followed by autoclaving for 30 min at 121 °C (for reduce tannins) and dried by tray drier at 23 °C According to (Legesse, & Admassu, 2012). The dried material was ground using a laboratory electronic mill into a powdery form (BRAWN, Model 2001 DL, Germany), (Lattanzio, Linsalata, Palmieri, & Van Sumere, 1989). After that dried MAKF were milled and kept in polyethylene bags at 4 °C until further analysis and processing. Molasses were separated from foreign matters.

Formulation of biscuit samples using different ratios of MAKF and SBM

The basic formulation of biscuit and composite of flour biscuit are outlined in Table (1)

Table 1. Formulation of different biscuit samples (1000 g flour basis):

Ingredients	A	B	C	D	E	F	G	H	H	I
WF (g)	1000	950	900	850	900	800	700	600	900	800
SBM (g)	0.00	50	100	150	0.00	0.00	0.00	0.00	50	100
MAKF (g)	0.00	0.00	0.00	0.00	100	200	300	400	50	100
Sugar (g)	195	195	195	195	195	195	195	195	195	195
Margarine (g)	50	50	50	50	50	50	50	50	50	50
Milk powder (g)	2.5	2.5	2.5	2.5	2.5	2.5	2.5	2.5	2.5	2.5
Ammonium bicarbonate (g)	15	15	15	15	15	15	15	15	15	15
Sodium metabisulphite (g)	0.1	0.1	0.1	0.1	0.1	0.1	0.1	0.1	0.1	0.1
Water (ml)	325	325	325	325	325	325	325	325	325	325
Salt (g)	3	3	3	3	3	3	3	3	3	3
Vanilla (ml)	1.2	1.2	1.2	1.2	1.2	1.2	1.2	1.2	1.2	1.2

Blend formulation and biscuit processing

Biscuit samples were prepared by replacing WF with different levels of composite flour in the basic formulation of biscuit (Table 1) as described in the methods of A.A.C.C. (2002). Blends of WF, MAKF and SBM for biscuit formulations were prepared and shown in Table (1).

Biscuit samples were processed from dough's containing 10, 20 and 30% MAKF and 5,10, 15% SBM as substituting levels for WF. Biscuit dough was formulated by blending WF, MAKF and SBM with other ingredients. The formulated blends were mingled for 15 min at 125 rpm (speed 2) using a mixer (type DITO - SAMA, Aubusson, France). Each boosts of the paste were removed from the mixer and allowed to rest for 10 min. The paste pieces were sheeted and flattened using roller into a sheet of about 8 mm thickness, and then cut into rectangular pieces with size, 4.5cm × 4.5 cm. Samples were baked in an electric oven (DiFioreForensic, Model, MLC80B, Fornimorello, Italy) at 249 ºC for 18 min.

After baking, biscuits were left to cool at room temperature and were wrapped tightly with polypropylene pouches and kept until further evaluation and analyses took place.

Gross chemical composition

Moisture, ash, protein, fiber and fat were determined according to A.O.A.C. (2000). Total carbohydrates were calculated by differences.

Texture profile analysis

Physical properties were recorded by texture profile analyzer. Texture measurements of samples were carried out with universal testing machine (Cometech, Btype, Taiwan) provided with software. 35 mm diameter compression disc was used. Two cycles were applied, at a constant cross head velocity of 1 mm/s, to 30-50% of sample depth, and then returned. From the resulting force-time, i.e. hardness (N) and adhesiveness (M.J) were calculated from the TPA graphic, according to Bourne (2003).

Sensory evaluation of biscuit samples

Sensory evaluation was carried out according to Lanza, Pagiarini, & Tamselli (1995). Biscuit samples were served to panel test of (10) judges to evaluate color, odour, taste, texture, appearance and overall acceptability using hedonic scale from (10) to (1). The scoring scheme was established as mentioned by Zobik, & Hoojjat (1984) as followed: Color (10), taste (10), odor (10), texture (10), appearance (10) and overall acceptability (10) degrees.

Physical measurements of biscuits

The spread factor, width and thickness of biscuits were evaluated according to A.A.C.C (2002), method no. 10-50D. The spread ratio was calculated by dividing width (W) by thickness (T).

Statistical analysis

One-way analysis of variance (ANOVA) was used to show the significant between biscuit samples. T-paired sample was used to study the significant between MAKF and SBM. The statistical software SPSS (Version 16.0, SPSS Inc., Chicago, IL) was used for analysis. All results were carried out in triplicate and data reported as mean ± standard deviation (SD).

Results and discussion

Chemical composition of MAKF and SBM

The prepared flours from MAKF and SBM were analyzed for chemical composition (Table 2) and compared to WF data reported by Bouazizi, Montevecchi, Antonelli, & Hamdi (2020). It could be noticed from Table (2) that the highest component in MAKF and SBM was carbohydrates (67.89 and 59.89%, respectively), while, the lowest component in both was fat which reached about 3.22 and 0.01%, respectively.

As shown in Table (2), MAKF had higher content of protein (8.78%) than SBM (6.76%), while molasses had higher content of ash (10.62%). Compared to the chemical

composition of WF reported by Bouazizi et al. (2020), it was found that, MAKF had the lowest moisture content (10.80%) followed by WF (14.00%) and SBM (22.35%). SBM contained higher ash content (10.62%) than the MAKF (6.97%), while WF reported the lowest ash content reached about 0.53%.

Table 2. Gross chemical composition of MAKF, SBM and biscuit samples.

Sample	Moisture	Protein	Fat	Ash	Fiber	Total carbohydrates
MAKF	10.80±0.18	8.78±0.13*	3.22±0.09*	6.97±0.09	2.34*	67.89±0.55
SBM	22.35±0.19*	6.76±0.11	0.01±0.04	10.62±0.10*	0.10±0.15	59.89±0.47
A	8.22±0.12^{f}	9.63±0.14^{a}	4.65±0.09^{a}	1.11±0.08^{d}	0.43±0.09^{e}	75.96±0.64^{a}
B	9.62±0.20^{c}	8.23±0.11^{c}	3.81±0.21^{b}	1.61±0.07^{b}	0.45±0.13^{e}	76.28±0.34^{a}
C	10.33±0.18^{b}	8.01±0.16^{c}	3.52±0.11^{bc}	1.93±0.12^{a}	0.40±0.16^{e}	75.81±0.39^{a}
D	11.31±0.22^{a}	7.15±0.18^{d}	3.17±0.08^{c}	1.88±0.14^{ab}	0.44±0.20^{e}	76.05±0.54^{a}
E	8.55±0.17^{e}	9.29±0.17^{ab}	4.99±0.19^{ab}	1.27±0.11^{cd}	0.67±0.11^{c}	76.09±0.29^{a}
F	8.86±0.19^{d}	9.11±0.15^{ab}	5.19±0.17^{b}	1.36±0.10^{c}	0.81±0.26^{b}	75.98±0.24^{a}
G	9.22±0.09^{cd}	8.55±0.19^{bc}	5.33±0.10^{c}	1.43±0.11^{c}	0.93±0.08^{a}	76.43±0.45^{a}
H	9.44±0.20^{c}	8.77±0.20^{b}	4.76±0.12^{ab}	1.66±0.12^{b}	0.59±0.04^{d}	75.31±0.20^{a}
I	9.5±0.19^{c}	8.19±0.14^{c}	4.87±0.19^{bc}	1.82±0.09^{ab}	0.64±0.16^{d}	75.87±0.33^{a}

- The data were presented as mean ± S.D.
(*) Means in MAKF and SBM are significantly different at ($p \leq 0.05$).
- Means having the different case letter(s) within a column are significantly different at $P \leq 0.05$.
- A= control 100% WF; B= 95% WF + 5% SBM; C= 90% WF + 10% SBM; D = 85% WF + 15% SBM; E = 90% WF + 10% MAKF; F = 80% WF + 20% MAKF; G = 70% WF + 30% MAKF; H = 90% WF + 5% SBM + 5% MAKF and I = 80% WF + 10% SBM + 10% MAKF.

Protein content of MAKF and SBM was lower than that of WF (8.78 and 6.76% vs. 12.60%), but MAKF had remarkably higher fat content (3.22%) compared to WF and SBM (1.16 and 0.01%, respectively). WF gave higher carbohydrate content (71.20%) than MAKF and SBM (67.89 and 59.89%, respectively). The high ash content of SBM and MAKF indicates that they can be good sources of minerals. Bandyopadhyay et al. (2014), Yatnatti, Vijayalakshmi, & Chandru (2014) and Das, Khan, Rahman, Majumder, & Islam (2019) reported similar carbohydrate (69.77, 73.10 and 72.02%, respectively) and protein (7.53, 7.53 and 8.03%) contents in MAKF. Higher fat content was obtained by Bandyopadhyay et al. (2014) and Joyce, Latayo, & Onyinye (2014) which reached about 9%. On the other hand, lower fat content was reported by Das et al. (2018) (0.64%). On the contrary, ash amount stated by Das et al. (2018) and Bandyopadhyay et al. (2014) was lower than out result. Different mango varieties and determination process may be the facts for deviation of the results. According to Odunsi (2005), mango seed kernel flour can be used in the manufacturing of cakes, cookies and breads for adults and children. Šarić et al. (2016) reported near results for protein and ash contents in SBM. Lower amount for ash content were mentioned by Lončar et al. (2020) and Pătraşcu, Râpeanu, Bonciu, Vicol, & Bahrim (2009).

Mineral content of SBM and MAKF

Data in Table (3) presented the minerals content (mg/100g) in MAKF and SBM. All minerals content in MAKF were significantly higher than in SBM. The predominate mineral in MAKF was K followed by Mg which reached about 83.60 and 74.66 mg/100g, respectively.

In molasses, K, Na and Fe were reported to be about 6 mg/100g. Ca in MAKF and SBM reached about 27.90 and 1.32 mg/100g. MAKF showed a small amount of Fe reached about 9.93 mg/100g. Close results were obtained by Abdelaziz (2018) and Yatnatti et al. (2014) for Fe in mango kernel (9.3 and 12 mg/100g, respectively). Also, for Ca Elgindy (2017) and Nzikou et al. (2010) reported near contents to our findings. While K and Mg were lower than the results demonstrated by Yatnatti et al. (2014), Abdelaziz (2018), Elgindy (2017), Gumte, Taur, Sawate, & Kshirsagar (2018). On the other side, Na showed higher content than the other reported by Abdelaziz (2018), Nzikou et al. (2010) and Yatantti et al. (2014) and in harmony with Gumte et al. (2018). For SBM, higher amounts of K, Ca, Mg and Na were reported by Lončar et al. (2020) and Lević, Razmovski, Vučurović, Koprivica, & Mišljenović (2008), while Fe amount which reported by Lončar et al. (2020) was near to our findings (5.32 mg/100g). Generally, variation in mineral contents between samples could be due to cultivation climate, ripening stage, variety of plant, harvesting time of seeds and extraction method used.

Chemical composition of biscuit samples

Biscuits were selected as a food matrix due to their global diffusion, long shelf-life and the possibility of being easily exported. Chemical composition of biscuit samples with MAKF and SBM was presented in Table (2). Adding MAKF and SBM in different levels to biscuits caused a significant increase in moisture amount as did ash content in comparison with control sample.

These results are supported by Ashoush, & Gadallah (2011) and Bolek (2020) who enriched biscuits with mango peels and olive stone powder. As the proportion of MAKF and SBM in the biscuit formulation increased, the protein content of biscuit samples decreased significantly. This was

expected for the lower protein content in MAKF and SBM than in WF.

On the other side, the higher the amount of MAKF in the biscuit formulation, the higher the fat content in biscuit samples. This result may be due to the high fat content of MAKF (Bandyopadhyay et al., 2014; Joyce et al., 2014). Different results were obtained in SBM for fat content in biscuits, which decreased as increasing of SBM percentage.

This result could be attributed to fat content of SBM which was lower than WF. Non-significant differences were mentioned between biscuit samples in total carbohydrates. Biscuit samples with 5 and 10% of SMB and MAKF, respectively, showed higher moisture and ash contents and lower protein and fat amounts in comparison with control sample. Fiber content did not change significantly as a result of using SBM in biscuit production.

On the other side, MAKF showed significant effect on fiber content of biscuits. Increasing the amount of MAKF caused an increase in fiber content reached the highest level by using 30% MAKF (0.93%).

Table 3. Minerals content of MAKF, SBM and biscuit samples.

Sample	Potassium (K)	Calcium (Ca)	Magnesium (Mg)	Sodium (Na)	Iron (Fe)
MAKF	83.60	27.90	74.66	20.36	9.93
SBM	6.64	1.32	3.17	6.24	6.99
A	65.32	25.17	40.73	51.68	2.02
B	60.18	18.77	32.50	52.43	3.13
C	53.27	13.03	25.82	53.12	3.88
D	49.91	10.67	20.19	53.87	4.01
E	76.16	26.52	51.11	64.23	4.21
F	81.01	27.16	62.32	78.40	4.56
G	90.79	27.93	73.54	89.04	4.96
H	67.34	24.71	42.81	65.57	4.08
I	68.12	25.33	46.14	77.05	4.28

- The data were presented as mean ± S.D.
- Means having the different case letter(s) within a column are significantly different at $P \leq 0.05$.
- A= control 100% WF; B= 95% WF + 5% SBM; C= 90% WF + 10% SBM; D = 85% WF + 15% SBM; E = 90% WF + 10% MAKF; F = 80% WF + 20% MAKF; G = 70% WF + 30% MAKF; H = 90% WF + 5% SBM + 5% MAKF and I = 80% WF + 10% SBM + 10% MAKF.

Minerals content of biscuit samples

The biscuit samples were estimated for minerals content and the results were shown in Table (3). In comparison to the control, Table (3) showed that, higher molasses content contributed to lower K (60.18 to 49.91 mg/100g), Ca (18.77 to 10.67 mg/100g) and Mg (32.50 to 20.19 mg/100g) contents and higher Na (52.43 to 53.78 mg/100g) and Fe (3.13 to 4.01 mg/100g) in the biscuits in comparison to the corresponding controls (65.32, 25.17, 40.73, 51.68 and 2.02 mg/100 for K, Ca, Mg, Na and Fe, respectively).

The reason for this is the low amount of K, Ca and Mg in SBM, while WF had more amounts of these minerals. Also, the increase in Fe amount in SBM than in WF led to an increase in Fe content in biscuit samples. MAKF is a perfect source of minerals. Its addition is expected to increase the content of minerals and the elevated mineral content in formulations with molasses confirms this.

Increasing the amount of MAKF replaced with WF caused a raise in mineral contents in biscuit samples. The highest mineral amount was recorded in 30% MAKF. K, Mg and Na recorded higher increase in biscuit samples than Ca and Fe as a result of adding MAKF. These results were in harmony with Salem (2020) who reported an increase in mineral contents in biscuit produced by different percentages of mango seed kernel. Filipčev, Mišan, Šarić, & Šimurina (2016) indicated that increasing molasses doses resulted in remarkable increases in the observed macro and microelements. This note was similar to Fe and Na content in our biscuit samples, but not with other minerals content. The minerals Mg, Ca and K are important for the effectiveness of insulin and their deficiency in the diet has been associated with increased risk of developing diabetes (Wright, Ellis, & Ilag, 2014).

Physical properties of biscuit samples

Data in Table (4) showed the width, thickness and spread ratio of biscuit samples. Among the attributes the physical properties of biscuit depends on the composition of matrix. For width, control sample showed the highest value (46.51 mm). The spread ratio, width and thickness values of control and biscuit samples were ranged from 8.38 to 11.01, 40.32 to 46.51 and 3.81 to 4.95 respectively The width of biscuits significantly decreased as adding MAKF and SBM corresponding to control sample.

This decrease may be due to the reduction of the gluten structure with increased levels of WF replacement (Choudhury, Badwaik, Borah, Sit, & Deka, 2015). 5% and 10% of SBM followed the control sample in width value (42.75 and 42.31 mm, respectively). The samples produced by blinding SBM and MAKF at 5 and 10% no significant differences were noticed between each other and 5 and 10% SBM.

Increasing the amount of SBM caused a decrease in biscuits width. While increasing the amount of MAKF caused an increase in the width of biscuits which reached

41.20 and 41.93 mm in 20 and 30% of MAKF without significant differences. The thickness of the biscuit samples significantly decreased with increasing fat content which is in line with the findings of Pareyt et al. (2009).

So, adding SBM by 5, 10 and 15% and MAKF by 20 and 30% showed a decrease in the thickness of biscuit samples. Using SBM by 10 and 15% and MAKF by 20 and 30% reported no significant differences in biscuits thickness. This was in agreement with Filipčev, Šimurina, & Bodroža-Solarov (2014) who mentioned that increasing the molasses content did not significantly affect thickness in any of the tested biscuit variants.

Increasing the percentage of replacement of WF with SBM caused an increase in spread ratio. SBM different percentages showed higher spread ratio than control reached the highest value by adding 15% SBM (11.01). This may be due to the addition of liquid molasses yielded softer gluten-free cookies with higher spread and better pronounced color properties (Filipčev et al., 2016). On the other side, 20 and 30% MAKF represented non-significant results with control. This was the same effect during using 10% SBM and 10% MAKF. Only using 10% MAKF and 5% SBM and 5% MAKF showed lower value of spread ratio than control sample (8.38 and 8.62, respectively).

Table 4. Physical properties and textural characteristics of biscuit samples.

Sample	Width	Thickness	Spread ratio	Hardness (N)	Adhesiveness
A	46.51±0.28^{a}	4.95±0.11^{a}	9.40±0.20^{c}	17.01±0.16^{a}	0.22±0.05^{a}
B	42.75±0.32^{b}	4.21±0.09^{b}	10.15±0.09^{b}	10.91±0.11^{e}	0.13±0.03^{b}
C	42.31±0.24^{b}	3.91±0.17^{c}	10.82±0.18^{ab}	10.75±0.19^{e}	0.14±0.06^{b}
D	41.98±0.18^{c}	3.81±0.10^{c}	11.01±0.15^{a}	10.42±0.22^{e}	0.11±0.08^{b}
E	40.32±0.31^{d}	4.81±0.19^{a}	8.38±0.12^{d}	12.52±0.11^{d}	0.01±0.009^{c}
F	41.20±0.12^{c}	4.42±0.12^{b}	9.32±0.17^{c}	10.27±0.13^{e}	0.02±0.05^{c}
G	41.93±0.22^{c}	4.41±0.16^{b}	9.50±0.16^{c}	9.55±0.18^{f}	0.04±0.004^{c}
H	42.51±0.20^{b}	4.93±0.20^{a}	8.62±0.20^{d}	16.21±0.22^{b}	0.22±0.20^{a}
I	41.45±0.11^{b}	4.42±0.10^{b}	9.37±0.20^{c}	15.47±0.16^{c}	0.20±0.04^{a}

- The data were presented as mean ± S.D.
- Means having the different case letter(s) within a column are significantly different at $P \leq 0.05$.
- A= control 100% WF; B= 95% WF + 5% SBM; C= 90% WF + 10% SBM; D = 85% WF + 15% SBM; E = 90% WF + 10% MAKF; F = 80% WF + 20% MAKF; G = 70% WF + 30% MAKF; H = 90% WF + 5% SBM + 5% MAKF and I = 80% WF + 10% SBM + 10% MAKF.

Textural characteristics of biscuit samples

The mechanical characteristics of biscuits are important to evaluate the acceptance point of view of consumer. The effects of MAKF and SBM on textural characteristics of biscuit dough were given in Table (4). Significant differences were reported between control and SBM and MKF samples. The use of different ratios of SBM to the biscuit formulation did not significantly affected hardness. Filipčev et al. (2016) stated that dry molasses increased hardness whereas liquid molasses decreased it. Using MAKF at different ratios caused significant differences in hardness. Using 10% from MAKF recorded the highest hardness result (12.52) among the other used ratios, while increasing the amount of MAKF in biscuit formulation caused low in hardness reached about 10.27 and 9.55 for 20% and 30% MAKF, respectively.

This behavior was related to the high fibre content (which was low in SBM and MAKF), and therefore to hydroxyl groups, which establish strong interactions with gluten proteins via water interactions through hydrogen bonds (Rosell, Rojas, & De Barber, 2001). Our results were in opposite with the others observed by Aslam et al. (2014) who stated that the biscuits with 15% mango kernel powder and 95% flour and with 15% was significantly harder than biscuits that made with 100% flour. Also, the hardness of the biscuit dough formulated with prickly pear peel flour significantly increased with increasing the amount of prickly pear peel flour (Bouazizi et al., 2020).

Similar results were obtained by Bolek (2020) who reported that hardness of biscuit dough increased significantly as the proportion of olive stone powder increased. Using MAKF and SBM caused a decrease in adhesiveness of biscuit samples in comparison with control. Non-significant differences were reported during increasing MAKF and SBM percentage in biscuit samples. Adhesiveness was higher in SBM than MAKF biscuit samples.

Dough adhesiveness was significantly affected by the fat content; higher fat content (MAKF had higher fat content than SBM) decreased dough adhesiveness (Filipčev et al., 2014). This was similar to Filipčev et al. (2014) who illustrated that no significant variations were reported in molasses biscuit types. Adding SBM and MAKF together with 5 and 10% to the biscuit formulation caused near result in hardness and adhesiveness in comparison with control sample.

Sensory evaluation of biscuit samples

Table (5) reveals the sensory attributes of biscuit from various blends of WF and MAKF and SBM. Control biscuit showed maximum color mean score of 9.7, which was the highest, obtained among the type of biscuit followed by 5 and 10% SBM which reported mean score 9.2 and 8.2, respectively.

In addition, sample 30% MAKF secured the lowest score (6.6) while sample 10% SBM and MAKF secured second lowest score (6.6) but both were equally acceptable. The decrease in color in MAKF samples is due to the fact that as blending ratio with MAKF increases, this in turn

affects and led to the color change of the biscuits to darkness (Legesse, & Emire, 2012).

This change in color while increasing the blending ratio of MAKF might be due to the nutrients interaction during processing and baking time with temperature combination (Legesse, & Emire, 2012). For flavor, ANOVA test revealed that there was significant difference among the biscuit samples at 5% level of significance. Among the MAKF supplanted biscuits, the sample 10% secured the highest score of 7.2 while sample 30% reported the lowest score of 6.5 among all samples.

Table 5. Sensory evaluation of biscuit samples.

Sample	Color	Taste	Adour	Texture	Appearance	Overall acceptability
A	9.7±0.12^{a}	9.3±0.14^{a}	9.1±0.16^{a}	9.2±0.11^{a}	9.4±0.12^{a}	9.4±0.10^{a}
B	9.2±0.15^{b}	8.7±0.11^{b}	9.1±0.09^{a}	9.0±0.09^{a}	9.2±0.09^{a}	9.1±0.18^{a}
C	8.2±0.13^{c}	8.1±0.08^{c}	8.4±0.21^{b}	8.6±0.13^{b}	8.2±0.16^{b}	8.3±0.21^{b}
D	7.7±0.11^{d}	7.5±0.16^{d}	7.8±0.13^{c}	7.7±0.16^{c}	7.9±0.20^{c}	7.7±0.15^{c}
E	6.8±0.11^{e}	7.2±0.13^{de}	7.2±0.10^{d}	7.5±0.18^{cd}	7.2±0.19^{d}	7.4±0.24^{cd}
F	6.9±0.09^{e}	6.8±0.10^{e}	6.8±0.14^{de}	7.0±0.10^{d}	7.0±0.20^{d}	7.0±0.24^{d}
G	6.6±0.10^{f}	6.3±0.09^{f}	6.2±0.17^{e}	6.4±0.19^{e}	6.5±0.18^{f}	6.5±0.11^{e}
H	7.2±0.13^{d}	7.1±0.14^{de}	7.0±0.15^{d}	6.9±0.12^{d}	7.1±0.15^{d}	7.0±0.24^{d}
I	6.6±0.14^{f}	6.8±0.20^{e}	6.9±0.15^{de}	6.5±0.20^{e}	6.8±0.12^{e}	6.7±0.14^{e}

- The data were presented as mean ± S.D.
- Means having the different case letter(s) within a column are significantly different at $P \leq 0.05$.
- A= control 100% WF; B= 95% WF + 5% SBM; C= 90% WF + 10% SBM; D = 85% WF + 15% SBM;E = 90% WF + 10% MAKF; F = 80% WF + 20% MAKF; G = 70% WF + 30% MAKF; H = 90% WF + 5% SBM + 5% MAKF and I = 80% WF + 10% SBM + 10% MAKF.

For SBM, the sample 5% SBM showed the highest score of taste (8.7) after control sample and as the percentage of SBM increased in samples, the taste score decreased. In case of adour, texture and appearance it was seen that the sample containing 100% WF secured the highest scores (9.1, 9.2 and 9.4, respectively) and was equally acceptable as sample having 90% WF and 10% SBM securing scores of 9.1, 9.0 and 9,2, respectively, while the sample containing 10% MAKF reported higher adour, texture and appearance scores (7.2, 7.5 and 7.2, respectively) than 20 and 30% of MAKF. The biscuits made by adding 5% MAKF + 5% SBM were better than the others produced by adding 10% MAKF + 10% SBM. From the previous results it could be noticed that biscuits produced by adding SBM were more acceptable than the samples with MAKF.

Blending of MAKF with WF significantly decreased the color, taste, odor, texture, appearance and overall acceptability of biscuit as the proportion of MAKF blend ratio increased. These findings were close to the results reported by Legesse, & Emire (2012) and Ifesan (2017). Finally, sample having 100% WF, 95% WF and 5% SBM were not varied significantly based on overall acceptability but rest samples differed significantly from former two.

Therefore, based on the sensory evaluation of the developed biscuits, it could be said that supplementation of SBM and MAKF with WF would result in lowering the consumer preference but up to 15% SBM and 30% MAKF supplementation had not affect much.

Conclusion

The physicochemical and phytochemical analyses carried out on MAKF and SBM revealed that they could be good source of balanced food material which could be utilized in food production especially confectionary industry. The utilization of MAKF with WE to produce biscuit resulted to a biscuit with improved ash content. Utilization of MAKF and SBM for commercial purposes can reduce the environmental pollution which resulted as by-product from mango and sugar beet processing industries and contribute to food security by converting waste to valuable food products. From the present study it could be concluded that blends containing up to 5 and 10% SBM was suitable for the development of biscuits.

Beyond 30% blends of MAKF, the color of the biscuits become darken attributable to the Maillard browning reaction, presence of high fiber composition and baking process parameters. Addition of MAKF significantly improved the micronutrient pattern in the biscuits by raising the levels of macro- and micro-minerals. While using SBM improved the level of Na and Fe in produced biscuits. The partial substitution of WF with MAKF and SBMF to produce biscuits is a promising strategy in the manufacturing of bakery products.

Acknowledgment

The last author is most grateful for the technical support provided by the members of the faculty of agriculture, University of Kafrelsheikh, Egypt.

Conflict of Interest

The authors declare that they have no conflict of interest.

References

1. A.A.C.C. (2002). Approval Methods of American Association of Cereal Chemists, in St. Paul, Minnesota, USA.

2. A.O.A.C. (2000). Association Official Analytical Chemists.Official Methods of Analysis.7th ed., Washington DC, USA.
3. Abdelaziz, S. A. (2018). Physico chemical characteristics of mango kernel oil and meal. *Middle East Journal of Applied Sciences, 8*(1), 1-6.
4. Ajila, C. M., Aalami, M., Leelavathi, K., PrasadaRao, U. J. S. (2010). Mango peel powder: A potential source of antioxidant and dietary fiber in macaroni preparations. *Innovative Food Science & Emerging Technologies, 11*, 219-224.
5. Ashoush, I. S., Gadallah, M. G. E. (2011). Utilization of mango peels and seed kernels powders as sources of phytochemicals in biscuit. *World Journal of Dairy & Food Sciences, 6*(1), 35–42.
6. Aslam, H. K., Raheem, M. L., Ramzan, R., Shakeel, A., Shoaib, M., Sakandar, H. A. (2014). Utilization of mango waste material (peel, kernel) to enhance dietary fiber content and antioxidant properties of biscuit. *Journal of Global Innovations in Agricultural and Social Sciences, 2*(2), 76-81.
7. Bandyopadhyay, K., Chakraborty, C., Bhattacharyya, S. (2014). Fortification of mango peel and kernel powder in cookies formulation. *Journal of Academia and Industrial Research, 2*(12), 661–664.
8. Bolek, S. (2020). Olive stone powder: A potential source of fiber and antioxidant and its effect on the rheological characteristics of biscuit dough and quality. *Innovative Food Science & Emerging Technology. 64*, 102423.
9. Bouazizi, S., Montevecchi, G., Antonelli, A., Hamdi, M. (2020). Effects of prickly pear (*Opuntia ficus-indica* L.) peel flour as an innovative ingredient in biscuits formulation. *LWT, 124*, 109155.
10. Bourne, M. C. (2003). Food texture and viscosity: Concept and measurement. Elsevier Press, New York/London.
11. Chen, M., Zhao, Y., Yu, S. (2015). Optimisation of ultrasonicassisted extraction of phenolic compounds, antioxidants, and anthocyanins from sugar beet molasses. *Food Chemistry, 172*, 543–550.
12. Chou, C. C. (2003). Preparation antioxidants enriched functional food products from sugar cane and beet. United States Patent Applications127141.
13. Choudhury, M., Badwaik, L. S., Borah, P. K., Sit, N., Deka, S. C. (2015). Influence of bamboo shoot powder fortification on physico-chemical, textural and organoleptic characteristics of biscuits. *Journal of food science and technology, 52*(10), 6742–6748.
14. Das, P. C., Khan, M. J., Rahman, M. S., Majumder, S., Islam, M. N. (2019). Comparison of the physico-chemical and functional properties of mango kernel flour with wheat flour and development of mango kernel flour based composite cakes. *NFS Journal, 1*(17),1-7.
15. Das, P. C., Sattar, S., Jony, M. E., Islam, M. N. (2018). Rehydration kinetics of flour from dehydrated mango kernel. *Food Research, 2*(5), 474–480.
16. Douglas, M. C., Glenn, D. C. (1982). Foods and food production encyclopedia. Van nostrandReinhold . P1941
17. Elegbede, J., Achoba, I., Richard, H. (1995). Nutrient composition of mango (*Mangnifera indica*) seed kernel from Nigeria. *Journal of food biochemistry, 19*(5), 391–398.
18. Elgindy, A. A. (2017). Chemical and technological studies of mango seed kernel. *European Journal of Food Science and Technology, 5*(2), 32-40.
19. Filipčev, B., Bodroža-Solarov, M., Šimurina, O., Cvetković, B. (2012). Use of sugar beet molasses in processing of gingerbread type biscuits: effect on quality characteristics, nutritional profile, and bioavailability of calcium and iron. *Acta alimentaria. 41*(4), 494-505.
20. Filipčev, B., Lević, L., Bodroža-Solarov, M., Mišljenović, N., Koprivica, G. (2010). Quality characteristics and antioxidant properties of breads supplemented with sugar beet molasses-based ingredients. *International Journal of Food Properties, 13*(5), 1035-53.
21. Filipčev, B., Mišan, A., Šarić, B., Šimurina, O. (2016). Sugar beet molasses as an ingredient to enhance the nutritional and functional properties of gluten-free cookies. *International Journal of Food Sciences and Nutrition, 67*(3), 249-256.
22. Filipčev, B., Šimurina, O., Bodroža-Solarov, M. (2014). Quality of gingernut type biscuits as affected by varying fat content and partial replacement of honey with molasses. *Journal of food science and technology, 51*(11), 3163-71.
23. Gumte, S. V., Taur, A. T., Sawate, A. R., Kshirsagar, R. B. (2018). Effect of fortification of mango (*Mangifera indica*) kernel flour on nutritional, phytochemical and textural properties of biscuits. *Journal of Pharmacognosy and Phytochemistry, 7*(3), 1630-1637.
24. Ifesan, B. O. (2017). Chemical properties of mango kernel and seed and production of biscuit from wheat-mango kernel flour blends. *International Journal of Food and Nutrition Research, 1*, 5.
25. Jahurul, M. H. A., Norulaini, N. A. N., Zaidul, I. S. M., Jinap, S., Sahena, F., Azmir, J., Sharif, K. M. Omar, A. M. (2015). Mango (*Mangifera indica* L.) by-products and their valuable components: a review. *Food Chemistry, 183*, 173–180.
26. Joyce, O. O., Latayo, B. M., Onyinye, A. C. (2014). Chemical composition and phytochemical properties of mango (*Mangifera indica*.) seed kernel. *International Journal of Advanced Chemistry, 2*,185-7.
27. Khammuang, S., Sarnthima, R. (2011). Antioxidant and antibacterial activities of selected varieties of Thai mango seed extract. *Pakistan journal of pharmaceutical sciences, 24*(1), 37–42.
28. Kotsianis, I. S., Giannou, V., Tzia, C. (2002). Production and packaging of bakery products using MAP technology. *Trends in Food Science & Technology, 13*, 319–324.

29. Lanza, C. M., Pagiarini, E., Tamselli, F. (1995). Sensory and chemical evaluation of frozen blood orange juice. *Agricoltura Mediterranea, 125*, 421-426.
30. Lattanzio, V., Linsalata, V., Palmieri, S., Van Sumere, C. F. (1989). The beneficial efficial effect of citric acid and ascorbic acid on the phenolic browning reaction in stored artichoke (*Cynara scolymus*, L.) heads. *Food Chemistry, 33*, 93-106.
31. Legesse, M. B., Admassu, S. (2012). Functional and physicochemical properties of mango seed kernels and wheat flour and their blends for biscuit production. *African Journal of Food Science and Technology, 3*(9), 193-203.
32. Legesse, M. B., Emire, S. A. (2012). Functional and physicochemical properties of mango seed kernels and wheat flour and their blends for biscuit production. *African Journal of Food Science and Technology, 3*(9), 193-203.
33. Lević, L., Razmovski, R., Vučurović, V., Koprivica, G., Mišljenović, N. (2008). Appliance of sugar beet molasses after osmotic dehydration of apple for bioethanol production. *Časopis za procesnu tehniku i energetiku u poljoprivredi/PTEP. 12*(4), 219-221.
34. Loelillet, D. (1994). The European mango market: A promising tropical fruit. *Fruit, 49*, 5-9.
35. Lončar, B., Nićetin, M., Filipović, V., Knežević, V., Pezo, L., Šuput, D., Kuljanin, T. (2020). Osmotic dehydration in sugar beet molasses-food safety and quality benefits. *Journal of Hygienic Engineering and Design,* 15-20.
36. Menon, L., Majumder, S. D., Ravi, I. (2014). Mango (*Mangifer aindica* L.) kernel flour as a potential ingredient in the development of composite flour bread. *Indian Journal of Natural Products and Resources, 5*(1), 75–82.
37. Nzikou, J. M., Kimbonguila, A., Matos, L., Loumouamou, B., Pambou-Tobi, N. P. G., Ndangui, C. B., Abena, A. A., Silou, Th., Scher, J., Desobry, S. (2010). Extraction and characteristics of seed kernel oil from mango (*Mangifera indica*). *Research Journal of Environmental and Earth Sciences, 2*(1), 31–35.
38. Odunsi, A. (2005). Response of laying hens and growing broilers to the dietary inclusion of mango (*Mangifera indica* L.) seed kernel meal. *Tropical Animal Health and Production, 37*(2), 139-150.
39. Pareyt, B., Talhaoui, F., Kerckhofs, G., Brijs, K., Goesaert, H., Wevers, M., Delcour, J. (2009). The role of sugar and fat in sugar-snap cookies: structural and textural properties. *Journal of Food Engineering, 90*, 400–408.
40. Pătraşcu, E., Râpeanu, G., Bonciu, C., Vicol, C., Bahrim, G. (2009). Investigation of yeast performances in the fermentation of beet and cane molasses to ethanol production. *Ovidius University Annals of Chemistry, 20*(2), 199-204.
41. Rosell, C. M., Rojas, J. A., De Barber, C. B. (2001). Influence of hydrocolloids on dough rheology and bread quality. *Food Hydrocolloids, 15*, 75–81.
42. Salem, B. R. (2020). Use of tomato pomace, mango seeds kernel and pomegranate peels powders for the production of functional biscuits. *Zagazig Journal of Agricultural Research, 47*(4), 1011-1023.
43. Šarić, L. C., Filipčev, B. V., Šimurina, O. D., Plavšić, D. V., Šarić, B. M., Lazarević, J. M., Milovanović, I. L. (2016). Sugar beet molasses: properties and applications in osmotic dehydration of fruits and vegetables. *Food and Feed Research, 43*(2), 135-44.
44. Šimurina, O., Filipčev, B., Lević, L., Pribiš, V., Pajin, B. (2006). Sugar beet molasses as an ingredient in tea-cookie formulation. *Journal on Processing and Energy in Agriculture, 10*(3-4), 93-6.
45. Wright, A. G., Ellis, T. P., Ilag, L. L. (2014). Filtered molasses concentrate from sugar cane: natural functional ingredient effective in lowering the glycaemic index and insulin response of high carbohydrate foods. *Plant foods for human nutrition, 69*, 310–316.
46. Yatnatti, S., Vijayalakshmi, D., Chandru, R. (2014). Processing and nutritive value of mango seed kernel flour. *Current Research in Nutrition and Food Science Journal, 2*(3), 170-5.
47. Zobik, M. E., Hoojjat, P. (1984). Sugar-snap cookies with wheat-navy bean sesame seed flour blend. *Cereal Chemistry, 61*, 41-44.

ISSN print: 1224-5984
ISSN online: 2248-3942

Rom Biotechnol Lett. 2022; 27(1): 3200-3207
doi: 10.25083/rbl/27.1/3200-3207

Received for publication, October, 10, 2020
Accepted, December, 15, 2021

Original paper

Influence of high-voltage electric field thawing on frozen tilapia fillets quality

ATEF MOHAMED ELSBAAY[1], ASMAA AHMED ELATTAR[1], ROWIDA YOUNIS ESSA[2]

[1] Agricultural Engineering Department, Faculty of Agric. Kafrelsheikh University, 33516 Egypt.
[2] Food Technology Department, Faculty of Agric. Kafrelsheikh University, Egypt.

Abstract In the food sector, high voltage electric field (HVEF) has recently been regarded as a novel thawing technique. The variance in the quality was compared between frozen tilapia fish fillets thawed by high voltage electrostatic field (HVE) and those thawed conventionally as control. Frozen tilapia fish fillets were thawed under HVEF and were exposed to three different corona voltages from 4.5 to 14 kV at electrode gaps of 3, 4.5, and 6 cm; the control was thawed at 20°C without HVEF treatment. Thawing rate, evaporation, thawing, and drip losses, as well as total volatile binding nitrogen (TVB-N), thiobarbituric acid reactive substances, protein solubility, and color variations, have been employed as the quality indicators. The results revealed that thawing under HVEF greatly enhances the thawing rates of frozen tilapia fish fillets. The greatest rate of thawing was 2.16 times that of the control specimen. However, thawing HVEF reduced the protein solubility and color of fish specimens. In comparison to the control, increasing the applied voltage reduced the protein solubility of the fish specimens High electrostatic field intensities caused frozen tilapia fish fillets to oxidize quicker than lower ones.

Keywords Thawing, High voltage electric field (HVEF), TVB-N, tilapia, Protein solubility

To cite this article: ELSBAAY AM, ELATTAR AA, ESSA RY. Influence of high-voltage electric field thawing on frozen tilapia fillets quality. *Rom Biotechnol Lett*. 2022; 27(1): 3200-3207. DOI: 10.25083/rbl/27.1/3200-3207.

✉ *Corresponding author: ROWIDA YOUNIS ESSA, Food Technology Department, Faculty of Agric. Kafrelsheikh University, Egypt.
E-mail: rowida.essa@agr.kfs.edu.eg

Introduction

Fish is becoming a more essential source of food all around the world (Silva et al., 2011). The proportion of fisheries produce used for directly human consumption climbed from around 70% in the 1980s to more over 85% in 2012 (FAO, 2014).

Egypt is already one of the world's biggest aquaculture industry, which contributes significantly to income, jobs generation and food production. Nile tilapia was brought to undeveloped nations and sustenance cultivated to suit local protein demands (GAFRD, 2016). Nile tilapia, *Oreochromisniloticus*, is amongst the most significant fish species in tropical Africa's inland fisheries, particularly in the Great East African rift valley lakes.

Aside from its importance in caught fisheries, Tilapia is one of the most significant species for 21st-century aquaculture, with production in over 100 nations. Tilapias have become the world's 2nd most common cultured fish, trailing only carps (Elsebaieet al., 2021). Annual cultured tilapia output topped 2,002,087 metric tons (Yitayew, 2012). *O. niloticus* has a total length of 20 cm on average (FAO, 2012).

Egypt, China, Indonesia, and the Philippines are the top tilapia producers today. The benefits of tilapia include their quick growth, impedance against numerous illnesses and stresses, resilience to changing environmental circumstances, and readiness to breed in captivity (Shoemaker et al., 2000).

Freezing is a key intermediate stage in preparing fish for frozen storage, and among the most widely utilized ways is the air blast freezer. This technique eliminates heat out from fish via cycling cold air at temperatures ranging from-30 to - 40°C with speeds varying from 1.5 to 6ms-1 above the products (Ninan, 2018).

Freezing not only inhibits microbial growing but rather the chemical changes that cause quality degradation (Ordóez et al., 2005). This procedure is highly effective in retaining the nutritional and sensory properties of the fish, as long as the freezing, storage, and thawing stages are carried out correctly (Evangelista, 2008). The freeze-thawing process causes muscle proteins denaturation, resulting in undesirable textural changes in meat (Wang et al., 2015). Consequently, despite the effectiveness of freezing in ensuring either quality of meat and nutritional safety, various difficulties related to the freezing - thawing processes continue to be a major source of worry for the food consumers and manufacturers (Ali et al., 2015). A significant consideration when choosing the appropriate thawing procedure is that the technique is non-destructive, causing minimal damage to the fish quality. Various systems, including air, vacuum, water heat, radio frequency, high pressure, microwave, ultrasonic, and infrared have been used to thaw frozen fish, each of which has number of its issues, like as indolent rate, elevated weight losses, chemical spoilage, microbial spoilage, excessive heat, and expensive cost (Uyar et al., 2015 and Llave et al., 2015). As a result, it is critical to create a system capable of preserving quality while preventing unwanted changes in tilapia fish fillets.

Today, nonthermal systems have been used as a novel methods to prevent the negative effects of heat on food color, flavor, and nutritional content (Orlowska et al., 2014), such asohmic thawing and HVEF thawing Ohmic thawing is based on electricity flow via a food product with electrical resistance (Bozkurt and Icier, 2012). Heat is produced instantaneously within the foodstuff. Meanwhile, in HVE thawing, air is ionized by passing high voltage electricity between a needle electrode and a ground electrode, and the produced ions are propelled around the electrodes. Then, the bulk of the ionized fluid moved on the sample's surface by transferring momentum from air ions to neutral air molecules (Zhang and Ding, 2020).

Besides, its low power consumption, the HVEF retains food at freshness state, which has lately made it appealing for the production of high-quality products (Singh et al., 2012 and Dinani et al., 2014). Previous researches have shown that HVEF can cut the time required to thaw chicken (-3°C) and frozen pork (20°C) to two-thirds of the time required in still air (He et al., 2013). Thawing frozen eggs and beef with this novel process took 25–30% less time than the conventional procedures under the identical temperature (Orlowska et al., 2014). The HVEF method has been reduced the time required to thaw frozen pork tenderloin meat by raising voltage and reducing the distance between electrodes (He et al., 2014). Some researchers investigated the influence of an electrostatic field on the frozen items quality and discovered that electrostatic thawing process can restrict microbiological growth and minimize microbial loads; thus, the quantity of volatile nitrogen in thawed items via this way is lowered and storage duration is increased (He et al., 2013).Based on the foregoing, it appears that implementing an adequate technique for frozen fish thawing can be a significant achievement for food manufacturers. The current work is part of an ongoing investigation into the use of HVEF thawing for frozen tilapia fish fillets, with the goal of investigating the changes that may occur in the quality of the product throughout thawing beneath HVEF and storage duration, as well as comparing it to the traditional still air technique. Hence, it offers for the first time the practical and theoretical groundwork for using high-voltage electric field thawing technologies to thaw frozen tilapia fillets.

Materials and Methods

Materials

Nile tilapia fish

Nile tilapia (Orechromisniloticus) fish specimens (average weight = 300-450 g) were acquired on the same day of harvesting from a fish market in Kafr El-Shiekh City, Egypt.

All chemical used in this work of HPLC grade (99.9% purity) were obtained from Sigma company of chemicals and drugs, St. Louis, MO, USA.

HVE experimental apparatus included high voltage output from -50 to 50 kV and maximal electrical current (5 mA), a processing chamber and a high-voltage generator regulated by a multi-point plate electrode system. The ground electrode is a rectangular 20 x 15 cm^2 copper plate. A sharp 16-tip (0.4 mm diameter) connected to the positive pole of high voltage power supply creates a corona discharge electrode. The chamber was positioned in a low temperature incubator. Via varying the voltages and distance amidst the used electrodes, the intensity of the electric area is changed. The experiential device for applying the HVEF method is demonstrated in Figure 1.

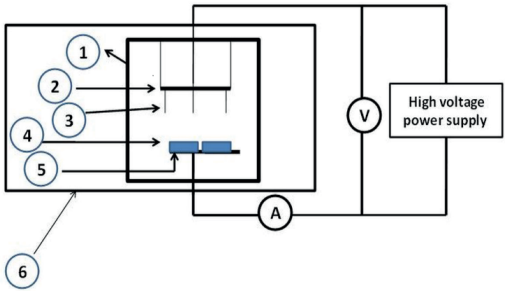

Figure 1. Schematic diagram of experimental set-up employed for HVE thawing process. Where, 1 is chamber, 2 is Aluminum, 3 is point electrode, 4 is frozen tilapia fish fillets, 5 is plate electrode (Copper) and 6 is incubator

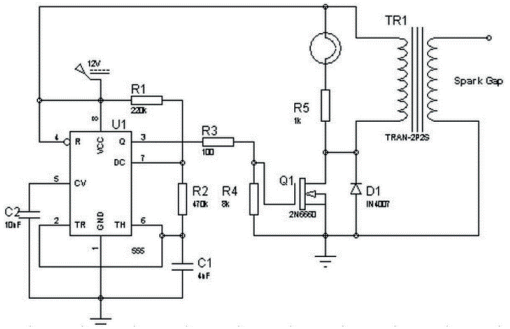

Figure 2. The schematic diagram of the electrical circle of the high voltage powersupply.

Methods

Nile tilapia fish fillets (NTFFs) preparation and freezing

Each fish was gutted, deheaded, cleaned, and filleted into two pieces weighing roughly 90 g each. The specimens were then wrapped in sterile polyethylene bags and sent immediately to the food technology laboratory, faculty of agriculture, Kafrelshiekh University using an icebox, where they were immediately frozen at -18°C in a freezer (Kiriazi, Egypt) for 24 hours to prepare for the thawing experiment.

Thawing

Frozen NTFFs(7 cm diameter × 1 cm thickness) thawing process were carried using HVE for each treatment. Frozen NTFFs was positioned over rectangular platelet electrode and an electrical area was formed between the positive and negative electrodes. Control sample thawing process was carried out by poisoning it into HVE room over the identical platelet electrode in the absence of the electric field. Fiber optic thermocouple (Digi-Sense® Traceable® Kangaroo) was used to regulate the temperature pending this process. To stabilize the thermocouple prior to freezing, a hole was formed in the geometric middle of each processed NTFFs via plurality of needles, and by finishing the freezing period, needles were pulled out of the sample. The optic fibers were put in the geometric middle of every one and keep it fixed in NTFFs. When the NTFFs internal temperature reaches up 0°C, the thawing is deemed finished. The applied voltages for the experimental groups were 4.5, 7.5, and 10.5 kV; 6, 10.5 and 13.5 kV; and 7.5, 10.5, and 14 kV for electrode gaps of 3, 4.5 and 6 cm.He et al. (2014) stated that both the geometric center and surface temperatures increased rapidly with increased applied voltages, and there was no significant difference in the inside and outside temperatures of frozen pork tenderloin meat from different HVEF treatments or in the control. Therefore, the temperature measured at the geometric center of the samples was taken as object of study. The experiments were triplicated.

Thawing rate measurement

The period needed for promoting the temperature in the position of frozen NTFFs from -18ºC to 0ºC, was possessed in consideration as thawing period. The thawing rate of frozen NTFFs was calculated by dividing the NTFFs weight by the thawing period (g/s)

Evaporation, thawing, and drip losses measurement

Evaporation, thawing, and drip losses values were measured using the procedure explained according to Ding et al. (2018). The results were calculated from the following equations:

$$\text{Evaporation loss (\%)} = \frac{M_F - M_{TB}}{M_F} \times 100$$

$$\text{Thawing loss (\%)} = \frac{M_F - M_{TA}}{M_F} \times 100$$

$$\text{Drip loss} = \frac{M_{TB} - M_{TA}}{M_F} \times 100$$

Where M_F, M_{TB}, and M_{TA} are the frozen weight, the thawed weight before removing surfacewater, and the thawed weight after surface water removal, respectively

Cooking and total losses determination

Ten grams of thawed samples were put in a polyethylene bag and cooked for 25 minutes in a water bath at 75°C until the temperature was reached 72°C. The following formulas were used to calculate cooking loss and total loss:

$$\text{Cooking loss (\%)} = \frac{\text{Raw weight - Cooking weight}}{\text{Raw weight}} \times 100$$

$$\text{Total loss} = \text{Thawing loss} + \text{Cooking loss}$$

Total Volatile Binding Nitrogen (TVB-N)

The TVBN of the tha wed NTFFs samples was measure dinstantly after 6 days of storage at 4±1Cusing a colorimetric method as defined by Mousakhani-Ganjeh*et al.* (2015).

Thiobarbituric acid reactive substances determination

The thawed NTFFs' thiobarbituric acid reactive substances content were measured using a colorimetric system, as described by Zeb and Ullah (2016).

Protein solubility

The protein solubility of the thawed NTFF was determined using the procedure stated byHe *et al.* (2015).

Color differences of NTFFs:

The thawed NTFFs sample color spacers were calculated in line with the CIE Lab method using the Hunter Lab Colorimeter in L* (lightness), a* (redness–greenness), and b* (yellowness-blue) (Colorflex, Hunter Associates laboratory, USA).

Thawing energy consumption and specific thawing energy consumption

Thawing energy consumption and specific thawing energy consumption calculated using following equations (Niazmand et al., 2020):

$$Thawing\ energy\ consumption\ (kW.h) = V \times I \times t \quad (1)$$

$$Specific\ thawing\ energy\ consumption\ (kW.h.kg^{-1}) = \frac{Thwaing\ energy\ consumption}{sample\ weight} \quad (2)$$

Where V is working electrical potential (in Volts), I is electrical current (A), t is thawing time (h)

Statistical analysis

ANOVA was conducted using the general linear regression model of SPSS (Ver.16.0, 2007) to assess variations between values. The probability degrees of $P \leq 0.05$ were significantly considered for statistical tests. All measurements and experiments were conducted in triplicate.

Results and discussion

Thawing rate

The effect of various voltages and electrodes gaps used in the HVEF process on the thawing rate is shown in Table 1. As the voltages increased, the thawing rate obviously increased for each electrode gap ($P \leq 0.05$). But at the other hand, increasing the gaps between electrodes, the thawing rate decreased at a constant voltage (10.5 kV). Thawing rate at the electrical field strength of 3.5 kV/cm (3cm electrodes gap and 10.5kV), was 2.16 times higher than that the control sample under conventional conditions (0.069 g/s and 0.032 g/s, respectively). It is worth noting that even at the low electrical field strength (1.25 kV/cm, 6cm electrodes gap and 7.5kV), an increase of approximately 1.34 times than that the control was reported. Hence, thawing beneath HVEF had a favorable influence on the process via enhancing the thawing rate, since the quality of tilapia fish fillets is less impacted by thawing time and much more quality is retained. These results are consistent with what has been stated in the previous investigations (He et al., 2013, Mousakhani-Ganji et al., 2016).

Table 1. Influence of voltage and gap on *the* thawing rate, thawing loss, drip loss, evaporation loss, cooking loss and total loss of tilapia fish fillets

Gap (cm)	Voltage (Kv)	Electrical field strength	Thawing rate (g/s)	Evaporation loss (%)	Drip loss (%)	Thawing loss (%)	Cooking loss (%)	Total loss (%)
3	4.5	1.5	0.049±0.01^{bc}	0.68±0.15^{d}	0.56±0.09^{cd}	1.46±0.32^{c}	18.60±1.21^{c}	20.06±1.03^{c}
	7.5	2.5	0.058±0.02^{ab}	1.09±0.42^{b}	0.74±0.12^{b}	1.98±0.29^{b}	20.74±0.97^{a}	22.72±1.44^{a}
	10.5	3.5	0.069±0.01^{a}	1.27±0.58^{a}	0.72±0.16^{b}	2.14±0.33^{b}	20.05±1.16^{a}	22.19±1.65^{a}
4.5	6.0	1.33	0.045±0.03^{c}	0.76±0.21^{c}	0.49±0.10^{d}	1.53±0.39^{c}	18.13±1.33^{c}	19.66±1.32^{d}
	10.5	2.33	0.056±0.02^{b}	1.06±0.53^{b}	0.76±0.19^{b}	1.96±0.46^{b}	20.69±0.99^{a}	22.65±1.39^{a}
	13.5	3.00	0.066±0.03^{a}	1.19±0.44^{a}	0.71±0.08^{b}	2.03±0.52^{b}	19.92±1.32^{b}	21.95±0.99^{b}
6.0	7.5	1.25	0.043±0.04^{c}	0.64±0.21^{d}	0.61±0.13^{c}	1.51±0.38^{c}	18.11±1.52^{c}	19.62±1.29^{d}
	10.5	1.75	0.051±0.01^{b}	0.65±0.19^{d}	0.62±0.16^{c}	1.54±0.29^{c}	20.62±1.12^{a}	22.16±1.38^{a}
	14.0	2.33	0.055±0.02^{ab}	1.07±0.54^{b}	0.76±0.14^{b}	1.97±0.51^{b}	20.35±1.08^{a}	22.32±1.52^{a}
Control		---	0.032±0.01^{d}	0.65±0.11^{d}	1.73±0.63^{a}	3.31±0.63^{a}	16.04±1.66^{d}	19.35±1.40^{d}

Means in same column with different small letters are significantly different ($P \leq 0.05$)

The ions formed in the tiny region surrounding the needle electrodes are accelerated by the electrical field, and the generated movement is transferred from the ionized air particles to uncharged air molecules and generates the corona winds, which propels the bulk fluid to the surface. In this instance, the bulk fluid interferes with the surface, causing disturbance on the surface's boundary layer and, as a result, increasing the heat transfer coefficient (Goodenough et al., 2007). As a result, the time necessary for thawing the frozen tilapia fish fillets is reduced.

Evaporation, drip, thawing, cooking, and total losses

In this work, five types of losses were calculated to investigate the impacts of varying voltages and electrode gaps on the quality of HVEF-thawed NTFFs.The results revealed that as the applied voltage was raised, evaporation loss rose; however, when the electrode gap was reduced for a fixed voltage, evaporation loss increased. The samples thawed in HVEF at 1.75 kV/cm (6cm electrode gap and 10.5kV) revealed the same evaporation loss as the ones thawed under ordinary conditions (control specimen). At 4.5 and 6 cm electrode gap, raising the voltage resulted in a small increase in evaporation loss. The thawing and drip losses values reduced by increasing the electric field intensity from 1.25 to 1.5 kV/cm, and then marginally raised at 3.5 kV/cm. However, at the same voltage, there were no significant variations between the electrode gaps of 3 cm and 4.5 cm. As may be observed, the control showed greater losses than the HVEF treatment (Table 1).

Cooking loss was smaller in the control group compared to the HVEF treatments. It increased considerably ($P \leq 0.05$) with increasing electric field strength, with 2.5 kV/cm electric field strength showing the greatest cooking loss at each electrode gap. Cooking and total losses rose as voltage rose, but there were no substantial increases at any of the electrode gaps. The increased water release during heating in the HVEF-treated samples is thought to be due to protein denaturation (Bouton and Harris, 1972). Protein solubility was observed to decrease with increasing voltage at all electrode spacing and decreasing electrode distance at a constant voltage (Mousakhani -Ganjeh et al., 2015). Denatured proteins lose their capacity to hold water, with a tiny fraction lost after thawing process and a significant percentage lost during cooking.

TVB-N

Bacteria and enzymes breakdown proteins in animal-derived foods, producing amines, ammonia, and other alkaline nitrogenous compounds that may be measured using the TVB-N content. As a result, the TVB-N value is a useful measure of fish freshness. TVB-N at a concentration of 20mg N/100g fish meat is suggested for rejection.The findings show that as the electric field strength increased, the rate of TVB-N changes decreased (Fig. 3). The control sample's changes in TVB-N values were slightly higher (81.17 percent) than those in the HVEF-thawed samples (Fig. 3). Changes in TVB-N values after 6 days of storage decreased with increased voltage at all electrode distances, as seen in Fig. 3. At a constant voltage (10.5 kV), narrower electrode gaps resulted in lower increases in TVB-N values. The removal of microbial load, as well as the formation and release of negative ions in the air, are some of the processes by which the corona influences product quality(MousakhaniGanjeh et al., 2015).

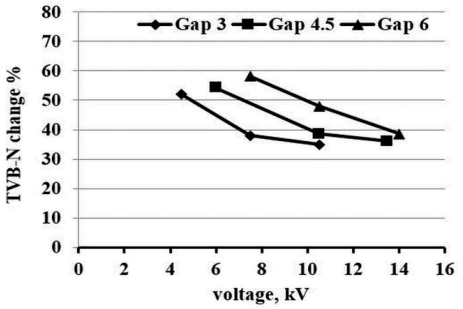

Figure 3. Changes in TVB-N of frozen tilapia fish fillets after thawing in different voltages and gaps.

The HVEF corona might have an impact on product quality by reducing microbial contamination as well as producing and releasing air ions negative charge (IANC) and ozone (Song et al., 2000). Ozone and IANC would prevent or eliminate spoilage and harmful bacteria, resulting in less degradation of fresh items (Starik et al., 2016 and Papachristodoulou et al., 2018). HVEF treatment will minimize TVB-N yield, allowing thawed Tilapia fillets to be stored for longer.

TBA

Malone aldehyde difference in thawed frozen tilapia fish fillets during cold storage is seen in Fig. 4. The findings show that as the applied voltage was increased, Malone aldehyde increased dramatically ($P \leq 0.05$). MDA levels have increased as storage time in the refrigerator at 4°C increased. Furthermore, the entire voltage electrode distances studied showed a growing pattern in these improvements. As a result of the reduced electrode distance, lipid oxidation during storage was more severe with rising voltage. However, when the electrode gap was raised with a constant voltage (10.5 kV) during the trial, lipid oxidation decreased. On days 0, 2, 4, and 6, the highest TBA values were 1.59, 1.81, 2.24, and 2.55 times greater than those recorded for the control at a voltage of 10.5 kV and a distance of 3 cm, respectively. It's possible that the high energy released during HVEF thawing causes lipid oxidation to occur. Lipid oxidation, as well as the formation and release in negative ions of air, are all involved in the influence of corona on product consistency. High levels of negative ions in the environment cause oxidation of the sample surface and taste degradation. The effect of electrical voltages producing air ionization may be the reason for this phenomenon.

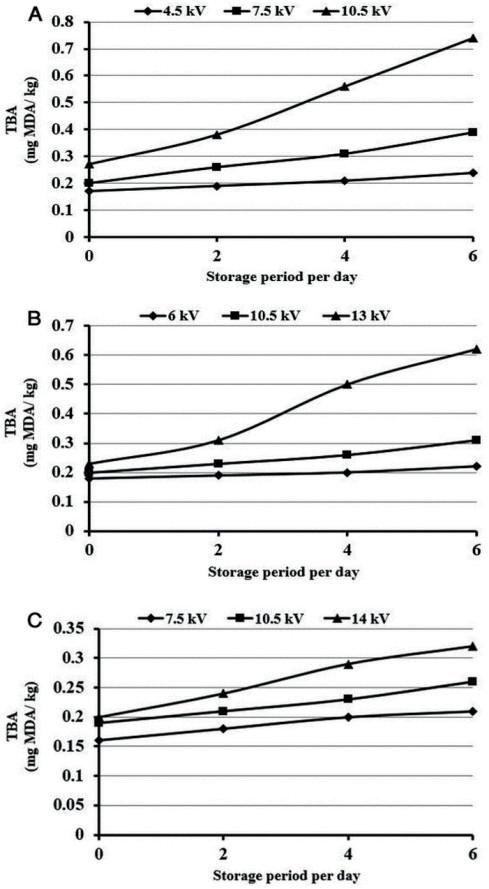

Fig. 4. Changes in TBA values during storage of frozen tilapia fish fillets thawed with different voltages, 3cm (A), 4.5cm (B), and 6cm (C) gaps.

Protein solubility

Protein denaturation can be assessed using a variety of measures. Measuring protein solubility is one of the most general. As seen in Table 2, protein solubility decreased as voltage increased, suggesting that higher voltages resulted in further protein denaturation. With a starting voltage of corona equal to that of air thawed samples (80.02 mg protein/g sample), the highest protein solubility was obtained. The effect of electrode distance on protein denaturation is also seen in the results. Reduced electrode gap has a detrimental effect on protein solubility, resulting in increased denaturation of proteins at constant voltage due to the lower effect of corona at higher electrode gaps. As a result, voltages greater than 10.5 kV generated the greatest influence of corona on protein solubility. The development of negative ions in the air during the application of HVEF appears to be a major factor in protein denaturation.Protein secondary and tertiary structures may be altered, resulting in decreased protein solubility. The thiol group of cysteine is converted to disulfide by the negative ions in the air. Disulfide crosslinks form, which denature the protein and alter its solubility (Cataldo, 2003). Protein solubility is reduced to a greater degree at lower electrode distances and higher voltages when more negative ions of the air are released.

Color differences of NTFFs

Consumers generally equate color with product freshness, improved taste, and higher quality, according to studies of seafood products. L* (lightness), a* (redness–greenness), and b* (yellowness–blueness) values were used to measure fish color in this analysis (He et al., 2013). Table 2 illustrates how variations in voltage and electrode difference affect the color parameters L*, a*, and b*. With increases in applied voltage and electrode distance, the values of a* and b* decreased. The L* values in the test sample were slightly smaller than those in the samples thawed at voltages greater than 10.5 kV. The changes in color parameters can in any way be linked to the development of ozone during the HVEF phase. The results of ozonation on the color parameters of Mackerel surimi were studied by Jiang et al. (1998). They also discovered that ozonation improved the L* value in surimi because the porphyrin ring was oxidized.

Table 2. Influence of voltage and gap on the protein solubility and colour parameters of tilapia fish fillets

Gap (cm)	Voltage (Kv)	Electrical field strength	Protein solubility (%)	Colour parameters		
				L*	a*	b*
3	4.5	1.5	81.03±1.02^{a}	49.44±1.82^{c}	2.60±0.49^{b}	18.43±1.06^{b}
	7.5	2.5	77.96±1.32^{d}	50.46±1.62^{b}	2.55±0.56^{c}	16.69±1.14^{d}
	10.5	3.5	71.84±1.41^{e}	51.50±1.10^{a}	2.52±0.82^{c}	15.03±1.27^{e}
4.5	6.0	1.33	82.16±1.33^{a}	49.26±1.94^{c}	2.61±0.99^{b}	18.96±1.22^{ab}
	10.5	2.33	79.35±1.46^{c}	50.23±1.77^{b}	2.56±.45^{c}	17.24±1.39^{c}
	13.5	3.00	72.15±1.52^{e}	50.98±1.40^{a}	2.54±0.71^{c}	15.75±1.20^{e}
6.0	7.5	1.25	82.19±1.30^{a}	48.61±1.71^{cd}	2.63±0.64^{b}	19.14±1.18^{a}
	10.5	1.75	80.0±1.51^{b}	49.69±1.66^{c}	2.58±0.50^{bc}	17.82±1.32^{c}
	14.0	2.33	79.35±1.29^{c}	50,21±1.58^{b}	2.56±0.62b^{c}	17.23±1.51^{c}
Control		---	80.02±1.73^{b}	50.58±1.79^{b}	2.94±0.55^{a}	19.07±1.98^{a}

Means in same column with different small letters are significantly different ($P \leq 0.05$)

Specific thawing energy consumption

Table 3 shows the influence of high voltage and gap on the energy consumption and specific energy consumption during frozen tilapia fish fillets thawing process. The results indicate that specific thawing energy consumption (Watt.h/kg) significantly increased with increasing applied voltage (P≤0.05). Furthermore, these changes took an increasing trend for all the voltage electrode distances examined. The highest specific thawing energy consumption values obtained at a voltage of 14 kV and a gap of 6 cm was 37.94 Watt.h/kg, combared with other investigated samples.

Table 3. Influence of high voltage and gap on the energy consumption and specific energy consumption

Gap, cm	High voltage, kV	Input power to power supply, Watt	Thawing time, h	Thawing energy consumption Watt.hr	Specific thawing energy consumption Watt.h/kg
3	4.5	2.55f	0.57ab	1.45f	14.54f
	7.5	3.96d	0.48c	1.90e	19.01e
	10.5	5.46c	0.40c	2.18d	21.84d
4.5	6	3.04e	0.62a	1.88e	18.85e
	10.5	5.46c	0.50b	2.73c	27.30b
	13.5	6.9b	0.42c	2.90b	28.98b
6	7.5	3.96d	0.65a	2.57c	25.74c
	10.5	5.46c	0.54b	2.95b	29.48b
	14	7.44a	0.51bc	3.79a	37.94a

Means in same column with different small letters are significantly different (P ≤ 0.05)

Conclusion

In the food sector, high voltage electric field (HVEF) has recently been regarded a novel thawing technique. The variance in the quality was compared between frozen tilapia fish fillets thawed by high voltage electrostatic field (HVE) and those thawed conventionally as control. The results revealed that thawing under HVEF greatly enhances the thawing rates of frozen tilapia fish fillets and their TVB-N values. In general, thawing frozen tilapia fillets using a high voltage electrostatic field can not only speed up the process, but also improve the quality of the fish..HVEF achieved at a voltage of 10.5 kV and an electrode gap of 3 cm is the optimum choice based on thaw rate and quality parameters.

Author contributions

Atef Mohamed Elsbaay: Conceptualization, Data curation, Formal analysis, Investigation, Methodology, Validation, Writing - original draft, Writing - review & editing.

Asmaa A. Elattar: Conceptualization, Data curation, Formal analysis, Investigation,Methodology, Writing - original draft.

Rowida Younis Essa: Data curation, Formal analysis, Investigation, Methodology, Software, Validation, Writing - original draft, Writing - review & editing.

Conflict of Interest

The authors have declared no conflicts of interest for this article.

References

1. Alem-Rajabif, A., & Lai, F. C. (2005). EHD-enhanced drying of partially wetted glass beads. *Drying Technology*, *23*(3), 597-609.
2. Ali, S., Zhang, W., Rajput, N., Khan, M. A., Li, C. B., & Zhou, G. H. (2015). Effect of multiple freeze-thaw cycles on the quality of chicken breast meat. *Food Chemistry*, 173(1), 808-814.
3. Bouton, P. E., Harris, P. V. (1972). The effect of cooking temperature and time on some mechanical properties of meat. *J. Food Sci.* 37,140–144.
4. Bozkurt, H., & Icier, F. (2012). Ohmic thawing of frozen beef cuts. *Journal of Food Process Engineering*, *35*(1), 16-36.Cataldo, F. (2003). On the action of ozone on proteins. *Polymer Degradation and Stability*, *82*(1), 105-114.
5. Ding, C., Ni, J., Song, Z., Gao, Z., Deng, S., Xu, J., &Bai, Y. (2018). High-voltage electric field-assisted thawing of frozen tofu: Effect of process parameters and electrode configuration. *Journal of Food Quality*, *2018*.
6. Drdóñez, J. A., Rodrigues, C. O. M., Álvarez, F. L., Sanz, G. L. M., Minguillón, F. G. G., Perales, H. L., &Cortecero, S. D. M. (2005). *Tecnologia de alimentos: alimentos de origem animal* (Vol. 2). Porto Alegre: Artmed.
7. Elsebaie, E. M., Younis, E. R., &Elsbaay, A.M. (2021). Impact of atmospheric cold Plasma (ACP) on maintaining bolti fish (Tilapia nilotica) freshness and quality Criteria during cold storing. Journal of Food Processing and Preservation, e15442.

8. Evangelista, J. (2008). *Tecnologia de alimentos* (2. ed.). São Paulo: Atheneu.
9. FAO .(2012). Cultured Aquatic Species Information Programme. Text by Rakocy, J. E. In: FAO Fisheries and Aquaculture Department [online]. Rome. [Cited 11 September 2012].
10. FAO. (2014). Web-based Reporting System for the Questionnaire on the Implementation of the Code of Conduct for responsible Fisheries. In: FAO Fisheries and Aquaculture Department[online]. Rome. [Cited 12 March 2014].
11. GAFRD. (2016). "General Authority of Fish Resources Development". Fish Statics Year Book. Ministry of agriculture, Egypt.
12. Goodenough, T. I., Goodenough, P. W., &Goodenough, S. M. (2007). The efficiency of corona wind drying and its application to the food industry. *Journal of food Engineering*, *80*(4), 1233-1238.
13. He, F.-Y., Kim, H.-W., Hwang, K.-E., Song, D.-H., Kim, Y.-J., Ham, Y-.K., Kim, C. (2015). Effect of ginger extract and citric acid on the tenderness of duck breast muscles. *Korean journal for food science of animal resources, 35*(6), 721 .
14. He, X., Liu, R., Nirasawa, S., Zheng, D., & Liu, H. (2013). Effect of high voltage electrostatic field treatment on thawing characteristics and post-thawing quality of frozen pork tenderloin meat. *Journal of Food Engineering*, *115*(2), 245-250.
15. He, X., Liu, R., Tatsumi, E., Nirasawa, S., & Liu, H. (2014). Factors affecting the thawing characteristics and energy consumption of frozen pork tenderloin meat using high-voltage electrostatic field. *Innovative Food Science & Emerging Technologies*, *22*, 110-115.
16. Jiang, S.T., Ho, M.L., Jiang, S.H., Lo, L., & Chen, H.C.(1998). Color and quality of mackerel surimi as affected by alkaline washing and ozonation. *Journal of Food Science*, *63*(4), 652-655.
17. Llave, Y., Liu, S., Fukuoka, M., & Sakai, N. (2015). Computer simulation of radiofrequency defrosting of frozen foods. *Journal of Food Engineering*, *152*, 32-42.
18. Mousakhani-Ganjeh, A., Hamdami, N., &Soltanizadeh, N. (2015). Impact of high voltage electric field thawing on the quality of frozen tuna fish (Thunnusalbacares). *Journal of Food Engineering*, *156*, 39-44.
19. Mousakhani-Ganjeh, A., Hamdami, N., Soltanizadeh, N. (2016). Thawing of frozen tuna fish (Thunnusalbacares) using still air method combined with a high voltage electrostatic field. J. Food Eng. 169, 149–154.
20. Niazmand, R., Jahani, M., Sabbagh, F., &Rezania, S. (2020). Optimization of Electrocoagulation Conditions for the Purification of Table Olive Debittering Wastewater Using Response Surface Methodology. *Water*, *12*(6), 1687.
21. Ninan, G., &Zynudheen, A. A. (2014). Evaluation of quality and shelf life of two commercially important fish species viz., tiger tooth croaker (Otolithesruber Bloch and Schneider) and flathead grey mullet (Mugilcephalus Linnaeus) in iced conditions. *Proceedings of the National Academy of Sciences, India Section B: Biological Sciences*, *84*(4), 1035-1042.
22. Orlowska, M., LeBail, A., &Havet, M. (2014). Electrofreezing, Ohmic Heating in Food Processing.
23. Papachristodoulou, M., Koukounaras, A., Siomos, A. S., Liakou, A., &Gerasopoulos, D. (2018). The effects of ozonated water on the microbial counts and the shelf life attributes of fresh-cut spinach. *Journal of Food Processing and Preservation*, 42(1).
24. Shoemaker, C. A., Klesius, P. H., & Evans, J. J. (2000, September). Diseases of tilapia with empasis on economically important pathogens. In *Proceedings of the 5th International Symposium on tilapia Aquaculture*.
25. Silva, T. M., Sabaini, P. S., Evangelista, W. P., & Gloria, M. B. A. (2011). Occurrence of histamine in Brazilian fresh and canned tuna. *Food Control*, *22*(2), 323-327.
26. Singh, A., Orsat, V., &Raghavan, V. (2012). A comprehensive review on electrohydrodynamic drying and high-voltage electric field in the context of food and bioprocessing. *Drying Technology*, *30*(16), 1812-1820.
27. Song, J., Fan, L., Hildebrand, P. D., & Forney, C. F. (2000). Biological effects of corona discharge on onions in a commercial storage facility. *Hort Technology,* 3(10),608–612.
28. Starik, A. M., Savelieva, V. A., Sharipov, A. S., &Titova, N. S. (2016). Enhancement of hydrogen sulfide oxidation via excitation of oxygen molecules to the singlet delta state. *Combustion and Flame,*170,124–134.
29. TaghianDinani, S., Havet, M., Hamdami, N., &Shahedi, M. (2014). Drying of mushroom slices using hot air combined with an electrohydrodynamic (EHD) drying system. *Drying Technology*, *32*(5), 597-605.
30. Uyar, R., Bedane, T. F., Erdogdu, F., Palazoglu, T. K., Farag, K. W., &Marra, F. (2015). Radio-frequency thawing of food products–A computational study. *Journal of Food Engineering*, *146*, 163-171.
31. Wang, H., Luo, Y., Shi, C., &Shen, H. (2015). Effect of different thawing methods and multiple freeze-thaw cycles on the quality of common carp (Cyprinuscarpio). *Journal of aquatic food product technology*, *24*(2), 153-162.
32. Yitayew, T. (2012). The effect of storage temperature and time on bacteriological load and physicochemical quality of Nile tilapia (*Oreochromisniloticus*) fillet from Lake Tana, Ethiopia. M. Sc. Thesis, Addis Ababa University, Ethiopia.
33. Zeb, A., &Ullah, F. (2016). A simple spectrophotometric method for the determination of thiobarbituric acid reactive substances in fried fast foods. *Journal of analytical methods in chemistry*.
34. Zhang, Y., & Ding, C. (2020). The Study of Thawing Characteristics and Mechanism of Frozen Beef in High Voltage Electric Field. *IEEE Access*, *8*, 134630-134639.

ISSN print: 1224-5984
ISSN online: 2248-3942

Rom Biotechnol Lett. 2022; 27(1): 3208-3214
doi: 10.25083/rbl/27.1/3208-3214

Received for publication, January, 04, 2022
Accepted, February, 10, 2022

Original paper

Antilipase, antiacetylcholinesterase and antioxidant activities of Moringa oleifera extracts

UMAR FARUK MAGAJI[1,2], OZLEM SACAN[1], REFIYE YANARDAG[1]

[1] Istanbul University- Cerrahpasa, Faculty of Engineering, Department of Chemistry, Biochemistry Section, 34320 Avcilar - Istanbul/Turkey.
[2] Federal University Birnin Kebbi, Department of Biochemistry and Molecular Biology, 1157 Birnin Kebbi - Kebbi State/Nigeria.

Abstract Pancreatic lipase is critical for the catabolism of lipids in the intestine, making it a prime target for obesity management. Acetylcholinesterase is an important enzyme that hydrolyses the neurotransmitter acetylcholine. It inhibition is paramount in enhancing systemic acetylcholine level. Side effects of conventional drugs lead to continued search for alternative anti-obesity and anticholinesterase agents. The present study assessed lipase and acetylcholinesterase inhibition, as well as antioxidant activity of *Moringa oleifera* extracts. The inhibitory activities of the extracts on lipase and acetylcholinesterase were dose dependent. Aqueous leaf extract (IC_{50} = 3.26 ± 0.26 mg/ml) and hexane root extract (IC_{50} = 0.08 ± 0.00 mg/ml) exhibited the highest antilipase and antiacetylcholinesterase activity respectively. Aqueous extracts of root and leaf (IC_{50} of 1.43 ± 0.03 mg/ml and 1.86 ± 0.10 mg/ml respectively) had the highest N, N-dimethyl-p-phenylene diamine dihydrochloride radical scavenging activity, while ethyl acetate leaf extract had the highest nitrite scavenging activity (IC_{50} = 2.20 ± 0.06 mg/ml). Compared to other extracts, methanol leaf extract exhibited the highest ferric reducing power. These findings suggest that *M. oleifera* possess promising antilipase, antiacetylcholinesterase and antioxidant potentials. Therefore, may be employed as food additive for the management of obesity, Alzheimer and other degenerative diseases.

Keywords Acetylcholinesterase, Alzheimer, antioxidant, lipase, Moringa, obesity

To cite this article: MAGAJI UF, SACAN O, YANARDAG R. Antilipase, antiacetylcholinesterase and antioxidant activities of *Moringa oleifera* extracts. *Rom Biotechnol Lett*. 2022; 27(1): 3208-3214. DOI: 10.25083/rbl/27.1/3208-3214.

✉ *Corresponding author: REFIYE YANARDAG, Istanbul University- Cerrahpasa, Faculty of Engineering, Department of Chemistry, Biochemistry Section, 34320 Avcilar - Istanbul/Turkey.
E-mail: yanardag@iuc.edu.tr

Introduction

Obesity is a life style disorder characterised by low body mass index. It is general associated with insulin resistance, hyperlipidaemia, coronary heart diseases, apoplexy, cancer of colon, social discrimination and depression[1]. The management of obesity and treatment of its accompanying morbidity are important 21st century public health challenge. Common regimen in the management of obesity involves suppressing food consumption, increasing energy expenditure, down regulation of lipocyte proliferation and pancreatic lipase (central for digestion of triglycerides in small intestine) inhibition. However, euphoric action, addiction, loss of appetite, risk of haemorrhage stroke and valvular heart disease, pulmonary hypertension, stimulant effect and gastrointestinal complications are common side effects associated with drugs used in this regimens[2-5]. These complications have led to the continuing search for natural anti-obesity agents, especially diet based lipase inhibitors[6].

Alzheimer is a neurological disease associated with memory loss, behavioural defects and disorientation. A generalised and progressive loss of nerve cells and brain function leading to dementia is observed among aged and young patients[7]. The most common agents used for Alzheimer management involves the inhibition of acetylcholinesterase. They prevent the hydrolysis of acetylcholine, thereby retaining higher systemic levels of acetylcholine especially at the synapses, and ultimately enhancing the transmission of nerve impulse[8]. Therefore, the continued search for acetylcholinesterase inhibitors and anti-Alzheimer agents remains indispensable.

Excessive free radical production and compromised antioxidant system may result to deleterious outcome such as mutagenesis, neurological disorders, cardiovascular dysfunction, and premature aging[9,10]. Plants are known to be excellent sources of compounds with remarkable antioxidant activities. A typical example is the ability of flavonoids and phenolic compounds to scavenge nitrites capable of oxidising haemoglobin to methaemoglobin or cause anaemia[11-13]. In addition, phytochemicals especially carotenoid, polyphenol, flavonoid, saponin, terpene and glycoside compounds are shown to be enzyme inhibitors, exhibit wound healing, regenerative, anti-inflammatory, antioxidants as well as antitumor activity. Consumption of plants rich in these compounds is positively correlated with lower degenerative diseases, low pathological defects and improved wellbeing[14,15].

Moringa oleifera is the commonest specie among 13 cultivars of *Moringaceae* family, due to its phytochemical and pharmacological properties. It is commonly consumed as food or as food additive in Africa and Asia. All the plant parts are used for various therapeutic and industrial purposes. Common therapeutic benefits of the plant include wound healing, treatment of inflammations and ulcers, cardio-vascular diseases, gastrointestinal disturbances, hepatorenal complications, haematological disorders, act as an antiplasmodic, antimicrobial and cytotoxic agent[16]. In present study, leaf, seed and root extracts of *M. oleifera* (aqueous, methanol, ethyl acetate and hexane) were assessed for pancreatic lipase and acetylcholinesterase inhibition, as well as antioxidant activity ($DMPD^+$ radical scavenging activity, nitrite scavenging activity and ferric reducing power).

Materials and Methods

Sample collection and preparation

Various parts of *M. oleifera* collected from North-West Nigeria, were extracted as reported by Magaji *et al*., the lyophilised aqueous extracts and residues of organic extracts were stored in Eppendorf tubes at -20 °C until use[17].

Lipase inhibition test

Pancreatic lipase was prepared by dissolving 10 mg/ml of pig pancreatic type II lipase (Sigma, L3126) in Tris-HCl buffer (0.1 M; pH 8.5), followed by centrifugation for 10 minutes at -4 °C and 7000 × g so as to obtain a clear supernatants[18]. Lipase activity was assayed spectrophotometrically via hydrolysis of 4-nitrophenyl caprate (4-NPC) to 4-nitrophenol. Briefly, reaction solution containing 5 µl of moringa extract (in DMSO) as inhibitor, 10 µl of lipase (10 mg/ml) and 200 µl of 0.1 M Tris-HCl buffer solution of pH 8.5 was incubated at 37 °C for 25 minute, after which 5 µl 4-NPC (5 mM) was added. Absorbance was read against reagent blank at 405 nm after incubation at 37 °C for 15 minute using a microplate reader[19]. Orlistat was used as standard inhibitor of lipase in this study. The percentage lipase inhibition was calculated as follows:

$$\% \text{ Lipase inhibition} = [1 - (Absorbance\ of\ Test/Absorbance\ of\ Control)] \times 100$$

Acetylcholinesterase inhibition test

The modified method of Ingkaninan *et al*. was employed for assaying acetylcholinesterase activity[20]. Briefly, 20 µl of inhibitor, 40 µl of 0.1 M Tris-HCl (pH 8.0), 100 µl of 3 mM 5,5'-dithiobis-(2-nitro-benzoic acid) and 20 µl of 15 mM acetylthiocholine iodide were added into a microplate and mixed. Thereafter, 20 µl of 0.28 U/ml acetylcholinesterase (Sigma, C3389-2KU) was added and incubated for 2 minutes at 37 °C. Absorbance was read at 405 nm against reagent blank. Tacrine was used as standard inhibitor of the enzyme. Percentage enzyme inhibition was calculated as shown below:

$$\% \text{ Acetylcholinesterase inhibition} = [1 - (Absorbance\ of\ Test/Absorbance\ of\ Control)] \times 100$$

Antioxidant assay

$DMPD^+$ radical scavenging test

$DMPD^+$ scavenging activity was analysed by incubating 0.1 ml test solution in 2.0 ml radical solution; composed of 1 ml of 100 mM DMPD, 100 ml acetate buffer

(0.1 M, pH 5.25) and 0.2 ml ferric chloride (0.05 M). After 10 minutes incubation in a dark cupboard, optical density (OD) was measured at 505 nm against acetate buffer[21]. The standard antioxidant used was L (+) ascorbic acid. The $DMPD^+$ scavenging effect was evaluated as follows:

$$\% \text{ DMPD}^+ \text{ scavenged} = [1 - (Absorbance\ of\ Test/Absorbance\ of\ Control)] \times 100$$

Nitrite scavenging assay

The method of Choi *et al*. was adapted for this assay[12]. A 0.1 ml of extract (in DMSO), 0.1 ml of 1 mM $NaNO_2$, 0.2 ml of 0.1 N HCl and 0.6 ml distilled water were vigorously mixed and kept for 3 hours at 37 °C. Then 0.5 ml of 2% acetic acid and 40 µl Griess reagent was thereafter added, shaken and kept in dark cardboard for 15 minute at 37 °C. Optical density was read spectrophotometrically at 540 nm. Quercetin was employed as standard control. The percentage nitrite scavenged was calculated as follows:

$$\% \text{ Nitrite scavenged} = [1 - (Absorbance\ of\ Test/Absorbance\ of\ Control)] \times 100$$

Ferric reducing power assay

To 0.1 ml test solution, 0.25 ml of 0.2 M phosphate buffer (pH 6.6) and 0.25 ml of 1% $K_3[Fe(CN)_6]$ were added and left to stand for 30 minutes at 50 °C. At 3000 rpm, the mixture was centrifugation for 10 minutes after adding 0.25 ml 10% TCA. To 0.25 ml of the supernatant, equal volume of distilled water and 0.05 ml of 0.1% $FeCl_3$ was added, and then incubated for 10 minutes in dark. Thereafter, absorbance was monitored at 700 nm[22]. Quercetin and ascorbic acid were employed as standard for the reducing test.

Statistical Analysis

Using regression analysis data, half maximum inhibition/scavenging concentration (IC_{50}) was calculated from % enzyme inhibition activities and % antioxidant activities (for $DMPD^+$ and nitrite scavenging). IC_{50} values are inversely correlated to inhibition/antioxidant activities. Results of ferric reducing power are presented as OD of test solution.

Results and discussion

Lipase inhibition

The inhibition activities of moringa extracts on pancreatic lipase are presented in Table 1. The inhibition activities were dose dependent. The highest lipase inhibition corresponding to IC_{50} of 3.26 ± 0.26 mg/ml was exhibited by aqueous leaf extract. This was closely followed by ethyl acetate leaf extract (IC_{50} = 4.73 ± 0.09 mg/ml), methanol seed extract (IC_{50} = 5.01 ± 0.03 mg/ml), hexane leaf extract (IC_{50} = 5.42 ± 0.33 mg/ml) and then aqueous seed extract (IC_{50} = 5.77 ± 0.24 mg/ml). The extracts with lowest lipase inhibition are: methanol leaf (IC_{50} = 7.68 ± 0.60 mg/ml) > aqueous root (IC_{50} = 11.97 ± 0.22 mg/ml) > hexane root (IC_{50} = 18.37 ± 0.47 mg/ml) > ethyl acetate root (IC_{50} = 19.11 ± 0.91 mg/ml). Contrary, both ethyl acetate and hexane seed extracts as well as methanol root extract did not exhibit lipase inhibitory effect. Orlistat which was used as standard had a remarkably high lipase inhibition of IC_{50} = 0.001 ± 6.81×10^{-5} mg/ml. Previous study indicates that red-pericarp mutant rice bran extracts inhibited lipase with IC_{50} value of between 35.95 to 35.97 mg/ml[23]. A 10 mg/ml of *Everniastrum cirrhatum* methanol extract gave an approximately 40 % inhibition of pancreatic lipase activity[24]. Also, report by Toma *et al*. showed that the IC_{50} of aqueous-ethanol *M. stenopetala* leaves extract was more than 5 mg/ml[25]. These findings are similar to the present study in which IC_{50} ranged between 3.26 mg/ml to 19.11 mg/ml. The overall lipase inhibition effect of Moringa can be credited to the rich phytochemical constituents of the plant extracts e.g. quercetin, caffeic acid, kaempferol, rutin, myricetin etc, or their various derivatives previously isolated from other plants and confirmed to exhibit pancreatic lipase inhibition[26-30].

Acetylcholinesterase inhibition

In Table 1, the acetylcholinesterase inhibition activity of moringa extracts are presented. Hexane root extract exhibited the highest acetylcholinesterase inhibition (IC_{50} = 0.08 ± 0.00 mg/ml), and was closely accompanied by aqueous leaf extract (0.10 ± 0.00 mg/ml), ethyl acetate leaf extract (0.10 ± 0.01 mg/ml), aqueous seed extract (0.10 ± 0.00 mg/ml), methanol leaf extract (0.10 ± 0.01 mg/ml), aqueous root extract (0.12 ± 0.01 mg/ml), methanol seed extract (0.12 ± 0.00 mg/ml) and ethyl acetate seed extract (0.13 ± 0.02 mg/ml). The least inhibition was observed in hexane extract of seed and leaf (0.21 ± 0.03 and 0.31 ± 0.01 mg/ml respectively). Methanol and ethyl acetate extract of root showed no inhibition activity. Tacrine had an exceptional inhibition with IC_{50} of 0.002 ± 6.96×10^{-5} mg/ml. Studies indicate that *Gentiana kurroo*[31] and *Areca catechu* L.[32] had neuroprotective effects and enhanced learning/memory ability. Also, *Withania somnifera* was shown to alleviate Alzheimer disease by inhibiting acetylcholinesterase with IC_{50} value of 0.00035 mM[33]. Sutalangka *et al*. demonstrated that that leaves extract of *M. oleifera* decreased malondialdehyde level and acetylcholinesterase activity of rat hippocampus tissue and increased antioxidant enzymes activities. Thus suggesting the plant had neuroprotective and memory enhancing effect[34]. Reports by Adefegha *et al*. indicates that aqueous extract of Moringa seed had inhibitory effect on acetylcholinesterase (IC_{50} =0.27 mg/ml) [35]. Similarly, Ghous *et al*. reported that methanol shoot extracts of Moringa had IC_{50} of 77.58 µg/ml on acetylcholinesterase activity[36]. These findings agree with the present studies where all parts of Moringa were found to exhibit promising antiacetylcholinesterase activity. Therefore supporting it uses as fold medicine for management and delaying the progression of Alzheimer disease in Northern Nigeria.

Table 1. Lipase and Acetylcholinesterase Inhibitory Activity of Moringa Extracts

Extract/Standard	Lipase (IC_{50}; mg/ml)*	Acetylcholinesterase (IC_{50}; mg/ml)*
Aqueous leaf extract	3.26 ± 0.26	0.10 ± 0.00
Methanol leaf extract	7.68 ± 0.60	0.11 ± 0.01
Ethyl acetate leaf extract	4.73 ± 0.09	0.10 ± 0.01
Hexane leaf extract	5.42 ± 0.33	0.31 ± 0.01
Aqueous root extract	11.97 ± 0.22	0.12 ± 0.01
Methanol root extract	ND	ND
Ethyl acetate root extract	19.11 ± 0.91	ND
Hexane troot extract	18.37 ± 0.47	0.08 ± 0.00
Aqueous seed extract	5.77 ± 0.24	0.10 ± 0.00
Methanol seed extract	5.01 ± 0.03	0.12 ± 0.00
Ethyl acetate seed extract	ND	0.13 ± 0.02
Hexane seed extract	ND	0.21 ± 0.03
Orlistat	$0.001 \pm 6.81\times10^{-5}$	-
Tacrine	-	$0.002 \pm 6.96\times10^{-5}$

*Mean ± SD of three replicate values; ND= Activity Not Detected

Antioxidant activity

The antioxidant activity of Moringa extracts are presented in Table 2. Amongst the extracts, aqueous extract of root and leaf had the highest DMPD radical scavenging activity with IC_{50} of 1.43 ± 0.03 mg/ml and 1.86 ± 0.10 mg/ml respectively. With an IC_{50} of 3.09 ± 0.19 mg/ml, aqueous seed extract closely followed. Extracts with comparatively moderate activity are ethyl acetate root (IC_{50} = 6.12 ± 0.34 mg/ml), methanol root (IC_{50} = 6.27 ± 0.10 mg/ml), methanol seed (IC_{50} = 7.46 ± 0.51 mg/ml) and ethyl acetate seed (IC_{50} = 13.82 ± 0.14 mg/ml). Methanol leaf extract exhibited the least scavenging activity (IC_{50} = 27.04 ± 6.18 mg/ml), while ethyl acetate extract of leaf, and the hexane extract of both leaf, root and seed did not exhibit DMPD radical mopping action. L (+) ascorbic acid had an outstanding IC_{50} value of 0.21 mg/ml. DMPD radical scavenging activity is a rapid antioxidant test based on the ability of compounds to donate hydrogen atom to $DMPD^+$, there by decolourizing the coloured radical cation formed from DMPD at acidic pH and in presence of a suitable oxidant solution. Antioxidant activity is proportional to intensity of decolouration[21]. There are no previous reports on the DMPD radical scavenging activity of *M. oleifera*. Findings of this study revealed that the Moringa extracts from polar solvents are more efficient antioxidants, with aqueous extract of all the three plant parts exhibiting higher DMPD radical scavenging activity than their methanol, ethyl acetate and hexane counterparts. This suggests that aqueous extraction was effective in abstracting antioxidant compound capable of donating hydrogen atom and possibly quenching radical/chain reaction..

Table 2. $DMPD^+$ scavenging activity, nitrite scavenging activity and ferric reducing power of moringa extracts

Extract/Standard	$DMPD^+$ Scavenging Activity (IC_{50}; mg/ml)*	Nitrite Scavenging Activity (IC_{50}; mg/ml)*	Ferric Reducing Power (O.D. at 4.0 mg/ml)
Aqueous leaf extract	1.86 ± 0.10	6.17 ± 0.01	0.47 ± 0.40
Methanol leaf extract	27.04 ± 6.18	5.06 ± 0.01	0.81 ± 0.01
Ethyl acetate leaf extract	ND	2.20 ± 0.06	0.41 ± 0.01
Hexane leaf extract	ND	7.39 ± 0.38	0.13 ± 0.00
Aqueous root extract	1.43 ± 0.03	3.19 ± 0.15	0.50 ± 0.01
Methanol root extract	6.27 ± 0.10	7.00 ± 0.75	0.48 ± 0.00
Ethyl acetate root extract	6.12 ± 0.34	7.95 ± 0.38	0.20 ± 0.01
Hexane root extract	ND	4.13 ± 0.12	0.11 ± 0.00
Aqueous seed extract	3.09 ± 0.19	34.08 ± 6.61	0.04 ± 0.01
Methanol seed extract	7.46 ± 0.51	7.63 ± 0.20	0.08 ± 0.01
Ethyl acetate seed extract	13.82 ± 0.14	ND	0.05 ± 0.00
Hexane seed extract	ND	ND	0.04 ± 0.00
L (+) Ascorbic Acid	0.21 ± 0.00	-	1.02 ± 0.00†
Quercetin	-	0.08 ± 0.00	0.93 ± 0.01†

*Mean ± SD of three replicate values; †Conc. = 0.20 mg/ml; ND= Activity Not Detected

In comparison to other extracts, ethyl acetate leaf extract, aqueous root extract and hexane root extract (with IC_{50} of 2.20 ± 0.06, 3.19 ± 0.15 and 4.13 ± 0.12 mg/ml respectively) exhibited the highest nitrite scavenging activities. Moderate scavenging activities were exhibited by methanol leaf extract (IC_{50} = 5.06 ± 0.01 mg/ml), aqueous leaf extract (IC_{50} = 6.17 ± 0.01 mg/ml), methanol root extract (IC_{50} = 7.00 ± 0.75 mg/ml), hexane leaf extract (IC_{50} = 7.39 ± 0.38 mg/ml), methanol seed extract (IC_{50} = 7.63 ± 0.20 mg/ml) and ethyl acetate root extract (IC_{50} = 7.95 ± 0.38 mg/ml). The least scavenging activity was found in aqueous seed extract (IC_{50} = 34.08 ± 6.61 mg/ml), while ethyl acetate and hexane extract of the seed had no nitrite scavenging activity at the tested extract concentration. Quercetin had superior scavenging activity with an IC_{50} of 0.08 mg/ml. Nitric oxide is an important intermediate produced by nitric oxide synthases. In human, it is an indispensable pleiotropic molecule with signalling function. It helps modulate secretion of insulin, neural and blood vessels development, peristalsis and airway tone. It also has neurotransmitter function and immune defence function[37]. As a free radical, nitric oxide reacts with superoxide anion forming peroxynitrite (a potentially cytotoxic molecule). More so, the overproduction of nitric oxide is associated with autoimmune diseases, inflammation, arthritis, diabetes, hypertension, stroke, carcinomas as well as septic shock[38-41]. Therefore regulation of tissue nitric oxide level and scavenging it is an important target in attenuation of some disease conditions[42]. Report by Aju *et al*. indicated that methanol extract of Moringa leaves had the higher scavenging action (IC_{50} = 0.32 mg/ml) when compared to hydro alcohol extract (IC_{50} = 1.46 mg/ml), while water extract had a lower activity than the former (IC_{50} = 1.50 mg/ml) [43]. However, these IC_{50} values were below those found in the present study, indicating higher nitrite scavenging activity of Moringa from Kerala compared to that used in present study.

As shown in Table 2, methanol leaf extract (at 4.00 mg/ml) exhibited the highest ferric reducing power with an OD of 0.81 ± 0.01. However, the leaf extracts reducing power was lower than that of both ascorbic acid (OD = 1.02 ± 0.00) and quercetin (OD = 0.93 ± 0.01) at 0.20 mg/ml. Other extracts with appreciably high reducing power at 4.00 mg/ml are aqueous root extract, methanol root extract, aqueous leaf extract and ethyl acetate leaf extract. Those with least scavenging activities are: ethyl acetate root extract > hexane leaf extract > hexane root extract > methanol seed extract > ethyl acetate seed extract > aqueous seed extract > hexane seed extract. These findings suggest that polar solvent had better extraction power for antioxidants present in leaves and roots. Ferric reducing power is based on capability of compounds to donate electrons, there by facilitating the reduction of ferric ions (Fe^{3+}) to ferrous ions (Fe^{2+}). The intensity of the blue colour formed is positively correlated to reducing power of test solution. A study by Pakade *et al*. indicates that *M. oleifera* cultivated in South Africa had higher ferric reducing power than common vegetables such as peas, cabbage, spinach, broccoli and cauliflower[44]. Hydro alcohol and then aqueous extract of Moringa leaves were reported to have more potent ferric reducing power than methanol extract[43]. In a separate report, Luqman *et al*. disclosed ethanol and aqueous extract of Moringa seed had higher ferric reducing power than their corresponding leaf extracts[45]. These are in contrast to the findings of this study where methanol leaf extract displayed better reducing power compared to aqueous leaf extract, and both of these leaf extracts had higher reducing power than their counterpart seed extracts.

Conclusion

The findings of the present study suggest that *M. oleifera* can serve as a dietary source of anti-obesity and acetylcholinesterase inhibitors. Coupled with the antioxidant property, the plant can serve as an alternative herb for attenuating or managing obesity, Alzheimer and other degenerative diseases if properly exploited. More so, the strong antioxidant properties of the leaf can help lessen the impact of oxidative stress and progression of degenerative diseases when employed as food additives.

Acknowledgement

Our gratitude goes to the Biochemistry Unit, Chemistry Department, Istanbul University-Cerrahpasa for providing both laboratory space and research equipment that was utilised during this experiment.

Conflict of interest

The authors declare no conflict of interest.

References

1. Aronne LJ, Classification of obesity and assessment of obesity-related health risks, *Obesity*, 10 (2002) 105–115.
2. Silverstone T, Appetite suppressants: a review, *Drugs,* 43 (1992) 820–836.
3. Gardin JM, Schumacher D & Constantine G, Valvular abnormalities and cardiovascular status following exposure to dexfenfluramine or phentermine/ fefluramine, *JAMA*, 283 (2000) 1703–1709.
4. Kernan WN, Viscoli CM & Brass LM, Phenylpropanolamine and the risk of hemorrhagic stroke, *The New England Journal of Medicine*, 343 (2000) 1826–1832.
5. Kang J & Park C, Anti-obesity drugs: a review about their effects and safety, *Diabetes & Metabolism Journal*, 36 (2012) 13-25.
6. Lunagariya NA, Patel NK, Jagtap SC & Bhutani KK, Inhibitors of pancreatic lipase: state of the art and clinical perspectives, *EXCLI Journal*, 13 (2014) 897–921.
7. Burns A & Iliffe S, Alzheimer's disease, *BMJ*, 338 (2009) b158.

8. Heinrich M & Teoh HL, Galanthamine from snowdrop-the development of a modern drug against Alzheimer's disease from local Caucasian knowledge, *Journal of Ethnopharmacology*, 92 (2004) 147–162.
9. Aruoma OI, Nutrition and health aspects of free radicals and antioxidants, *Food and Chemical Toxicology*, 32 (1994) 671–683.
10. Bagchi K & Puri S, Free radicals and Antioxidants in health and diseases, *Eastern Mediterranean Health Journal*, 4 (1998) 350–360.
11. Frei B, Stocker R & Ames BN, Antioxidant defences and lipid peroxidation in human blood plasma, *Proceedings of the National Academy of Sciences*, 85 (1988) 9748–9752.
12. Choi JS, Park SH & Choi JH, Nitrite scavenging effect by flavonoids and its structure-effect relationship, *Archives of Pharmacal Research*, 12 (1) (1989) 26–33.
13. Kang YH, Park YK & Lee GD, The nitrite scavenging and electron donating ability of phenolic compounds, *Korean Journal of Food Science and Technology*, 28 (2) (1996) 232–239.
14. 14 Mahato D & Sharma HP, Phytochemical profiling and antioxidant activity of *Leea macrophylla* Roxb. ex Hornem.-*in vitro* study, *Journal of Traditional Knowledge*, 18 (3) (2019) 493-499.
15. Willcox JK, Ash SK & Catignani GL, Antioxidants and prevention of chronic diseases, *Critical Reviews in Food Science and Nutrition*, 44 (2004) 275–295.
16. 16 Pandey A, Pandey RD, Tripathi P, Gupta PP, Haider J, Bhatt S & Singh AV, *Moringa oleifera* Lam. (Sahijan) - a plant with a plethora of diverse, Therapeutic benefits: an updated retrospection, *Medicinal Aromatic Plants*, 1 (2012) 101.
17. Magaji UF, Sacan O & Yanardag R, Alpha amylase, alpha glucosidase and glycation inhibitory activity of *Moringa oleifera* extracts, *South African Journal of Botany*, 128 (2020) 225–230.
18. Lehner R & Verger R, Purification and characterization of a porcine liver microsomal triacylglycerol hydrolase, *Biochemistry*, 36 (1997) 1861–1868.
19. Jeong JY, Jo YH, Lee KY, Do SG, Hwang BY & Lee MK, Optimization of pancreatic lipase inhibition by *Cudrania tricuspidata* fruits using response surface methodology, *Bioorganic & Medicinal Chemistry Letters*, 24 (2014) 2329–2333.
20. Ingkaninan K, Temkitthawon P, Chuenchon K, Yuyaem T & Thongnoi W, Screening for acetylcholinesterase inhibitory activity in plants used in Thai traditional rejuvenating and neurotonic remedies, *Journal of Ethnopharmacology*, 89 (2003) 261–264.
21. Fogliano V, Verde V, Randazzo G & Ritieni A, Method for measuring antioxidant activity and its application to monitoring the antioxidant capacity of wines, *Journal of Agricultural and Food Chemistry*, 47 (1999) 1035–1040.
22. Yildirim A, Mavi A & Kara A, Determination of antioxidants and antimicrobial activities of *Rumex crispus* L. extracts, *Journal of Agricultural and Food Chemistry*, 49 (2001) 4083–4089.
23. Chiou S, Lai J, Liao J, Sung J & Lin S, *In vitro* inhibition of lipase, α-amylase, α-glucosidase, and angiotensin-converting enzyme by defatted rice bran extracts of red-pericarp rice mutant, *Cereal Chemistry*, 95 (2018) 167–176.
24. Anil KHS, Prashith KTR, Vinayaka KS, Swathi D & Venugopal TM, Anti-obesity (Pancreatic lipase inhibitory) activity of *Everniastrum cirrhatum* (Fr.) Hale (Parmeliaceae), *Pharmacognosy Journal*, 3 (19) (2011) 65-68.
25. Toma A, Makonnen E, Mekonnen Y, Debella A & Addisakwattana S, Intestinal α-glucosidase and some pancreatic enzymes inhibitory effect of hydroalcholic extract of *Moringa stenopetala* leaves, *BMC Complementary and Alternative Medicine*, 14 (2014) 180.
26. Nakai M, Fukui Y, Asami S, Toyoda-Ono Y, Iwashita T, Shibata H, Mitsunaga T, Hashimoto F & Kiso Y, Inhibitory effects of oolong tea polyphenols on pancreatic lipase *in vitro*, *Journal of Agricultural and Food Chemistry*, 53 (2005) 4593–4598.
27. Moreno DA, Ilic N, Poulev A & Raskin I, Effects of *Arachis hypogaea* nutshell extract on lipid metabolic enzymes and obesity parameters, *Life Sciences*, 78 (2006) 2797–2803.
28. Han L, Li W, Narimatsu S, Liu L, Fu H, Okuda H & Koike K, Inhibitory effects of compounds isolated from fruit of *Juglans mandshurica* on pancreatic lipase, *Journal of Natural Medicines*, 61 (2007) 184–186.
29. Wikiera A, Mika M & Zyla K, Methylxanthine drugs are human pancreatic lipase inhibitors, *Polish Journal of Food and Nutrition Sciences*, 62 (2012) 109–113.
30. Habtemariam S, Antihyperlipidemic components of *Cassia auriculata* aerial parts: identification through in vitro studies, *Phytotherapy Research*, 27 (2013) 152–155.
31. Nasreena S, Rohaya A, Sumaya H, Seema A, Rabia H, Bashir AG & Eijaz AB, Pharmacological evaluation of *Gentiana kurroo* plant extracts against Alzheimer's disease, *Biomedical Journal of Scientific & Technical Research*, 14 (5) (2019) 10946–10951.
32. Bhat SK, Ashwin D, Mythri S & Bhat S, Arecanut (*Areca catechu L*) decreases Alzheimer's disease symptoms: Compilation of research works, *Journal of Medicinal Plants Studies*, 5 (5) (2017) 04–09.
33. Mahrous R, Ghareeb DA, Fathy HM, EL-Khair RMA & Omar AA, The protective effect of Egyptian *Withania somnifera* against Alzheimer's, *Medicinal & Aromatic Plants*, 6 (2017) 285.
34. Sutalangka C, Wattanathorn J, Muchimapura S, Thukham-mee W, *Moringa oleifera* mitigates memory impairment and neurodegeneration in animal model of age-related dementia, *Oxidative Medicine and Cellular Longevity*, 695936 (2013) 9.
35. Adefegha SA, Oboh G, Oyeleye SI, Dada FA, Ejakpovi I & Boligon AA, Cognitive enhancing and antioxidative potentials of velvet beans (*Mucuna pruriens*) and horseradish (*Moringa oleifera*) seeds

extracts: a comparative study, *Journal of Food Biochemistry*, 41 (2017) e12292.
36. Ghous T, Rasheed A, Yasin K, Nasim F, Younas F & Andleeb S, Exploring anti-acetylcholinesterase, antioxidant and metal chelating activities of extracts of *Moringa oleifera* L. for possible prevention and cure of Alzheimer's disease, *Scientific Research and Essays*, 9 (11) (2014) 523–527.
37. Delker SL, Xue F, Li H, Jamal J, Silverman RB & Poulos TL, Role of zinc in isoform-selective inhibitor binding to neuronal nitric oxide synthase, *Biochemistry*, 49 (51) (2010) 10803–10810.
38. Shami PJ, Moore JO, Gockerman JP, Hathorn JW, Misukonis MA & Weinberg JB, Nitric oxide modulation of the growth and differentiation of freshly isolated acute non-lymphocytic leukemia cells, *Leukemia Research*, 19 (1995) 527–533.
39. Nathan C, Inducible nitric oxide synthase: What difference does it make? *Journal of Clinical Investigation*, 100 (1997) 2417–2423.
40. Taddei S, Virdis A, Ghiadoni L, Sudano I & Salvetti A, Endothelial dysfunction in hypertension, *Journal of Cardiovascular Pharmacology*, 38 (2) (2001) S11–S14.
41. Sims NR & Anderson MF, Mitochondrial contributions to tissue damage in stroke, *Neurochemistry International*, 40 (2002) 511–526.
42. Hobbs AJ, Higgs A & Moncada S, Inhibition of nitric oxide synthase as a potential therapeutic target, *Annual Review of Pharmacology and Toxicology*, 39 (1999) 191-220.
43. Aju BY, Rajalakshmi R & Mini S, Evaluation of proximate principles and antioxidant activity of *Moringa oleifera* Lam. (drum stick tree) in Kerala, *International Journal of Advanced Research*, 5 (8) (2017) 2101-2106.
44. Pakade V, Cukrowska E & Chimuka L, Comparison of antioxidant activity of *Moringa oleifera* and selected vegetables in South Africa, *South African Journal of Science*, 109 (3/4) (2013) 5.
45. Luqman S, Srivastava S, Kumar R, Maurya AK & Chanda D, Experimental assessment of *Moringa oleifera* leaf and fruit for its antistress, antioxidant, and scavenging potential using *In vitro* and *In vivo* assays, *Evidence-Based Complementary and Alternative Medicine*, 519084 (2012) 12.

ISSN print: 1224-5984
ISSN online: 2248-3942

Rom Biotechnol Lett. 2022; 27(1): 3215-3224
doi: 10.25083/rbl/27.1/3215-3224

Received for publication, January, 06, 2021
Accepted, February, 14, 2022

Original paper

Characterization of a lipolytic strain of Pseudomonas stutzeri SN-3 and production of triacylglycerol hydrolase with concomitant biodegradation of palm oil

SANA AHMAD[1], ALIYA RIAZ[2], MUHAMMAD NOMAN SYED[3]

[1]Assistant Professor, Department of Biochemistry, Bahria University Medical and Dental College, 74400, Karachi, Pakistan
sanaahmad_185@yahoo.com
[2]Assistant Professor, Department of Biochemistry, Jinnah University for Women, 74600, Karachi, Pakistan
aliyariaz103@hotmail.com
[3]Assistant Professor, Department of Biochemistry, University of Karachi, 75270, Karachi, Pakistan
nomansyed@uok.edu.pk

Abstract Lipases are triacylglycerol hydrolases (3.1.1.1) that under aqueous condition catalyzes the hydrolysis of triglycerides. Lipases are the ubiquitous enzymes with their applications ranging from food industry to cosmetics, pharmaceuticals and bioremediation purposes. The present research involves 16S rDNA sequencing of a lipase producing strain isolated indigenously. The strain was identified as a novel *Pseudomonas stutzeri* SN-3, the gene sequence of which was deposited in GenBank with accession number MH639065. The research design also includes the exploration of alternative fermentation conditions for maximum production of triacylglycerol hydrolase from the novel strain. Different physical and chemical parameters were studied which includes temperature, pH, fermentation time course, nitrogen sources, carbon sources, phosphate sources, different salts and their concentrations for getting optimal yield of triacylglycerol hydrolase. Utilization of olive oil for production of lipases is a conventional approach, which is quite costly for commercial applications; therefore, palm oil was incorporated in cultivation medium as an alternative cheap substrate for triacylglycerol hydrolase production. Enzyme yield from *Pseudomonas stutzeri* SN-3 was optimized by using 1 gm% palm oil and 4 gm% yeast extract as carbon and nitrogen sources respectively in the presence of 2 gm% $CaCl_2$ as enzyme stabilizer and 0.01% KH_2PO_4 as bacterial growth promoter. The maximum enzyme production was observed after 48 hours of fermentation with medium pH 7 at 37 ^{0}C. Conclusively, we had a novel *Pseudomonas stutzeri* SN-3 specie and a cost-effective and eco-friendly medium for commercial production of triacylglycerol hydrolase.

Keywords *Pseudomonas stutzeri*, Biocatalysis, Biodegradation, Lipase, Optimization

To cite this article: AHMAD S, RIAZ A, SYED MN. Characterization of a lipolytic strain of *Pseudomonas stutzeri* SN-3 and production of triacylglycerol hydrolase with concomitant biodegradation of palm oil. *Rom Biotechnol Lett*. 2022; 27(1): 3215-3224. DOI: 10.25083/rbl/27.1/3215-3224.

✉ *Corresponding author: SANA AHMAD, Assistant Professor, Department of Biochemistry, Bahria University Medical and Dental College, 74400, Karachi, Pakistan.
Phone Number: +92333-2434533, Fax Number: 36620614
E-mail: sanaahmad_185@yahoo.com

Introduction

The Triacylglycerol hydrolases or lipases (E.C. 3.1.1.1) are the enzymes which catalyze the degradation of triglycerides into diacylglycerol, monoacylglycerol, fatty acids and glycerol (Jaeger *et al.,* 1999). They bear the tremendous potential of catalyzing the reverse reaction i.e. esterification along with acidolysis and alcoholysis (Stergiou *et al.,* 2013). The water interface favors hydrolytic reaction by lipases whereas in the oil interface, lipases catalyze the esterification. Thus, the action of lipases is medium dependent (Gupta *et al.,* 2004). Lipases exhibit both condition and catalytic promiscuity (Busto *et al.,* 2010; Wu *et al.,* 2010 ; Kapoor and Gupta, 2012). This is one of the reasons of tremendous applications of lipases in various industries. The regular substrates of lipases are glycerol esters. Lipases are highly specific in their action being stereo, regio and enantioselective (Jaeger and Eggert, 2002; Anobom *et al.*, 2014). Lipases are produced by a variety of fauna and flora; from microbes to higher organisms and plants. Among all these sources, microbial lipases are the most utilized and studied. Bacterial lipases play an imperative role in commercial sectors due to the ease of production (Salihu & Alam, 2012). Many bacterial genera produces potential triacylglycerol hydrolases but the *Pseudomonas* lipases are more economic, highly stable and provide a wide range of specificity (Lee *et al.*, 2015). Related to the eminent characteristics of lipases, they are equally important in the industries (Woittiez *et al.*, 2017). The applications of lipases are growing rapidly in organic synthesis, pharmaceuticals, biofuel production, cleaners and degreasing formulations, flavor development, food modification, the production of fine chemicals, paper making, manufacturing of cosmetics, and in oleochemical industry. Triacylglycerol hydrolases are equally important for bioremediation processes from oil spill to the degradation of plastics (Salihu & Alam, 2012).

Application of the enzymes produced by living organisms for the disintegration of organic substances is known as biodegradation. Triacylglycerol hydrolases being the hydrolases of triglycerides contribute significantly in cleaning the oil based wastes via biodegradation. Biodegradation of oil is not only fruitful for the environment but also for the assessment of eco friendliness of the oil. Palm oil is the major vegetable oil produced in the world (Woittiez *et al.*, 2017). Palm oil encompasses 66.83 million metric tons or 34% of the total vegetable oil production across the globe and since 2015 its domestic utilization has climbed from 702 million metric tons to 75.098 million metric tons (Shahbandeh, 2019). The increased concentration of palm oil in waste water is an outcome of this raised level of its utilization globally (Saranya *et al.*, 2014). Lipid rich waste water is harmful for the living organisms and its proper handling is essential to create a safe living environment (Gombert *et al.*, 1999). Concerning this, use of bioresources such as enzymes for lipid hydrolysis is the most appropriate approach. Enzymatic hydrolysis of lipid rich waste water is preferred because of their ecofriendly and highly specific nature. By revealing the new and economic sources for large-scale enzyme preparations, mass production would become easy and inexpensive to meet the industrial demands of microbial lipases. The present research was therefore designed to optimize the fermentation parameters for maximum triacylglycerol hydrolase production from the isolated strain.

Materials and Methods

Chemicals

All analytical grade chemicals used in this study were procured from Sigma-Aldrich USA.

Bacterial strain

Bacterial culture used in this research was obtained from Enzyme Technology Unit, Department of Biochemistry, University of Karachi, Pakistan. The strain was previously isolated and identified as *Pseudomonas* specie SN-3 on morphological and biochemical characteristics. The strain was found to be gram negative, non-spore former, motile, acidophilic, halotolerant (Ahmad & Syed, 2019).

Molecular Identification

The bacterial strain was identified by using 16S rDNA sequencing. It is the most widely used technique for genotypic identification of bacterial strains (Drancourt *et al*., 2000). The molecular identification includes separation of genomic DNA, augmentation of 16S rDNA gene and its sequencing. EZ-10 Spin Column Genomic DNA Kit (Bacterial Samples) was used to separate genomic DNA. Isolation of the genomicDNA was tracked by using 1% agarose gel electrophoresis. 16S rDNA gene was amplified in the isolated genomic DNA using primers. Primer FD1 (10µM) 5'-AGAGTTTGATCCTGGCTCAG-3' and Primer RS16 (10µM) 5'-TACGGCTACCTTGTTACGACTT-3' were used as forward and reverse primer respectively.

Commercially available kit was use to purify amplified gene and then the purified product was subjected to Sanger's sequencing.

Culture maintenance

The strain revived primarily in nutrient broth and continually grown on nutrient broth complemented with olive oil (1%) at 37ºC for 24 hours. The strain was preserve at 4ºC in an olive oil (1%) agar medium and subculture routinely.

Inoculum preparation

For preparation of inoculum, nutrient broth was accompanied with palm oil (1% v/v), yeast extract (4% w/v) and $CaCl_2$ (2% w/v) and seed culture (10% v/v) was prepared by inoculating a 100 µL of preserved culture into it. For inoculum preparation, this culture then incubated at 37ºC for 24 hours and then used in cultivation.

Enzyme Production Medium

Fermentation was conducted in 100 ml Erlenmeyer flask. The basic fermentation medium consisted of 1% tryptone, 1.0 % olive oil, 0.05% $CaCl_2$, 0.05% $MgSO_4$ and 0.001% K_2HPO_4. (Syed *et al.*, 2010). A 24hr old 10% v/v inoculum was shifted into the basic cultivation medium and incubated for 48hrs at 37ºC. Subsequently the bacterial cells were pallet at 10,000x g at 0ºC for 10 minutes. The clear supernatant was pooled and utilized as the source of crude enzyme

Estimation of biomass

Growth of *Pseudomonas* strain estimated with the help of the absorbance at 600nm (Mobarak-Qamsari *et al.*, 2011).

Enzyme Assay

The total triacylglycerol hydrolase activity was monitored spectrophotometrically by using *p*-nitrophenyl-palmitate as chromogenic substrate as documented by Pencreac'h and Baratti (Pencreac'h and Baratti, 1996). The reaction mixture comprises of 1 mL of 40mM *p*-nitrophenylpalmitate (dissolved in n-hexane and 50mM phosphate buffer of pH 7.0) and 0.5 mL of CFF. After 15 minutes, Enzyme activity was ceased by adding 1 mL of 5% NaOH and the obtained product was read at 410 nm. One enzyme unit equals to the amount of enzyme that liberate one micromole of *p*-nitrophenol per mL under activity analysis conditions.

Optimization of Fermentation Parameters

The standard media was optimized for maximum lipase induction at the optimum pH 7.0 and temperature 37ºC by replacing the specific constituents of the production medium. Physical and chemical parameters for enriched yield of lipase were optimized. Physical parameters include temperature, time course and pH of fermentation medium. Whereas under the route of chemical parameters; different carbon sources, nitrogen sources, salts and various concentrations of the selected nutrients were optimized. At each step after fermentation, CFF was collected and evaluated for lipase production via the enzyme assay and total protein.

Chemical Parameters

Carbon Source and its concentration

Fermentation medium was tested for enhanced turnout of lipase with diverse carbon sources which were olive oil, almond oil, palm oil, glycerol, fructose and lactose. Optimization was studied at pH 7.0 and at 37ºC. These parameters studied individually at the concentration of 1%. The most efficient carbon source with highest lipase titer was then further optimized at different concentrations ranging from 1%-6%

Nitrogen Source and its Concentration

Various nitrogen sources which include ammonium chloride, urea, yeast extract, peptone, ammonium phosphate, and tryptone were incorporated in the cultivation medium for greater lipase formation (pH 7.0, 37^0C). These parameters studied individually at the concentration of 1%. Different concentrations (1%-6%) of most efficient nitrogen source for lipase production were further varied for selection of optimum one.

Metal ions and its concentrations

Enriched lipase turnout was tested with different salts such as $FeCl_3$, MgCl, NaCl, $MgSO_4$, KCl and $CaCl_2$. The assessment was taken individually with each salt and the most effective salt was studied at different concentrations (1%-6%).

Phosphate source and its concentrations

Suitable phosphate source was selected for enhanced lipase induction by incorporating various phosphate compounds includingKH_2PO_4, NaH_2PO_4, K_2HPO_4 and Na_2HPO_4. The selected source was further observed on varying concentration (0.01% to 0.06%).

Physical Parameters

Effect of cultivation time on lipase production

Time effect was observed by incubating the fermentation medium for varying time periods such as 3, 6, 24, 48 and 72 hrs.

Effect of pH on lipase induction

Media was studied for enriched lipase induction with the change in pH (from 3-10)

Effect of Temperature on lipase production

Different temperatures were also tested for maximum lipase yield. The fermentation media was incubated at diverse temperatures ranging from 30^0C-70^0C.

Results and discussion

Molecular Identification

The 16S rDNA of *Pseudomonas stutzeri* was found to consist of 598 base pairs (Fig.1). The obtained gene sequence was deposited to Genbank with the accession number MH639065 (*Pseudomonas stutzeri* SN-3). The gene sequence was further explored through BLAST analysis for determination of specie origin (https://blast.ncbi.nlm.nih.gov/Blast.cgi.). The gene sequence of *Pseudomonas stutzeri* SN-3 was aligned with selected twentyfour gene sequences of data base for the development of phylogenetic tree.

Optimization of Fermentation

Triacylglycerol hydrolases are extracellular enzymes. They are strongly influenced by composition and conditions of the growth medium. Optimization of these elements affects microbial growth, which ultimately enhances the enzyme induction. The chemical and physical factors of the cultivation medium not only play an important role in cost reduction of overall process but also govern the proper applicability of enzyme.

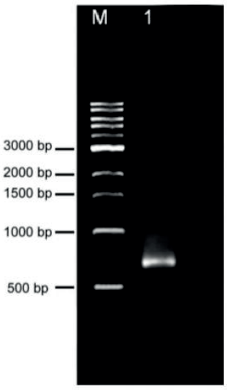

Figure 1. Molecular weight determination of amplified 16S rDNA. Lane M represents DNA ladder and Lane 1 denotes amplified PCR product

Chemical Parameters

Carbon Source and its concentration

Outcomes concerning with the effect of various carbon sources on the production of triacylglycerol hydrolase are depicted in Fig.3. It showed that all the carbon sources used, influence triacylglycerol hydrolase production varyingly but maximum triacylglycerol hydrolase production was attained when the medium was supplemented with palm oil. Highest triacylglycerol hydrolase production (82.09 ± 0.565 U) and cell growth (1± 0.05 mg/mL) was obtained when the palm oil used as carbon source. However, high cell mass was also observed when the cultivation medium was enriched with fructose and lactose. Outcomes of varying concentrations of palm oil on triacylglycerol hydrolase titer showed a sharp decline in enzyme yield with every rise in percent concentration of palm oil in the cultivation medium (Fig. 3B). The cell mass also observed to follow the same decline with increasing concentration of palm oil in the production medium.

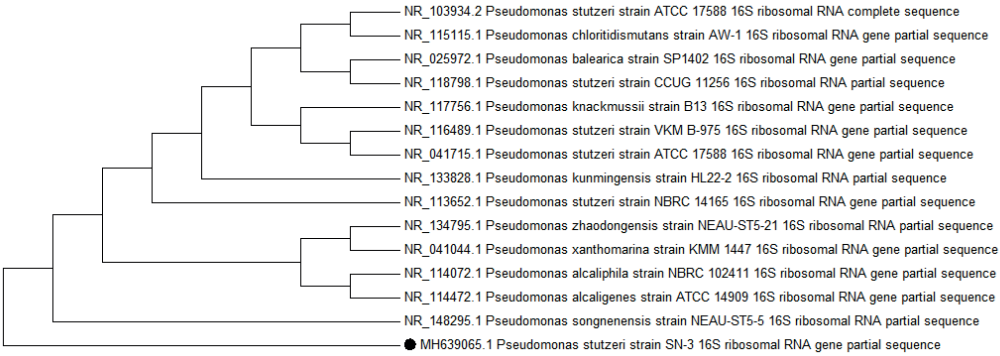

Figure 2. Phylogenetic tree by maximum likelihood method exhibiting the 16S rDNA sequence similarity against the available 16S rDNA sequences in Genbank database.

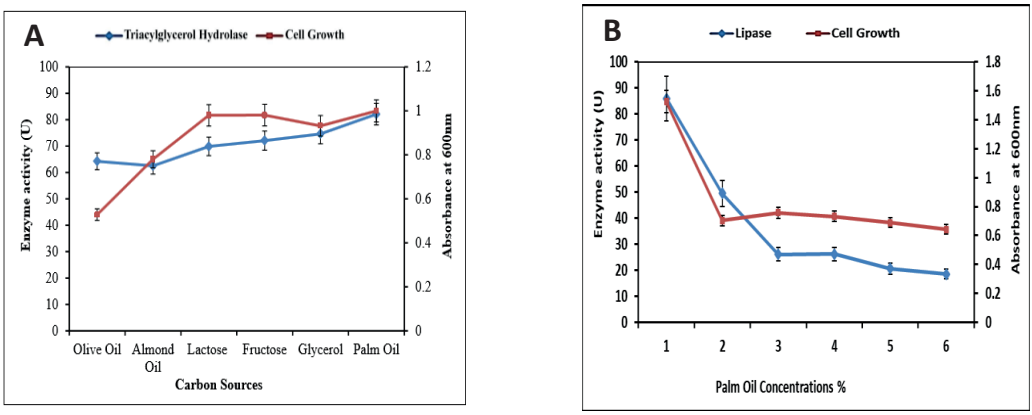

Figure 3. Effect of different carbons sources (A) and concentration of appropriate carbon source (B) on induction of lipase and bacterial growth. (Values are expressed as Mean ± S.E, n=3).

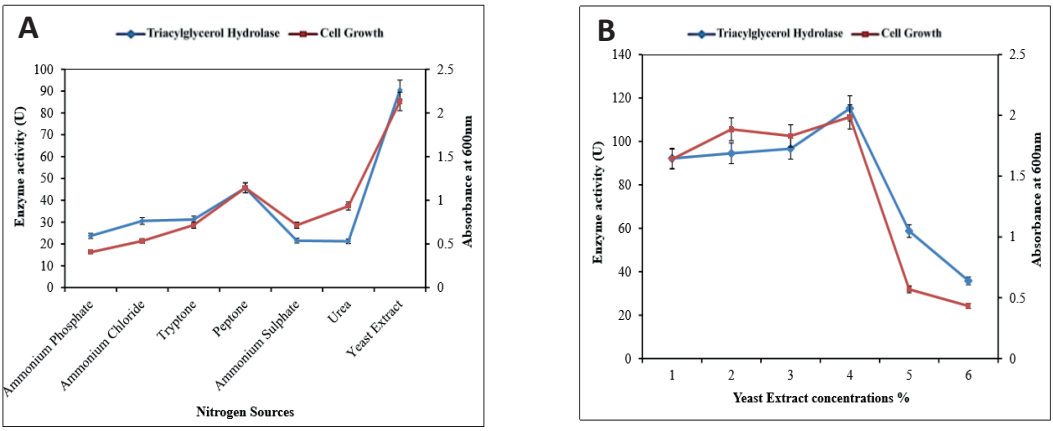

Figure 4. Effect of different nitrogen sources (A) and concentration of appropriate nitrogen source (B) on lipase induction and bacterial growth. (Values are expressed as Mean + S.E, n=3).

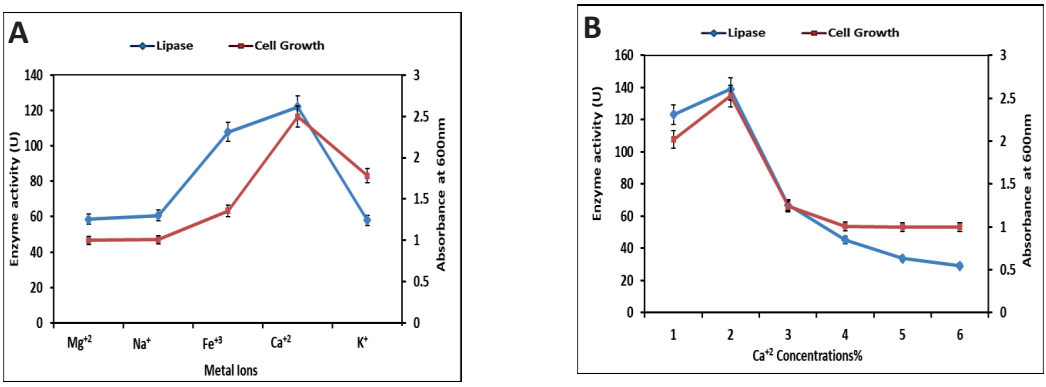

Figure 5. Influence of various metal ions (A) and concentration of appropriate metal ion i.e. Ca^{+2} (B) on induction of lipase and bacterial growth. (Values are expressed as Mean $\pm$ S.E, n=3).

Nitrogen Source and its Concentration

The effect of different nitrogen sources and the concentration of appropriate source on triacylglycerol hydrolase induction were evaluated as shown in Fig.4. Initially, various organic and inorganic nitrogen sources were analyzed and yeast extract was found to be the most preferred nitrogen source as reflected by the high titer of triacylglycerol hydrolase (90.52 ± 0.406 U) and highest cell mass. It was also observed that triacylglycerol hydrolase production by *Pseudomonas stutzeri* SN-3 indicate a direct relationship with the rise in yeast extract concentration up-to four percent and then decreases with five and six percent concentrations of yeast extract (Fig.4B). The isolated *Pseudomonas stutzeri* SN-3 was also observed to grow abundantly in the medium at 4% concentration of yeast extract.

Metal ions and its concentrations

Data plotted in Fig.5 shows the effect of different metal ions on triacylglycerol hydrolase induction and bacterial growth. All the metal ions tested improved the triacylglycerol hydrolase induction distinctly however, $CaCl_2$ resulted in maximum secretion of triacylglycerol hydrolase (122.059 ± 1.341 U) at 2% concentration (Fig.5B). The parallel pattern of the cell growth was observed in metal ions and the different concentrations of Ca^{+2} ions.

Phosphate source and its concentrations

Data presented in figure 6 (A) displayed that all the phosphate sources added to the cultivation medium affect bacterial cell division and triacylglycerol hydrolase titer. Maximum triacylglycerol hydrolase production (205.67 ± 5.283U) with a subsequent highest cell biomass was found when medium was supplemented with KH_2PO_4. Yield of triacylglycerol hydrolase was shown to drop significantly, when the fermentation medium was incorporated with K_2HPO_4, NaH_2PO_4, and Na_2HPO_4.The Na_2HPO_4 existence in growth medium displayed uppermost cell growth; however

the triacylglycerol hydrolase titer was found to drop comparatively. Various Concentrations of KH_2PO_4 supplementation were also explored to efficiently formulate the cultivation medium for enhanced triacylglycerol hydrolase induction. Obtained results were plotted in figure 6B. It was found that 0.01% $KH_2PO_4$was suitable for *Pseudomonas stutzeri* SN-3 to produce maximum triacylglycerol hydrolase. Further increase in $KH_2PO_4$was found to be inhibitory for both cell proliferation and triacylglycerol hydrolase induction.

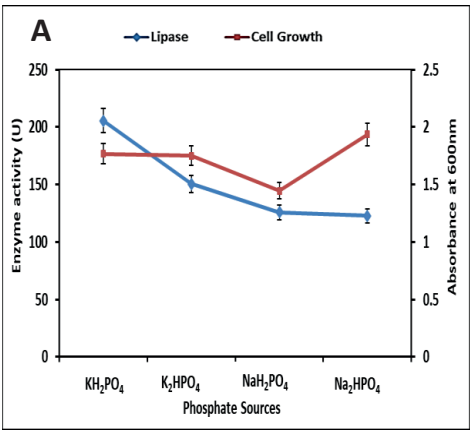

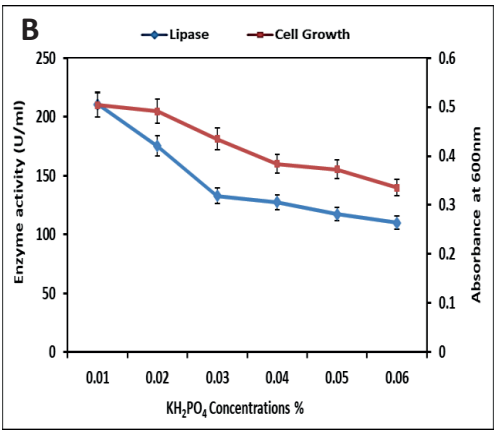

Figure 6. Effect of different phosphate sources on cell proliferation and lipase production by *Pseudomonas stutzeri* SN-3. (Values are expressed as Mean + SD, n=3).

Fermentation Optimization with Physical Parameters

Effect of cultivation time on lipase production

Outcomes of cultivation time exhibited that utmost 48hours required by *Pseudomonas stutzeri* SN-3 to produce high triacylglycerol hydrolase titer (Fig. 7). The graph of cell growth displayed that the appearance of triacylglycerol hydrolase titer into the growth medium was initiated in exponential phase and then gradually increases, reached to its upper limit at the commencement of stationary phase (Fig. 7). A gradual decline in triacylglycerol hydrolase titer was obtained after 48 hours of fermentation.

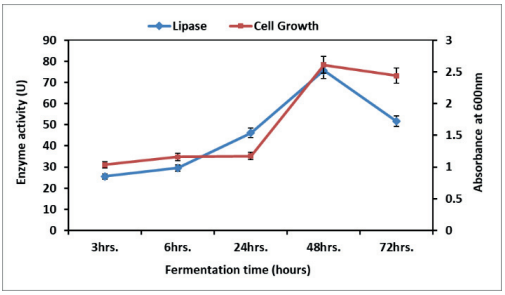

Figure 7. Time course optimization for maximum induction of lipase and bacterial growth. (Values are expressed as Mean ± S.E, n=3).

Effect of pH on lipase induction

Concerning triacylglycerol hydrolase induction in present research, pH 7.0 was found to be the most appropriate pH as it showed highest triacylglycerol hydrolase titer and highest cell mass (Fig 8).

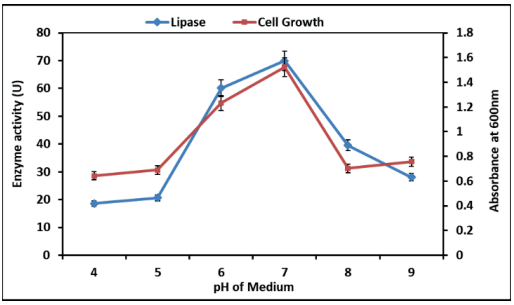

Figure 8. Effect of pH on induction of lipase and bacterial growth. (Values are expressed as Mean ± S.E, n=3).

Effect of Temperature on lipase production

Temperature was found to be the inducer of triacylglycerol hydrolase production as the enzyme yield affects with all the temperatures tested. Results interpret 40ºC as the suitable temperature for *Pseudomonas stutzeri* SN-3 as it was observed to grow adequately and produced maximum triacylglycerol hydrolase at 40ºC.

Triacylglycerol hydrolasess are the most versatile enzymes used in the industries. Their promiscuous nature makes them the most suitable candidate for use in various industries. Due to the increasing demand of microbial triacylglycerol hydrolasess in industrial site, this study was therefore conducted to isolate potential triacylglycerol hydrolase producing bacteria and to evaluate the effect of different physico-chemical parameters for hyper production of triacylglycerol hydrolase.

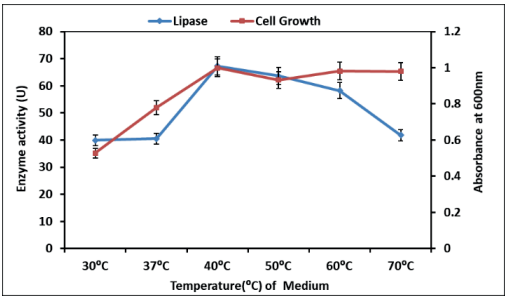

Figure 9. Effect of temperature on induction of lipase and bacterial growth. (Values are expressed as Mean ± S.E, n=3).

Molecular identification of the previously isolated *Pseudomonas* strain encompasses the exploration of 16S rDNA sequence. The obtained dendrogram presented in figure 2 showed that isolated *Pseudomonas stutzeri* SN-3 originated from other strains of *Pseudomonas stutzeri* and form an exclusive array with *Pseudomonas songnenensis* which has its origin from other *Pseudomonas* species. Based on these findings, the isolated *Pseudomonas stutzeri* SN-3 is placed in genus *Pseudomonas Sensustricto*, *Protobacteria* phyla and class *Gammaproteobacteria* (Parwata *et al.*, 2014; Lalucat *et al.*, 2006).

Carbon has always been the chief considerable component for the expression of triacylglycerol hydrolase activity due to the inducible nature of lipases (Marina *et al.*, 1998; Fabiszewska *et al.*, 2015). Consequently lipases are generally produced in the presence of lipid sources such as oil, hydrolysable esters like glycerol (Gupta *et al.*, 2004) and other carbon sources which include sugars (Ghanem *et al.*, 2000; Rashid *et al.*, 2001). Therefore, the effects of various carbon sources on production of triacylglycerol hydrolase have been included in this research design.

According to the available literature, palm oil industrial residues shown promising potential to induce triacylglycerol hydrolase production by *Aspergillus niger* (Charles and James, 2011). Palm oil mill effluent (POME) was found to be a significant factor in induction of triacylglycerol hydrolases from fungal species (Ibegbulam-Njoku and Achi, 2014). Palm agro-industrial waste has reported to enhance lipase production from the nonpathogenic yeast *Yarrowia lipolytica* (Fraga *et al*., 2021). The *Bacillus pumilus* lipase produced with palm oil as substrate (Saranya *et al.*, 2014). The current research exhibited comparable outcomes with Saranya *et al* (Saranya, 2014) validating the efficiency of palm oil in lipase synthesis by *Pseudomonas* sp. In addition to palm oil, fructose and glycerol were also observed to be the appropriate substrates for lipase induction. The high cell growth may be due to the inclination of microbes towards simple sugars for cell division and growth (Mazmira *et al.*, 2012).

Formerly olive oil was an extensively used source for lipase production (Amin *et al.*, 2014; Erick *et al.*, 2016). However, in present research, palm oil has shown promising potential for lipase production besides olive oil. Hence it can be predicted that palm oil is a comparatively new bioresource to enhance triacylglycerol hydrolase induction in *Pseudomonas.* At the same time the isolated *Pseudomonas stutzeri* SN-3 can be utilized for bioremediation of palm oil contaminated soil and water.

Organic nitrogen sources were found to increase lipase production by *Pseudomonas sp*. (Mobarak-Qamsari *et al.*, 2011). However, concerning to the cell growth, other organic nitrogen sources also exhibited positive results. These sources used as active ingredients during cell multiplication and therefore they are preferable over their inorganic counterparts (Djekrif-Dakhmouche *et al.,* 2006).

According to present research findings, triacylglycerol hydrolase induction has been greatly enhanced in presence of 4% yeast extract and the cell growth also perfectly coincides with this result. Traditionally, enriched triacylglycerol hydrolase production was obtained by using both organic and inorganic nitrogen sources. Yeast extract has proven to be the best source for maximum lipase induction in *Bacillus* sp. (Laachari *et al.*, 2014) in *Pseudomonas aeruginosa* UKHL1 (Patel *et al.,* 2020). Yeast extract supports greater cell yield as it comprises of the essential amino acids, peptides and water soluble vitamins necessary for microbial growth (Mobarak-Qamsari *et al.*, 2011; Peighamy-Ashnaei *et al.*, 2006). Therefore, the present results are valuable addition in evidences to the previous studies.

Besides macromolecules, micromolecules (minerals) are also necessary for proliferation and growth of microorganisms. Therefore, in this study, the effect of various metal ions was examined on isolated strain for triacylglycerol hydrolase production. These minerals were found to augment triacylglycerol hydrolase activity by modifying the structure and removal of fatty acids from the reaction site. Therefore, enhance the induction of triacylglycerol hydrolase by providing a suitable environment to it (Kumar and Valsa, 2007). Various studies showed that triacylglycerol hydrolase yield improve significantly by varying the concentrations of $CaCl_2$ (Patel *et al*., 2020; Bokhari *et al.*, 2013; Kumar *et al.*, 2012).

Phosphorous compounds also play crucial role in bacterial multiplication and development. They serve as regulatory and structural sources in bacterial cultures. In excess amount, they may render the phosphate metabolism and thereby reduces bacterial cell growth (Kulakovskaya, 2014). Therefore various phosphate compounds (KH_2PO_4, NaH_2PO_4, K_2HPO_4, and Na_2HPO_4) were included into the fermentation medium to document their effects on cell division of *Pseudomonas stutzeri* SN-3 and triacylglycerol hydrolase titer. In present research, KH_2PO_4 was found to stimulates triacylglycerol hydrolase production. The same phosphate source that is KH_2PO_4 was reported as microbial

stimulant for yield enhancement of lipid degrading enzyme (). In combination to soy meal, KH_2PO_4 was also found to prefer by *Botryosphaeriaribis* EC-01 to produce lipase proficiently (Barbosa *et al.*, 2011). Fungal preference of KH_2PO_4 has also been reported such as in *Trichodermaviride* (Osman *et al.*, 2012). A lipid hydrolyzing enzyme from *Aspergillusniger* was also found to produce in higher amounts when 0.2% KH_2PO_4 was incorporated in the growth medium (Pokorny *et al.*, 1994).

After optimizing chemical parameters, effect of various physical parameters on enzyme production was also observed. The decline in triacylglycerol hydrolase titer may be due to presence of other extracellular metabolites that are responsible to change the pH of enzyme production medium (Saranya *et al.*, 2014). The rise in pH and level of proteases results in low triacylglycerol hydrolase production (Gupta *et al.*, 2004). All these observation are in accordance with previous studies that also reported maximum lipase production in 48hours by different bacterial species (Bokhari *et al.*, 2013; Esteban-Torres *et al.*, 2015; Paul *et al.*, 2015 and Deyaa *et al.*, 2016).

The pH of the production medium plays a critical role in maintenance of microbial physiological functions and movement of nutrient and mineral sources through cellular membrane. Consequently, optimum pH ultimately enhances the enzyme production. The optimal pH of fermentation medium was found to be 7.0 reflecting the preference of *Pseudomonas stutzeri* towards neutral pH (Lalucat *et al.*, 2006). Inclination of bacterial lipases for pH 7.0 has been evident from the literature (Paul *et al.*, 2015; Deyaa *et al.*, 2016).

Optimum temperature of fermentation medium was found to be 40^0C. The same temperature was observed for lipase production by an *Actinomycete* (Patel *et.al.*, 2021). The results of effect of temperature on triacylglycerol hydrolase production reflects that the isolated *Pseudomonas stutzeri* SN-3 is mesophilic in nature. Many lipase producing bacterial strains were reported to cultivate in temperature ranges 25-40^0C (Fatima *et.al.*, 2021). As the high cell growth associated with increased enzyme yield therefore many bacterial strains exhibited maximum lipase production at 37^0C including *lactobacillus plantarum* and g*eobacillus thermoleovorans* DA2 (Esteban-Torres *et al.*, 2015; Paul *et al.*, 2015; Kanimozhi *et al.*, 2011).

Conclusion

Triacylglycerol hydrolases are crucial enzymes for the growing field of Biotechnology. Through present research, a novel lipase producing strain was identified molecularly as *Pseudomonas stutzeri* SN-3. The sequence of 16S rDNA was deposited in the Genbank [MH639065]. Further, an economical fermentation medium was designed for maximum lipase yield. The property of *Pseudomonas stutzeri* SN-3 to degrade palm oil as carbon source efficiently by the action of triacylglycerol hydrolase made it a useful bioresource for management of palm oil industrial effluents and palm oil containing wastewater. Future research on purification and characterization studies of *Pseudomonas* SN-3 triacylglycerol hydrolase may reveal its possible forthcoming applications.

Acknowledgement

The authors are grateful to University of Karachi for funding this research.

Conflict of interest

There are no conflicts of interest.

References

1. Jaeger KE, Dijkstra BW, Reetz MT. Molecular biology,three dimensional structures and biotechnolo gical application of lipases. *Annu Rev Microbiol*. 1999; 53:315–51.
2. Stergiou PY, Foukis A, Filippou M, Koukouritaki M, et al. Advances in lipase-catalyzed esterification reactions. *Biotechnol Adv*. 2013; 31:1846-59.
3. Gupta R, Gupta N, Rathi P. Bacterial lipases: an overview of production, purification and biochemical properties. *Appl Microbiol Biotechnol*. 2004; 64:763–781.
4. Wu Q, Liu BK, Lin XF. Enzyme promiscuity for organic synthesis and cascade process. *Curr Org Chem.* 2010; 14:1966–88.
5. Busto E, Gotor-Fernandez V, Gotor V. Hydrolases: catalytically promiscuous enzymes for non-conventional reactions in organic synthesis. *Chem Soc Rev.* 2010; 39:4504–23.
6. Kapoor M, Gupta MN. Lipase promiscuity and its biochemical applications. *Process Biochem*. 2012; 47:555–569.
7. Jaeger KE, Eggert T. Lipases for biotechnology. *Curr Opin Biotechnol*. 2002; 13: 390-397.
8. Anobom CD, Pinheiro AS, De-Andrade RA, Aguieiras EC, et al. From structure to catalysis: recent developments in the biotechnological applications of lipases. *Biomed Res Int.* 2014; article ID 684506.
9. Salihu A, Alam MZ. Production and applications of microbial lipases: a review. *Sci Res Essays*. 2012; 7:2667-2677.
10. Lee, Li P, Hudzaifah MK, Marimuthu C, et al . Lipase-secreting *Bacillus* species in an oil-contaminated habitat: promising strains to alleviate oil pollution. *BioMed Res Int*. 2015: Article ID. 820575.
11. Woittiez, Lotte S, Mark T, Wijk V, et al. Yield gaps in oil palm: A quantitative review of contributing factors. *Eur J Agron*. 2017; 83:57-77.
12. Shahbandeh M. Palm oil consum ption worldwide from 2015/2016 to 2019/2020. Statista. https://www. statista.com/statistics/274127/world-palm-oil-usage-distribution. 2019; Accessed 15 January 2020.
13. Fraga JL, Souza CP, Pereira AD, Aguieiras EC, de Silva LO, Torres AG, Freire DG, Amaral PF. Palm oil wastes as feedstock for lipase production by Yarrowia lipolytica and biocatalyst application/reuse. *3 Biotech*. 2021; 11(4):1-9.
14. Saranya P, Kumari HS, Rao BP, Sekaran G. Lipase production from a novel thermo-tolerant and extreme

acidophile *Bacillus pumilus* using palm oil as the substrate and treatment of palm oil-containing wastewater. *Environ Sci Pollut Res.* 2014; 21:3907–3919.
15. Gombert AK, Pinto AL, Castilho LR, Freire DMG. Lipase production by *Penicillium restrictum* in solid-state fermentation using babassu oil cake as substrate. *Process Biochem*. 1999; 35:85–89.
16. Ahmad S, Syed MN. Isolation of a Novel Halotolerant Lipase Producing Strain of *Pseudomonas Stutzeri*. *International journal of biology and biotechnology.* 2019; 161: 37-43.
17. Drancourt M, Bollet C, Carlioz A, Martelin R, et al. 16S ribosomal DNA sequence analysis of a large collection of environmental and clinical unidentifiable bacterial isolates. *J. Clin. Microbiol.* 2000; 38: 3623-3630.
18. Syed MN, Iqbal S, Bano S, Khan AB, et al. Purification and characterization of 60 kD lipase linked with chaperonin from *Pseudomonas aeruginosa* BN-1. *Afr J Biotechnol.* 2010; 9: 7724-7732.
19. Mobarak-Qamsari E, Kasra-Kermanshahi R, Moosavi-nejad Z. Isolation and identification of a novel, lipase-producing bacterium, *Pseudomnas aeruginosa* KM110. *Iran J Microbiol*. 2011; 3:92-98.
20. Pencreac'h G, Baratti JC. Hydrolysis of p-nitrophenyl palmitate in n-heptane by the *Pseudomonas cepacia* lipase: a simple test for the determination of lipase activity in organic media. *Enzym Microb Technol*. 1996; 18:417–422.
21. Parwata IP, Asyari M, Hertadi R. Organic solvent-stable lipase from moderate halophilic bacteria *Pseudomonas stutzeri* isolated from the mud crater of bleduk kuwu, central java, Indonesia. *J Pure Appl Microbiol*. 2014; 8: 31-40.
22. Lalucat J, Bennasar A, Bosch R, García-Valdés E, et al. Biology of *Pseudomonas stutzeri*. *Microbiol. Mol. Biol. Rev.* 2006; 70: 510-547.
23. Marina L, Silvia M, José LM, Stefania B, et al. Physiological control on the expression and secretion of *Candida rugosa* lipase. *Chem Phys Lipids*. 1998; 93:143–148.
24. Fabiszewska AU, Kotyrba D, Nowak D. Assortment of carbon sources in medium for *Yarrowia lipolytica* lipase production: A statistical approach. *Ann Microbiol*. 2015; 65:1495-1503.
25. Ghanem, Essam H, Hashim A, Al-Sayed, Saleh KM. An alkalophilic thermostable lipase produced by a new isolate of *Bacillus alcalophilus*. *World J Microbiol Biotechnol*. 2000; 16(5):459-464.
26. Rashid N, Shimada Y, Ezaki S, Atomi H, et al. Low temperature lipase from psychrotrophic *Pseudomonas sp*. Strain KB700A. *Appl Environ Microbiol*. 2001; 67:4064–4069.
27. Charles ON, James CO. Isolation of lipase producing fungi from palm oil Mill effluent (POME) dump sites at Nsukka. *Braz Arch Biol Technol*. 2011; 54(1):113-116.
28. Ibegbulam-Njoku PN, Achi OK. Lipase Production by Fungal Isolates Grown in Palm Oil Mill Effluent. *Br Biotechnol*. 2014; J 4: 1191-1200.
29. Mazmira MM, Ramlah SSA, Rosfarizan M, Ling TC, et al. Effect of saccharides on growth, sporulation rate and δ-endotoxin synthesis of *Bacillus thuringiensis*. *Afr J Biotechnol*. 2012; 11: 9654-9663.
30. Amin M, Bhatti HN, Zuber M, Bhatti IA, Asgher M. Potential use of agricultural wastes for the production of lipase by *Aspergillus melleus* under solid state fermentation. *J Anim Plant Sci*. 2014; 24:1430-1437.
31. Erick A, Silveira Paulo W, Farinas TCS. Valorization of Palm Oil Industrial Waste as feedstock for lipase production. *Appl Biochem Biotechnol*. 2016; 179:558–571.
32. Djekrif-Dakhmouche S, Gheribi-Aoulmi SZ, Meraihi Z, Bennamoun L. Application of a statistical design to the optimization of culture medium for α-amylase production by *Aspergillus niger* ATCC 16404 grown on orange waste powder. *J Food Eng*. 2006; 73:190-197.
33. Laachari F, Bergadi FE, Bahafid W, Sayari A, et al. Biochemical study of lipases from *Bacillus subtilis*. *Moroccan J Biol*. 2014; 11:1-9.
34. Patel H, Ray S, Patel A, Patel K, Trivedi U. Enhanced lipase production from organic solvent tolerant Pseudomonas aeruginosa UKHL1 and its application in oily waste-water treatment. *Biocatal. Agric*. 2020; 28:101731.
35. Peighamy-Ashnaei S, Sharifi-Tehrani A, Ahmadzadeh M, Behboudi K. Effect of carbon and nitrogen sources on growth and biological efficacy of *Pseudomonas fluorescens* and *Bacillus subtilis* against *Rhizoctonia solani*, the causal agent of bean damping-off. *Communi Agric Appl Biol Sci*. 2006; 72:951-956.
36. Kumar MP, Valsa AK. Optimization of culture media and cultural conditions for the production of extracellular lipase by *Bacillus coagulans*. *Indian J Biotechnol*. 2007; 6:114-117.
37. Kumar D, Kumar L, Nagar S, Raina C, et al. Screening, isolation and production of lipase/esterase producing *Bacillus sp.* strain DVL2 and its potential evaluation in esterification and resolution reactions. *Archives of Applied Science Research*. 2012; 4: 1763-1770.
38. Bokhari DM, Gohar UF, Hussain Z. Optimization Studies of Lipase Production from locally isolated *Bacillus spp. Biologia*. 2013; 59:259-265.
39. Kulakovskaya T. Phosphorus storage in Microorganisms: diversity and evolutionary insight. *Biochemistry and Physiology*. 2014; 4:e130. doi:10.4172/2168-9652.1000e130
40. Amenaghawon AN, Odika P, Aiwekhoe SE. Optimization of nutrient medium composition for the production of lipase from waste cooking oil using response surface methodology and artificial neural networks. *Chem Eng Commun*. 2021; 15:1-1.
41. Barbosa AM, Messias JM, Andrade MM, Dekker RF, et al. Soybean oil and meal as substrates for lipase production by *Botryosphaeria ribis*, and soybean oil to enhance the production of botryosphaeran by *Botryosphaeria rhodina*. In *Soybean-Biochemistry, Chemistry and Physiology*.

2011; IntechOpen. Prof. Tzi-Bun Ng (Ed.), ISBN: 978-953-307-219-7, InTech 101-119.
42. Osman ME, Amany A, Abo El-Nasr, Nashwa H. Screening of Some Fungal Isolates for Lipase Production and Optimization of Cultural Conditions for the Most Potent Isolate. *Egypt J Microbiol*. 2012; 47: 79- 95.
43. Pokorny D, Friedrich J, Cimerman A. Effect of nutritional factors on lipase biosynthesis by *Aspergillus niger*. *Biotechnol let*. 1994; 16: 363-366.
44. Esteban-Torres M, Mancheño JM, Rivas BDL, Muñoz RLWT. Characterization of a halotolerant lipase from the lactic acid 3 bacteria *Lactobacillus plantarum* useful in food fermentations. *Food Sci Technol*. 2015; 60:246–252.
45. Paul D, Saha S, Pramanick S, Chattopadhyay S. Standardization of process parameters for the maximum production of extracellular lipase by bacteria, isolated from indigenous sources. *IRJET*. 2015; 02:682-688. Corpus ID: 212579290.
46. Deyaa M, Abol Fotouh M, Reda A, Bayoumi, et al. Production of Thermoalkaliphilic Lipase from *Geobacillus thermoleovorans* DA2 and Application in Leather Industry. *Enzyme Res*. 2016; Article ID 9034364.
47. Patel GB, Shah KR, Shindhal T, Rakholiya P, Varjani S. Process parameter studies by central composite design of response surface methodology for lipase activity of newly obtained Actinomycete. *Environ. Technol. Innov*. 2021; 23:101724.
48. Fatima S, Faryad A, Ataa A, Joyia FA, Parvaiz A. Microbial lipase production: A deep insight into the recent advances of lipase production and purification techniques. *Biotechnol. Appl. Biochem*. 2021; 68(3):445-58.
49. Kanimozhi K, Wese EG, Devairrakan J, Jegadeeshkumar D. Production and Optimization of Lipase from *Bacillus subtilis*. *Inter J of Bio Techn*. 2011; 2(3):6-10.

ISSN print: 1224-5984
ISSN online: 2248-3942

Rom Biotechnol Lett. 2022; 27(1): 3225-3234
doi: 10.25083/rbl/27.1/3225-3234

Received for publication, December, 11, 2021
Accepted, January, 14, 2022

Original paper

Some atmospheric trace metals deposition in selected trees as a possible biomonitor

KAAN ISINKARALAR

Kastamonu University, Faculty of Engineering and Architecture, Department of Environmental Engineering, Kastamonu, Türkey

Abstract Several trees are effectively used to biomonitor of trace metals in urban environmental pollution. It gives information about the speciation of trace metals and their transition between organs in the plant. In the wood of the trees, it can be determined which part is formed in which year with the help of organs formed by the effect of seasonal differences. Air pollutants damage to humans and other living things in nature is generally referred to as a sign of pollution. They are released from anthropogenic sources accumulate in the bodies of nearby species over time. They give information about the history of air pollutants due to the accumulation in their wood, inner bark, and outer bark. In this study, organs of *Robinia pseudoacacia* L., *Cupressus arizonica* G., and *Platanus orientalis* L. were analyzed as biomonitors with Inductively Coupled Plasma Mass Spectrometry (ICP-MS). All samples were taken from Kocaeli province industrial zone which has quite a wide industrial area. The concentration of selected trace elements as Iron (Fe), Magnesium (Mg), and Zinc (Zn) their emission caused by industrial activities and transport vehicle density. The results of the study show that *Robinia pseudoacacia* L. was the most suitable species for Fe, Mg, and Zn concentration levels as a biomonitor.

Keywords Atmospheric deposition; biomonitor; trace elements; trees

To cite this article: ISINKARALAR K. Some atmospheric trace metals deposition in selected trees as a possible biomonitor. *Rom Biotechnol Lett*. 2022; 27(1): 3225-3234. DOI: 10.25083/rbl/27.1/3225-3234.

✉ *Corresponding author: KAAN ISINKARALAR, Kastamonu University, Faculty of Engineering and Architecture, Department of Environmental Engineering, Kastamonu, Türkiye.
E-mail: kisinkaralar@kastamonu.edu.tr

Introduction

Clean air is a vital requirement for sustainable life including plants, which is necessary for metabolism processes such as respiration, digestion, photosynthesis, which are necessary for living things to survive (Isinkaralar et al. 2021). Despite all air pollution is a global problem that increasingly threatens the ecosystem with the development of technology and irregular urbanization (Greg et al. 2003; Sevik et al. 2018; Shen et al. 2021; Yılmaz and Işınkaralar 2021a, b). It has many sources that trace metals release does not deteriorate and disappear easily in nature also bioaccumulate in their cells (Jayakumar et al. 2021). They can be toxic, poisonous, or carcinogenic on organs which cause various damages depending on their amount (Dai et al. 2021; Rahaman et al. 2021). They can occur with fossil fuel combustion, mining activities, fertilizer application, agricultural activities, and dispersing to certain distances by movements of the wind. It is aimed to identify the sources of each pollutant such as heavy metal, polycyclic aromatic hydrocarbons (PAHs) and volatile organic compounds (VOCs), trace metal, a toxic metal, and macronutrients and micronutrients (can be dangerous in high concentration) (Isinkaralar 2020; Ghoma et al. 2022; Isinkaralar et al. 2022). Therefore, it is important to detect the accumulation levels in plants and trees in the urban environment (Tong et al. 2021). Trace elements that can be needed in very small quantities by humans, animals, and plants despite they play a very important role with high concentrations (Soetan et al. 2010). Especially in plants, high concentrations of these chemicals reduce the growth rate and demonstrate negative effects on cells (Soetan et al. 2010; Adamec et al. 2021).

Although 53 of the 90 elements found in nature are considered heavy metals, only 17 of them can be found in living life and ecosystems according to their solubility level. Iron (Fe) is the 4th most abundant element in the lithosphere and is one of the most vital elements in the life of living things (Abdu et al. 2017). It is a limiting element for the plant mainly due to the low solubility of ferric in an aerobic environment (Emerson et al. 1999). Fe, which is an important micronutrient for the functioning of metabolic activities, biochemical and physiological processes, plays an active role in the formation of many enzymes, DNA and chlorophyll synthesis, respiration, and photosynthesis, increasing yield and plant health (Oleszkiewicz and Sharma 1990). Although abundant in well-aerated soil, its biological activity is low. This is mainly because it forms insoluble iron compounds at neutral pH levels (Kasotia et al. 2021). Due to its presence in insoluble oxidized forms, 30% of globally cultivated soils have low iron concentrations (Rout and Sahoo 2015). However, in soils filled with water, the iron concentration can be found in high amounts in the form of Fe^{+3} (insoluble ferric) due to its low redox potential (Rehman et al. 2021). In this case, high amounts of iron taken into their bodies can turn into toxic effects through lipid peroxidation. Another important heavy metal is Zinc (Zn), a micronutrient necessary for plants. It is one of the major global pollutants in the atmosphere because it releases into the soil and atmosphere from minerals containing Zn, volcanic activities, forest fires, and biotic processes (Pacyna and Pacyna 2001; Shah 2021). Zinc isotopes were found in remote arctic areas due to atmospheric deposition (Simonetti et al. 2000). Although plants take in the form of Zn^{+2} or their compounds with their roots, leaves, cuticles, and stomata thanks to protein carriers from the soil, it is still not known how they are taken into their structures (Rawashdeh and Florin 2015). High concentrations of Zn cause some negative effects on plant bodies (Suresh and Ravishankar 2004). Foremost among them, it has been seen in the studies that it causes weakening of the roots, retardation of growth and development, oxidative stress, disruption of DNA and proteins, photosynthesis, and thus loss of biomass (Fryzova et al. 2017). Magnesium (Mg) is an essential element used in the formation of protein structure and phosphorylation enzymes in plants (Santos et al. 2017). In its deficiency, it causes retardation in plant growth and a decrease in yield, as well as losses in the photosynthesis stage due to it being an essential macronutrient for plants (Guo et al. 2015). Depending on the structure and genotypes of the plants, if they are taken in high amounts, they show different toxic effects. It has a higher level of toxic effect, especially in soils with high acidity but insufficient drainage (Peres et al. 2016). Especially Mg^{+2} has an important mission for climate regulation and carbon sequestration (Goddard et al. 2007; Groshans et al. 2019). Although the presence of the elements that are the subject of the study in the soil is low, their level is increasing thanks to atmospheric transports (from ocean, sea, desert dust, etc.) (Mahowald et al. 2009). The transport, accumulation, and transformation of all these elements into other forms primarily occur with atmospheric deposition including wet, dry, and total (Keesstra et al. 2016).

Biomonitoring with plants is being increasingly used as an alternative method compared to the active methods of working locally and anthropogenic substances range from the atmosphere to the soil. This is due to the high-cost implications of the active and traditional instrumental method. Biomonitors accumulate some environmental pollutants that occur in anthropogenic activities that can tell more information about quantitative (Gómez-Arroyo et al. 2021). Several studies show that the ability of the species to be used as biomonitors to accumulate heavy metals in their bodies and the fact that we can measure their levels have enabled them to become biological receptors (Blevins 1994). The tree species used as biomonitors should not be disinformation immediately due to the accumulation of air pollutants, and they should have stayed in that area for many years. In addition to these, it is desired that they be more in number and have a sufficient amount of organs and tissues in that region so that the correlation can be easily seen (Maresca et al. 2020). Many studies have been conducted on the usability of plants as biomonitors, bioindicators, and bio accumulators since plants are the creatures that provide easy identification and sampling (Guéguen et al. 2012; Turkyilmaz et al. 2018). A variety of

environmental conditions as well as anthropogenic differences have emerged about the use of plants as biomonitors (Pellegrini et al. 2014; Dadea et al. 2017). It is not known how long plants such as moss and lichens are exposed to heavy metal pollution in the air (He et al. 2005). As the best alternative to these plants, the use of leaves of annual plants that are not evergreen solved this problem, and their leaves can easily give data on heavy metal pollution that occurs in a vegetation season (Stojanowska et al. 2020; Isinkaralar and Erdem 2021a, b). It is stated that the healthiest information is obtained with the use of biomonitors by pine, spruce, and fir. The needles of this species have remained on the tree and whose needle ages can be determined clearly for many years. The using barks of trees as biomonitors, the availability of biological material throughout the year healthier, and longer years of information have been obtained from the past to the present. Especially in regions with four seasons, in areas with traffic and industry, the barks of tree species taken from areas very close to the pollutant source clearly showed the level of pollutants. While the ages of the trees are determined by their rings, the change in trees that live for many years reveals the situation more clearly.

This study has been carried out in Fe, Mg, and Zn elements (another name as nutrient elements) accumulation due to their transition between atmosphere to plants. The use of wood, inner bark, and outer bark was evaluated in selected trees as biomonitors grew in Kocaeli province industrial zone. The *Robinia pseudoacacia* L., *Cupressus arizonica* G., and *Platanus orientalis* L. were determined deposition of Fe, Mg, and Zn in organs.

Materials and Methods

Sample site

This study was the preferred species as *Robinia pseudoacacia* L. (Locust tree), *Cupressus arizonica* G. (Arizona cypress), and *Platanus orientalis* L. (Eastern sycamore). All samples were taken from the main trunk of trees in the organized industrial zone (OSB) of Kocaeli city. A 10 cm thick log sample was taken from the northern part and approximately 50-60 cm high from the ground. The organs of *Robinia pseudoacacia* L., *Cupressus arizonica* G., and *Platanus orientalis* L. were coded as W (wood), IB (inner bark), and OB (outer bark). They were determined different age portions as to be 30 years old, have come from 1991-1993 to 2018-2020 within three years (taking into account their widths).

Preparation of samples

The samples were not washed due to organs do not have direct contact with the external environment (such as atmosphere and soil) that were physically trapped on the surfaces of the bark. All samples were kept in room conditions until they became air-dry without being exposed to direct sunlight for two weeks after pre-treatment. The samples were brought to the 1-2 cm interval without using metal and weighed as powder as 0.5 g each sample. Samples taken into glass containers were dried in a controlled oven at 50 ^{o}C for 7 days. The samples were taken as 0.5 g weighed and 5 mL nitric acid (65% HNO_3, Merck, Germany) and 2 mL hydrogen peroxide (30% H_2O_2, Merck, Germany) were added to vessels. The combustion process was carried out in the microwave oven at 200 ^{o}C for 15 minutes in the 3052 Method (USEPA 1996). The resulting samples were made up to 25 mL with ultrapure water for dilution and Fe, Mg, and Zn analyzes were made by atomic emission spectrometry (ICP-OES) with a plasma source device (SpectroBlue, Spectro). All solutions were prepared using analytical reagent grade and ultrapure water was used for sample digestion.

Statistical data analyses

Statistical analyses were carried out by using SPSS 22.0 statistical package program. All measurements are repeated in triplicate and the obtained data are analyzed by analysis of variance (ANOVA) and Duncan test. The ANOVA was also used to specify significant differences among varied species for the organs.

Results and discussion

Changing of the Fe Concentration

The biomonitor chosen was the bark and organ of a *Robinia pseudoacacia* L., *Cupressus arizonica* G., and *Platanus orientalis* L. which, due to its widely used as plants in parks, roads, and landscape. Table 1 has been proven that they can provide information on the presence of the Fe element in the district.

As regards the ANOVA that the change in the concentration of Fe element on an organ basis in all three species is statistically significant (p<0.001). Considering the Duncan test results, the lowest values are obtained in the W and the highest values were obtained in the OB. In the W and IB, the values were obtained as the same group of *Platanus orientalis* L., and in other species, each organ formed a separate group. It is noteworthy that the values obtained in the OB are many times higher than the values obtained in the IB and W in all species. The lowest value in the OB is obtained in *Platanus orientalis* L. with 137.7 ppm, the highest value is obtained in *Robinia pseudoacacia* L. with 3008.4 ppm, the highest value in the IB is obtained in *Robinia pseudoacacia* L. with 60 ppm, and the lowest value is obtained in *Platanus orientalis* L. with 6.6 ppm. In the W, the lowest value is obtained in *Robinia pseudoacacia* L. with 14.7 ppm, and the highest value is obtained in *Platanus orientalis* L. with 16.9 ppm. According to these results, it can be said that the lowest values are obtained in *Platanus orientalis* L. and the highest values are obtained in *Robinia pseudoacacia* L. The change in the Fe concentration in W depending on the age range is given in Table 2.

Table 2. The Fe concentration (ppm) age interval and species change of in wood**.**

Table 1. Change of Fe concentrations (ppm) based on species

Organ	Species			*F* value
	Robinia pseudoacacia L.	*Cupressus arizonica* G.	*Platanus orientalis* L.	
W	14.7 a	15.4 a	16.9 a	0.214 ns
IB	60 Cb	33.4 Bb	6.6 Aa	4918***
OB	3008.4 Cc	2937.3 Bc	137.7 Ab	150839.7***
F value	118349.1***	185795.1***	64.9***	

Uppercase letters: horizontal direction, Lowercase letters: vertical direction, ***significant level at 0.001, ns: not significant

Table 2. The Fe concentration (ppm) age interval and species change of in wood

Range of age	Species			*F* value
	Robinia pseudoacacia L.	*Cupressus arizonica* G.	*Platanus orientalis* L.	
2018-2020	16.7 Cg	11.4 Be	7.3 Ae	179***
2015-2017	11.1 Ad	23.2 Ch	11.7 Bg	16280.9***
2012-2014	8 Bb	9.3 Cc	5.9 Ac	1248.5***
2009-2011	14.4 Bf	10.6 Ad	55.2 Cj	121256.5***
2006-2008	33.6 Ch	17.6 Ag	19.9 Bh	167844.7***
2003-2005	9.2 Bc	25.6 Ci	3.3 Ab	41708***
2000-2002	13.5 Be	7.3 Ab	50.6 Ci	223201.3***
1997-1999	34.5 Ci	6.4 Aa	7.6 Bf	396930.2***
1994-1996	3.1 Ba	30 Cj	1 Aa	57430.1***
1991-1993	3 Aa	12.5 Cf	6.7 Bd	23315***
F Value	3178.6***	17870.1***	290581.9***	

Uppercase letters: horizontal direction, Lowercase letters: vertical direction, ***significant level at 0.001

When the values showing the change of Fe element according to the age range were examined, it is seen that the highest value in *Robinia pseudoacacia* is obtained with 34.5 ppm in 1997-1999, the lowest value with 3 ppm in 1991-1993. In *Cupressus arizonica* G., the lowest value was obtained 6.4 ppm in 1997-1999, the highest value is obtained as 30 ppm in 1994-1996. In *Platanus orientalis* L., the highest value with 55.2 ppm in the years 2009-2011, and the lowest value with 1 ppm in the years 1994-1996. According to the ANOVA, it is determined that the variation of Fe concentration depending on the species is statistically significant at least 99% confidence level (p<0.001) in all age ranges. When the values were examined, it is very difficult to say that the Fe concentration changes regularly based on species or year. This situation can be interpreted as the change of Fe concentration in plants does not change primarily depending on the species or year, and other factors are more dominant.

Changing of the Mg Concentration

The biomonitor chosen was the bark and organ of a species in the variation of the Mg concentration assessed depending on the species in Table 3.

Table 3. Change of Mg concentrations (ppm) based on species

Organ	Species			*F* value
	Robinia pseudoacacia L.	*Cupressus arizonica* G.	*Platanus orientalis* L.	
W	78.6 Aa	119.6 Ba	376 Ca	351.086***
IB	206.4 Ab	857.6 Bb	3486.8 Cc	459489.9***
OB	1639 Ac	1744.2 Bc	3224.6 Cb	1921.4***
F value	876.2***	7484.5***	12764.9***	

Uppercase letters: horizontal direction, Lowercase letters: vertical direction, ***significant level at 0.001

According to the ANOVA, it is determined that the change of Mg element in all organs is statistically significant (at least p<0.001) in both species and organ basis in all species. When the average values and Duncan test results are examined, the lowest value is obtained in the OB is *Robinia pseudoacacia* L. with 1639 ppm, the highest value in *Platanus orientalis* L. with 3224.6 ppm, and the highest value in the IB with 3486.8 ppm in *Platanus orientalis* L., the lowest value with 228.4 ppm in *Platanus orientalis* L. and the lowest value in the W part with 78.6 ppm in *Robinia pseudoacacia* L. and the highest value is obtained in *Platanus orientalis* L. with 376 ppm. However, it can be said that the Mg concentration is generally listed as W<IB<OB (There is no statistically significant difference between W and IB in *Platanus orientalis* L.). In addition, it is seen that the values obtained in the OB are much higher than the values obtained in the IB and W. The change in the Mg concentration in W is given depending on the age in Table 4.

Table 4. Age interval and directional change of Mg (ppm) element in wood

Range of age	Species			F value
	Robinia pseudoacacia L.	*Cupressus arizonica* G.	*Platanus orientalis* L.	
2018-2020	254.9 Bj	65.2 Aa	478.4 Ci	18109.6***
2015-2017	51.6 Ad	104.4 Bb	393.1 Cg	14902***
2012-2014	24.6 Aa	122 Be	327.7 Ca	27538.2***
2009-2011	31 Ab	134.3 Bg	366.9 Ce	74288.3***
2006-2008	45.2 Ac	166 Bh	349.6 Cb	14127.7***
2003-2005	82.7 Ah	129.8 Bf	416.2 Ch	120178.8***
2000-2002	56.7 Ae	128.3 Bf	357.6 Cc	33548.6***
1997-1999	60.4 Af	123 Be	327.5 Ca	33506.6***
1994-1996	69.9 Ag	108.5 Bc	380.1 Cf	33147***
1991-1993	109.5 Ai	114.3 Bd	362.6 Cd	28626.4***
F Value	3798.5***	587.5***	2182.6***	

Uppercase letters: horizontal direction, Lowercase letters: vertical direction, ***significant level at 0.001

Table 5. Change of Zn concentrations (ppm) based on organ and direction

Organ	Species			*F* value
	Robinia pseudoacacia L.	*Cupressus arizonica* G.	*Platanus orientalis* L.	
W	2.8 Aa	3.8 Bb	2.5 Aa	11.347***
IB	4.9 Ab	11.8 Cc	5.6 Bb	4961.4***
OB	178.4 Cc	0.2 Aa	10.3 Bc	157246.2***
F value	28931.6***	57.2***	294.5***	

Uppercase letters: horizontal direction, Lowercase letters: vertical direction, ***significant level at 0.001

Table 6. Age interval and directional change of Zn (ppm) element in wood

Range of age	Species			*F* value
	Robinia pseudoacacia L.	*Cupressus arizonica* G.	*Platanus orientalis* L.	
2018-2020	3.3 Cf	3.1 Bc	2.6 Ag	142.8***
2015-2017	2.5 Bd	4.5 Ch	2.2 Ad	10310.2***
2012-2014	1.4 Ab	4.0 Cg	2.6 Bf	21501.6***
2009-2011	2.1 Bc	3.6 Cd	1.8 Ab	9516.8***
2006-2008	1.4 Ab	7.6 Ci	3.5 Bj	48562***
2003-2005	3.1 Be	4.0 Cg	2.0 Ac	14522.8***
2000-2002	4.4 Ch	3.7 Be	2.8 Ah	3577.6***
1997-1999	4.6 Ci	1.8 Aa	2.5 Be	22632.8***
1994-1996	1 Aa	2.4 Cb	1.5 Ba	23277.2***
1991-1993	4.1 Cg	3.8 Bf	3.1 Ai	605.3***
F value	4616.4***	16115.8***	3069.7***	

Uppercase letters: horizontal direction, Lowercase letters: vertical direction, ***significant level at 0.001

The Mg concentration was examined based on species in all periods it is statistically significant (at least $p<0.001$) except for 1991-1993. The highest value in *Robinia pseudoacacia* L. is 254,9 ppm in 2018-2020, the lowest value with 24.6 ppm in 2012-2014, the lowest value in *Cupressus arizonica* G. with 65.2 ppm in 2018-2020, the highest value with 166 ppm in 2006-2008, the highest value in *Platanus orientalis* L. with 478.4 ppm in 2018-2020, the lowest value is obtained between 1997-1999 with 327.5 ppm. When the average values are examined, it is seen that the Mg concentration generally tends to increase until the period of 2006-2011, but it shows a general decrease after these dates, and *Platanus orientalis* L. more clearly reflects variance.

Changing of the Zn Concentration

Another element Zn evaluated on the organ is given in Table 5.

According to the ANOVA that the change of Zn element in all organs is statistically significant ($p<0.001$), both based on species and in all species. The highest value in the IB is found to be in *Cupressus arizonica* G. with 11.8 ppm, the lowest value with 4.9 ppm in *Robinia pseudoacacia* L., the highest value in the OB part with 178.4 ppm in *Robinia pseudoacacia* L., the lowest value is found to be in *Cupressus arizonica* G. with 0.2 ppm, the highest value in the W part with 3.8 ppm in *Cupressus arizonica* G., the lowest value is found to be in *Platanus*

orientalis L. with 2.5 ppm. It is seen that in *Robinia pseudoacacia* L. and *Cupressus arizonica* G., the Zn concentration is listed as W<IB<OB and the values obtained in the OB are much higher than the values obtained in the IB and W, as in other elements. The change in the Zn concentration in W is given depending on the age range in Table 6.

The ANOVA results related to the change of Zn element concentrations according to age range were examined, it is seen that the variation based on species in all organs and statistically significant (p<0.001). When the average values are examined, the highest values are obtained between 1997-1999 with 4.6 ppm in *Robinia pseudoacacia* L. and 7.6 ppm between 2006-2008 in *Cupressus arizonica* G., in *Platanus orientalis* L. between 2006-2008 with 3.5 ppm. When the table values are examined, the first striking result is that the lowest values in all age ranges have been obtained in *Platanus orientalis* L. species. Apart from this, generally, the highest values are obtained in *Cupressus arizonica* G. species. In addition, it can be said that the Zn concentration in *Cupressus arizonica* G. and *Platanus orientalis* L. woods generally tends to increase.

The Fe, Mg, and Zn changes are statistically significant at least at the 99% confidence level on the organ. They are an important factor in atmospheric deposition controlling which can cause global carbon cycling and climate change (Jickells et al. 2005; Lin et al. 2014). The data was obtained that the Fe, Mg, and Zn can firstly accumulate in the outer bark (OB) than inner bark (IB), and finally woods (W) of the trees. While the lowest in W, it is noteworthy that their concentrations were quite high in the industrial zone. In the studies, it is stated that the pollutant concentrations differ greatly depending on the organ. The values can change with the traffic density or some pollutant releases. Studies on Fe have shown that it may have soil pH and redox potential, but may also be due to reactions of macronutrients and auxiliary heavy metals (Bienfait 1988; Briat et al. 2010). Madejón et al. (2004) showed that the heavy metals in *Populus alba* they found in the air were in positive correlation with the amounts in the soil. Currently, researchers have executed many studies on the change of heavy and trace metals that the lowest were obtained in W and the highest in the OB (Akarsu, 2019). Moreira et al. (2016) were revealed a hierarchy of element concentrations according to the street classification by traffic density Another study was obtained the highest concentrations of Pb, Co, and Fe in the outer shell, and the lowest was obtained in W (Sevik et al. 2020). In both studies, while the concentrations of the elements are not significant in the OB facing the direction of traffic and industry, the highest concentrations were obtained in the OB in the part facing the direction of traffic and industry. Drava et al. (2020) was established a relationship between Fe concentration in the bioindicator reflect the mortality in the various areas of the city. Turkyilmaz et al. (2019) have stated that some heavy metal concentrations in the OB are found higher than in other organs. Zhang et al. (2019) was shown that the Pb found in the species analyzed as a biomonitor is air-borne rather than soil. In parallel with this, it has been stated that Hg-based pollution is more caused by air pollution than soil. Ateya (2020) supported that Pb, Cd, Cr, and Ni concentrations are attained a high level in barks than in wood. Alaqouri et al. (2020) stated that although the Cu concentration did not change, Zn and Pb concentrations in the annual rings shifted to a certain extent. As a matter of fact, in many studies, it has been stated that traffic and industrial facilities are the most important source of many heavy metals (Al-Thani et al. 2018; Aricak et al. 2020). Olowoyo et al. (2010) were investigated the *Jacaranda mimosifolia* tree as a biomonitor of atmospheric trace metals in Tshwane City, South Africa. The Zn concentration is necessary although they found high Zn concentration in traffic areas due to emissions of fuel. In addition, Zn is an element used in the production of motor oil and tires and accumulates in tree species as these are eroded and released into the environment over time. Previous work showed that these elements uptake by microorganisms and higher plants due to adsorption on organic and inorganic surfaces (Weiss et al. 2007).

It is thought that the reason why the heavy metal concentrations in the OB are at higher levels than in other organs. This pollution is seen more clearly in industrial regions due to the rough structure of the bark and the heavy metals adhering to this structure and the particulate matter contaminated (Kumar and Khan 2021). Studies have shown that other pollutants adhere to particulate matter and infect particulate matter with heavy metals. Then heavy metal concentrations in these organs increase as these particulate substances settle on plant organs (Çobanoğlu 2019; Cetin et al. 2021). The rough surface structure of the OB facilitates the adhesion of particulate materials. The high concentration of heavy metals is explained in the barks from traffic and industry areas. So contamination of particulate materials with heavy metals originating from intense emission (Sevik et al. 2020). Because traffic and industry release many pollutants (Turkyilmaz et al. 2020; Savas et al. 2021). The ability of each plant or tree species to absorb pollutants depends on its physiological character, as well as the accumulation and behavior of each heavy metal (Sert et al. 2019; Świsłowski et al. 2020). Thus, the accumulation of these pollutants is shaped under many factors such as the presence, over years, the tolerance capacities in different bodies, climate, prevailing wind direction (Sevik et al. 2019; Karacocuk et al. 2022). Because many factors affect the entry and accumulation of heavy metals in the plant body (Vymazal 2016). In addition to plant structure and environmental factors such as plant type, rainfall and moisture amount, plant habitus, organ structure, the type of heavy metal and its interaction with the plant are also important factors affecting the accumulation of heavy metals in plant organs (Belimov et al. 2003). The concentrations of the elements in different periods are at different levels reveals this situation again because many factors are affecting the entry and accumulation of heavy metals into the plant body (Wang et al. 2018). It shows that the transfer of heavy metals within the plant, especially in the wood part, is limited. For this reason, the fact that the heavy metal concentration in the atmosphere during the formation of woods is variable

causes the heavy metal concentrations in the woods formed in different years to be at different levels.

Conclusion

One of the main purposes of the study is to obtain information about the movement of trace metals into the plant from industrial and transportation over the years. It is determined that there may be great differences between the OB, IB, and W adjacent to each other in the same direction, as well as the element concentrations of the trees formed in the OSB, Kocaeli. This shows that the transfer of Fe, Mg ve Zn between organs can be interpreted as very limited. The level of knowledge about the speciation and displacement of heavy metals from their entry into the plant is quite limited. The Fe, Mg ve Zn concentrations can accumulate in *Robinia pseudoacacia* L., *Cupressus arizonica* G., and *Platanus orientalis* L. over the years depending on the organ factor in the industrial area. Trees organs have an accumulation of atmospheric trace metals from the recent past to the present. Although the most suitable species to be used for Fe concentration levels is *Robinia pseudoacacia* L., Mg concentration levels are *Platanus orientalis* L. and *Cupressus arizonica* G. is the most suitable species for Zn accumulation.

References

1. Abdu N, Abdullahi AA, Abdulkadir A (2017) Heavy metals and soil microbes. Environmental chemistry letters, 15(1), 65-84. https://doi.org/10.1007/s10311-016-0587-x
2. Adamec L, Matušíková I, Pavlovič A (2021) Recent ecophysiological, biochemical and evolutional insights into plant carnivory. Annals of Botany. https://doi.org/10.1093/aob/mcab071
3. Akarsu H (2019) Determination of Heavy Metal Accumulation in Atmosphere by Being Aid of Annual Rings, Kastamonu University Graduate School of Natural and Applied Sciences Department of Sustainable Agriculture and Natural Plant Resources, MsC Thesis, 71 pages
4. Alaqouri HAA, Genc CO, Aricak B, Kuzmina N, Menshikov S, Cetin M (2020) The possibility of using Scots pine needles as biomonitor in determination of heavy metal accumulation. Environmental Science and Pollution Research, 27(16), 20273-20280. https://doi.org/10.1007/s11356-020-08449-1
5. Al-Thani H, Koç M, Isaifan RJ (2018) A review on the direct effect of particulate atmospheric pollution on materials and its mitigation for sustainable cities and societies. Environmental science and pollution research, 25(28), 27839-27857. https://doi.org/10.1007/s11356-018-2952-8
6. Aricak B, Cetin M, Erdem R, Sevik H, Cometen H (2020) The Usability of Scotch Pine (Pinus sylvestris) as a Biomonitor for Traffic-Originated Heavy Metal Concentrations in Turkey. Polish Journal of Environmental Studies, 29(2). DOI: https://doi.org/10.15244/pjoes/109244
7. Ateya TAA (2020) The Availability of Picea pungens Engelm. Installation in Monitoring The Change of Heavy Metal Pollution in Urban Planning Studies, Kastamonu University Graduate School of Natural and Applied Sciences Department of Engineering Management, MsC Thesis, 79 pages
8. Belimov AA, Safronova VI, Tsyganov VE, Borisov AY, Kozhemyakov AP, Stepanok VV, Martenson AM, Gianinazzi-Pearson V, Tikhonovich IA (2003) Genetic variability in tolerance to cadmium and accumulation of heavy metals in pea (Pisum sativum L.). Euphytica, 131(1), 25-35. https://doi.org/10.1023/A:1023048408148
9. Bienfait HF (1988) Mechanisms in Fe-efficiency reactions of higherplants. Journal of Plant Nutrition 116, 605e629. https://doi.org/10.1080/01904168809363828
10. Blevins DG (1994) Uptake, translocation, and function of essential mineral elements in crop plants. Physiology and determination of crop yield, 259-275. DOI:10.1016/B978-0-12-385531-2.00004-9
11. Briat JF, Duc C, Ravet K, Gaymard F (2010) Ferritins and iron storage in plants. Biochimica et Biophysica Acta (BBA)-General Subjects, 1800(8), 806-814. https://doi.org/10.1016/j.bbagen.2009.12.003
12. Çetin M, Şevik H, Türkyılmaz A, Işınkaralar K (2021) Using Abies's Needles as Biomonitors of Recent Heavy Metal Accumulation. Kastamonu University Journal of Engineering and Sciences, 7(1), 1-6. Retrieved from https:// dergipark.org.tr /en/pub/kastamonujes/ issue/ 63105/892118
13. Dadea C, Russo A, Tagliavini M, Mimmo T, Zerbe S (2017) Tree species as tools for biomonitoring and phytoremediation in urban environments: A review with special regard to heavy metals. Arboriculture & Urban Forestry, 43(434), 155-167. https://doi.org/10.1007/ s10653-020-00605-3
14. Dai Y, Shi J, Zhang N, Pan Z, Xing C, Chen X (2021) Current research trends on microplastics pollution and impacts on agro-ecosystems: A short review. Separation Science and Technology, 1-14. https://doi.org/10.1080/01496395.2021.1927094
15. Drava G, Ailuno G, Minganti V (2020) Trace Element Concentrations Measured in a Biomonitor (Tree Bark) for Assessing Mortality and Morbidity of Urban Population: A New Promising Approach for Exploiting the Potential of Public Health Data. Atmosphere, 11(8), 783. https://doi.org/10.3390/atmos11080783
16. Emerson D, Weiss JV, Megonigal JP (1999) Iron-oxidizing bacteria are associated with ferric hydroxide precipitates (Fe-plaque) on the roots of wetland plants. Applied and Environmental Microbiology, 65(6), 2758-2761. https://doi.org/10.1128/AEM.65.6.2758-2761.1999 •
17. Fryzova R, Pohanka M, Martinkova P, Cihlarova H, Brtnicky M, Hladky J, Kynicky J (2017) Oxidative

stress and heavy metals in plants. Reviews of environmental contamination and toxicology volume 245, 129-156.
18. Ghoma WEO, Sevik H, Isinkaralar K (2022) Using indoor plants as biomonitors for detection of toxic metals by tobacco smoke. Air Quality, Atmosphere & Health, https://doi.org/10.1007/s11869-021-01146-z
19. Goddard MA, Mikhailova EA, Christopher JP, Schlautman MA (2007) Atmospheric Mg2+ wet deposition within the continental United States and implications for soil inorganic carbon sequestration. Tellus B: Chemical and Physical Meteorology, 59(1), 50-56. https://doi.org/10.1111/j.1600-0889.2006.00228.x
20. Gómez-Arroyo S, Zavala-Sánchez MÁ, Alonso-Murillo CD, Cortés-Eslava J, Amador-Muñoz O, Jiménez-García LF, Morton-Bermea O (2021) Moss (Hypnum amabile) as biomonitor of genotoxic damage and as bioaccumulator of atmospheric pollutants at five different sites of Mexico City and metropolitan area. Environmental Science and Pollution Research, 28(8), 9849-9863. https://doi.org/10.1007/s11356-021-16153-x
21. Gregg JW, Jones CG, Dawson TE (2003) Urbanization effects on tree growth in the vicinity of New York City. Nature, 424(6945), 183-187. https://doi.org/10.1038/nature01728
22. Groshans GR, Mikhailova EA, Post CJ, Schlautman MA, Cope MP, Zhang L (2019) Ecosystem services assessment and valuation of atmospheric magnesium deposition. Geosciences, 9(8), 331. https://doi.org/10.3390/ geosciences9080331
23. Guéguen F, Stille P, Geagea ML, Boutin R (2012) Atmospheric pollution in an urban environment by tree bark biomonitoring–Part I: Trace element analysis. Chemosphere, 86(10), 1013-1019. https://doi.org/10.1016/j.chemosphere.2011.11.040
24. Guo W, Chen S, Hussain N, Cong Y, Liang Z, Chen K (2015) Magnesium stress signaling in plant: just a beginning. Plant Signaling & Behavior, 10(3), e992287. https://doi.org/10.4161/15592324.2014.992287
25. He ZL, Yang XE, Stoffella PJ (2005) Trace elements in agroecosystems and impacts on the environment. Journal of Trace elements in Medicine and Biology, 19(2-3), 125-140. https://doi.org/10.1016/j.jtemb.2005.02.010
26. Isinkaralar K (2020) Removal of formaldehyde and BTEX in indoor air using activated carbon produced from horse chestnut (Aesculus Hippocastanum L.) Shell. Ph.D. Thesis Hacettepe University Institute of Science, Department of Environmental Engineering. Ankara, Turkey
27. Isinkaralar K, Erdem R (2021a) Landscape Plants as Biomonitors for Magnesium Concentration in Some Species. International Journal of Progressive Sciences and Technologies, 29(2), 468-473.
28. Isinkaralar O, Tonuk UG, Isinkaralar K, Yilmaz D (2021) An Analysıs on Sustainability Assessment Tools at Neighborhood Scale. Sosyal, Beşeri ve İdari Bilimler Alanında Uluslararası Araştırmalar VIII. Eğitim Yayınevi, Konya, pp 517-530
29. Işınkaralar K, Erdem R (2021b) Changes of Calcium Content on Some Trees in Kocaeli. Kastamonu University Journal of Engineering and Sciences, 7(2), 148-154. Retrieved from https://dergipark.org.tr/en/pub/kastamonujes/issue/66389/1015387
30. Isinkaralar K, Gullu G, Turkyilmaz A (2022) Experimental study of formaldehyde and BTEX adsorption onto activated carbon from lignocellulosic biomass. Biomass Conversion and Biorefinery. https://doi.org/10.1007/s13399-021-02287-y
31. Jayakumar M, Surendran U, Raja P, Kumar A, Senapathi V (2021) A review of heavy metals accumulation pathways, sources and management in soils. Arabian Journal of Geosciences, 14(20), 1-19. https://doi.org/10.1007/s12517-021-08543-9
32. Jickells TD et al. (2005) Global iron connections between desert dust, ocean biogeochemistry, and climate, Science, 308(5718), 67–71, doi:10.1126/science.1105959.
33. Karacocuk T, Sevik H, Isinkaralar K, Turkyilmaz A, Cetin M (2022) The change of Cr and Mn concentrations in selected plants in Samsun city center depending on traffic density. Landscape and Ecological Engineering 18, 75–83. https://doi.org/10.1007/s11355-021-00483-6
34. Kasotia A, Varma A, Choudhary DK (2021) Deployment of Benign Bacterial Strains to Improve Soil Productivity Under Drought Stress. In Climate Change and the Microbiome (pp. 477-489). Springer, Cham.
35. Keesstra SD, Bouma J, Wallinga J, Tittonell P, Smith P, Cerdà A, ... & Fresco LO (2016) The significance of soils and soil science towards realization of the United Nations Sustainable Development Goals. Soil, 2(2), 111-128. https://doi.org/10.5194/soil-2-111-2016
36. Lin YC, Chen JP, Ho TY, Tsai IC (2015) Atmospheric iron deposition in the northwestern Pacific Ocean and its adjacent marginal seas: the importance of coal burning. Global Biogeochemical Cycles, 29(2), 138-159. https://doi.org/10.1002/2013GB004795
37. Madejón P, Maranon T, Murillo JM, Robinson B (2004) White poplar (Populus alba) as a biomonitor of trace elements in contaminated riparian forests. Environmental Pollution, 132(1), 145-155. https://doi.org/10.1016/j.envpol.2004.03.015
38. Mahowald NM, Engelstaedter S, Luo C, Sealy A, Artaxo P, Benitez-Nelson C, ... & Siefert RL (2009) Atmospheric iron deposition: global distribution, variability, and human perturbations. Annual Review of Marine Science, 1, 245-278. https://doi.org/10.1146/annurev.marine.010908.163727
39. Maresca V, Sorbo S, Loppi S, Funaro F, Del Prete D, Basile A (2020) Biological effects from environmental pollution by toxic metals in the “land of fires” (Italy) assessed using the biomonitor species Lunularia cruciata L. (Dum). Environmental

Pollution, 265, 115000. DOI: 10.1016/j.envpol.2020.115000
40. Moreira TCL, de Oliveira RC, Amato LFL, Kang CM, Saldiva PHN, Saiki M (2016) Intra-urban biomonitoring: source apportionment using tree barks to identify air pollution sources. Environment international, 91, 271-275. https://doi.org/10.1016/j.envint.2016.03.005
41. Oleszkiewicz JA, Sharma VK (1990) Stimulation and inhibition of anaerobic processes by heavy metals—a review. Biological Wastes, 31(1), 45-67. https://doi.org/10.1016/0269-7483(90)90043-R
42. Pacyna JM, Pacyna EG (2001) An assessment of global and regional emissions of trace metals to the atmosphere from anthropogenic sources worldwide. Environmental reviews, 9(4), 269-298. https://doi.org/10.1016/j.gca.2007.04.026
43. Pellegrini E, Lorenzini G, Loppi S, Nali C (2014) Evaluation of the suitability of Tillandsia usneoides (L.) L. as biomonitor of airborne elements in an urban area of Italy, Mediterranean basin. Atmospheric Pollution Research, 5(2), 226-235. https://doi.org/10.5094/APR.2014.028
44. Peres TV, Schettinger MRC, Chen P, Carvalho F, Avila DS, Bowman AB, Aschner M (2016) Manganese-induced neurotoxicity: a review of its behavioral consequences and neuroprotective strategies. BMC Pharmacology and Toxicology, 17(1), 1-20. DOI: 10.1186/s40360-016-0099-0
45. Rahaman MS, Rahman MM, Mise N, Sikder T, Ichihara G, Uddin MK, Kurasaki M, Ichihara S (2021) Environmental arsenic exposure and its contribution to human diseases, toxicity mechanism and management. Environmental Pollution, 117940. https://doi.org/10.1016/j.envpol.2021.117940
46. Rawashdeh HM, Florin S (2015) Foliar application with iron as a vital factor of wheat crop growth, yield quantity and quality: A Review. International Journal of Agricultural Policy and Research, 3(9), 368-376. DOI: 10.15739/IJAPR.062
47. Rehman AU, Nazir S, Irshad R, Tahir K, ur Rehman K, Islam RU, Wahab Z (2021) Toxicity of heavy metals in plants and animals and their uptake by magnetic iron oxide nanoparticles. Journal of Molecular Liquids, 321, 114455. https://doi.org/10.1016/j.molliq.2020.114455
48. Rout GR, Sahoo S (2015) Role of iron in plant growth and metabolism. Reviews in Agricultural Science, 3, 1-24. https://doi.org/10.7831/ras.3.1
49. Santos EF, Santini JMK, Paixão AP, Júnior EF, Lavres J, Campos M, Dos Reis AR (2017) Physiological highlights of manganese toxicity symptoms in soybean plants: Mn toxicity responses. Plant physiology and biochemistry, 113, 6-19. https://doi.org/10.1016/j.plaphy.2017.01.022
50. Savas DS, Sevik H, Isinkaralar K, Turkyilmaz A, Cetin M (2021) The potential of using Cedrus atlantica as a biomonitor in the concentrations of Cr and Mn. Environ Sci Pollut Res 28, 55446–55453. https://doi.org/10.1007/s11356-021-14826-1
51. Sert EB, Turkmen M, Cetin M (2019) Heavy metal accumulation in rosemary leaves and stems exposed to traffic-related pollution near Adana-İskenderun Highway (Hatay, Turkey). Environmental monitoring and assessment, 191(9), 1-12. https://doi.org/10.1007/s10661-019-7714-7
52. Sevik H, Isinkaralar K, Isinkaralar O (2018) Indoor air quality in hospitals: the case of Kastamonu Turkey. J Chem Biol Phys Sci Sect D 9(1):67–73
53. Sevik H, Cetin M, Ozel HB, Ozel S, Cetin IZ (2020) Changes in heavy metal accumulation in some edible landscape plants depending on traffic density. Environmental Monitoring and Assessment, 192 (2), 78. https://doi.org/10.1007/s10661-019-8041-8
54. Sevik H, Ozel HB, Cetin M, Özel HU, Erdem T (2019) Determination of changes in heavy metal accumulation depending on plant species, plant organism, and traffic density in some landscape plants. Air Quality, Atmosphere & Health, 12 (2), 189-195. https://doi.org/10.1007/s11869-018-0641-x
55. Shah SB (2021) Heavy metals in the marine environment—an overview. Heavy Metals in Scleractinian Corals, 1-26.
56. Shen H, Luo, Z, Xiong R, Liu X, Zhang L, Li Y, Du W, Chen Y, Cheng H, Shen G, Tao S (2021) A critical review of pollutant emission factors from fuel combustion in home stoves. Environment International, 157, 106841. https://doi.org/10.1016/j.envint.2021.106841
57. Simonetti A, Gariépy C, Carignan J (2000) Pb and Sr isotopic compositions of snowpack from Québec, Canada: Inferences on the sources and deposition budgets of atmospheric heavy metals. Geochimica et Cosmochimica Acta, 64(1), 5-20. https://doi.org/10.1016/S0016-7037(99)00207-0
58. Soetan KO, Olaiya CO, Oyewole OE (2010) The importance of mineral elements for humans, domestic animals and plants-A review. African journal of food science, 4(5), 200-222. https://doi.org/10.5897/AJFS.9000287
59. Stojanowska A, Rybak J, Bożym M, Olszowski T, Bihałowicz JS (2020) Spider Webs and Lichens as Bioindicators of Heavy Metals: A comparison study in the vicinity of a copper smelter (Poland). Sustainability, 12(19), 8066. https://doi.org/10.3390/su12198066
60. Suresh B, Ravishankar GA (2004) Phytoremediation—a novel and promising approach for environmental clean-up. Critical reviews in biotechnology, 24(2-3), 97-124. https://doi.org/10.1080/ 07388550490493627
61. Tong R, Fang Y, Zhang B, Wang Y, Yang X (2021) Monitoring and evaluating the control effect of dust suppressant on heavy metals based on ecological and health risks: a case study of Beijing. Environmental Science and Pollution Research, 28(12), 14750-14763. https://doi.org/10.1007/s11356-020-11648-5
62. Turkyilmaz A, Cetin M, Sevik H, Isinkaralar K, Saleh EAA (2020) Variation of heavy metal accumulation in certain landscaping plants due to traffic density.

Environment, Development and Sustainability, 22 (3), 2385-2398. https://doi.org/10.1007/s10668-018-0296-7
63. Turkyilmaz A, Sevik H, Isinkaralar K, Cetin M (2018) Using Acer platanoides annual rings to monitor the amount of heavy metals accumulated in air. Environ Monit Assess 190:578. https://doi.org/10.1007/s10661-018-6956-0
64. Turkyilmaz A, Sevik H, Isinkaralar K, Cetin M (2019) Use of tree rings as a bioindicator to observe atmospheric heavy metal deposition, Environmental Science and Pollution Research, 26 (5), 5122-5130. https://doi.org/10.1007/s11356-018-3962-2
65. USEPA E (1996) Method 3052: Microwave assisted acid digestion of siliceous and organically based matrices. United States Environmental Protection Agency, Washington, DC USA.
66. Vymazal J (2016) Concentration is not enough to evaluate accumulation of heavy metals and nutrients in plants. Science of the total environment, 544, 495-498. https://doi.org/10.1016/j.scitotenv.2015.12.011
67. Yılmaz D, Işınkaralar Ö (2021a) How Can Natural Environment Scoring Tool (Nest) be Adapted for Urban Parks?. Kastamonu University Journal of Engineering and Sciences, 7(2), 127-139. Retrieved from https:// dergipark.org.tr /tr/pub /kastamonujes /issue/66389/ 1013821
68. Yılmaz D, Işınkaralar Ö (2021b) Climate Action Plans Under Climate-Resilient Urban Policies. Kastamonu University Journal of Engineering and Sciences, 7(2), 140-147. Retrieved from https://dergipark.org.tr/tr/pub/kastamonujes/issue/66389/1014599
69. Wang R, Shafi M, Ma J, Zhong B, Guo J, Hu X, Xu W, Yang Y, Ruan Z, Wang Y, Ye Z, Liu D (2018) Effect of amendments on contaminated soil of multiple heavy metals and accumulation of heavy metals in plants. Environmental Science and Pollution Research, 25(28), 28695-28704. https://doi.org/10.1007/s11356-018-2918-x
70. Weiss DJ, Rausch N, Mason TF, Coles BJ, Wilkinson JJ, Ukonmaanaho L, Arnold T, Nieminen TM (2007) Atmospheric deposition and isotope biogeochemistry of zinc in ombrotrophic peat. Geochimica et Cosmochimica Acta, 71(14), 3498-3517. https://doi.org/ 10.1016/j.gca.2007.04.026
71. Zhang X (2019) The history of pollution elements in Zhengzhou, China recorded by tree rings. Dendrochronologia, 54, 71-77. https://doi.org/10.1016/ j.dendro.2019.02.004

ISSN print: 1224-5984
ISSN online: 2248-3942

Rom Biotechnol Lett. 2022; 27(1): 3235-3241
doi: 10.25083/rbl/27.1/3235-3241

Received for publication, January, 08, 2022
Accepted, February, 16, 2022

Original paper

The influence of a two-point contralateral crutch gait on the loading of the lower limb using a forearm crutch

CRISTINA REYNDERS-FREDERIX[1], PETER REYNDERS-FREDERIX[2], BERNARDO INNOCENTI[3], MIHAI BERTEANU[4]

[1] University Hospitals Brussels, campus Saint-Pierre, Department of Internal Medicine – Physiotherapy and Revalidation, Free University of Brussels.
[2] University Hospitals Brussels, campus Brugmann, Department of Orthopedic Surgery, Free University of Brussels.
Orcid 0000-0001-9198-1155
[3] BEAMS, (Bio Electro and Mechanical Systems) Free University of Brussels.
[4] Department of Revalidation & Physiotherapy, Carol Davila University of Medicine and Pharmacy, Bucharest, Romania.

Abstract

Objectives: This biomechanical study was conducted to validate the assumption that using an elbow crutch on one side diminishes the loading of the contralateral lower limb.
Methods: This study included in total 49 subjects: 39 patients and 10 healthy volunteers with a total of 114 observations divided in two groups. Group I, control group, (forearm crutch) contained 24 subjects (5 healthy volunteers and 19 Orthopedic patients). Group II (electronic forearm crutch) was made up of 25 subjects (5 healthy volunteers and 20 Orthopedic patients) with 60 observations. The electronic crutch recorded the speed of the crutch movement in the sagittal plane, the axial force exerted on the shaft of the crutch and the position of the crutch in the frontal plane in relation to the central axis of the subject.
Results: holding the forearm crutch contralateral of the examined limb, we documented a 74% lower amount of limb loading.
Holding the elbow crutch on the same side as the examined limb, we reported in 53.6% less loading.
Conclusions: These results do not corroborate with the theoretical mechanical analysis of limb loading, where a diminishing load of the limb is predicted contralateral to an elbow crutch.

Keywords Fracture care, walking aids, biomechanics of walking, force platform

To cite this article: REYNDERS-FREDERIX C, REYNDERS-FREDERIX P, INNOCENTI P, BERTEANU M. The influence of a two-point contralateral crutch gait on the loading of the lower limb using a forearm crutch *Rom Biotechnol Lett*. 2022; 27(1): 3235-3241. DOI: 10.25083/rbl/27.1/3235-3241.

✉ *Corresponding author: CRISTINA REYNDERS-FREDERIX, University Hospitals Brussels, campus Saint-Pierre, Department of Internal Medicine – Physiotherapy and Revalidation, Free University of Brussels.
E-mail: cristina_reynders-frederix@stpierre-bru.be

Introduction

Walking aids are often used as an essential rehabilitation tool to help patients in their functional recovery during treatment for an orthopaedic ailment. The simplest way of walking aid is the cane. With the walking stick, the transmission of force to the ground is via the forearm and wrist. The weaker forearm muscles limit the transmission of forces via the walking stick to the ground. With the forearm crutch, due to the double contact (wrist and forearm), the transmission of force is much more efficient in magnitude and in time. The use of a crutch broadens the base of support of the patient, improving balance and reducing the load placed on one of the lower limbs (**Kaye 2000, Alexander 1996, Verbrugge 1997, Whittle 2012**). Although crutches are often prescribed by a physiotherapist to facilitate post-operative walking, an exact determination of the forces acting on the affected limb in specific clinical situations are difficult to obtain (**Brand 1980, Rasouli 2019**). There are many types of crutches. For this study we utilised the forearm crutch, also called Lofstrand or Canadian crutch. This crutch has a cuff at the end that goes around the forearm (**Whittle 2012**). This study aimed to validate the assumption that with a two-point contact gait, the contralateral leg opposite from the crutch receives a lesser load while the leg next to the crutch takes a greater load.

Materials and Methods

We reported on 49 subjects (39 patients and 10 healthy volunteers) to participate in the current study. The patients were allocated according to the first-come, first-served principle. They had all different orthopaedic ailments of their lower leg and were at the end of their rehabilitation period. No patient refused to take part in this study. Walking patterns were defined in both groups by the walk ratio. The walk ratio, step-length divide by step-rate, is a speed independent index of walking (**Sekiya 1998**).

There was a significant difference in walking ratio between the young healthy subjects (0.033) and the patient group (0.019). Group I, control, used a forearm crutch and included 24 subjects: 5 healthy volunteers (5 females) with a mean age of 43.6 (range: 23–80) years and 19 orthopaedic patients (12 females and 7 males) with a mean age of 33.0 (range: 21–45) years. The difference in age and weight between the volunteers and patients was significant ($p = 0.0087$ and $p = 0.0160$, respectively). Group II included subjects who used an instrumented, electronic elbow crutch (Figure 1) and contained 25 subjects: 5 healthy volunteers (2 females and 3 males) with a mean age of 28 (range: 25–32) years and 20 patients (11 females and 9 males) with various orthopaedic ailments with a mean age of 52.5 (range: 22–69) years. The difference in age between the volunteers and patients was significant ($p = 0.0004$).

In addition, only age was significantly different between Groups I and II.

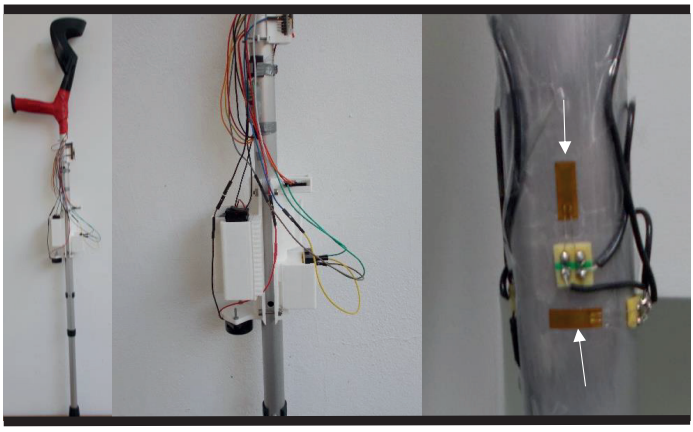

Figure 1. Instrumented crutch with the full Wheatstone bridge configuration (white arrows)

We made in total 114 observations: 54 in Group I and 60 in Group II. An observation was defined as an episode of walking with a crutch. In both groups, we combined the crutch with a foot pressure plate (Footscan 9, RSScan, Belgium) to determine the amount of load being exerted beneath the foot. The instrumented crutch used in this study is a unique instrument which records the axial force on the crutch, the crutch's angular speed in the sagittal plane and the crutch's position in the frontal plane relative to the axis of the body. It is described in detail in a previous publication (**Reynders-Frederix 2020**) .The foot pressure platform assessed the load distribution in time and also per area on the sole of the foot. The pressure with this system is expressed in Newton/cm $^{2.}$ We chose to use a two-point contralateral crutch gait, the crutch on one side is moved forward on the same time as the contralateral limb, because

this type of support is often prescribed at the end of the revalidation period following an orthopaedic injury (**Smidt 1980, Stallard 1980, Pierson 1994**).

Before testing each participant, we calibrated the axial force exerted on the crutch using a compression bench (Tinius Olsen H5KL-Salfords UK). For this step, the bottom region of the crutch was dismantled and positioned on the compression bench. The crutch underwent cycled compression at 100 N, and the value noted on the compression bench was compared with the recorded force/time curb on the PyCharm display.

Before the observation, the participants were asked to practice walking with regular elbow crutches for 15 minutes. After that, they were asked to walk with bare feet across an inside trajectory course three times for a distance of 10 metres (30 metres) without and with an elbow crutch. Walking test was done on a nonslip conductive rubber walkway. The test was repeated for every crutch position (contralateral/ipsilateral from the injured leg).

In Group II (instrumented crutch), the axial force on the crutch shaft, the angular velocity of the crutch in the sagittal plane and the crutch positions in the frontal plane were recorded by a portable computer equipped with Bluetooth capabilities. The position of the crutch in respect to the body axis, is represented by a curve with both positive and negative areas. An index was created determined by dividing the positive area by the negative area.

An index > 1 indicated that the crutch was leaning away from the body's centre and that the patient was putting more pressure on the crutch, while an index of < 1 showed that the crutch was kept closer to the midline of the body with more pressure on the contralateral limb.

A force plate that was 50 x 50 cm in size was placed in the middle of the trajectory. This foot scan obtains precise plantar pressure measurements using 4096 sensors at a scanning rate of up to 300 Hz using Footscan 9 software (Rsscan, Beringen, Belgium). The loading of the ipsilateral and contralateral crutch, as recorded by the force plate, was measured in five timeframes at 10%, 25%, 40%, 60% and 80% of the stance phase and compared with the recordings without an elbow crutch (Figure 2).

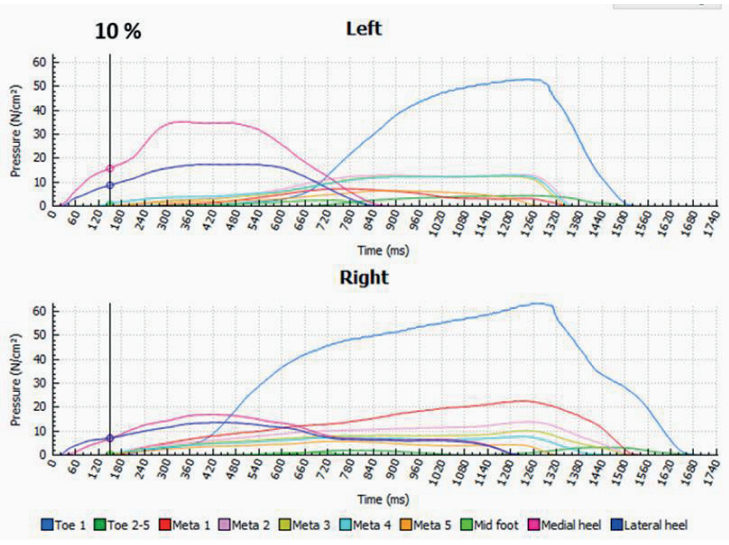

Figure 2. Normalizing pressure for time. Five time frames at 10 %, 25%, 40%, 60% and 80 % from the stance phase were used to calculate the pressure.

Design of the instrumented crutch

The crutch used in the current study was a standard elbow crutch with an aluminium frame that was selected because of its lightness (2.700 kg/m^3), tensile strength (70–700 MPa) and Young's modulus (69 GPa). The prototype was built by the BEAMS department at Free University in Brussels (**Reynders-Frederix 2020**) (Figure 1).

We installed four strain gauges as a full Wheatstone bridge to assess the pure amount of compression on the crutch shaft. In addition, a gyroscope and tri-axial accelerometer (GY-521) were used to determine the roll and pitch angle of the crutch. Finally, a microcontroller (Arduino Uno) sent the data via Bluetooth to a developed end-user programme created in Python (ESP32). Synchronous readings of the different biomechanical parameters were carried out using PyCharm (PyCharm version 2019.1.3; JetBrains Czech Republic).

Statistics

GraphPad Instat® 3 (San Diego, California 92108, USA) software was used for statistical calculations. The statistical analysis assessed the Gaussian distribution using

the Kolmogorov-Smirnoff test. An unpaired nonparametric Mann-Whitney U test was chosen to compare the means. The regressions and correlations were tested with multiple X variables (multiple regression). The level of significance was set at 5%. To calculate the ideal sample size and its power, we used GraphPad StatMate® (San Diego, California 92108, USA).

Results and discussion

We included 49 subjects divided into two groups for a total of 114 observations (Group I: 24 participants with 54 observations; Group II: 25 participants with 60 observations). Both groups did not differ significantly in their weight, height or shoe sizes. There was a significant difference in age between Groups I and II (mean age in Group I: 43.35 [range: 23–80] years and mean age Group II: 52.7 [range: 22–75] years; p=0.0043).

In 114 observations, we observed less force on the limb contralateral to the crutch in 74% (43 of 58 observations) of subjects with a mean of -14.6% (range: -1% to -46%) and an SD of 12 (95% confidence interval [CI]: -10.3% ± -18.5%). In 26% (15 of 58 observations) of subjects, there was an increase in force loading on the limb contralateral to the crutch with a mean of +7.3% (range: +1% to +10%) and an SD of 5.9% (95% CI: +9.8% ± +4.7%).

In 53.6% (30 of 56 observations) of subjects, there was less loading on the limb ipsilateral from the crutch with a mean of -15.75% (range: -1% to -34%) and an SD of 10.3 (95% CI: -11, 37% ± -20, 13%). In 46.4% (26 of 56 observations), more loading was recorded on the limb ipsilateral from the crutch with a mean +13.8% (range: +1% to +35%) and an SD of 10.36 (95% CI: +17.6% ± +9.9%).

There was a significant difference in the number of cases with positive loading of the limb opposite the crutch (CL) with the positive loading of the limb nearest the crutch (IP) in Groups I and II. A descriptive analysis of the test results and their significance in Groups I and II is shown in Tables III and IV. In Group I (normal elbow crutch), we found a significant difference in the number of positive (more loading) and negative (less loading) loading of the contralateral limb (opposite from the elbow crutch) and ipsilateral limb loading (same site as the crutch). The descriptive statistics of Group I (normal elbow crutch) and also the subject- and crutch-specific variables are shown in Table I.

Table I. Descriptive statistics of Group I (normal elbow crutch): subject- and crutch-specific variables.

Characteristics	**Variables**	**Variables**	**p-value**	
CL	Group I	Group II	0.1805	
IP	Group I	Group II	0.5640	
Age (Group I)	Age	IP	0.3708Ω	NS
Age (Group I)	Age	CL	0.9668Ω	NS
Weight (Group I)	Weight	IP	0.2116Ω	NS
Weight (Group I)	Weight	CL	0.5913Ω	NS
Height (Group I)	Height	IP	0.8881Ω	NS
Height (Group I)	Height	CL	0.6764Ω	NS
IP (Group I)	***More load***	***Less load***	***<0.0001****	
CL (Group I)	***More load***	***Less load***	***<0.0001****	
IP (Group I)	Patients	Volunteers	0.1426§	NS
CL (Group I)	Patients	Volunteers	0.2235§	NS
CL (Group I)	Male	Female	>0.9999§	NS
IP (Group I)	Male	Female	0.3698§	NS
More loading	***CL Groups I and II***	***IP Groups I and II***	***0.0157****	
Less loading	CL Groups I and II	IP Groups I and II	0.445§	NS
Ratio neg. vs pos.	CL Groups I and II	IP Groups I and II	0.132§	NS

***Mann-Whitney U test/**§**Fischer's exact test/**Ω** Correlation: Spearman rank/**NS**: not significant
$: unpaired t-test/**IP**: Loading on the lower limb near the crutch/**CL**: loading on the lower leg contralateral from the crutch.

In Group II (electronic crutch), when examining loading forces exerted on the contralateral and ipsilateral limb, we found that the difference between more loading versus less loading was significant. In these same subjects, we found a correlation between the loading of the ipsilateral limb (near to the crutch) and tallness. Tall participants had a greater load on the ipsilateral holding crutch that was significantly greater than that of participants with a shorter height.

In a multiple regression analysis within the patients and volunteer groups, we could not find any correlation between limb loading contralateral or ipsilateral from the used crutch and the force exerted on the crutch, the angle velocity of the crutch in the sagittal plane or the position of the crutch in relation to the centre of the body. In addition, the position of the crutch in relation to the centre of the body did not differ between volunteers and patients.

The descriptive statistics of Group II (instrumented crutch) subject- and crutch-specific variables are shown in Table II.

Table II. Descriptive statistics of **Group II** (instrumented elbow crutch): subject- and crutch-specific variables.

Characteristics	**Variables**	**Variables**	**p-value**
CL	*Positive (more)*	*Negative (Less)*	*0.000**
Length/Position	Length (subjects)	Position (crutch)	0.289§ NS
IP	*Positive (more)*	*Negative (Less)*	*<0.0001**
CL	Patients	Volunteers	0.6206§ NS
IP	Patients	Volunteers	0.4118§ NS
IP	Male	Female	0.1032§ NS
CL	Male	Female	0.6980§ NS
CL	Tall (>1.63 m)	Short (<1.63 m)	0.6683§ NS
IP	*Tall (>1.63 m)*	*Short (<1.63 m)*	*0.0498§*
CL	CL	Force on crutch	0.7434**Ω** NS
IP***	CL	Force on crutch	0.2921**Ω** NS
CL	CL	Weight	0.0520**Ω** NS
IP	CL	Weight	0.3636**Ω** NS
CL	Old (>60 years)	Young (<60 years)	0.3003§ NS
IP	Old (>60 years)	Young (<60 years)	1.0§ NS
IP	CL	Age	0.5374**Ω** NS
CL	CL	Age	0.8195**Ω** NS
Force/Position	Axial force on the crutch	Position of the crutch	0.2326**Ω** NS

*Mann-Whitney U test/§Fischer's exact test/**Ω** Correlation: Spearman rank/**NS**: not significant/*** when holding the crutch on the same side of the limb, there is a relationship between the force exerted on the crutch and the amount of contralateral limb loading.**CL**: Load on the lower leg contralateral to the crutch.**IP**: Load on the lower limb near the crutch.

Multiple Regression Analysis

*Multiple regression **Load Contra Lateral Leg** as the dependent variable, or **Y**, and **Force, Velocity** and **Crutch position** as independent variables or X.
Equation that fits the data the best.
Load CL = 108.82 + 0.05322 (Force) – 0.4249 (Speed) – 0.06542 (Crutch position)
R squared = 21.95%
The P-value is 0.0972, which is not considered significant.
Angular speed makes a significant contribution.
*Multiple regression **Load Ipsilateral Leg** as the dependent variable, or **Y**, and **Force, Velocity** and **Crutch position** as independent variables, or X.
Equation that fits the data the best.
Load Cr = 100.15 + 0.04791 (Force) – 0.1668 (Speed) – 0.4370 (Crutch position)
R squared = 8.54%
The P-value is 0.5528, which is not considered significant.
No variable made a significant contribution.

The decision to use a crutch is based on a theoretical model that calculates the condition of equilibrium of the pelvis during a slow gait in a stance phase, where one foot is on the ground and the other is lifted off the floor (**Whittle 2012, Brinckmann 2016**). Because the progression in walking is slow, it is assumed that the inertial (horizontal) forces generated during acceleration and deceleration during the stance phase are negligible.

In this situation, there is an equilibrium between the *gravitational weight of the body minus one leg* which is in a swing phase and the *contraction force of abductor muscles of the loading hip.* Adding a crutch on the opposite side as the injured leg diminishes the abductor muscle force needed for this equilibrium. The theoretical reduction of the load on the lower leg opposite the crutch equals five times the force between the hand and the crutch (**Brinckmann 2016**) (Figure 3).

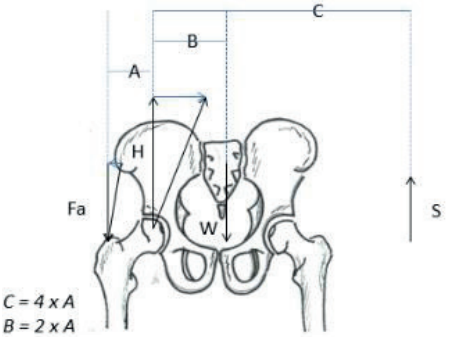

Figure 3. Theoretical analysis of the mechanical influence of unloading the leg using a crutch on the contralateral side.

Knowledge of this principle is paramount and is often used in the post-trauma revalidation of patients. In our study, we combined the data obtained from the electronic crutch and force platform in a group of healthy volunteers and in a group of Orthopedic patients. We could not corroborate this presumed correlation between the position of the crutch in relation to the centre of the body and the loading of the limb.

In our study, out of a total of 114 observations (an observation was defined as a bout of walking with a crutch), 15 out of 58 observations gave rise to more loading of the limb opposite to the one holding the crutch. In 43 out of 58 observations, there was less loading force exerted on the contralateral limb. The variation of less loading was important (range: -1% to -46%).

When the limb loading force near the crutch was examined, 46.6% of our subjects demonstrated a greater loading force, with a mean of +13.8% (range: +1% to +35%).

This study also produced a few other observations. Although the patient group differ from the healthy volunteer group in walking patterns (walking ratio). There was no difference in the loading characteristics between the volunteers and the patients. In addition, we were unable to find a correlation between the force exerted on the crutch and any reduction of the limb loading opposite the crutch. Other factors (such as age, weight, height, crutch position or sex) did not influence the loading or unloading of the crutch on either side of the body.

The most striking result was the unreliable and unpredictable change of limb loading with crutches. The fact that the reduction in loading can vary this much is difficult to understand. In some cases, patients may unintentionally exert more pressure on the affected lower limb, which is potentially dangerous and may jeopardize the healing of the skeletal injury (**Aro 1993**).

There is no clear explanation for our results. The literature on this topic is scarce. Statistical analyses of our data revealed only a significant contribution of height and weight to the loading forces of the leg near the crutch. We hoped to partially explain the results with the positioning of the crutch during walking. It seems reasonable to consider overloading of the leg contralateral from the crutch when the patient's body is leaning towards the affected leg. However, we did not find a significant influence of the crutch position on the contralateral or ipsilateral leg loading. One possible explanation for our results is the disturbed proprioception of the injured leg. With this disturbance of proprioception, the damping of the surrounding muscles' is reduced or absent. An indication for this can be found in the volunteers' results in Group II, where all subjects reduced the load on the leg contralateral from the crutch. This effect was not seen in the volunteers of Group I. Also, the Hawthorne effect plays probably a role in which studied subjects could artificially adapt their walking style (**Levitt 2011**).

The work of Bergmann explained the importance of the subject's muscular tonus. His in vivo measurements of a hip prosthesis revealed that significant variations in hip contact forces exist in the presence of a disturbed gait. Bergmann hypothesized that these exceptionally high peak contact forces are partly due to muscular dysfunction (**Bergmann 2001**).

A limitation of this study is that the patient population in both groups was heterogeneous. We hypothesized that the walking patterns and lack of proprioception would be the same for all patients. Nevertheless, it is still possible that one orthopaedic pathology has more effect on the load transmission of the crutch than another. Another limitation is the length of the pathway. It is possible that with a more extended walkway, walking would be more fluent, less artificial, than with the short walkway (10 m) we used in this study. Also, targeting the pressure platform in the middle of the walkway could hinder the walking pattern of a subject. Another limitation could be that the same study persons did not use both types of crutches. However, we found only a difference in age between the two groups. Even then, the outcome was the same in both groups. Another pitfall when making pressure measurements with pressure platforms is that patients with the painful area will not fully load this area to avoid pain. In this case, lower pressure will be recorded. We did not have patients with an ongoing painful foot sole in the patient group. The strength of the present study is the inclusion of orthopaedic patients and able-body subjects. In most studies, only healthy persons were used for the gait analyses. Another strength was the inclusion of standard crutches beside the instrumented crutch. Because of encasing issues, seen with the instrumented crutch, it was thought that adding a standard elbow crutch would better reflect the normal walking behaviour of the study subjects.

Conclusions

In the present study, we could not corroborate the commonly cited concept of orthopaedic and rehabilitation medicine that the load of a leg contralateral from a used crutch is less and the leg load near the crutch is more. In post-surgery physiotherapy, one crutch can be valuable to keep a patient's balance but is likely not enough to protect the injured lower limb from overloading. Considering the seemingly considerable and unreliable variation in lower limb loading opposite from the crutch, our data indicate that walking with two crutches throughout the rehabilitation phase seems safer.

Ethical review statement:

The ethics committee does not raise ethical or legal reservations against a publication of the results of this project. Permission of the clinical research ethical committee was obtained: CE 2020/90 BUN:B0772020000023, 09.06.2020.

References

1. Kaye HS, Kang T, LaPlante MP. Mobility device use in the United States. *National Institute on Disability and Rehabilitation Research* 2000;14: 23-52.

2. Alexander NB. Gait disorders in older adults. *J Am Geriatr Soc* 1996; 44:434-451.
3. Verbrugge LM, Rennert C, Madans JH. The greater efficacy of personal and equipment assistance in reducing disability. *Am J Public Health* 1997; 87:384-392.
4. Whittle WW. Whittle's Gait Analysis. Fifth edition. 2012; p78-82.
5. Brand RA, Crowninshield RD. The effect of cane use on hip contact force. *Clin Orthop Rel Res* 1980; 147:181-184.
6. Rasouli F, Kyle BR. Walking assistances using crutches: A state of the art. *Journal of biomechanics* 2019; 98: 109489.
7. Sekiya N, Nagasaki H. Reproducibility of walking patterns of normal young adults: test-retest reliability of the walk ratio (step-length/step-rate).*Gait and Posture* 1998;7:225-227.
8. Reynders-Frederix C, Reynders-Frederix PA, Innocenti B, Berteanu M. Development of an electronic assistive walking device. Rom Biotechnol Lett.2020;25(5):1992-1997
9. Smidt GL, Mommens MA. System of reporting and comparing influence of ambulatory aids on gait. *Phys.Ther* 1980; 60: 551-558. Https://doi.org/ 10.1093/ ptj/60.5.551
10. Stallard J, Dounis E, Major RE, Rose GK. One leg swing through gait using two crutches. An analysis of the ground reaction forces and gait phases. Acta Orthop. Scand. 1980; 51:71-77
11. Pierson FM. Principles and Techniques of Patient Care. WB Saunders, Philadelphia, PA, 1994.
12. Brinckmann P. Hip biomechanics. In: *Orthopedic Biomechanics*. Georg Thieme Publishers Stuttgart, 2016: 272-293.
13. Aro H, Chao E. Bone-Healing Patterns Affected by Loading, Fracture Fragment Stability, Fracture Type, and Fracture Site Compression. *Clinical Orthopaedics and Related Research* 1993; 293:8-17.
14. Levitt SD., List JA. Was there really a Hawthorne effect at the Hawthorne plant? An analysis of the original illumination experiments. American Economic Journal: Applied economics 2011; 3: 224-238.
15. Bergmann G. et al. Hip contact forces and gait patterns from routine activities *Journal of Biomechanics* 2001; 34: 859–871.

ISSN print: 1224-5984
ISSN online: 2248-3942

Rom Biotechnol Lett. 2022; 27(1): 3242-3251
doi: 10.25083/rbl/27.1/3242-3251

Received for publication, January, 06, 2022
Accepted, February, 15, 2022

Original paper

Optimization of some fish by-products using tilapia and mullet head fortification of rice

BADAWY WZ, FATHYA AM, AMAR AK, EL-NEMR KM

Food Technology Department, Faculty of Agriculture, Kaferelsheikh University, Egypt.

Abstract Fish processing waste is either discarded or considered as a low-value raw material. The chemical composition and fatty acid profile of the tilapia and mullet by-products (heads, viscera, and liver) were determined. Also, the possibility of rice fortification with tilapia head flour (THF) and mullet head flour (MHF) and its effect on the chemical composition and sensory properties of rice were evaluated. Results indicated that, the tilapia and mullet by-products could be considered as a good source of protein and ether extract. Furthermore, the Head had significantly the highest content of crude protein, ash, crude fiber and unsaturated fatty acids among other different parts of tilapia and Mullet by-products. Apparent, fortification rice with various levels of THF and MHF lead to increased significantly protein, ether extract, and ash content. Also, Sensory properties were significantly ((P<0.05) decrease in cooked rice sample fortified with mullet head at the 6 and 9 % compared with the control sample. Finally, THF and MHF is an inexpensive and environmentally friendly alternative source of protein, ether extract, and ash can be converted to the healthy value-added products to increase of the amount of protein, ether extract, and mineral content in food production.

Keywords Fish, by-Products, nutritional evaluation, rice, fortification

To cite this article: BADAWY WZ, FATHYA AM, AMAR AK, EL-NEMR KM. Optimization of some fish by-products using tilapia and mullet head fortification of rice. *Rom Biotechnol Lett*. 2022; 27(1): 3242-3251. DOI: 10.25083/rbl/27.1/3242-3251.

✉ *Corresponding author: BADAWY WZ, Food Technology Department, Faculty of Agriculture, Kaferelsheikh University, Egypt.
E-mail: walid.metwali@agr.kfs.edu.eg

Introduction

The total fish production in Egypt is 1.71 million tons annually where 1.4 million tons were produced through aquaculture, it represents more than 80% of the total fish production (Gafrd, 2018). tilapia and mullet are dominant species. They account for 85.1% of the total aquaculture production. In addition, Egypt is the world's top producer of cultured mullet **(EL-SAYED {1}).** A large number of fish meat-based consumer convenient products are emerging and thus a huge quantity of by-products are generated which accounts for about 65-70% of the weight of the raw material **(KUMAR *& al.* {2}).**

In the tilapia and Mullet processing procedure, only 30%-40% (weight) of the fish is consumed as a fillet, and the other party (heads, viscera, fins, and bones) are discarded. However, these by-products may be used to produce flour, pates, and soups. This application minimizes the production costs (lower costs of raw material) and reduces the environmental impact caused by fishery activity **(LEONHARDT *& al.* {3} and PETENUCI *&al.* {4}).** Generally, fish processing waste is either discarded or considered as a low-value raw material, which meets the demand of the fish meal industry **(GHALY *& al.* {5}).** However, fish by-products are increasingly being recognized as secondary raw material and being utilized for the production of high-value products with functional and bioactive properties such as gelatin, protein hydrolysate, and omega-3 fatty acids concentrate. Fish by-products could also be used as an important source of nutrition **(TAHERGORABI *& al.* {6}; RENUKA *& al.* {7}).**

Fish by-products can entail significant environmental and food-technical challenges due to their high microbial and endogenous enzyme load, rendering them susceptible to rapid degradation if not processed properly or stored in appropriate conditions **(ARVANITOYANNIS *&* KASSAVETI {8})** Fish by-products can be classified into two types: One that includes easily degradable products with high enzyme content, such as viscera and blood, and a second one that includes the more stable products (bones, heads, and skin) **(RUSTAD *& al.*{9}).**

Discarding these by-products caused two major problems. First, is not benefiting from a large number of nutrients such as protein, oil, minerals, and vitamins. Second, disposal of such large quantities that contains polluting organic matter causes many of the major environmental and economic problems. **(SAYANA *&* SIRAJUDHEEN {10})**. Hence, the efficient use of fish processing waste is gaining importance and nowadays fish processing waste is a secondary raw material due to the richness of proteins, fats, and minerals. Developing appropriate technology to recover or isolate valuable components can be of paramount importance. Among the various by-products are fish heads, viscera, and liver. Fish processing is an important need for large fish companies to reduce costs related to transporting inedible parts of fish, increase product stability and quality, and remove parts, such as offal, that may contain bacteria and enzymes, which present risks to fish processing and storage. **(GHALY *& al.* {5}).**

The known healthy compounds and properties associated with fish are also present in their by-products. A great number of bioactive compounds can be obtained from fish by-products: collagen, chitin, enzymes, gelatin, glycose-minoglycans , polyunsaturated fatty acids (PUFA), minerals, protein, and peptides, and vitamins. It should be noted that the long-chain omega-3 fatty acids (LC-PUFAs), eicosapentaenoic acid (EPA), and docosahexaenoic acid (DHA), are among the most successful compounds extracted from fish by-products, achieving a high value in the market due to their beneficial health effects **(FERRARO *& al.* {11}; OLSEN *& al.* {12}; ZAMORA-SILLERO *& al.* {13}).** These Fish by-products can also be used for the production of various value-added products such as proteins, oil, amino acids, minerals, enzymes, bioactive peptides, collagen, and gelatin. The fish proteins are found in all parts of the fish. The amino acids present in the fish can be utilized in animal feed in the form of fishmeal and sauce or can be used in the production of various pharmaceuticals **(ESTEBAN *& al.* {14}; ZHAO *&al.* {15}).**

Rice is considered one of the most important foods worldwide, as it is cultivated on a large scale in all continents and consistently consumed by more than half of the world's population. Cooked rice is known as an excellent source of energy due to its high content in starch, while it also contains rice proteins which offer all the essential amino acids to human nutrition, some of which, though, in limited quantities **(RYAN {16}).** The unique taste of rice provides an easy way to combine rice with the other food to achieve a better taste and nutritional balance **(WALTER *& al.* {17}).** Rice is also one of the foods which are considered to be a potential food vehicle for the fortification of micronutrients because of its regular consumption. Many studies tried to add iron and zinc to rice in order to reduce the nutritional problems, especially micronutrient deficiencies. A study in Bangladeshi children and their caregivers showed that rice was the main source of zinc intake, providing 49% of dietary zinc to children and 69% to women **(ARSENAULT *& al.* {18}).**

Fortification of main foods is generally accepted as an effective way for providing the daily requirements for a range of vitamins and minerals **(BABARYKIN *& al.* {19}).** Thus, the aim of this study was to evaluate the by-products of tilapia and mullet and studied the possibility of rice fortification with tilapia head flour (THF) and mullet head flour (MHF) and its effect on the chemical and sensory properties of rice.

Materials and Methods

Materials

The tilapia and mullet by-products (heads, viscera, and liver) used in this study were bought from the local market in Kaferelsheik city Egypt during April 2020.

Sex kg of rice variety “Sakha 106” was used in this study. Samples (Freshly harvested grains) from the 2020 season were dehulled and polished at the grain quality Lab., RRTC. Sakha, Egypt. All samples were taken and well mixed and cleaned.

Chemicals

All of the chemicals used in this study were obtained from EL-Gomhouria pharmaceutical company, of Tanta city at EL-Gharbia Governorate, Egypt. All other chemicals were analytical grads.

Methods

Preparation of tilapia and mullet by-products

The tilapia and mullet by-products (heads, viscera, and liver) were separated from the fish manually by the market vendors then were cleaned and carefully washed with tap water. After that, these samples were boiled in water for 10 min in order to prevent contamination by disease pathogens, and then dried in an oven at 60±5˚C overnight till complete drying. Finally, the sample was milled into a fine powder and packed in multilayer flexible packages, kept at -20˚C for further analyses**. (JAYASINGHE *& al.* {20}).**

Chemical composition of samples

Chemical compositions as moisture content, crude protein, ether extract, and the ash content were determined according to **AOAC {21}.** Total carbohydrates were determined by subtracting.

Fatty acid profile of samples

The fatty acids composition of the oil extracted from samples were determined at room temperature using the method described by **CONKERTON *&* al {22}.** The ISO 1995 method was used to prepare fatty acids methyl ester of samples, which were then, analyzed using a gas chromatograph (GC-1000, DANI, Italy) and a flame ionization detector that was slightly modified according to **AZADMARD *&* DUTTA {23}.** Fatty acids were identified by acquiring chromatograms and comparing their retention times to those of normal fatty acid methyl esters (Sigma Aldrich, St. Louis, MO).

Preparation of cooking rice

Cooking Rice fortification with levels (3, 6 and 9%) of tilapia head flour (THF) and mullet head flour (MHF) was produced as described by **PANAGIOTIS *& al.* {24}.**

Sensory evaluation of cooked rice

A semi-trained panel of twenty members using ten-point hedonic-scale ratings for color, taste, odor, texture, and overall acceptability in order to provide organoleptic characteristics for different fortification cooked rice, **EL-BANA *& al.* {25}.** Liked extremely 9, Like very much 8, Liked moderately 7, Liked slightly 6, Neither liked nor disliked 5, Disliked slightly 4, Disliked moderately 3, Disliked very much 2 and Disliked extremely 1.

Statistical analysis

Data were analyzed using analysis of variance (one way ANOVA), while comparisons were done by Duncan's test at $P<0.05$ level of significance using SPSS (2008) version 17 program for windows.

Results and discussion

Proximate Composition of tilapia by-products

The Gross chemical composition of tilapia by-products (Head, viscera, and Liver) are given in table (1). The results pointed to, significant differences ($p<0.05$) were found in the moisture, protein , ether extract , ash , crude fiber, and carbohydrate contents of tilapia by-Products (Head, viscera, and Liver). The results in Table (1) revealed that, tilapia By-Products could be considered as a good source of protein and ether extract. Where they recorded (15.42 and 42.23%) in the head, (8.95 and 55.92%) in viscera, and (9.61 and 23.33%) in the Liver. These values point to tilapia by-products flour as an important nutritional alternative, due to its high levels of proteins and minerals, as compared to other human foods. High values of protein, ether extract, and minerals are directly related to low moisture content, since a reduction in meal moisture content causes an increase in the concentration of other compounds. These results are in agreement with **STEVANATO *& al.* {26}.** Also, results presented in the above-mentioned Table, it could be observed that, Head had significantly the highest content of crude protein, ash and crude fiber (15.42, 20.25 and 18.87 %) respectively among other different parts of tilapia. while, Liver had a significantly higher percentage of Moisture and Carbohydrates (5.81 and 60.94%) respectively, meanwhile, viscera had a significantly higher percentage of ether extract (55.92%) among other different parts of tilapia. These results are in agreement with **SHIRAHIGUE *& al.* {27}.** The composition of the fish waste varies according to the type of species, sex, age, nutritional status, time of year, and health **(SUVANICH *& al.* {28}).**

Table 1. Chemical composition of different parts of tilapia (% on a dry weight basis)

Parts of tilapia	Chemical composition (%)					
	Moisture	Crude protein	Ether extract	Ash	Crude fiber	*Carbohydrates
Head	3.36^{c} ±0.15	15.42^{a} ±0.12	42.23^{b} ±0.23	20.25^{a} ±0.10	18.87^{a} ±0.18	3.23^{c} ±0.14
viscera	4.66^{b} ±0.19	8.95^{c} ±0.25	55.92^{a} ±0.22	5.57^{b} ±0.17	0.17^{b} ±0.09	29.39^{b} ±0.22
Liver	5.81^{a} ±0.13	9.61^{b} ±0.10	23.33^{c} ±0.26	5.87^{b} ±0.15	0.25^{b} ±0.15	60.94^{a} ±0.31

Each value is an average of three determinations ± standard deviation.
Values followed by the same letter in columns are not significantly different at P<0.05.
*Carbohydrates were calculated by differences.

Proximate composition of mullet by-products

The chemical composition of mullet by-Products analyzed is presented in Table (2). The different parts of Mullet showed a significant difference in ($p<0.05$) on the moisture, protein, ether extract, ash, crude fiber, and carbohydrate contents. Moisture values ranged between 3.25% and 5.88%, being liver the part that had higher percentages. The obtained results indicated that, the head had a significantly higher content of ether extract, ash, and crude fiber (49.61,20.25 and 5.63%) respectively compared to that of other by-products. Meanwhile, viscera had a significantly higher content of carbohydrate (40.66%) Following with liver (35.60%) and head (10.82%) These results are in agreement with **PATEIRO *& al.* {29}.** Ash contents in the head were higher than those found in other fish by-products. Regarding ash content, fish heads had large amounts of minerals. These results are in agreement with **HE *& al*. {30}; PATEIRO *&al.* {29}.**

Mullet by-Products could be considered as a good source of protein and ether extract where they recorded (13.69 and 49.61%) in the head, (12.02 and 39.90%) in viscera and (14.56 and 42.61%) in the Liver. These values point to mullet by-products flour as an important nutritional alternative, due to its high levels of proteins and minerals, as compared to other human foods. These results are in agreement with **ELAVARASAN *& al.* {31}.**

Table 2. Chemical composition of different parts of mullet (% on a dry weight basis).

Parts of Mullet	Chemical composition (%)					
	Moisture	Protein	ether extract	Ash	Fiber	* Carbohydrates
Head	$3.25^{c}\pm0.10$	$13.69^{b}\pm0.18$	$49.61^{a}\pm0.29$	$20.25^{a}\pm0.11$	$5.63^{a}\pm0.09$	$10.82^{c}\pm0.13$
viscera	$4.17^{b}\pm0.19$	$12.02^{c}\pm0.15$	$39.90^{c}\pm0.11$	$5.76b^{c}\pm0.10$	$1.66^{b}\pm0.04$	$40.66^{a}\pm0.31$
Liver	$5.88^{a}\pm0.12$	$14.56^{a}\pm0.17$	$42.61^{b}\pm0.23$	$6.26^{b}\pm0.13$	$0.97^{c}\pm0.08$	$35.6^{b}\pm0.24$

Each value is an average of three determinations ± standard deviation.
Values followed by the same letter in columns are not significantly different at $P<0.05$
* Carbohydrates were calculated by differences.

Fatty acids composition of tilapia by-products oil

The fatty acids composition of tilapia by-products oils is presented in Table (3). The evaluation of the fatty acid profile indicated significant differences ($p < 0.05$) among samples regarding the fractions of fatty acids. The results shown in Table (3) are illustrated that, the fatty acid composition of lipids extracted from the head, liver, and Viscera of tilapia had a higher amount of saturated fatty acids (SFA) and monounsaturated fatty acids (MUFA) and a lower amount of polyunsaturated fatty acids (PUFA). Generally, the total saturated fatty acid of the viscera was higher (51.15%) than that of the head (43.01%) than the liver (39.46%). Among the saturated fatty acids, the highest concentration was Palmitic acid (32.30, 30.99, and 31.90% respectively) following by stearic acid (7.04,5.58 and 14.68% respectively) for head, liver, and viscera respectively. This agreement with found by **EL-SHERIF {32}.** As for unsaturated fatty acids, it could be cleared that, all tilapia by-products had higher oleic acid and linoleic acid (43.67and 6.88; 40.16 and 7.77; 33.77 and 5.46%) in the head, liver, and viscera respectively. Meanwhile, the liver contained a higher concentration of Linolenic acid (2.58%) comparing with other tilapia by-products. these results agree with **SUSENO *& al.* {33}; KHODDAMI *& al*. {34}; ABD EL-RAHMAN *& al*. {35}.**

Linoleic and oleic acids rich oils are particularly important for the human diet. They help maintain membrane fluidity at the water barrier of the epidermis, and can be further enzymatically oxidized to a variety of derivatives involved in cell signaling. Interestingly, the studied oils are rich in palmitic and stearic acids, which are at the origin of these two fatty acids, explaining the presence in small amounts, The presence of high amounts of the essential fatty acid linoleic acid suggests that these oils are highly nutritious oils due to the ability of unsaturated oils to reduce serum cholesterol **(OUASSOR *& al.* {36}).**

Fatty acids composition of mullet by-products oil

The nutritional importance of fish consumption is to great extent associated with its advantageous fatty acid profile. Lipids and fatty acids play an important role in the biochemistry of membranes and have a direct impact on membrane-mediated processes such as osmosis regulation and nutrient uptake and transport. On the other hand, the nature and quantity of these fats in fish varies according to species and habits **(KUMARAN *& al.* {37}).** A comparison of the fatty acid composition of lipids extracted from the head, liver, and Viscera of mullet is presented in Table (4). The obtained results show that, the fatty acid profile evaluation showed significant differences ($P < 0.05$) between samples with respect to the fatty acid fractions.

Table 3. Fatty acids composition of tilapia by-products oil

Type of Fatty acids		Different parts of tilapia		
		Head (%)	Liver (%)	Viscera (%)
C12 : 0	Laurie acid	0.47	0.26	0.10
C14:0	Myristic a cid	3.20	2.63	4.47
C16:0	Palmitic a cid	32.30	30.99	31.90
C18:0	Stearic a cid	7.04	5.58	14.68
Total saturated fatty Acids(SFA)		**43.01**	**39.46**	**51.15**
C16:1	Palmitaleic a cid	3.22	8.00	6.40
C18:1	Oleic a cid	43.67	40.16	33.77
C20:1	Arachidonic a cid	2.35	1.41	1.38
Total mono unsaturated fatty Acids (MUFA)		**49.24**	**49.57**	**41.55**
C18:2	Linoleic a cid	6.88	7.77	5.46
C18:3	Linolenic a cid	0.86	2.58	1.83
Total polyunsaturated fatty Acids (PUFA)		**7.74**	**10.35**	**7.29**
Unsaturated fatty Acids(UFA)		**56.98**	**59.92**	**48.84**
Total fatty Acids		**99.99**	**99.38**	**99.99**

Table 4. Fatty acid Composition of mullet by-products

Type of Fatty acids		Different parts of mullet by-products		
		Head (%)	Liver (%)	Viscera (%)
C12 : 0	Laurie acid	0.44	0.78	-
C14:0	Myristic a cid	10.05	4.23	9.11
C16:0	Palmitic a cid	31.14	31.26	33.6
C18:0	Stearic a cid	6.24	8.04	11.35
Total saturated fatty Acids(SFA)		**47.87**	**44.31**	**54.06**
C16:1	Palmitaleic a cid	12.57	5.13	9.66
C18:1	Oleic a cid	27.58	30.65	26.6
C20:1	Arachidonic a cid	4.43	5.49	0.50
Total mono unsaturated fatty Acids (MUFA)		**44.58**	**41.27**	**36.76**
C18:2	Linoleic a cid	5.60	12.87	2.60
C18:3	Linoleic a cid	0.57	1.04	4.75
Total polyunsaturated fatty Acids (PUFA)		**6.17**	**14.01**	**7.35**
Unsaturated fatty Acids(UFA)		**50.75**	**55.18**	**44.11**
Total fatty Acids		**98.62**	**99.59**	**98.17**

The results shown in Table (4) are illustrated that, the fatty acid composition of lipids extracted from the head, liver, and Viscera of mullet had a higher amount of saturated fatty acids (SFA) and monounsaturated fatty acids (MUFA) and a lower amount of polyunsaturated fatty acids (PUFA). Furthermore, the total saturated fatty acid of the viscera was higher (54.06%) than that of the liver (44.31%) than the head (47.87%). Among the saturated fatty acids, the highest concentration was Palmitic acid and stearic acid (33.60 and 11.35% respectively) in viscera, while the highest concentration of Palmitic acid and stearic acid in the liver were (31.26 and 8.04% respectively) but, the highest concentration in the head was palmitic acid and meristic acid (|31.14 and 10.05% % respectively) this agreement with found by **KACEM *&al.* {38}; ELAVARASAN *& al.*{39}.** As for monounsaturated fatty acids (MUFA), it could be cleared that, the major types of (MUFAs) in all samples were oleic and Palmitoleic acid. The highest contents of the total (MUFAs) were in the Head (44.58%) while, the lowest content was observed in the viscera (36.76%). Furthermore, the contents of polyunsaturated fatty acids (PUFA) in the head, liver, and Viscera of mullet were 6.17, 14.01, and 7.35% respectively. The predominant (PUFA) in all samples was linoleic, these results this agreement with **PUDTIKAJORN *&* BENJAKUL {40}.**

Sensory evaluation of cooked rice fortified by different levels of tilapia head

The sensory properties of any food product are the major part of important attributes that affect the consumer choice (**SALEM {41}**). Sensory properties of cooked rice

fortified by levels) 3.0, 6.0, and 9.0 %) of the tilapia head are shown in Table (5). From statistical analysis of these data, it could be noticed that there was no significant difference at (P<0.05) in Appearance, texture, odor, taste, color, and overall acceptability between the control sample and cooked rice fortified with tilapia head at the 3.0% level, while, Sensory properties were significantly (P<0.05) decrease in cooked rice sample fortified with tilapia head at the 6.0 and 9.0% compared with the control sample. The highest values of Appearance, Texture, Odor, Taste, Color, and Overall acceptability were noticed in control cooked rice (9.4,9.3 ,9.7, 9.5, 9.6, and 9.5 respectively) while, the lowest values were noticed in cooked rice fortified by tilapia head at level 9.0% (8.7, 8.4, 9.0, 8.7, 8.6 and 8.6 respectively) compared to all samples This result was agreements with **DE CESARO *& al.* {42}.**

Sensory evaluation of cooked rice fortified by different levels of mullet's head

Sensory properties of cooked rice fortified by levels) 3.0, 6.0, and 9.0 %) of Mullet's head are shown in Table (6). According to statistical analysis of these data, there was no significant change in Appearance, Texture, Odor, Taste, Color, and Overall Acceptability between the control sample and cooked rice fortified with mullet head at the 3.0% level (P<0.05). While, Sensory properties were significantly ((P<0.05) decrease in cooked rice sample fortified with mullet head at the 6.0 and 9.0% compared with the control sample. The highest values of Appearance, Texture, Odor, Taste, Color, and Overall acceptability were noticed in control cooked rice (9.2, 9.1, 9.5, 9.3, 9.4, and 9.3 respectively) while, the lowest values were noticed in cooked rice fortified by Mullet's head at level 9.0% (8.5, 8.2, 8.8, 8.5, 8.4 and 8.4 respectively) compared to all samples.

Table 5. Sensory evaluation of cooked rice fortified by different levels of tilapia head

Samples	Sensory properties					
	Appearance	Texture	Odor	Taste	Color	Overall acceptability
Control	9.4^{a} ±0.11	9.3^{a} ±0.15	9.7^{a} ±0.26	9.5^{a} ±0.11	9.6^{a} ±0.22	9.5^{a} ±0.17
3%	9.3^{a} ±0.21	9.2^{a} ±0.29	9.6^{a} ±0.13	9.3^{a} ±0.24	9.4^{a} ±0.21	9.3^{a}±0.12
6%	9.1^{ab} ±0.27	9.0^{b} ±0.39	9.3^{b} ±0.29	9.1^{b} ±0.38	9.1^{b} ±0.16	9.1^{b}±0.11
9%	8.7^{b} ±0.31	8.4^{c} ±0.17	9.0^{c} ±0.40	8.7^{c} ±0.29	8.6^{c} ±0.15	8.6^{c}±0.30

Each value is an average of twenty determinations ± standard deviation.
Values followed by the same letter in columns are not significantly different at P<0.05.

Table 6. Sensory evaluation of cooked rice fortified by different levels of mullet's head

Samples	Sensory properties					
	Appearance	Texture	Odor	Taste	Color	Overall acceptability
Control	9.2^{a}±0.41	9.1^{a} ±0.35	9.5^{a} ±0.56	9.3^{a} ±0.41	9.4^{a} ±0.32	9.3^{a}±0.19
3%	9.1^{a}±0.31	9.0^{a} ±0.49	9.4^{a} ±0.43	9.1^{a} ±0.14	9.2^{a} ±0.41	9.1^{a}±0.13
6%	8.9^{b}±0.47	8.8^{b} ±0.19	9.1^{b} ±0.19	8.9^{b} ±0.28	8.9^{b} ±0.26	8.9^{b}±0.28
9%	8.5^{c}±0.21	8.2^{c} ±0.37	8.8^{c} ±0.30	8.5^{c} ±0.39	8.4^{c} ±0.45	8.4^{c}±0.24

Each value is an average of twenty determinations ± standard deviation.
Values followed by the same letter in columns are not significantly different at P<0.05.

Nutritional composition of rice fortified by different levels of tilapia head

The tilapia head which presented high nutritional value, being considered a solution to waste disposal problems, as well as an ingredient that can be incorporated in different food product formulas with the purpose of enrichment, as performed on food product formulas (**IBRAHIM {43}).** The changes in the chemical composition of control cooked rice and cooked rice fortified by levels (3, 6 and 9%) of the tilapia head (% on a dry weight basis) are shown in table (7). From statistical analysis of these data, it could be noticed that there was a significant difference at (P<0.05) in Moisture, Crude Protein, ether extract, ash, and total

carbohydrates between all samples. It should be noted from the given data that, the moisture contents ranged between 43.63 % in control to 49.01% in fortification rice with 9.0% tilapia head flour. The increased moisture content can be explained by the higher content of protein which also increases the water-binding capacity of dough with higher levels of tilapia head flour. It is also reported that, moisture content of bread increased resulted in the addition of tilapia-waste flour (**MONTEIRO *& al.* {44}**). Apparent also from the same Table that, fortification rice with various levels of tilapia head flour leads to increased significantly protein, ether extract, and ash content from 7.04, 2.35, and 2.30 % in control to 9.92, 7.24, and 5.05% in fortification rice with 9.0% tilapia head flour. The protein, ether extract, and ash content of fortification rice with tilapia head flour increase ($P < 0.05$) by increasing the concentrations of fortification tilapia head flour. This increment may be due to the tilapia head flour were high protein, ether extract, and ash content as compared to the cooked rice as reported by **WIDODO *&* SIRAJUDIN {45}.** The increase of protein content in each treatment was influenced by the protein content of the base ingredients used. On the other hand, the total carbohydrate content in cooked rice fortified by various levels of tilapia head flour was significantly decreasing by increasing tilapia head flour. It was decreased from 88.31% in control to 77.97 in fortification rice with 9.0% tilapia head flour. This is maybe due to tilapia head flour are rich in protein, ether extract, and ash. Data of the present study are in agreement with those found by **MONTEIRO *& al.* {44}.**

Table 7. Quality properties of rice fortified by different levels of tilapia head flour (on a dry weight basis)

Samples	Quality properties (%)				
	Moisture	Crud Protein	Ether extract	Ash	*Total carbohydrates
Control	$43.63^{a}\pm0.39$	$7.04^{d}\pm0.19$	$2.35^{d}\pm0.11$	$2.30^{d}\pm0.07$	$88.31^{a}\pm0.53$
3%	$45.51^{b}\pm0.22$	$8.00^{c}\pm0.10$	$4.11^{c}\pm0.14$	$2.93^{c}\pm0.11$	$84.96^{b}\pm0.44$
6%	$46.83^{c}\pm0.13$	$8.96^{b}\pm0.15$	$5.55^{b}\pm0.18$	$3.77^{b}\pm0.09$	$81.72^{c}\pm0.36$
9%	$49.01^{d}\pm0.18$	$9.92^{a}\pm0.17$	$7.24^{a}\pm0.11$	$5.05^{a}\pm0.10$	$77.79^{d}\pm0.18$

Each value is an average of three determinations ± standard division.
Values followed by the same letter in rows are not significantly different at $P<0.05$.
* Total carbohydrates were calculated by difference.

Nutritional composition of rice fortified by different levels of mullet's head

The changes in the chemical composition of control cooked rice and cooked rice fortified by levels (3, 6 and 9 %) of mullet's head (% on a dry weight basis) are shown in table (8). From statistical analysis of these data, it could be noticed that there were the significant differences at ($P<0.05$) in Moisture, Crude Protein, ether extract, ash, and total carbohydrates between all samples. From the same Table (6) it could be noticed that, the moisture contents ranged between 50.63 % in control to 49.66 % in fortification rice with 9.0% mullet head flour. The increased moisture content can be explained by the higher content of protein which also increases the water-binding capacity of dough with higher levels of Mullet head flour. It is also reported that, moisture content of bread increased resulted in the addition of Mullet head flour. These results agree with **EL-BELTAGI *&* *al.* {46} ; DE CESARO *& al.* {42}.** Apparent also from the same Table that, fortification rice with various levels of Mullet head flour leads to increased significantly protein, ether extract, and ash content from 7.04, 2.35, and 2.30 % in control to 9.83, 6.33, and 4.98% in fortification rice with 9.0% Mullet head flour . This increment may be due to the Mullet head flour were high protein, ether extract, and ash content as compared to the cooked rice. **EL-BELTAGI *&* *al.* {46} ; ABRAHA *&* al. {47}** reported that the nutritive value of cereal proteins can be increased when fortified with fish protein . On the other hand, the total carbohydrate content in cooked rice fortified by various levels of mullet head flour was significantly decreasing by increasing Mullet head flour. It was decreased from 88.31% in control to 78.86 in fortification rice with 9.0% Mullet head flour. This is maybe due to Mullet head flour are rich in protein, Ether extract, and ash. Data of the present study are in agreement with those found by **BASTOS *& al.* {48}.**

Table 8. Quality properties of rice fortified by different levels of mullet head flour (on a dry weight basis).

Samples	Quality properties				
	Moisture	Crud Protein	Ether extract	Ash	*Total carbohydrates
Control	$50.63^{a}\pm0.30$	$7.04^{d}\pm0.15$	$2.35^{d}\pm0.11$	$2.30^{d}\pm0.07$	$88.3^{a}\pm0.53$
3%	$51.60^{b}\pm0.25$	$7.97^{c}\pm0.12$	$3.82^{c}\pm0.21$	$2.90^{c}\pm0.09$	$85.31^{b}\pm0.34$
6%	$52.93^{c}\pm0.36$	$8.90^{b}\pm0.17$	$5.01^{b}\pm0.10$	$3.70^{b}\pm0.13$	$82.39^{c}\pm0.41$
9%	$49.66^{d}\pm0.31$	$9.83^{a}\pm0.19$	$6.33^{a}\pm0.23$	$4.98^{a}\pm0.10$	$78.86^{d}\pm0.33$

Each value is an average of three determinations ± standard division.
Values followed by the same letter in rows are not significantly different at $P<0.05$.
* Total carbohydrates were calculated by difference.

Conclusions

The tilapia and mullet head flour had high nutritional value in relation to their protein, total lipids, and ash (minerals) contents. The omega-3 fatty acid content is proved to be satisfactory by the PUFA/SFA and the n-6/n-3 ratios and within the recommended levels. It is considered a solution to fish waste disposal problems as well as ingredients that can be fortification in different food products.

References

1. A. M. EL-SAYED. Regional review on status and trends in aquaculture development in the Near East and North Africa –2015, by. FAO Fisheries and Aquaculture Circular No. 1135/6. Rome, Italy. (2015)
2. A. KUMAR, K. ELAVARASAN, P. KISHORE, D. UCHOI, H. M. DEVI, G. NINAN, A. A. ZYNUDHEEN. Effect of dehydration methods on physico-chemical and 2 sensory qualities of restructured–dehydrated fish product. *J. Food Process. Pres.* DOI 10.1111/jfpp.13277. (2017).
3. J. H. LEONHARDT, M. CAETANO-FILHO, H. FROSSARD, A. M. MORENO. Morphometrics, fillet yield and fillet composition in Nile tilapia, Oreochromics niloticus, strains thai chitralada, Brazil local and their hybrid. Semina: Ciências Agrárias, 27(1), 125-132. (2006).
4. M. E. PETENUCI, F. B. STEVANATO, D. R. MORAIS, L. P. SANTOS, N. E. SOUZA, J. V. VISENTAINER. Composição e estabilidade lipídica da farinha de espinhaço de tilápia. Ciência e Agrotecnologia, 34 (5), 1279-1284. (2010).
5. A. E. GHALY, V. V. RAMAKRISHNAN, M. S. BROOKS, S. M. BUDGE, D. DAVE. Fish processing wastes as a potential source of proteins, amino acids and oils: A critical review. *J. Microb. Biochem. Tech*., 5: 107- 129. (2013).
6. R. TAHERGORABI, K.E. MATAK, J. JACZYNSKI. Fish protein isolate: development of functional foods with nutraceutical in-gredients. *J. of Functional Foods* 18: 746–756. (2015).
7. V. RENUKA, R. ANANDAN, M. SUSEELA, C.N. RAVISHANKAR, G.K. SIVARAMAN. Fatty acid profile of yellowfin tuna eye (Thunnus albacares) and oil sardine muscle (Sardinella longiceps). *Fish. Tech*., 53: 151-154. (2016).
8. I.S. ARVANITOYANNIS, A. KASSAVETI. Fish industry waste: Treatments, environmental impacts, current and potential uses. *Int. J. Food Sci. Technol*., 43, 726–745. (2008).
9. T. RUSTAD, I. STORRØ, R. SLIZYTE. Possibilities for the utilization of marine by-products. *Int. J. Food Sci. Tech*., 46, 2001–2014. (2011).
10. K. S. SAYANA, T. K. SIRAJUDHEEN. By-products from Tuna processing wastes an economic approach to coastal waste management. Proceedings of the International Seminar on Coastal Biodiversity Assessment, 411-420. (2017).
11. V. FERRARO, A.P. CARVALHO, C. PICCIRILLO, M.M. SANTOS, P.M. CASTRO, M.E. PINTADO. Extraction of high added value biological compounds from sardine, sardine-type fish and mackerel canning residues—A review. Mater. Sci. Eng. C, 33, 3111–3120. (2013).
12. R.L. OLSEN, J. TOPPE, I. KARUNASAGAR. Challenges and realistic opportunities in the use of by-products from processing of fish and shellfish. *Trends Food Sci. Tech*., 36, 144–151. (2014).
13. J.; ZAMORA-SILLERO, A. GHARSALLAOUI, C. PRENTICE. Peptides from fish by-product protein hydrolysates and its functional properties: An overview. Mar. Biotechnol., 20, 118–130. (2018).
14. M.B. ESTEBAN, A.J. GARCÍA, P. RAMOS, M.C. MÁRQUEZ. Evaluation of fruit–vegetable and fish wastes as alternative feedstuffs in pig diets. , 27(2), 193–200. (2007).
15. H. ZHAO, M. JIANG, S. XUE, S. XIE, X. WU, A. GUO. Fish meal can be completely replaced by soy protein concentrate by increasing feeding frequency in nile tilapia (Oreochromisniloticus). Department of Aquaculture Nutritional.16:648-655. (2011).
16. E. P. RYAN. Bioactive food components and health properties of rice bran. Journal of the American Veterinary Medical Association, 238(5), 593–600. (2011).
17. M. WALTER, E. MARCHESAN, P.F. SACHET MASSONI, D.A. PICOLLI L. SILVA, G. MENEGHETTI SARZI SARTORI, R. BRUCK FERREIRA. Antioxidant properties of rice grains with light brown, red and black pericarps colors and the effect of processing. *Food Res. Int*., 50, 698–703. (2013).
18. J. E. ARSENAULT, E. A. YAKES, M. B. HOSSAIN, M. M. ISLAM, T. AHMED, C. HOTZ, L. LEWIS, A. S. RAHMAN, K. M. JAMIL, K. H. BROWN. The Current High Prevalence of Dietary Zinc Inadequacy among Children and Women in Rural Bangladesh Could Be Substantially Ameliorated by Zinc Biofortification of Rice. *Journal of Nutrition* 140: 1683 - 1690. (2010).
19. D. BABARYKIN, I. ADAMSONE, D. AMERIKA, A. SPUDASS, V. MOISEJEV, N. BERZINA, L. MICHULE, R. ROZENTAL. Calcium enriched bread for treatment of uremic hyperphosphatemia. *J. of Renal Nutrition* 14: 149-156. (2004).
20. P. JAYASINGHE, I. ADEOTI, K. A. HAWBOLDT. study of process optimization of extraction of oil from fish waste for use as a low-grade fuel. *J. of the American Oil Chemists' Society*, 90: 1903- 1915. (2013).
21. AOAC. Official Methods of Analysis of AOAC International. 18th Edition, AOAC International, Gaitherburg, 2590. (2010).
22. E. J. CONKERTON, P.J. WAN, O.A. RICHARD. Hexane and heptane as extraction solvents for cottonseed: A laboratory-scale study. *J. of the American Oil Chemists' Society,*72: 963–965. (1995).
23. S. AZADMARD, P.C. DUTTA. Rapid separation of methyl- sterols from vegetable oils by solid- phase extraction. Lipid Technology,18 :231–234. (2006).

24. E. PANAGIOTIS, E. IGOUMENIDIS, V. LEKKA, T. KARATHANOS. Fortification of white milled rice with phytochemicals during cookingin aqueous extract of Mentha spicata leaves. An adsorption study. LWT - *Food Sci. and Tech*., 65: 589-596. (2016).
25. M. A. EL-BANA, R. A. GOMA, A.S. ABD EL-SATTAR. Effect of parboiling process on milling quality, physical and chemical properties of two rice varieties. Menoufia *J. Food and Dairy Sci*., 5: 35 – 51. (2020).
26. F. B. STEVANATO, M. E. PETENUCCI, M. MATSUSHITA, M. C. MESOMO, N. E. SOUZA, J. E. L. VISENTAINER, J.V. VISENTAINER. Fatty acids and nutrients in the flour made from tilapia (Oreochromis niloticus) heads. Ciênc. Tecnol. Aliment., Campinas, 28(2): 440-443. (2007).
27. L. D. SHIRAHIGUE, M. O. SILVA, A. C. CAMARGO, L. F. SUCASAS, R. BORGHESI, I. S. R. CABRAL, M. OETTERER. The feasibility of increasing lipid extraction in tilapia (Oreochromisniloticus) waste by proteolysis. *J. of Aquatic Food Product Tech.,* 25, 265-271. (2016).
28. V. SUVANICH, R. GHAEDIAN, R. CHANAMAI, E.A. DECKER, D.J. MCCLEMENTS. Prediction of proximate fish composition from ultrasonic properties: catfish, cod, flounder, mackerel and salmon. *J. of Food Sci*., 63: 966-968. (2006).
29. M. PATEIRO, P. E. S. MUNEKATA, R. DOMÃ¬NGUEZ, M. WANG, F.J. BARBA, R. BERMÃDEZ, J. M. LORENZO. Nutritional Profiling and the Value of Processing By-Products from Gilthead Sea Bream (Sparus aurata). Marine Drugs, 18(2), 101–.119. (2020).
30. S. HE, C. FRANCO, W. ZHANG. Characterisation of processing wastes of Atlantic Salmon (Salmo salar) and Yellowtail Kingfish (Seriola lalandi) harvested in Australia. *Int. J. Food Sci. Tech*., 46, 1898–1904. (2011).
31. K. ELAVARASAN, A. KUMAR, D. UCHOI, C. S. TEJPAL, G. NINAN, A. A. ZYNUDHEEN. Extraction and characterization of gelatin from the head waste of tiger tooth croaker (Otolithes ruber). Waste Biomass Valor. 8: 851-858. (2017).
32. S.A. EL-SHERIF. Utilization of Fayoum Fisheries by Products in the Production of Fish Meal High Nutritional Quality and Microbiological Safety. *Int. J. of Chem. Tech. Res*., 10 (5): 458-469. (2017).
33. H. S. SUSENO, Y. NURJANAH, A. SARASWATI. Determination of extraction temperature and period of fish oil from tilapia (Oreochromis Niloticus) by product using wet rendering method. The 1st International Symposium on Aquatic Product Processing .1:124-135. (2015).
34. A. KHODDAMI, A. A. ARIFFIN, J. BAKAR, H. M. GHAZALI. Fatty acid profile of the oil extracted from fish waste (Head, Intestine and Liver) (Sardinella lemuru). World *Appl. Sci. J*. 7:127-131. (2009).
35. F. ABD EL-RAHMAN, N.S. MAHMOUD, B. ABO EL – KHAIR, M. Y. SAMY. Extraction of Fish Oil from Fish Viscera. Egypt, J.Chem., 61(.2): 225 – 235. (2018).
36. I. OUASSOR, Y. AQIL, W. BELMAGHRAOUI, S. EL HAJJAJI. Characterization of two Moroccan watermelon seeds oil varieties by three different extraction methods. OCL, 27, 13–. doi:10.1051/ ocl/2020010. (2020).
37. R. KUMARAN, V. RAVI, B. M. GUNALAN, A. S. SUNDRAMANICKAM. Estimation of proximate, amino acids, fatty acids and mineral composition of mullet (Mugil cephalus) of Parangipettai, Southeast Coast of India. Adv. *Appl. Sci. Res*., 3(4):2015-2019. (2012).
38. M. KACEM, M. SELLAMI, W. KAMMOUN, F.FRIKHA, N. MILED, F. BEN REBAH. Seasonal Variations in Proximate and Fatty Acid Composition of Viscera of Sardinella aurita, Sarpa salpa, and Sepia officinalis from Tunisia. *J. of Aquatic Food Product Tech.,* 20 (2), 233–246. (2011).
39. K. ELAVARASAN, A. KUMAR, C. S. TEJPAL, K. D. SATHISH, G. N. UCHOI, A. A. ZYNUDHEEN. Quality and Fatty Acid Composition of Lipids from Head of Indian Mackerel (Rastreliger kanagurta) and Tigertooth Croaker (Otolithes ruber). Fishery Technology 54: 112 – 117. (2017).
40. K. PUDTIKAJORN, S. BENJAKUL. Simple Wet Rendering Method for Extraction of Prime Quality Oil from Skipjack Tuna Eyeballs. *Eur. J. Lipid Sci. Tech*.,122, 1–29. (2020).
41. R.H. SALEM. Quality characteristics of beef sausages with tomato peel as a color and functional additive during frozen storage. *J. World Applied Sciences,* 22 (8):1085-1093. (2013).
42. E. DE CESARO, F. MELINA, G. GISLAINE, M. G. JANE, P. GIULIANA, S. D. G. ELENICE. Evaluation of cookies with inclusion of different levels of barred sorubim (Pseudoplatystoma fasciatum) flour. *Brazilian Journal of Development, Curitiba*, 7(5), 47223-47238. (2021).
43. S.M. IBRAHIM. Evaluation of production and quality of salt-biscuits supplemented with fish protein concentrate. *World J. Dairy and Food Sci*. 4: 28-31. (2009).
44. M.L.G. MONTEIRO, E.T. MA´RSICO, M.S. SOARES JUNIOR, R. DELIZA, D.C.R. DE OLIVEIRA, C.A. CONTE-JUNIOR. Tilapia-waste flour as a natural nutritional replacer for bread: A consumer perspective. PLoS ONE 13(5): e0196665. https:// doi.org/10.1371/journal.pone.0196665. (2018).
45. S. WIDODO, S. SIRAJUDIN. Effect of Drying Time on Quality of Mozambique tilapia Fish (Oreochromis Mossambicus) and Round Sardinella (Sardinella Aurita) Flour, in International Conference ADRI -5 ("Scientific Publications toward Global Competitive Higher Education) .1:. 157–163. (2017).
46. H.S. EL-BELTAGI, N.A. EL-SENOUSI, Z.A. ALI, A.A. OMRAN. The impact of using chickpea flour

and dried carp fish powder on pizza quality. PLoS ONE 12(9): 1-15. (2017).

47. B. ABRAHA, A. MAHMUD, H. ADMASSU, F. YANG, N.T. SIGHE. Production and Quality Evaluation of Biscuit Incorporated with Fish Fillet Protein Concentrate. *J. Nutr Food Sci.,* 8: 744. (2018).
48. S.C. BASTOS, T. TAVARES, M.E.S.G. PIMENTA, R. LEAL , L.F. FABRI ´CIO, C.J. PIMENTA, C.A. NUNES, A.C.M. PINHEIRO. Fish filleting residues for enrichment of wheat bread: chemical and sensory characteristics. *J Food Sci Technol*. 51(9): 2240–2245. (2014).

ISSN print: 1224-5984
ISSN online: 2248-3942

Rom Biotechnol Lett. 2022; 27(1): 3252-3263
doi: 10.25083/rbl/27.1/3252-3263

Received for publication, January, 04, 2022
Accepted, February, 16, 2022

Original paper

In vitro Angiotensin Converting Enzyme Inhibitory and Antioxidant Activities of Some Sulfur Compounds

SEBAHAT YILMAZ, BERTAN BORAN BAYRAK, REFIYE YANARDAG

Istanbul University-Cerrahpasa, Faculty of Engineering Block A, Department of Chemistry, Division of Biochemistry, 34320-Avcilar/Istanbul/TURKEY.

Abstract The angiotensin converting enzyme (ACE) catalyzes the conversion of angiotensin I to a key vasoconstrictor angiotensin II in renin-angiotensin system (RAS), thus playing an important role in both regulating blood pressure and maintaining fluid balance through RAS. Free radicals are continuously produced in the biological system. Therefore, organisms need both exogenous and endogenous antioxidants to guard against the damage caused by these free radicals. In this way, they prevent the occurrence of numerous diseases via protecting cellular components and biomolecules. The aim of the current study was to investigate the ACE inhibitory and antioxidant activities of sulfur compounds. The ACE inhibitory and antioxidant activities of all sulfur compounds increased in a concentration-dependent manner. Among these compounds, methionine had the highest ACE inhibitory and antioxidant activityes based on reducing power, DPPH radical scavenging and ORAC methods. Cystine had the highest ABTS radical scavenging, FRAP and nitrite scavenging activities. However, S-benzyl cysteine and S-phenyl cysteine exhibited the lowest ACE inhibitory and antioxidant activities, respectively. These outcomes indicate that sulfur compounds have both ACE inhibitory and antioxidant activities and may serve as gateways for research toward understanding the beneficial pharmacological effects of sulfur compounds against cell damage caused by oxidative stress.

Keywords Free radicals; angiotensin converting enzyme; inhibitors; antioxidant activity; sulfur compounds

To cite this article: YILMAZ S, BAYRAK BB, YANARDAG R. *In vitro* Angiotensin Converting Enzyme Inhibitory and Antioxidant Activities of Some Sulfur Compounds. *Rom Biotechnol Lett*. 2022; 27(1): 3252-3263. DOI: 10.25083/rbl/27.1/3252-3263.

✉ *Corresponding author: BERTAN BORAN BAYRAK, Istanbul University-Cerrahpasa, Faculty of Engineering Block A, Department of Chemistry, Division of Biochemistry, 34320-Avcilar/Istanbul/TURKEY.
E-mail: bertanb@iuc.edu.tr

Introduction

The angiotensin converting enzyme (ACE; EC 3.4.15.1) is a zinc metalloprotease of paramount significance in the renin-angiotensin system (RAS). As a result of its peptidyl-dipeptidase activity, ACE hydrolyzes the C-terminal His-Leu dipeptide from angiotensin (Ang)-I to form a key vasoconstrictor octapeptide Ang-II. Thus, it plays an important role in both regulating blood pressure and maintaining fluid/electrolyte/salt balances through RAS in the organism. More so, ACE inhibits a potent vasodilator bradykinin (Tipnis et al., 2000). After discovered as a homologue of human ACE, the ACE2 acts as a carboxypeptidase, cleaves the basic amino acid in C-terminal residue, thereby hydrolyzing Ang-II to Ang (1-7) or produces Ang (1-9) (Simões e Silva et al., 2016; Shukla and Banerjee, 2021). Besides, ACE2, an important regulator of the RAS system, has been proven to have a very crucial role (by acting as a receptor mediating viral entry to the organism) in the pathogenesis of severe acute respiratory syndrome coronavirus 2 (SARS-CoV-2), which causes coronavirus disease 2019 (Coto et al., 2021; Mascolo et al., 2021; Pagliaro et al., 2022). ACE and ACE2 participate in the synthesis of bioactive peptides of the RAS, thereby are involved in the inflammatory process of conditions such as cardiac hypertrophy, pulmonary hypertension, lung injury, and sepsis (Gaddam et al., 2014). Because of these properties, the main strategy for the prevention of diseases that may result from the alteration of ACE activity may be the search for new molecules for ACE inhibition.

Free radicals are atoms or molecules that have one or more unpaired electrons in their outer orbital electron shell. They are highly unstable, have low activation energy and short life. Because of their high reactivity, excessive formation of free radicals [especially reactive oxygen species (ROS)] disrupts the balance of cellular metabolic processes/reactions, thereby causing inevitable and detrimental effects on important biomolecules such as lipids, proteins, and DNA in cells (Juan et al., 2021). Under normal physiological conditions, there is a balance between ROS that are constantly being formed in cells and antioxidants that neutralize them. Disruption of this balance in favor of ROS leads to oxidative stress, a condition characterized by the accumulation of cellular ROS. Accumulating findings have shown that there is a strong relationship between oxidative stress and many ailments, such as immune deficiency, inflammatory conditions, and several types of cancers, cardiovascular and respiratory diseases (Forman and Zhang, 2021). Antioxidants are chemical compounds not only responsible for preventing oxidative damage, but also detoxifying ROS. They prevent or delay the oxidation of biomolecules by reducing the reactivity of ROS (Sánchez, 2017).

Sulfur is an abundant element that plays a crucial role as a component of proteins, vitamins, and other important biomolecules that are essential for life. Sulfhydryl (thiol)-containing amino acids include methionine (Met), cysteine, homocysteine, and taurine (Bin et al., 2017). These are involved in the synthesis of intracellular antioxidants such as glutathione and N-acetyl cysteine (Čolović et al., 2018). On the other hand, some organosulfur compounds such as diallyl sulfide, diallyl disulfide, N-acetyl cysteine, S-allyl cysteine, S-methyl cysteine (SMC), S-ethyl cysteine and S-propyl cysteine have reducing power, metal chelating ability, and superoxide ion scavenging activity (Hsu et al., 2004; Corzo-Martínez et al., 2007; Bayrak and Yanardag, 2021). Antioxidant effects of sulfur compounds have been studied by several researchers (Atmaca, 2004; Battin and Brumaghim, 2008). Sulfur-containing amino acids can be used to reduce cell damage induced by oxidative stress, because of their ROS removing ability (Moskovitz, 2005). Dagsuyu and Yanardag (2021) have revealed that some sulfur compounds have urease and trypsin inhibitory activities. Although vast majority of antioxidants have an active hydroxyl group in their phenolic ring structure which neutralizes free radicals by easily donating hydrogen atoms (Lü et al., 2010), it has been stated that natural or synthetic mixtures consisting of sulfur and nitrogen-containing amino acids, peptides, polypeptides and protein hydrolysates have also antioxidant potential (de Oliveira Filho et al., 2021). Reports show that sulfur-containing amino acids (or their derivatives) with antioxidant activity can be used in the food industry as additives or can be applied as dietary supplements, thereby extending the shelf-life of food because of their free radical scavenging activity (Udenigwe and Aluko, 2011). On the other hand, it has been revealed that cysteine S-conjugates [e.g., S-benzyl cysteine (SBC) and S-phenyl cysteine (SPC)] are intermediary and/or final products in xenobiotic metabolism (Okajima et al., 1984; Hanway et al., 2000). Another cysteine derivative, SMC, has been reported to have chemopreventive effects against hepatocarcinogenesis (Wei et al., 2000), antioxidative and antiinflammatory effects against neurotoxicity (Chen et al., 2007). Senthilkumar et al., (2013) have suggested that SMC shows hypoglycemic and antihyperlipidemic effects in experimental obesity model in rats. Besides, it has been revealed that SMC could be an effective compound against *Cryptosporidium parvum* infection via restoring structural alterations in different tissues of albino mice (Elmahallawy et al., 2020).

Presently, there are only few research articles reporting the *in vitro* ACE inhibitory activities and antioxidant potentials of Met, cystine, SBC, SMC, SPC, and taurine. Thus, the present study was aimed to investigate the *in vitro* ACE inhibitory and antioxidant activities of these sulfur compounds.

Materials and Methods

Chemicals

Cystine and Met were supplied by Merck Chemical Company (Darmstadt, Germany). SBC, SMC, SPC, taurine, N-[3-(2-Furyl)acryloyl]-Phe-Gly-Gly (FAPGG), 6-hydroxy-2,5,7,8-tetramethylchromane-2-carboxylic acid (Trolox), 2,2′-azino-bis(3-ethylbenzothiazoline-6-sulphonic acid)

diammonium salt (ABTS), 2,2-diphenyl-1-picrylhydrazyl (DPPH), N,N-dimethyl-4-phenylenediamine (DMPD), 2,4,6-tri(2-pyridyl)-s-triazine (TPTZ), ferrozine (3-(2-pyridyl)-5,6-diphenyl-1,2,4-triazine-4′,4″-disulfonic acid sodium salt), 2,2′-azobis(2-methylpropionamidine) dihydrochloride (AAPH), and fluorescein disodium salt were purchased from Sigma-Aldrich (St. Louis, MO, USA). All other chemicals used were of analytical grade.

ACE Inhibitory Activity Assay

ACE inhibitory activities of sulfur compounds were estimated according to Shalaby et al., (2006). In this assay, lamb kidney homogenate (10 %, weight/volume) was used as a source of ACE. Captopril was used as a standard inhibitor. The percent inhibition of the ACE was calculated using the following equation:

$$\text{ACE inhibitory activity (\%)} = \left[\frac{(A_0 - A_1)}{A_0}\right] \times 100 \qquad (1)$$

Where: A_0 represents the activity of the enzyme without the inhibitor, and A_1 is the activity of the enzyme in the presence of the sulfur compounds (or standard inhibitor).

Reducing Power Assay

The reducing power of the sulfur compounds was determined using method of Oyaizu (1986). As reference solution, Trolox was used. The intensity of the blue color is directly proportional to the reducing power of the tested sulfur compounds. A high absorbance of the reaction mixture indicates a greater reducing power of the tested sulfur compounds.

ABTS Radical Scavenging Activity Assay

ABTS radical scavenging activities of the sulfur compounds and reference antioxidant were assessed by the procedure of Arnao et al., (2001). Trolox was used as a reference antioxidant.

DPPH Radical Scavenging Activity Assay

DPPH radical scavenging activities of the sulfur compounds were estimated by the method of Brand-Williams et al., (1995). Trolox was used as a reference antioxidant.

DMPD Radical Scavenging Activity Assay

The determination of DMPD radical scavenging activity was performed using method of Fogliano et al., (1999). Ascorbic acid and Trolox were used as the reference antioxidants.

Ferric Reducing Antioxidant Power (FRAP) Assay

The FRAP assay was carried out according to Benzie and Strain (1996). Reference solutions of $FeSO_4.7H_2O$ were employed to obtain calibration curve. Ascorbic acid and Trolox were used as the positive control. The results were expressed as μM Fe^{2+} per 100 mL sample.

Metal Chelating Activity Assay

The metal chelating activities of the sulfur compounds were determined using the method of Decker and Welch (1990). EDTA was used as a reference metal chelator. A low absorbance indicates a higher chelating activity of the tested sulfur compounds.

Nitrite Scavenging Activity Assay

Nitrite scavenging activities of the sulfur compounds and quercetin (as a reference antioxidant) were carried out according to Liu et al., (2011).

Oxygen Radical Absorbance Capacity (ORAC) Assay

To measure ORAC of the sulfur compounds and Trolox (as a reference antioxidant), a modified method of Huang et al., (2002) was employed. The fluorescence was measured at 37° C every min for 35 min at 485 nm as the excitation wavelength and 528 nm for the emission wavelength. The following formula was used to calculate ORAC values, and the results were given as % inhibition value.

$$\text{ORAC value (\%)} = \frac{[(I_2 - I_1)]}{[(I_0 - I_1)]} \times 100 \qquad (2)$$

I_0 is initial fluorescence intensity value of fluorescein
I_1 is fluorescence intensity value of fluorescein remaining intact during incubation medium in the absence of the sulfur compounds or standard
I_2 is fluorescence intensity value of fluorescein remaining in the incubation medium in the presence of the sulfur compounds or standard

For antioxidant activities (ABTS, DPPH, DMPD, metal chelating, and nitrite scavenging activities) of the sulfur compounds (or standards) were calculated using the following equation:

$$\text{Radical scavenging activity (\%)} = \frac{[(A_0 - A_1)]}{A_0} \times 100 \qquad (3)$$

A_0 is the absorbance of the control, A_1 is the absorbance of the sulfur compounds

For ACE inhibitory and antioxidant activities, the sulfur compounds (or standard) concentration providing 50 % inhibitions (IC_{50}) were calculated by the regression equations (by plotting concentration of sulfur compounds versus percentage inhibition). A low IC_{50} indicates a higher inhibitory potential and antioxidant activity of the tested compounds.

Results and discussion

Free radicals are extremely reactive and unstable atoms, molecules or molecular fragments. They have one or more unpaired electrons that can easily interact with many other biomolecules (e.g., nucleic acids, proteins, and lipids) in the physiological conditions (Kumar et al., 2021). Besides, they can quickly propagate radical chain reactions, which have harmful effects on cells. The continuous formation and elimination of free radicals (i.e., ROS) in living cells are precisely kept under control by a phenominum called redox-balance (Pizzino et al., 2017; Ramana et al., 2018).

The disruption of this redox balance in favor of ROS causes oxidative stress, which in turn promotes the development of a wide variety of disorders that include cancer, diabetes, aging, Alzheimer's, and Parkinson's diseases (Suleman et al., 2019; Forman and Zhang, 2021).

The sulfur atom is present in all living cells, and is also essential for life. Besides, it is a structural component of some amino acids, proteins, and many other biomolecules that have important biological functions. Met, cysteine, cystine, homocysteine, N-acetyl cysteine, and taurine are well known sulfur-containing amino acids. Among them, Met and cysteine are designated as proteinogenic amino acids, whereas the others are called non-proteinogenic amino acids. Moreover, they are involved in many biochemical processes such as methylation reaction in the form of S-adenosylmethionine and biosynthesis of one of the most important intracellular antioxidants known as glutathione (Čolović et al., 2018).

The present study investigated the ACE inhibitory activity as well as antioxidant potential of Met, cystine, SBC, SMC, SPC, and taurine based on electron and hydrogen atom transfer methods. The outcomes were compared with activities of some natural and synthetic antioxidant compounds.

The activity of the ACE enzyme is very crucial because of its important role in both regulating blood pressure and maintaining fluid/electrolyte/salt balance in the organism through RAS (Fagyas et al., 2014). An increase in the activities of ACE is associated with cardiovascular and renal disorders (e.g., high blood pressure, heart failure, acute kidney injury, diabetes-mediated kidney disease). Because of being a key factor of experimental and clinical approaches in the treatment of the aforementioned diseases, inhibition of the ACE is at the center of research and paramount for the discovery of new and safe molecules with inhibitory properties (Giani et al., 2021). The inhibition effects of sulfur compounds as well as that of captopril against ACE activity are summarized in Table 1. The results depict IC_{50} values of ACE inhibitory activities of the sulfur compounds. IC_{50} values were calculated by plotting the inhibition percentage values as function of concentrations. According to the results, all the sulfur compounds and captopril had an IC_{50} values in the range of 0.11-389.07 µM. Considering the high inhibitory activities (associated with the lower IC_{50} values) these compounds demonstrated lower inhibitory activity against ACE in comparison to captopril (IC_{50} values of 0.11±0.02 µM). On the other hand, it was observed that Met had approximately two times more inhibitory effect than that of SMC. In addition, Met was observed to have the best ACE inhibitory activity among the sulfur compounds. The ACE inhibitory activity of sulfur compounds and the standard decreased in the order of: captopril>Met>SMC>taurine>cystine> SBC>SPC (Table 1). The various inhibitors may bind to the amino acids such as aspartate, histidine, phenylalanine, and serine at the binding pocket in the active center of the enzyme, thereby giving rise to inhibition of the ACE (Masuyer et al., 2012). Bioactive sulfur compounds in *Asparagus officinalis* have been revealed to possess anti-ACE activity (Nakabayashi et al., 2015). Sulfur-containing N-mercaptoalkanoyl amino acids had been reported to be potent ACE inhibitors whose SMC and SEC derivatives had the same IC_{50} value for SMC and lower IC_{50} value for SEC when compared to captopril (Komori et al., 1987). In the current study, SMC and other compounds showed weaker ACE inhibitory activities than that of captopril. This may be due to lack of sulfhydryl group in the substances we used in the current study or these substances may not fully interact with the amino acids in the active site of the enzyme.

Table 1. Inhibitory activities of the sulfur compounds on ACE.

Compounds / Standard	Concentrations (µM)	IC_{50} (µM)*
Cystine	0.1 1 10	90.97 ± 9.25
Met	0.01 0.1 0.5	1.46 ± 0.16
SBC	1 10 100	274.18 ± 38.74
SMC	0.5 1 2	2.46 ± 0.17
SPC	0.1 1 100	389.07 ± 98.03
Taurine	1 10 20	83.53 ± 14.69
Captopril	0.01 0.05 0.1	0.11 ± 0.02

*Mean ± SD of triplicate values.

ACE: Angiotensin converting enzyme; Met: Methionine; SBC: S-benzyl cysteine; SMC: S-methyl cysteine; SPC: S-phenyl cysteine.

The reducing power of molecules is related to the ability of a test sample to donate an electron or hydrogen atom to ferric iron (Shen et al., 2019). In the present study, the reducing power of the all compounds were estimated based on reducing Fe^{3+} to Fe^{2+}. FRAP method measures the antioxidant capacities of compounds with redox potential to form the Fe^{2+}-TPTZ complex, by giving an electron to the Fe^{3+}-TPTZ complex in an acidic pH (Magalhães et al., 2008). The findings in Table 2 show reducing power and the FRAP values of all tested compounds. It was observed that the reducing power of the sulfur compounds and standard antioxidant increased with concentration. Cystine and Met had the highest reducing power, whereas taurine had the lowest reducing power value. On the other hand, the reducing power of 500 µM Trolox was almost 5.5 times greater than that of Met (Table 2). The fact that the sulfur compounds have lower reducing power values than Trolox

is an indication of their lesser ability to reduce Fe^{3+}. In the current study, the FRAP values of all sulfur compounds exhibited low FRAP activities than that of standard antioxidant. Cystine was found to have the highest FRAP values. On the other hand, aromatic amino acids have been reported to have very good antioxidant potential, especially non-radical single electron transfer-based experimental systems such as FRAP (Munteanu and Apetrei, 2021). Theoretically, any compound whose redox potential is less than that of Fe(III)/Fe(II) pair can reduce Fe(III) to Fe(II) (Amin et al., 2013). On the contrary, FRAP method is reported to insufficiently measure the antioxidant capacities of compounds possessing free thiol groups such as glutathione (Gulcin, 2020). The reason for having the moderate FRAP values of the sulfur compounds in our study may be due to the presence of an aryl group with an electron delocalized system or an alkyl group covalently bonded to the sulfur atom (Guidea et al., 2020). However, FRAP value of cystine at 500 µM was nearly four-fold less than that of Trolox (Table 2). The FRAP values of all tested compounds in the present study were much lower than that of the standard antioxidant. FRAP values decreased in the order of: ascorbic acid>Trolox>cystine>SBC>SPC>SMC> taurine>Met (Table 2).

Table 2. Reducing power and FRAP values of the sulfur compounds.

Compounds / Standards	Concentrations (µM)*	Reducing Power (Absorbance)*	Concentrations (µM)*	Ferric Reducing Antioxidant Power (Fe^{2+} µM)*
Cystine	100 250 500	0.035±0.009 0.049±0.006 0.061±0.006	300 400 500	35.40±3.92 46.23±1.42 57.81±0.71
Met	100 250 500	0.026±0.002 0.070±0.003 0.125±0.003	1250 1500 2000	1.66±0.36 2.92±0.01 18.53±2.85
SBC	100 250 500	0.015±0.001 0.023±0.012 0.026±0.014	1250 1500 2000	44.72±4.45 51.26±8.43 75.69±1.95
SMC	100 250 500	0.014±0.001 0.026±0.013 0.032±0.018	1250 1500 2000	25.08±2.85 32.88±1.07 53.03±1.07
SPC	100 250 500	0.051±0.011 0.068±0.012 0.094±0.013	1000 1250 1500	23.57±2.82 33.89±2.04 43.71±5.84
Taurine	100 250 500	0.005±0.005 0.008±0.004 0.013±0.008	1250 1500 2000	4.94±0.01 16.01±1.42 21.80±0.36
Trolox	100 250 500	0.367±0.002 0.489±0.001 0.671±0.006	250 500 1000	130.83±2.85 211.15±5.34 242.88±0.36
Ascorbic acid	-	-	250 500 1000	107.92±0.36 194.28±1.42 246.15±2.14

*Mean ± SD of triplicate values.

Met: Methionine; SBC: S-benzyl cysteine; SMC: S-methyl cysteine; SPC: S-phenyl cysteine.

The ABTS radical scavenging activity method is frequently used to determine the antioxidant activities of both lipophilic and hydrophilic compounds based on electron and/or hydrogen atom transfer. Radical scavenging capability of complex mixtures and individual compounds is inversely proportional to the discolorizing of ABTS and DPPH radicals (Gulcin, 2020; Muntenau and Apetrei, 2021). The outcomes of ABTS and DPPH radical scavenging activities of the sulfur compounds and standard antioxidant are presented in Table 3. Standard antioxidant was better ABTS radical scavenger than the sulfur compounds. The IC_{50} values of the sulfur compounds were found to be high and ranged from 2029.67 to 10350.25 µM. The present findings suggest that ABTS radical scavenging activity can be employed in a wide pH range for both hydrophilic and hydrophobic molecules (Osman et al., 2006). Cystine (2029.67±106.54 µM) was found to have the lowest IC_{50} value among sulfur compounds (Table 3). For all the tested sulfur compounds, an increase in concentration resulted in elevation of the DPPH radical scavenging potential. Trolox had the strongest antiradical activity with IC_{50} of 27.28±0.76 µM compared to the sulfur

compounds. The antiradical power of the sulfur compounds are ordered as: Met>cystine>taurine>SMC>SPC>SBC (Table 3). Ripoll et al. found that taurine mildly scavenged DPPH radicals whereas it did not exhibit ABTS scavenging effect (Ripoll et al., 2012). More so, the findings of Kim et al., revealed that Met and taurine have no ABTS and DPPH radical scavenging activities (Kim et al., 2020). Similarly, Heng et al., (2020) revealed that Met did not exhibit DPPH radical scavenging activity at room temperature, but had a valuable antioxidant activity based on the oxidative stability index test at a higher temperature. The outcomes of the current study are not in line with the findings of the aforementioned researchers. In addition, the present findings show that sulfur compounds do not completely bleach ABTS radical cations. This may be due to the lack of hydrogen atoms that can be transferred to the ABTS radical cation in the side chains of these compounds. A recent study revealed that organic oligosulfides had not shown DPPH scavenging activity. Like in our study, this was associated with the fact that the organic oligosulfides are not strongly involved in hydrogen atom transfer to the DPPH radical (Osipova et al., 2021).

Table 3. ABTS and DPPH radical scavenging activities of the sulfur compounds.

Compounds / Standard	ABTS Radical Scavenging Activity		DPPH Radical Scavenging Activity	
	Concentration (µM)	IC_{50} (µM)*	Concentration (µM)	IC_{50} (µM)*
Cystine	250 350 500	2029.67±106.54	100 200 300	495.51±31.85
Met	1500 2000 3000	5325.61±229.40	100 200 300	318.43±17.31
SBC	1500 2000 3000	8099.15±726.43	500 1000 2000	5516.57±263.37
SMC	1500 2000 3000	6337.68±75.21	500 1000 2000	2959.77±25.47
SPC	1500 2000 3000	5199.90±25.67	500 1000 2000	3512.74±200.51
Taurine	1500 2000 3000	10350.25±569.48	100 200 300	756.11±1.75
Trolox	250 300 500	515.41±2.02	10 25 50	27.28±0.76

*Mean ± SD of triplicate values.

Met: Methionine; SBC: S-benzyl cysteine; SMC: S-methyl cysteine; SPC: S-phenyl cysteine.

DMPD radical scavenging activity method can be used for both hydrophilic and lipophilic molecules. When the $DMPD^{\bullet+}$ cation radical abstracts hydrogen atoms from surrounding molecules, it turns into a purple-colored product that is proportional to the antioxidant capacity of the test molecule (Gulcin et al., 2020). Metal chelators may act as important secondary antioxidants, due to their ability to lessen the redox potentials and stabilizations of the oxidized form of the transition metals such as Fe(II) (Končić et al., 2011). The results in Table 4 shows IC_{50} values of DMPD radical scavenging and metal chelating activities of the sulfur compounds and standard antioxidants and chelator (EDTA). According to DMPD radical scavenging activities, IC_{50} values of 8.12-9.82 µM were recorded for the sulfur compounds, while IC_{50} values of 0.73±0.01 µM and 0.88±0.01 µM were found for ascorbic acid and Trolox, respectively. The lowest IC_{50} value was exhibited by SPC (8.12±0.02 µM) (Table 4). The lower IC_{50} values of standard antioxidants for DMPD radical scavenging activity compared to the sulfur compounds are in line with the outcomes of both ABTS and DPPH radical scavenging activities. In DMPD experimental system, the dependence on the DMPD radical scavenging activity on the sulfur atoms in the structure of the compounds could not be fully established. Therefore, the standard antioxidants had better scavenging effects in comparison to the sulfur compounds, with ascorbic acid having a better antiradical effect than Trolox. Similar findings were reported by Schlesier et al., (2002). It was observed that ascorbic acid scavenged DMPD radical in a much shorter time than Trolox. Like ABTS, DMPD radical has a positively charged chromophore molecule that reacts with antioxidant in reaction media (Ahmed et al., 2020) in a process that can be explained by the different kinetic

properties of both compounds (Fogliano et al., 1999). As for metal chelating activities, it was found that SPC (IC_{50} value of 42.83±0.41 µM) had the highest metal chelating activity. IC_{50} values of standard compound and other sulfur compounds are as follows: 60.00±6.47 µM for EDTA, 74.87±8.15 µM for SBC, 105.03±4.02 µM for cystine, 153.11±0.59 µM for Met, 154.18±2.00 µM for SMC, and 181.54±7.37 µM for taurine (Table 4). The high metal chelating activities of SPC and SBC is likely related to the presence of the aromatic group in their structure (Carrasco-Castilla et al., 2012). Owing to the resonance structures of aromatic amino acids, they are suggested to act as effective radical scavengers, and can easily neutralize free radicals by donating protons (Rajapakse et al., 2005). Kim et al., (2020) reported that sulfur amino acids (such as Met, cysteine and taurine) failed to chelate Fe^{2+} ions but could chelate both Cu^{2+} and Zn^{2+}. This may vary depending on the different number of metal binding sites of the chelator (for example, hexadentate as in EDTA) and the affinity of the chelator to the metal. In addition, dietary supplements containing cysteine and Met have been shown to reduce oxidative stress in animals by acting as metal chelators (Patra et al., 2001; Nandi et al., 2005; Martínez et al., 2017).

Table 4. DMPD radical scavenging and metal chelating activities of the sulfur compounds.

Compounds / Standards	DMPD Radical Scavenging Activity		Metal Chelating Activity	
	Concentration (µM)	IC_{50} (µM)*	Concentration (µM)	IC_{50} (µM)*
Cystine	10 100 200	9.82±0.01	25 50 100	105.73±4.02
Met	10 100 1000	8.75±0.03	50 100 150	153.11±0.59
SBC	10 100 1000	9.66±0.04	25 50 100	74.87±8.15
SMC	10 100 1000	9.56±0.13	50 100 150	154.18±2.00
SPC	10 100 1000	8.12±0.02	25 50 100	42.83±0.41
Taurine	10 100 1000	9.32±0.05	50 100 150	181.54±7.37
Ascorbic Acid	1 100 500	0.73±0.01	-	-
Trolox	1 100 500	0.88±0.01	-	-
EDTA	-	-	50 100 150	60.00±6.47

*Mean ± SD of triplicate values.

EDTA: Ethylenediaminetetraacetic acid; Met: Methionine; SBC: S-benzyl cysteine; SMC: S-methyl cysteine; SPC: S-phenyl cysteine.

Nitrite (or nitrate), found in residual pesticides, protein-rich foods, and cosmetics/medicines, can react with secondary amine groups to form S-nitroso compounds such as nitrosamines. Nitrosamines are then converted to alkane-linked DNA, proteins and nitrogenous intracellular components that may increase the risk of cancer (Zhan et al., 2016). Also, they are important molecules that can precipitate methemoglobinemia (Choi et al., 2008). Therefore, the nitrite scavenging activity method is widely used to investigate the antioxidant potential of both natural and synthetic compounds. The ORAC method is an accepted standard method used in nutraceutical, pharmaceutical and food industry to assess the antioxidant capacity (Gorinstein et al., 2009). Moreover, it is widely employed in other sectors assessing antioxidant power and oxidative stress. IC_{50} values of the nitrite scavenging activities and ORAC values of the sulfur compounds and standard antioxidant are depicted in Table 5. Nitrite scavenging activity (IC_{50} value of 2185.27±76.50 µM) of quercetin was found to be lower than that of the sulfur

compounds. Alongside this, the IC_{50} value of cystine (812.78±41.74 μM) was lower than that of other sulfur compounds. The nitrite scavenging activity of the sulfur compounds are ordered as follows: cystine>SMC>Met> SPC>taurine>SBC>quercetin (Table 5). The present findings indicate that sulfur compounds are potentially powerful nitrite scavengers. In contrast, a report by Vriesman et al., (1997) demonstrated that some sulfur compounds having disulfide group (-S-S-) and S-methyl group (e.g., oxidized glutathione and S-methyl glutathione) do not exhibit nitrite scavenging activity at physiological pH. Thus, the *in vitro* nitrite scavenging activity exhibited by all sulfur compounds in the present study may be linked to the acidic reaction medium used. More so, the dependence of capability of nitrite scavenging on the sulfur atoms in the structure of the compounds may be due to different reaction kinetics. As of the ORAC values, in the present study showed that Trolox with an IC_{50} value of 32.77±0.47 μM was a more effective scavenger of peroxyl radicals when compared to sulfur compounds. Met (IC_{50} value of 220.19±13.53 μM) had the best antioxidant activity as compared to other compounds (Table 5). The ORAC values of all tested compunds are ordered as follows: Trolox>Met> taurine>SMC>SPC>cystine>SBC. It has been revealed that biologically active sulfur compounds (cystine, taurine, and Met, etc.) had close ORAC values by using both spectrophotometric and voltammetric methods and Met had the lowest whereas cystine had the highest ORAC values (Dorozhko and Korotkova, 2011). These findings were not in harmony with our results. In an inhibitory diagrams study of the ORAC values of 10 amino acids and some other natural components it was suggested that cystine had higher ORAC values than Met (Nakajima et al., 2016). In another study involving a combination of tripeptides and 20 amino acids, Met was shown to have the highest ORAC value after tryptophan and tyrosine (Ohashi et al., 2015).

Table 5. Nitrite scavenging scavenging activities and ORAC values of the sulfur compounds.

Compounds / Standards	Nitrite Scavenging Activity		Oxygen Radical Absorbance Capacity	
	Concentration (μM)	IC_{50} (μM)*	Concentration (μM)	IC_{50} (μM)*
Cystine	100 300 500	812.78±41.74	250 500 1000	680.14±5.42
Met	1000 1500 2000	896.27±33.30	250 500 1000	222.19±13.53
SBC	1000 1500 2000	2161.96±28.65	250 500 1000	807.93±23.92
SMC	1000 1500 2000	846.34±61.45	250 500 1000	470.46±11.73
SPC	1000 1500 2000	1094.62±19.80	250 500 1000	637.31±12.00
Taurine	1000 1500 2000	1486.81±11.05	250 500 1000	430.23±9.77
Quercetin	1000 1500 2000	2185.27±76.50	-	-
Trolox	-	-	25 37.50 50	32.77±0.47

*Mean ± SD of triplicate values.

Met: Methionine; SBC: S-benzyl cysteine; SMC: S-methyl cysteine; SPC: S-phenyl cysteine.

Conclusions

In the current study, *in vitro* ACE inhibitory and antioxidant activities of the several sulfur compounds were determined. The outcomes show that the ACE inhibitory and antioxidant activities of all the sulfur compounds increased with an increase in concentration. Among the sulfur compounds, Met was found to have the highest ACE inhibitory activity, as well as the highest reducing power, DPPH radical scavenging, and the ORAC effect. Cystine had the highest ABTS radical

scavenging, FRAP, and nitrite scavenging activity. While SPC was the sulfur compound with the lowest ACE inhibitory activity, SBC had the lowest antioxidant activity. Our findings indicate that sulfur compounds have moderate *in vitro* ACE inhibitory activity and antioxidant effect. On the basis of present outcomes, consumption of sulfur compounds might be beneficial for not only the regulation of inflammatory processes (e.g., cardiac hypertrophy, pulmonary hypertension, lung injury, and sepsis) but also for the prevention of some diseases caused by oxidative stress resulting from the detrimental effects of ROS. We suggest further research (*in vivo*) should be conducted so as to understand and unravel the biological activities of these compounds.

Acknowledgement

This work was supported by Istanbul University-Cerrahpaşa Scientific Research Projects Unit with Project Number: FYL-2018-31299.

Author Contributions

Conception/Design of Study-B.B.B. and R.Y.; Data Acquisition-S.Y., B.B.B.; Data Analysis/Interpretation-S.Y., B.B.B. and R.Y.; Drafting Manuscript-S.Y., B.B.B. and R.Y.; Critical Revision of Manuscript-B.B.B. and R.Y.; Final Approval and Accountability-B.B.B. and R.Y.; Technical or Material Support-S.Y., B.B.B. and R.Y.; Supervision-R.Y.

Data Availability

All data generated or analyzed during this study are included in this published article.

Declarations

Ethics Approval

This article does not contain any studies with human participants or animal subjects performed by any of the authors.

Informed Consent

All authors declare that the current paper has not been under review by other journals, besides approving its submission on Applied Biochemistry and Biotechnology.

Conflict of Interest

The authors have no conflict of interest to declare.

References

1. Ahmed ZB, Mohamed Y, Johan V, Dejaegher B et al. Defining a standardized methodology for the determination of the antioxidant capacity: case study of *Pistacia atlantica* leaves. *Analyst,* 2020; 145: 557-571. doi: 10.1039/C9AN01643K
2. Amin MM, Sawhney SS, Jassal MS. Comparative antioxidant power determination of *Taraxacum officinale* by FRAP and DTPH method. *Pharm Anal Acta*, 2013; 4: 221. doi: 10.4172/2153-2435.1000221
3. Arnao MB, Cano A, Acosta M. The hydrophilic and lipophilic contribution to total antioxidant activity. *Food Chem.* 2001; 73(2): 239-244. doi: 10.1016/S0308-8146(00)00324-1
4. Atmaca G. Antioxidant effects of sulfur-containing amino acids. *Yonsei Medical Journal,* 2004; 45(5): 776-788. doi: 10.3349/ymj.2004.45.5.776
5. Battin EE, Brumaghim JL. Metal specificity in DNA damage prevention by sulfur antioxidants. *J Inorg Biochem.* 2008; 102(12): 2036-2042. doi: 10.1016/j.jinorgbio.2008.06.010
6. Bayrak BB, Yanardag R. Antioxidant activities of *Eremurus spectabilis* M. Bieb. extracts and sulfur compounds. *Eur J Biol.* 2021; 80(2): 154-163. doi: 10.26650/EurJBiol.2021.1028656
7. Benzie IFF, Strain JJ. The ferric reducing ability of plasma (FRAP) as a measure of antioxidant power: the FRAP assay. *Anal Biochem.* 1996; 239(1): 70-76. doi: 10.1006/abio.1996.0292
8. Bin P, Huang R, Zhou X. Oxidation resistance of the sulfur amino acids: methionine and cysteine. *BioMed Res Int.* 2017; 2017: 9584932. doi: 10.1155/2017/9584932
9. Brand-Williams W, Cuvelier ME, Berset C. Use of a free radical method to evaluate antioxidant activity. *LWT-Food Sci Technol.* 1995; 28(1): 25-30. doi: 10.1016/S0023-6438(95)80008-5
10. Carrasco-Castilla J, Hernández-Álvarez AJ, Jiménez-Martínez C, Jacinto-Hernández C et al. Antioxidant and metal chelating activities of *Phaseolus vulgaris* L. var. Jamapa protein isolates, phaseolin and lectin hydrolysates. *Food Chem.* 2012; 131(4): 1157-1164. doi: 10.1016/j.foodchem.2011.09.084
11. Chen CM, Yin MC, Hsu CC, Liu TC. Antioxidative and anti-inflammatory effects of four cysteine-containing agents in striatum of MPTP-treated mice. *Nutrition,* 2007; 23(7-8): 589-597. doi: 10.1016/j.nut.2007.05.004
12. Choi DB, Cho KA, Na MS, Choi HS et al. Effect of bamboo oil on antioxidative activity and nitrite scavenging activity. *J Ind Eng Chem.* 2008; 14(6): 765-770. doi: 10.1016/j.jiec.2008.06.005
13. Čolović MB, Vasić VM, Djurić DM, Krstić DZ. Sulphur-containing amino acids: protective role against free radicals and heavy metals. *Curr Med Chem.* 2018; 25: 324-335. doi: 10.2174/0929867324666170609075434
14. Corzo-Martínez M, Corzo N, Villamiel M. Biological properties of onions and garlic. *Trends Food Sci Technol.* 2007; 18: 609-625. doi: 10.1016/j.tifs.2007.07.011
15. Coto E, Avanzas P, Gómez J. The renin-angiotensin-aldosterone system and coronavirus disease 2019. *Eur Cardiol Rev.* 2021; 16: e07. doi: 10.15420/ecr.2020.30
16. Dagsuyu E, Yanardag R. *In vitro* urease and trypsin inhibitory activities of some sulfur compounds. *Istanbul J Pharm.* 2021; 51(1): 85-91. doi: 10.26650/IstanbulJPharm.2021.844783
17. de Oliveira Filho JG, Rodrigues JM, Valadares ACF, de Almeida AB et al. Bioactive properties of protein hydrolysate of cottonseed byproduct: antioxidant, antimicrobial, and angiotensin-converting enzyme

(ACE) inhibitory activities. *Waste Biomass Valorization,* 2021; 12*:* 1395-1404. doi: 10.1007/s12649-020-01066-6

18. Decker EA, Welch B. Role of ferritin as a lipid oxidation catalyst in muscle food. *J Agric Food Chem.* 1990; 38(3): 674-677. doi: 10.1021/jf00093a019
19. Dorozhko EV, Korotkova EI. Biologically active substances studied by voltammetric and spectrophotometric techniques. *Pharm Chem J.* 2011; 44(10): 582-584. doi: 10.1007/s11094-011-0521-2
20. Simões e Silva AC, Teixeira MM. ACE inhibition, ACE2 and angiotensin-(1-7) axis in kidney and cardiac inflammation and fibrosis. *Pharmacol Res.* 2016; 107: 154-162. doi: 10.1016/j.phrs.2016.03.018
21. Elmahallawy EK, Elshopakey GE, Saleh AA, Agil A et al. S-Methylcysteine (SMC) ameliorates intestinal, hepatic, and splenic damage induced by *Cryptosporidium parvum* infection via targeting inflammatory modulators and oxidative stress in Swiss albino mice. *Biomedicines,* 2020; 8(10): 423. doi: 10.3390/biomedicines8100423
22. Fagyas M, Úri K, Siket IM, Daragó A et al. New perspectives in the renin-angiotensin-aldosterone system (RAAS) I: endogenous angiotensin converting enzyme (ACE) inhibition. *PLoS One,* 2014; 9(4): e87843. doi: 10.1371/journal.pone.0087843
23. Fogliano V, Verde V, Randazzo G, Ritieni A. Method for measuring antioxidant activity and its application to monitoring the antioxidant capacity of wines. *J Agric Food Chem.* 1999; 47(3): 1035-1040. doi: 10.1021/jf980496s
24. Forman HJ, Zhang J. Targeting oxidative stress in disease: promise and limitations of antioxidant therapy. *Nat Rev Drug Discov.* 2021; 20: 689-709. doi: 10.1038/s41573-021-00233-1
25. Gaddam RR, Chambers S, Bhatia M. ACE and ACE2 in inflammation: a tale of two enzymes. *Inflamm Allergy Drug Targets,* 2014; 13(4): 224-234. doi: 10.2174/1871528113666140713164506
26. Giani JF, Veiras LC, Shen JZY, Bernstein EA et al. Novel roles of the renal angiotensin-converting enzyme. *Mol Cell Endocrinol.* 2021; 529: 111257. doi: 10.1016/j.mce.2021.111257
27. Gorinstein S, Jastrzebski Z, Leontowicz H, Leontowicz M et al. Comparative control of the bioactivity of some frequently consumed vegetables subjected to different processing conditions. *Food Control,* 2009; 20(4): 407-413. doi: 10.1016/j.foodcont.2008.07.008
28. Guidea A, Zăgrean-Tuza C, Moț AC, Sârbu C. Comprehensive evaluation of radical scavenging, reducing power and chelating capacity of free proteinogenic amino acids using spectroscopic assays and multivariate exploratory techniques. *Spectrochim Acta A Mol Biomol Spectrosc.* 2020; 233: 118158. doi: 10.1016/j.saa.2020.118158
29. Gulcin I. Antioxidants and antioxidant methods: an updated overview. *Arch Toxicol.* 2020; 94(3): 651-715. doi: 10.1007/s00204-020-02689-3
30. Hanway R, Cavicchioli A, Kaur B, Parsons J et al. Analysis of S-phenyl-L-cysteine in globin as a marker of benzene exposure. *Biomarkers,* 2000; 5(4): 252-262. doi: 10.1080/135475000413809
31. Heng HFE, Ong XL, Chow PYE. Antioxidant action and effectiveness of sulfur-containing amino acid during deep frying. *J Food Sci Technol.* 2020; 57(3): 1150-1157. doi: 10.1007/s13197-019-04150-5
32. Hsu CC, Huang CN, Hung YC, Yin MC. Five cysteine-containing compounds have antioxidative activity in Balb/cA mice. *J Nutr.* 2004; *134,* 149-152. doi: 10.1093/jn/134.1.149
33. Huang D, Ou B, Hampsch-Woodill M, Flanagan JA et al. High-throughput assay of oxygen radical absorbance capacity (ORAC) using a multichannel liquid handling system coupled with a microplate fluorescence reader in 96-well format. *J Agric Food Chem.* 2002; 50(16): 4437-4444. doi: 10.1021/jf0201529
34. Juan CA, Pérez de la Lastra JM, Plou FJ, Pérez-Lebeña E. The chemistry of reactive oxygen species (ROS) Revisited: outlining their role in biological macromolecules (DNA, lipids and proteins) and induced pathologies. *Int J Mol Sci.* 2021; 22(9): 4642. doi: 10.3390/ijms22094642
35. Kim JH, Jang HJ, Cho WY, Yeon SJ et al. *In vitro* antioxidant actions of sulfur-containing amino acids. *Arab J Chem.* 2020; 13(1): 1678-1684. doi: 10.1016/j.arabjc.2017.12.036
36. Komori T, Asano K, Sasaki Y, Hanai H et al. Sulfur-containing acylamino acids. I. Syntheses and angiotensin I converting enzyme-inhibitory activities of sulfur-containing n-mercaptoalkanoyl amino acids. *Chem Pharm Bull.* 1987; 35(6): 2382-2387. doi: 10.1248/cpb.35.2382
37. Končić MZ, Barbarić M, Perković I, Zorc B. Antiradical, chelating and antioxidant activities of hydroxamic acids and hydroxyureas. *Molecules,* 2011; 16(8): 6232-6242. doi: 10.3390/molecules16086232
38. Kumar M, Pratap V, Nigam AK, Sinha BK et al. Plants as a source of potential antioxidants and their effective nanoformulations. *J Sci Res.* 2021; 65(3): 58-72. doi: 10.37398/JSR.2021.650308
39. Liu J, Lin S, Wang Z, Wang C et al. Supercritical fluid extraction of flavonoids from *Maydis stigma* and its nitrite-scavenging ability. *Food Bioprod Process.* 2011; 89(4): 333-339. doi: 10.1016/j.fbp.2010.08.004
40. Lü JM, Lin PH, Yao Q, Chen C. Chemical and molecular mechanisms of antioxidants: experimental approaches and model systems. *J Cell Mol Med.* 2010; 14(4): 840-860. doi: 10.1111/j.1582-4934200900897.x
41. Magalhães LM, Segundo MA, Reis S, Lima JLFC. Methodological aspects about in vitro evaluation of antioxidant properties. *Anal Chim Acta,* 2008; 613: 1-19. doi: 10.1016/j.aca.2008.02.047
42. Martínez Y, Li X, Liu G, Bin P et al. The role of methionine on metabolism, oxidative stress, and diseases. *Amino Acids,* 2017; 49(12): 2091-2098. doi: 10.1007/s00726-017-2494-2

43. Mascolo A, Scavone C, Rafaniello C, De Angelis A et al. The role of renin-angiotensin-aldosterone system in the heart and lung: focus on COVID-19. *Front Pharmacol.* 2021; 12: 667254. doi: 10.3389/fphar.2021.667254
44. Masuyer G, Schwager SL, Sturrock ED, Isaac RE et al. Molecular recognition and regulation of human angiotensin-I converting enzyme (ACE) activity by natural inhibitory peptides. *Sci Rep.* 2012; 2: 717. doi: 10.1038/srep00717
45. Moskovitz J. Methionine sulfoxide reductase: ubiquitous enzymes involved in antioxidant defense, protein regulation, and prevention of aging-associated diseases. *Biochim Biophys Acta Proteins Proteom.* 2005; 1703(2): 213-219. doi: 10.1016/j.bbapap.2004.09.003
46. Munteanu IG, Apetrei C. Analytical methods used in determining antioxidant activity: a review. *Int J Mol Sci.* 2021; 22(7): 3380. doi: 10.3390/ijms22073380
47. Nakabayashi R, Yang Z, Nishizawa T, Mori T et al. Top-down targeted metabolomics reveals a sulfur-containing metabolite with inhibitory activity against angiotensin-converting enzyme in Asparagus officinalis. *J Nat Prod.* 2015; 78(5): 1179-1183. doi: 10.1021/acs.jnatprod.5b00092
48. Nakajima A, Sakurai Y, Tajima K. Reactive oxygen species inhibitory diagrams and their usability for the evaluation of antioxidant ability. *Oxid Antioxid Med Sci.* 2016; 5(1): 1-7. doi: 10.5455/oams220216.rv.022
49. Nandi D, Patra RC, Swarup D. Effect of cysteine, methionine, ascorbic acid and thiamine on arsenic-induced oxidative stress and biochemical alterations in rats. *Toxicology,* 2005; 211(1-2): 26-35. doi: 10.1016/j.tox.2005.02.013
50. Ohashi Y, Onuma R, Naganuma T, Ogawa T et al. Antioxidant properties of tripeptides revealed by a comparison of six different assays. *Food Sci Technol Res.* 2015; 21(5): 695-704. doi: 10.3136/fstr.21.695
51. Okajima K, Inoue M, Morino Y, Itoh K. Topological aspects of microsomal N-acetyltransferase, an enzyme responsible for the acetylation of cysteine S-conjugates of xenobiotics. *Eur J Biochem.* 1984; 142(2): 281-286. doi: 10.1111/j.1432-10331984.tb08282.x
52. Osipova V, Polovinkina M, Gracheva Y, Shpakovsky D et al. Antioxidant activity of some organosulfur compounds *in vitro. Arab J Chem.* 2021; 14(4): 103068. doi: 10.1016/j.arabjc.2021.103068
53. Osman AM, Wong KKY, Hill SJ, Fernyhough A. Isolation and the characterization of the degradation products of the mediator ABTS-derived radicals formed upon reaction with polyphenols. *Biochem Biophys Res Commun.* 2006; 340(2): 597-603. doi: 10.1016/j.bbrc.2005.12.051
54. Oyaizu M. Studies on products of browning reaction: antioxidative activities of browning reaction prepared from glucose amine. *Jpn J Nutr Diet.* 1986; 44(6): 307-315. doi: 10.5264/eiyogakuzashi.44.307
55. Pagliaro P, Thairi C, Alloatti G, Penna C. Angiotensin-converting enzyme 2: a key enzyme in key organs. *J Cardiovasc Med.* 2022; 23(1): 1-11. doi: 10.2459/JCM.0000000000001218
56. Patra RC, Swarup D, Dwivedi SK. Antioxidant effects of α tocopherol, ascorbic acid and L-methionine on lead induced oxidative stress to the liver, kidney and brain in rats. *Toxicology,* 2001; 162(2): 81-88. doi: 10.1016/S0300-483X(01)00345-6
57. Pizzino G, Irrera N, Cucinotta M, Pallio G et al. Oxidative stress: harms and benefits for human health. *Oxid Med Cell Longev.* 2017; 2017: 8416763. doi: 10.1155/2017/8416763
58. Rajapakse N, Mendis E, Jung WK, Je JY et al. Purification of a radical scavenging peptide from fermented mussel sauce and its antioxidant properties. *Food Res Int.* 2005; 38(2): 175-182. doi: 10.1016/j.foodres.2004.10.002
59. Ramana KV, Reddy ABM, Majeti NVRK, Singhal SS. Therapeutic potential of natural antioxidants. *Oxid Med Cell Longev.* 2018; 2018: 9471051. doi: 10.1155/2018/9471051
60. Ripoll C, Coussaert A, Waldenberger FR, Vischer C et al. Evaluation of natural substances' protective effects against oxidative stress in a newly developed canine endothelial cell-based assay and in cell-free radical scavenging assays. *Int J Appl Res Vet Med.* 2012; 10(2): 113-124.
61. Sánchez C. Reactive oxygen species and antioxidant properties from mushrooms. *Synth Syst Biotechnol.* 2017; 2: 13-22. doi: 10.1016/j.synbio.2016.12.001
62. Schlesier K, Harwat M, Böhm V, Bitsch R. Assessment of antioxidant activity by using different in vitro methods. *Free Radic Res.* 2002; 36, 177-187. doi: 10.1080/10715760290006411. doi: 10.1080/10715760290006411
63. Senthilkumar GP, Thomas S, Sivaraman K, Sankar P et al. Study the effect of s-methyl L-cysteine on lipid metabolism in an experimental model of diet induced obesity. *J Clin Diagn Res.* 2013; 7(11): 2449-2451. doi: 10.7860/JCDR/2013/7304.3571
64. Shalaby SM, Zakora M, Otte J. Performance of two commonly used angiotensin-converting enzyme inhibition assays using FA-PGG and HHL as substrates. *J Dairy Res.* 2006; 73: 178-186. doi: 10.1017/S0022029905001639
65. Shen Q, Ou A, Liu S, Elango J et al. Effects of ion concentrations on the hydroxyl radical scavenging rate and reducing power of fish collagen peptides. *J Food Biochem.* 2019; 43(4): e12789. doi: 10.1111/jfbc.12789
66. Shukla AK, Banerjee M. Angiotensin-converting-enzyme 2 and renin-angiotensin system inhibitors in COVID-19: An update. *High Blood Press Cardiovasc Prev.* 2021; 28: 129-139. doi: 10.1007/s40292-021-00439-9
67. Suleman M, Khan A, Baqi A, Kakar MS et al. Antioxidants, its role in preventing free radicals and infectious diseases in human body. *Pure Appl Biol.*

2019; 8(1): 380-388. doi: 10.19045/bspab.2018.700197

68. Tipnis SR, Hooper NM, Hyde R, Karran E et al. A human homolog of angiotensin-converting enzyme: cloning and functional expression as a captopril-insensitive carboxypeptidase. *J Biol Chem.* 2000; 275(43): 33238-33243. doi: 10.1074/jbc.M002615200
69. Udenigwe CC, Aluko RE. Chemometric analysis of the amino acid requirements of antioxidant food protein hydrolysates. *Int J Mol Sci.* 2011; 12(5): 3148-3161. doi: 10.3390/ijms12053148
70. Vriesman MF, Haenen GRMM, Westerveld GJ, Paquay JBG et al. A method for measuring nitric oxide radical scavenging activity. Scavenging properties of sulfur–containing compounds. *Pharm World Sci.* 1997; 19(6): 283-286. doi: 10.1023/A:1008601327920
71. Wei M, Wanibuchi H, Yamamoto S, Iwai S et al. Chemopreventive effects of S-methylcysteine on rat hepatocarcinogenesis induced by concurrent administration of sodium nitrite and morpholine. *Cancer Lett.* 2000; 161(1): 97-103. doi: 10.1016/S0304-3835(00)00606-6
72. Zhan G, Pan L, Tu K, Jiao S. Antitumor, antioxidant, and nitrite scavenging effects of Chinese water chestnut (*Eleocharis dulcis*) peel flavonoids. *J Food Sci.* 2016; 81: H2578-H2586. doi: 10.1111/1750-3841.13434

ISSN print: 1224-5984
ISSN online: 2248-3942

Rom Biotechnol Lett. 2022; 27(1): 3264-3269
doi: 10.25083/rbl/27.1/3264-3269

Received for publication, December, 11, 2021
Accepted, January, 15, 2022

Original paper

Diversity, pathogenicity and biocontrol efficacy of Pseudomonas syringae isolated from plants in northern Jordan

FOUAD A. ALMOMANI[1], IHAB MANASREH[2], YOUSEF M. ABU-ZAITOON[3], ABDEL RAHMAN AL TAWAHA[3]

[1] Department of Applied Biology, Jordan University of Science and Technology, Irbid-22110, Jordan
[2] Department of Applied Biology, Jordan University of Science and Technology, Irbid-22110, Jordan
[3] Department of Biology, Faculty of science, Al-Hussein Bin Talal University, Maan-Jordan.

Abstract Diversity, pathogenicity, and biocontrol efficacy of *Pseudomonas syringae* strains isolated from a wide range of habitats in Jordan were investigated. Thirty-five infected plant samples (vegetable leaves and woody plant twig) were randomly collected. King's B agar medium was implemented and 124 colonies of *P. syringae* candidates were selected. Phenotypic, biochemical and pathogenicity tests were further carried out to confirm the identity of *P. syringae* isolates. The frequency of fluorescent isolates varied between 11- 50 %. Even though all isolates were shown to induce chlorosis of tobacco leaves, only two were able to macerate potato slices causing their rotting. This may be due to variation in secretion of cellulase and pectinase enzymes involve in pathogenicity as clearly discussed in this study. Interestingly, 55% of isolates were found to clearly inhibit growth of *E. coli*. Exceptional inhibition was noticed in *P. syringae* isolated from tomato and a possible effect of syringomycin was suggested. Therefore, *P. syringae* obtained in this study was recommended to have a pivotal role in the biological control system. Results obtained from the experiment of ice nucleation activity revealed that this phenotypic feature dominates woody plants.

Keywords *Pseudomonas syringae,* cellulase, pectinase, ice nucleation activity, biocontrol efficacy, and King's B medium.

To cite this article: ALMOMANI FA, MANASREH I, ABU-ZAITOON YM, AL TAWAHA AR. Diversity, pathogenicity and biocontrol efficacy of *Pseudomonas syringae* isolated from plants in northern Jordan. *Rom Biotechnol Lett*. 2022; 27(1): 3264-3269. DOI: 10.25083/rbl/27.1/3264-3269.

✉ *Corresponding author: YOUSEF M. ABU-ZAITOON, Department of Biology, Faculty of science, Al-Hussein Bin Talal University, Maan (postal address 20), Jordan.
E-mail: yousefaz@yahoo.com

Introduction

Since *Pseudomonas syringae* is first described as a plant pathogen in 1902, outbreaks of infections around the world have been documented and greater economic loss in a wide variety of crops has been reported (Cunty *et al.,* 2015, Berge *et al.,* 2014). Pathogenicity of some *P. syringae* pathovars is associated with the secretion of extracellular enzymes namely cellulase, pectinase and gelatinase cause tissue maceration or soft rot disease (Skerman *et al*., 1980; Andro *et al.,* 1984). *P. syringae* has two interconnected growth phases; epiphytic and endophytic phase. One of the most important features of epiphytic phase is the ice nucleation activity that known to produce ice from water supercooled at a temperature above normal freezing condition (Lindow *et al.,* 1982, Bultreys and Kaluzna, 2010). This activity creates openings in the hos plant releasing water and nutrients and leads to the frost injury which subsequently facilitation of infection by other pathogens (Xiu-Fang *et al.,* 2018).

Isolation and identification of this deleterious bacteria are laborious due to the considerable phenotypic and genotypic diversity. Additionally, an outgrowing list of newly isolated strains further complicate the scene. Phenotypic tests including production of levan, cytochrome c oxidase, arginine dihydrolase, as well as tobacco pathogenicity, potato rotting, ice nucleation activity and cross pathogenicity tests are routinely used to identify *P. syringae* isolates (Young *et al.,* 1996, Berge *et al.,* 2014). *P. syringae, a* fluorescent Pseudomonas, fluoresces under ultraviolet radiation due to the production of extracellular yellow green pigment (Nobutaka *et al.*, 2020) when cultivated on King's B agar selective medium (King *et al*., 1954).

Several studies reported the isolation of fluorescent pseudomonads showing high biocontrol efficacy. Effective strains were reported to protect host plants from across the plant kingdom in a wide range of environments (Takeuchi *et al.,* 2015; Ma *et al.,* 2016; Nandi *et al.,* 2017; Nobutaka *et al.,* 2020). As such, investigating the diversity of florescent pseudomonads from various habitats and plant species is a priority. In this study isolation, identification and characterization of the fluorescent *Pseudomonas syringae* in a wide spectrum of geographical locations and agronomical crops in Jordan is presented. This includes regions located 200 m below sea level to regions located 1100 m above sea level. In addition to discrepancy in altitudes, examined regions differ largely in temperature, humidity, as well as soil physical and chemical properties. This piece of work is therefore expected to fill a gap in this field in Jordan. Candidate isolates that could exhibit biocontrol activities and protect host plants was presented.

Materials and Methods

Sample collection and bacterial isolation

Thirty-five samples were collected from a wide array of infected plants, showing symptoms of *Pseudomonas* infection, including: tomato, green pepper, squash, almond, and olive. Plant samples were collected from different locations of the north part of Jordan. Samples were initially surface sterilized and then macerated in sterilized distilled water. After that, serial dilutions in distilled water were prepared and 0.1 ml from the appropriate dilution was spread on King's B agar selective medium (King *et al*., 1954). All plates were incubated at 27 °C for 72 h and randomly selected colonies were picked for further analysis.

Identification and characterization

Colony morphology of bacterial isolates was initially used to identify *Pseudomonas* isolates. White, convex, mucous and glistening colonies on King's B medium were selected for further identification. Gram staining and basic biochemical testes routinely used to discriminate *P. syringae* including: cytochrome c oxidase, levan production, arginine hydrolysis were performed (Cindy *et al.,* 2007; Berge *et al.,* 2014).

Tobacco Pathogenicity & Potato rotting tests

Tobacco pathogenicity test was performed according to Klement method (1964). Briefly, tobacco young leaves (20-day old) were wounded with sterilized needles, and inoculated with a loopful of 48 hour-old active *Pseudomonas* cultures obtained from the collected infected plant samples. Wounded leaf inoculated with a sterilized distilled water was used as a negative control. Pathogenicity was confirmed by observing symptoms of chlorosis which generally appear after 4 days of infection.

For potato rotting test, tubers were surface sterilized, peeled and sliced (1 mL thickness each). 100 µL of 48 hour-old active *Pseudomonas* cultures were spread on the surface of these slices in sterilized Petri plates. To keep slices moist, sterilized filters papers were plated in each plate before inoculation. As a negative control 10 mL of sterilized nutrient medium were added to the potato slices under the same conditions. Soft texture of the slice surface is a direct indicator of rotting which was appeared in average after seven days of infection.

Production of extracellular enzymes

Cellulase production was examined by inoculating a loopful of 48-hour old bacterial culture on 15% (w/v) agar medium containing the following components per 1L: yeast extract (1g), sodium carboxymethylcellulose (10g), KH_2PO_4 (4g), $FeSO_4.7H_2O$ (0.5g), as well as two g each of NaCl, $CaCl_2.2H_2O$ and NH_4Cl. The final pH was adjusted to 7.0. After 3days of incubation at 27°C, plates were flooded with 1% (w/v) aqueous congo red solution for 30 minutes at room temperature. Excess stain was poured off plates, destined with 1M NaCl, and kept at 4°C overnight. Colorless zones around inoculums indicate positive results (Mushtaq *et al*., 2019).

To test pectinase activity, 48-hour old active *Pseudomonas* was inoculated on a 15% pectin agar medium containing the following ingredients/1L: pectin (5g), KH_2PO_4 (4g), NH_4Cl (2g), $CaCl_2.2H_2O$ (2g), NaCl (2g), $MgSO_4.7H_2O$ (1g), $MnSO_4$ (0.05g), $FeSO_4.7H_2O$ (0.05 g),

as well and 0.1%. yeast extract. The final pH was adjusted to 7.0 and cultures were incubated at 27°C for 3 days. Plates were then flooded with 1% (w/v) acetyltrimethylammonium bromide and destined with 15% alcohol solution. Colorless zones around the inoculums, generally appear after 30 minutes, indicate positive results (Mushtaq *et al.,* 2019).

Ice nucleation activity and Induction of biotoxins against *E. coli*

To perform ice nucleation activity, freshly grown bacterial cultures were inoculated on a 15% agar medium containing per one L five g each of yeast extract, glucose, and peptone. Plates were incubated at -4.0°C. Crystal formation, usually appears after five minutes, is an indication of positive results (Berge *et al.,* 2014).

Induction of biotoxins against *E. coli* B strain was performed following Gasson method (1980). In this assay, sterilized cotton swabs were used to add 10^8 colony-forming cells of *E. coli* to Mueller Hinton agar medium. Cork borer was then used to create 5 mm diameter wells. Broth filtrate (50 µl) of freshly grown *Pseudomonas* cultures obtained from infected plants were placed in wells. Plates were then incubated at 27°C for 24h and clear zones around wells indicate positive biotoxin production against *E. coli*.

Results and discussion

This study was intended to characterize pathogenic *Pseudomonas* bacteria isolated from a wide taxonomic group of infected plants in different places of Jordan. Out of 35 samples obtained from infected tomato, green pepper, squash, almond, and olive, 124 colonies were isolated using King's B agar selective medium (King *et al*., 1954). The percentage of fluorescent inducing colonies was found to be 24% and varied from 11 % in olive and green pepper to 50 % in apple (Figure 1). Even in the same plant, percent of fluorescent colonies was varied from one place to the other.).

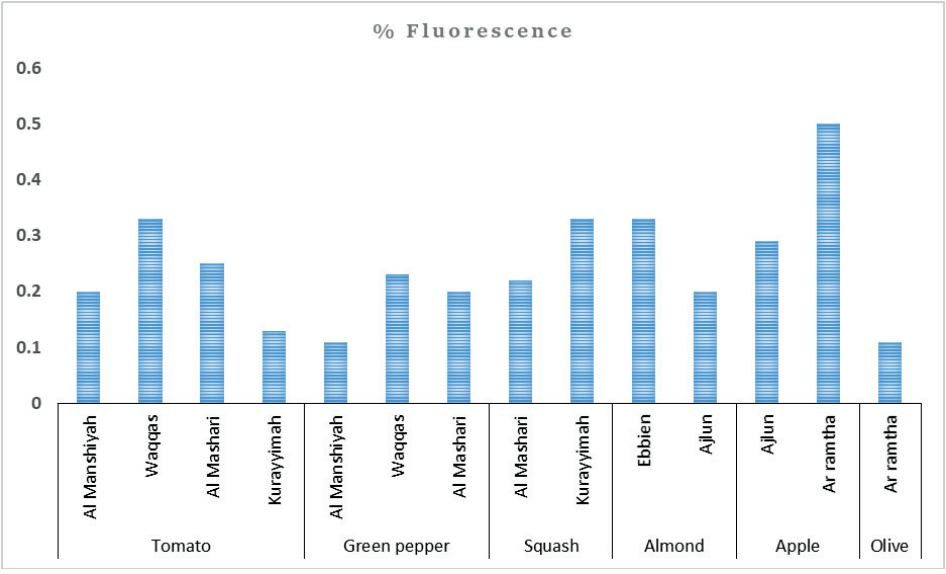

Figure 1. Percentage of fluorescent *Pseudomonas syringae* cultures (A) and the number of pathogenic isolate on tobacco leaves (B).

Pathogenicity tests by both induction of chlorosis of tobacco leaves and rotting of potato slices revealed that 18 out of 124 isolates (15%) were pathogenic. As shown in Figure 2, the highest percentage of pathogenic isolates was recovered from almond and the lowest one in green pepper.

Biological activity of pathogenic *Pseudomonas* isolates is indicated in Table 1. All isolates showed chlorosis or yellowish spots of the tested tobacco leaves whereas only two isolates (Gm1 and Ala2) were able to induce rotting on potato slices. Most bacterial isolates were able to hydrolyze cellulose, whereas only four *Pseudomonas* isolates (Tm, Gm1, Sal2, Ala2) isolated from tomato, green pepper, squash and almond respectively showed pectinase activity. The ability to hydrolyze gelatin is restricted to seven bacterial isolates including Tk, Gm2, Sal1, Sal2, Ale, Apa2, and Or collected from tomato, green pepper, squash, almond, apple and olive respectively. Toxicity or antibiotic activity for investigated isolates was tested against *E. coli* B strain (table 1).

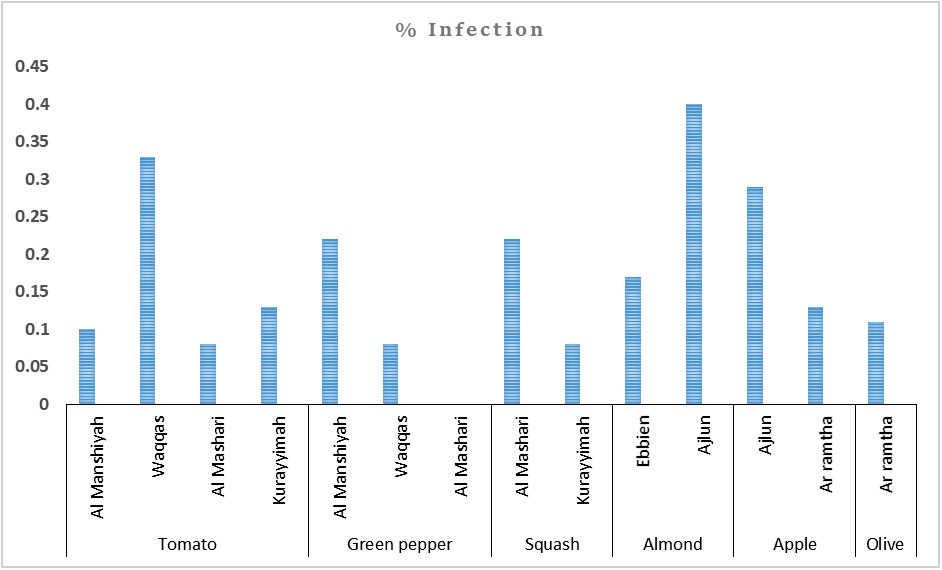

Figure 2. Number of pathogenic *Pseudomonas syringae* isolates on tobacco leaves.

Table 1. Biological activity of pathogenic isolates of fluorescent *Pseudomonas syringae.* INA= ice nucleation activity.[a] Symptoms of chlorosis as observed in the tobacco pathogenicity test. [b] Rotting as observed in the potato rotting test.

Plant material	Isolate number	Collection site	Hydrolytic Enzyme			*E.coli* inhibition	INA	Pathogenicity	
			Cellulase	Pectinase	Gelatinase			Chlrosis[a]	Rotting[b]
Tomato	Tm	Al Manshiyah	-	+	-	-	+	+	-
	Tw1	Waqqas	+	-	-	+	-	++	-
	Tw2		+	-	-	-	-	+	-
	Tk	Kurayyimah	+	-	+	+	-	++	-
	Tal	Al Mashari	++	-	-	+	+	+	-
Green Pepper	Gm1	Al Manshiyah	++	+	-	-	-	+	+
	Gm2		+	-	+	+	-	++	-
	Gw	Waqqas	+	-	-	+	-	+	-
Squash	Sal1	Al Mashari	-	-	+	+	-	++	-
	Sal2		-	+	+	+	-	+	-
	Sk	Kurayyimah	++	-	-	-	+	+	-
Almond	Ala1	Ajlun	+	-	-	-	-	+	-
	Ala2		+	+	-	-	-	++	+
	Ale	Ebbien	+	-	+	+	+	+	-
Apple	Apr	Ar ramtha	+	-	-	-	+	+	-
	Apa1	Ajlun	-	-	-	+	-	+	-
	Apa2		+	-	+	+	+	+	-
Olive	Or	Ar ramtha	+	-	+	-	+	+	-

Most of the phytopathogenic isolates were able to inhibit the growth of E. coli indicating their ability to induce biotoxin that could be used for biological control. For ice nucleation test, isolates numbers; Tm, Ta1, Sk, Ale, Apr, Apa2, and Or collected from tomato, squash, almond, apple and olive showed positive results.

Pseudomonas syringae is a common pathogen in diverse crops. The current study aimed to get a clear picture about the diversity, pathogenicity and biocontrol efficacy of P. syringae isolated from across a wide array of habitats in Jordan. This included regions located 200 m below sea level to 1100 m above sea level. The percentage of fluorescent Pseudomonas was found to be ranged from 11-50 % among the total Pseudomonas isolates collected from different habitats in Jordan. This frequency is in agreement with what was reported by Lindow et al. (1981), and Margaret & Hagedorn (1981).

Tobacco and potato show varying susceptibility to P. syringae isolates. All isolates were found to induce chlorosis of tobacco leaves. The high percentage of pathogenicity to tobacco is in agreement with Cindy et al. (2007). This could be due to host range specificity as reported by Gross et al. (1984) or cytotoxic production by the pathogenic isolates as reported by Fahy and Hayward (1983). Another possibility is that cellulase activity may be enough to induce pathogenicity to tobacco and other plants (He, 1996; Cindy et al., 2007). On the other hand, only two isolates were able to induce rotting to potato slices. This could be due to inability of isolates to secret pectinase enzyme as shown in table 1, a similar finding was obtained by Isabel et al. (1987). The scarcity of affecting potato may refer to the fact that P. syringae causes necrosis to aerial parts of plants rather than parts below the ground as the case with potato.

Among all tested bacterial isolates, 55% of them were found to inversely affect growth of E. coli (table 1). Three bacterial isolates out of five obtained from tomato were found to produce toxins and therefore inhibit growth of E. coli. Cindy et al., (2007) investigated the possibility of syringomycin production by 31 strains of P. syringae. They found that among seven host plants studied, syringomycin is almost exclusively produced by P. syringae infects tomato with a 13 mm zone of inhibition. Antimicrobial activity of the examined isolates could be due to the production of syringomycin and related biotoxins known to widely affect pathogenic bacteria. This activity makes P. syringae isolates as a possible strong candidate in the biological control system (Bender et al., 1999). On the other hand, yellowish symptoms or necrosis appears on tested plants could be due to the biotoxicity of these isolates as reported by Turner (1984) and Kang et al. (2015).

Data from the ice nucleation activity experiment revealed that unlike vegetables, ice nucleation substance is dominant in woody plants as four out of 7 isolates were found to have this phenotypic feature. Only 3 isolates out of 11 isolated from vegetables including tomato and squash were found to be ice nucleation active. Similar results were obtained for tomato by Cindy et al., (2007) who reported that a limited percent (22%) of tomato plants infected by P. syringae were found have this phenotype at an average temperature of -3 °C.

of the pathogenic isolates proved that 39% of them were with ice nucleation activity. Two of the pathogenic isolates from vegetables were with ice nucleation activity, this finding was in disagreement with Wolber et al. (1988) finding, they found that ice nucleation members are recovered from fruit pathogens especially stone fruit, this could be duo to genetic modification as the result of environmental conditions variation. Fahy and Hayward (1983) reported that 87% of their isolates were ice nucleation inducer and they were from stone fruit trees. This is an indication that there is no inconsistency of ice nucleation among phytopathogenic Fluorescent Pseudomonas.

References

1. Andro T, Chambost J, Kotoujauskya J, Cattaneo Y et al.. Mutants of *E. chrysanthemi* defective in secretion of pectinase and cellulose. *J Bact.* 1984; 160: 1199-1203.
2. Berge O, Monteil CL, Bartoli C, Chandeysson C et al. A user's guide to a data base of the diversity of *Pseudomonas syringae* and its application to classifying strains in this phylogenetic complex. *PLoS One*. 2014; 9(9): e105547. doi: 10.1371.
3. Bender CL, Alarcon-Chaidez F, Gross DC. *Pseudomonas syringae* phytotoxins: Mode of action, regulation and biosynthesis by peptide and polyketide synthetases. *Microbiol Molec Biol Rev*. 1999; 63: 266–292.
4. Bultreys A, and Kaluzna M. Bacterial cankers caused by *Pseudomonas syringae* on stone fruit species with special emphasis on the pathovars syringae and morsprunorum race 1 and race 2. *J. Plant Pathol.* 2010: S21-S33.
5. Cunty A, Poliakoff F, Rivoal C, Cesbron S et al. Characterization of *Pseudomonas syringae* pv. actinidiae (Psa) isolated from France and assignment of Psa biovar 4 to a de novo pathovar: *Pseudomonas syringae* pv. actinidifoliorum pv. nov. *Plant Pathol*. 2015; 64: 582–596.
6. Daub, Margaret E, and Hagedorn DJ. Epiphytic populations of *Pseudomonas syringae* on susceptible and resistant bean lines. *Phytopathol.* 1981; 71: 547-550.
7. Fahy P, and Hayward A. Pseudomonas: the fluorescence pseudomonas. 1983. In Plant Bacterial Disease: A diagnostic Guide, (eds). Fahy P, and Persley A. Academic Press Inc, Australia, 141-178
8. Gardan L, Shafic H, Belouin S, Broch F et al. DNA relatedness among the pathovars of *Pseudomonas syringae* and description of tremae sp. Nov. and P.cannabina sp. nov. (ex Sutic and Dowson 1959). *Int J of Syst Bact.* 1999; 49: 469-478.
9. Gasson J. Indicator technique for antimetabolite toxin production by plant pathogenic species of Pseudomonas. *Appl Enviro Microbiol.* 1980; 39: 25-29.

10. Gross D, Cody L, Procbsting J and Spott A. Ecotypes and pathogenicity of ice-nucleation active *Pseudomonas syringae* isolated from deciduous fruit tree orchards. *Phytpathol*. 1984; 74: 241-248.
11. He SY. Elicitation of plant hypersensitive response by bacteria. *Plant Physiol*. 1996; 112: 865–869.
12. Hildebrand D. Pectate and pectin gels for differentiation of Pseudomonas sp. and other bacterial plant pathogens. *Phytopathol.* 1970; 61: 1430-1436.
13. Isabel M, Roos M and Hattingh M. Pathogenicity and numerical analysis of phenotypic features of *Pseudomonas syringae* strains, isolated from deciduous fruit trees. *Phytopathol*. 1987; 77: 900-908.
14. Isabel M, Roos M and Hattingh M. Systemic invasion of cherry leaves and petioles by *Pseudomonas syringae* pv. *Morsprunorum*. *Phytopathol.* 1987; 77: 1246-1252.
15. Kang, In Jeong. Effective selection of soybean cultivars to wildfire disease pathogen *Pseudomonas amygdali* pv. *tabaci*. *J of crop sci and biotechnol*. 2015; 18(4): 279-284.
16. Khalaf H. Olive Knot Disease in Jordan. *Jordan J of Agri Sci*. 2006; 2(4): 387-400.
17. Kings EO, Ward MK and Raney DE. Two simple media for the demonstration of pyocyanin fluorescin. *J Lab Clin Med*. 1954; 44: 301-307
18. Klement Z. Rapid detection of the pathogenic pseudomonades. *Nature*. 1964; 199: 299-300.
19. Lelliott A, Billing G and Hayward EC. A degenerative scheme for the fluorescent plant pathogenic pseudomonades. *J of Appl Bact.* 1966; 29: 470-489.
20. Lindow E, Hirano S and Upper D. Relationship between ice nucleation frequency of bacteria and frost injury. *Plant Physiol*. 1982; 70: 1090-1093.
21. Ma Z, Geudens N, Kieu NP, Sinnaeve D et al. Biosynthesis, chemical structure, and structure-activity relationship of orfamide lipopeptides produced by Pseudomonas protegens and related species. *Front Microbiol*. 2016; 7: 382.
22. Mahaureh B. Isolation and characterization of Pseudomonads isolation from soil and root of the citrus trees. Master thesis, *Yarmook Univ*. 1987; 126
23. Margaret E and Hagedom D. Epiphytic populations of *Pseudomonas syringae* on susceptible and resistance bean lines. *Phytopathol.* 1981; 70: 5-8.
24. Mushtaq S, Shafiq M, Ashraf T, Haider MS et al. Characterization of plant growth promoting activities of bacterial endophytes and their antibacterial potential isolated from citrus. *The J of Animal & Plant Sci.* 2019; 29(4): 978-991.
25. Morris CE, Kinkel LL, Xiao K, Prior P et al. Surprising niche for the plant pathogen *Pseudomonas syringae*. *Infect Genet Evol*. 2007; 7(1): 84-92.
26. Nandi M, Selin C, Brawerman G, Dilantha F et al. Hydrogen cyanide, which contributes to *Pseudomonas chlororaphis* strain PA23 biocontrol, is upregulated in the presence of glycine. *Biol Control*. 2017; 108: 47–54.
27. Nobutaka S, Masaharu K, Kasumi T, Yusuke U et al. Diversity of Antibiotic Biosynthesis Gene-possessing Rhizospheric Fluorescent Pseudomonads in Japan and Their Biocontrol Efficacy. *Micro Env*. 2020; 35(2): doi:10.1264/jsme2.ME19155
28. Schippers B, Schippers A and Bakker P. Interactions of deleterious and Beneficial rhizosphere microorganisms and the effect of cropping practices. *Ann Rev Phytopathol*. 1987; 25: 339-358.
29. Skerman VBD. A guide to the Identification of the Genera of Bacteria. Baltimore, Maryland, Williams and Wilkins. 1961. 2nd ed. https://doi.org/10.1002/jobm.19610010307.
30. Skerman D, Mcgowan V and Sneath A. Approved list of bacterial name. *Int J of Syst Bact.* 1980; 30: 225-420
31. Takeuchi K, Noda N, Katayose Y, Mukai Y et al. Rhizoxin analogs contribute to the biocontrol activity of newly isolated Pseudomonas strain. *Mol Plant-Microbe Interact.* 2015; 28: 333–342.
32. Turner JG, and Taha RR. Contribution of tabtoxin to the pathogenicity of *Pseudomonas syringae* pv. *tabac*i. *Physiol Plant Pathol.* 1984; 25(1): 55-69.
33. Wolberts DP, Denny TP and Schell MA. Cloning of egl gene of *Pseudomonas selanacearum* and analysis of its role in phytopathogenicity. *J Bact*. 19881; 70: 1445-1451.
34. Xin, Xiu-Fang, Brian K, and Sheng YH. *Pseudomonas syringae*: what it takes to be a pathogen. *Nat Rev Microbiol.* 2018; 16(5): 316.
35. Xu A and Gross D. Evaluation of the role of syringomycin in plant pathogenisis by using Tn 5 mutants of *Pseudomonas syringae* pv *syringae*. *Appl Enviro Microbiol.* 1988; 84: 1345-1353.
36. Young JM, Saddler GS, Takikawa Y, Boer SH et al. Names of plant pathogenic bacteria 1864-1995. *Rev Plant Pathol.* 1996; 75(9): 721–763
37. Young J, Takikawa L, Gardan L and Stead D. Changing concepts the Taxonomy of plant pathogenic bacteria. *Annu Rev Phytopathol.* 1992; 30: 67-105.

ISSN print: 1224-5984
ISSN online: 2248-3942

Rom Biotechnol Lett. 2022; 27(1): 3270-3281
doi: 10.25083/rbl/27.1/3270-3281

Received for publication, December, 14, 2021
Accepted, January, 16, 2022

Original paper

Hybrid Approach for Human Diseases Prediction Using Air Quality Index

VENU D[1], D. YUVARAJ[2], M. MURALI[3], NITIKA VATS DOOHAN[4]

[1] Department of ECE, Kakatiya Institute of Technology and science, Warangal
[2] Dept of Computer science, Cihan University – Duhok, Kuridsitan Region, Iraq
[3] Department of IT, Sona College of Technology
[4] Medi-Caps University, Indore

Abstract

Air pollution has become an extremely serious issue as the air pollutants emitted from motor vehicles has a greater impact on human health than other contaminants. Air quality forecasting plays a major role in giving warning to people and controlling air pollution. The single technique forecasting has various drawbacks such as low accuracy, low performance and low speed. Our present work overcome the above drawbacks by using a hybrid model approach. Our proposed method aims to forecast air quality to predict the hourly concentration of air pollutants using a hybrid model of data mining and machine learning. It predicts diseases due to emission of air pollutants from the motor vehicles based on Air Quality Index level. The CLusteringInQUEst algorithm is used to cluster geo-spatial data for specific input region. The Air Quality Index (AQI) for desirable set of important air pollutant features was calculated from the datasets produced by air pollutants from atmosphere. The calculated AQI was the input to the eXtreme Gradient Boosting (XGB) decision tree. It then classifies AQI level for the specific air pollutants. Then the diseases were classified using XGB algorithm.CLIQUE method has chosen than any other data mining techniques for which it can accurately predict diseases based on AQI values. XGBoost classifier is known for its good performance gradient bosting tree models which is very fast and an efficient one for both computation time and memory. Hence the above two techniques were combined as a hybrid approach to get the benefits of those features.The hybrid model produces a result with a higher performance, accuracy and speed compared to other models. In this paper, we have compared accuracy and precision rates for the hybrid approach with two single techniques such as Support Vector Machine and Random Forest.An accuracy and Precision rates of our proposed hybrid approach was 98.6% and 98.7% than Support Vector Machine has 93.85% and 94.8% & Random Forest has 94.28% and 94.52% which proves that hybrid approach is an efficient diseases prediction technique in real-time environment.

Keywords Data Mining, CLustering In QUEst, Machine Learning, eXtremeGradiant Boosting, Air Quality Index, high performance, high-speed, accuracy.

To cite this article: VENU D, YUVARAJ D, MURALI M, DOOHAN NV. Hybrid Approach for Human Diseases Prediction Using Air Quality Index. *Rom Biotechnol Lett*. 2022; 27(1): 3270-3281. DOI: 10.25083/rbl/27.1/3270-3281.

✉ *Corresponding author: VENU D, Department of ECE, Kakatiya Institute of Technology and science, Warangal
E-mail: stamizharasu@outlook.com

Introduction

Getting worse of air quality due to vehicle emissions has become a main global cause for decreasing of ambient air quality, premature mortality and morbidity living near major roadways. Stroke, pulmonary failure, lung cancer, and chronic respiratory conditions are also linked to ambient air emissions, which accounts for an unprecedented 4.2 million deaths each year.More than 95 percent of the world's population breathes toxic or dangerous food. Air Pollution is the major environmental issue which results around seven million deaths per year and it is attributed to about 9% of deaths around the world. It is also one of the leading risk factors for disease burden.

Majority of the population who suffers from the harmful effects of air pollution are children, elderly and people with respiratory and cardiovascular problems. According to recent findings, there are greater associations between air quality and the onset of respiratory and cardiovascular disorders. Ischemic cardiac failure, pre-existing respiratory condition, pneumonia, stroke, Chronic Obstructive Pulmonary Disease (COPD), lung cancer, and acute lower respiratory infections are common diseases induced by toxic air contaminants released by motor vehicles along roadways in children. "Critieria Air Contaminants" are toxic air pollutants that cause diseases and harm people's health and the environment. Greenhouse smoke, Particulate Matter, Nitrogen oxides (NOx), Carbon Monoxide (CO), Sulphur Dioxide (SO2), and other pollution contaminants emitted by motor vehicles are the most common substances causing morbidity and mortality across the planet.

To address this issue, we proposed a hybrid approach which helps in learning about the air pollution level due to the emission of harmful air pollutants from motor vehicles. The required region was clustered for air pollutant datasets such as Ozone (O3), Sulfur Dioxide (SO2), Carbon Monoxide (CO), and Nitrogen Dioxide (NO2). The Air Quality Index was measured for each air pollutant per hour to determine the degree of air contamination in the environment as a result of toxic gas emissions from motor vehicles. It is used to forecast diseases induced by air pollutants in relation to the Air Quality Index. The AQI of the air pollutants were used to classify the diseases using a Decision Tree algorithm called eXtreme Gradient Boosting (XGB), which simplifies the process of classification as it is versatile in nature. Of all decision tree algorithms, XGB is the most accurate, high speed decision tree algorithm and also it reduces overfitting in classifying the disease caused by air pollutants. The proposed model helps in predicting the diseases caused by harmful air pollutants which helps in protecting human beings from health hazards. The main contribution of this paper includes,

To propose an effective regional clusteringusing Grid based partitioning algorithm CLIQUE to cluster the geo-spatial data in real-time environment.

For efficient classification process, eXtreme Gradient Boosting (XGB) is used to classify diseases according to the Air Quality Index values.

LITERATURE SURVEY

Agarwal et al. [1] dealt with six major megacities in India as well as six major cities in Hubei province, China, where shutdown steps were strictly enforced. For about three months, real-time PM2.5 and NO2 concentrations were observed at different monitoring stations. Those data concentrations were translated into AQI. After one week of lockout, cities in China and India saw an average decrease in AQI PM2.5 and AQI NO2 concentrations of 11.32 percent and 48.61 percent, respectively, and 20.21 percent and 59.26 percent. As a consequence, the findings reveal that the decrease in AQI NO2 concentration was instantaneous as opposed to the incremental drop in AQI PM2.5 concentration. The lockout in China and India results in a final decline in AQI PM2.5 of 45.25 percent and 64.65 percent, respectively, as well as a reduction in AQI NO2 concentrations of 37.42 percent and 65.80 percent. Thus it shows the significance of vehicle smoke in the environmental pollution.

Sarkar et al. [2] proposed a system for determining improvements in air quality in the municipal corporations of Kolkata and Howrah in West Bengal, India, from the pre-lockdown era to the post-lockdown period. GIS-based methods such as interpolation were used to determine the spatial and temporal distribution of contaminants, whereas statistical methods such as analysis of variance (ANOVA) were used to calculate the mean differences between two distinct systems, and a correlation matrix was used to examine the evolving relationship of pollutants during the pre-lockdown and lockdown phases.

Sanchez et al. [3] proposed a protocol to identify the strategies that could be used for a comprehensive data map (SEM), which would recognise and characterise information on policy measures that could be adopted at the city level to minimise traffic congestion and/or TRAP from on-road mobile sources, mitigating human exposures and adverse health effects.

Markendeya et al. [4] investigated seasonal variations in air emission levels in Lucknow while also reviewing the city's indoor air quality and emphasising the health impacts of major toxins such as PM10, PM2.5, SO2, NO2, Pb, Ni, and aerosols.

Fazziki et al.[5] suggested a method for combining the advantages of agent technology with machine learning and big data tools. For air quality prediction and the least polluted path finding in the road network, an artificial neural networks model and the Dijkstra algorithm are used. HBase and MapReduce are used to execute all data processing operations in a Hadoop-based architecture.

Bigazzi et al.[6] reviewed the effectiveness of traffic management strategies (TMS) for mitigating emissions, ambient concentrations, human exposure, and health effects of traffic-related air pollution in urban areas.TMS can improve urban air quality and pollution-related health outcomes for exposed populations.

The feasibility of a deep learning algorithm for forecasting asthma risk was investigated and validated by Kim et al. [7]. The researchers were interested in the peak expiratory flow rates (PEFR) of 14 paediatric asthma

patients at Korea University Medical Center, as well as the amounts of indoor particulate matter PM10 and PM2.

An et al. [8] suggested a prototype of an optical transmission device with wavelength division multiplexing for electromagnetic interference-free indoor dust monitoring. The ability to view precise dust information in real-time is critical for patients with respiratory diseases. Indoor atmosphere information such as dust accumulation, temperature, and relative humidity were relayed by RGB light sources.

According to Xia et al. [9], a spatial correlation examination was used to determine the associations between PM 2.5 emissions and ARI admissions, and a time series study using a distributed lag non-linear model was also used to assess the associations between PM 2.5 emissions and ARI admissions. There were significant differences in affect between children and adults, most notably in acute lower respiratory infection.

Neto et al. [10] looked at forecasting schemes that used ensembles of Artificial Neural Networks (ANNs), with the aim of improving prediction precision and efficiency. Trainable and non-trainable hybrid approaches were used in this paper to forecast PM 10 and PM 2.5 time series forecasting (particles with aerodynamic diameters smaller than 10 and 2.5 micrometres, respectively) for eight separate locations in Finland and Brazil across various time scales.

METHODOLOGY

SUBSPACE CLUSTERING

Clustering is the process of making a group of abstract objects into classes of similar objects. Traditional methods have the problem called “curse of dimensionality”. To overcome this, a combination of Partitioning algorithm and Grid-based algorithm called grid partitioning (i.e., subspace algorithm) is used. The Partitioning clustering method classifies the information into multiple groups based on the characteristics and similarity of the data. The Grid-based clustering minimizes the computational complexity, in clustering of large datasets.

CLIQUE

Clustering InQUEst (CLIQUE) is a subspace clustering algorithm that constructs static grids from the ground up. It uses the Apriori approach to narrow the search area. CLIQUE manipulates multidimensional data by processing a specific level in the first stage and then moving upward to the higher one. The clustering process in CLIQUE starts by dividing the number of measurements into non-overlapping rectangular units called grids based on the prescribed grid size, and then calculating the dense region based on a defined threshold value. If the amount of data points in a unit crosses a certain threshold, it is said to be large. After that, the Apriori approach is used to generate clusters from all dense subspaces. CLIQUE has unique features, such as the ability to locate clusters in orbitrary form. It can also find any number of clusters based on any number of measurements. Clusters can exist in any subspace, which implies they can be in a single or overlapping subspace. Instances can belong to more than one cluster if the clusters overlap.

The geospatial data was clustered using the CLIQUE subspace clustering algorithm in this process.

The CLIQUE algorithm contains the following steps:

1. Locate spaces that comprise clusters.
   Divide the data space into equal parts and tally how many of each are contained within each partition cell.
   Determine which subspaces comprise clusters using the Apriori principle.
2. Locate clusters
   Find dense classes in any of the target subspaces.
   Count the number of associated dense units in each of the subspaces of interest.
3. Create a brief overview of the clusters.
   Determine the maximum regions that comprise each cluster's cluster of linked dense units.
   Determine the bare minimum of cover for each cluster.

As a result, a subspace clustering algorithm is used to cluster the spatial results.

The advantages of using the CLIQUE algorithm include the ability to,

As long as massive density clusters appear in those spaces, automatically define subspaces with the highest dimensionality.

It is untouched by the order of the records in the input and has no assumptions about data delivery.

Scales linearly with input size and scales well as the number of data dimensions increases.

APRIORI APPROACH

It is a classic algorithm that is useful in mining frequent item sets and associated association rules, according to the Apriori theorem. If a k-dimensional unit is dense, so all of its representations in k-1 dimensional space are also dense, meaning that a dense field in one subspace generates dense regions when projected onto lower dimensional subspaces. Since CLIQUE is based on the Apriori property, its quest for dense units in high dimensions is limited to the intersection of dense units in subspaces.

Datasets of atmospheric air toxins were gathered and used for feature collection. Until qualifying for the decision tree, the appropriate features were chosen during the feature selection phase. The aim of the feature selection techniques is to (i) improve the interpretability of the domain by reducing the feature area, and (ii) improve the efficiency of the machine learning algorithms. The Air Quality Index is determined for each acquired air pollutant dataset after the feature selection phase by taking the average value for the appropriate data. The AQI is a regular air quality indicator that is used to report on the quality of the air. It shows you how safe or dirty the air is, as well as what health affects you might be concerned with. The Air Quality Index (AQI) was developed to determine the volume of pollution in the air as well as their health effects. The Air Quality Index is a number between 0 and 500 that indicates how polluted the air is. The higher the AQI ranking, the higher the level of air emissions and, as a result, the greater the risk to one's health. This importance helps us in giving guidance on how

to defend ourselves from the dangers of air contamination, as well as protecting individuals from developing heart and lung diseases. For e.g, an AQI of 50 or less indicates good air quality, while an AQI of 300 or more indicates dangerous air quality (see Table.1). The main aim of the AQI is to help you consider how local air quality affects your wellbeing. The AQI is split into six parts to make it simpler to understand:

Table. 1. Air Pollution Level based on Air Quality Index

AIR QUALITY INDEX	AIR POLLUTION LEVEL
0-50	Good
51-100	Moderate
101-150	Satisfactory
151-200	Unhealthy
201-300	Very Unhealthy
Above 301	Hazardous

Each group represents a particular degree of public health concern. The six degrees of health risk and their meanings are as follows:

“Good” Your community's AQI ranges between 0 and 50. Air quality is deemed acceptable, and air contamination is deemed to pose minimal or no danger.

“Moderate” is a word that has a lot of different meanings depending on who Your community's AQI is between 51 and 100. The air quality is acceptable; nevertheless, certain contaminants may pose a modest health risk to a very limited number of citizens. People that are unusually vulnerable to ozone, for example, can develop respiratory symptoms.

“Unhealthy for Sensitive Populations” Members of vulnerable groups can feel health consequences when AQI levels are between 101 and 150. As a result, they are more likely to be harmed than the general population. People with lung cancer, for example, are more vulnerable to ozone damage, while people with either lung or heart disease are more vulnerable to particle emissions. When the AQI is in this size, the general population is unlikely to be harmed.

"Unhealthy" When AQI levels are between 151 and 200, anyone can begin to see health effects. Members of vulnerable groups can suffer more severe health consequences.

“Extremely Unhealthy” A health warning is issued when the AQI falls between 201 and 300, indicating that anyone may suffer from more severe health effects.

“Dangerous” Over 300 AQI values prompt health alerts of emergency situations. The community as a whole is more likely to be impacted.

Finally, the Air Quality Index values obtained from the given datasets were implemented for further classification using the decision tree algorithm, which is a machine learning technique. We use an efficient algorithm called eXtreme Gradient Boosting, abbreviated as XGBoosting, for this operation. It is then improved further in terms of efficiency and speed using a random scan technique.

XGBOOST CLASSIFIER

The XGB classifier is a machine learning classifier that is both fast and has good performance gradient boosting tree models. The XGBoost outperforms the competition on a variety of challenging machine learning tasks.XGBoost is a great machine learning model that consistently produces the best outcomes in terms of accuracy. XGBoost evolved from the simple gradient tree boosting concept to severe gradient boosting. In general, XGBoost is faster than other gradient boosting implementations. XGBoost is designed for speed and performance. Its engineering goal is to drive boosted tree algorithms' computing resource boundaries. The algorithm allows efficient use of both computation time and memory. When teaching the model, it makes for the most effective use of resources. It dynamically handles missing values in the dataset. By re-teaching the original model with new data, we will strengthen it. It is faster than other gradient boosting random forest implementations as opposed to other gradient boosting benchmarking random forest implementations. It is memory-friendly, fast, and precise.

The hyperparameters are tuned to enhance XGBoost efficiency. The following XGBoost model hyperparameters must be optimised: maximum depth (max_ depth), a tree depth level parameter; minimum child weight, the amount of hessian weights; subsample, a training data sample ratio; colsample by a tree, the sample column ratio when building each tree; A shrinkage parameter is the learning intensity, and the L1 regularisation parameter is alpha. The number of trees to suit is described by the n estimator hyper parameter in XGBoost. It's also the amount of epochs the algorithm uses to connect a tree before the total number of trees exceeds n estimator count, which improves the model's accuracy. The value of the n estimator is set to 100 by design.

For hyperparameter tuning, the random search technique is used. In the random search process, we generate a grid of potential hyperparameter values. Each iteration tries a random combination of hyperparameters from this grid, records the results, and finally returns the best combination of hyperparameters. Randomsearchcv performs a search over a set number of random parameter combinations. At the end of the search, you can view all of the results through the class's attributes. The best observed score and the hyperparameters that obtained the best score are perhaps the most critical attributes. If you've determined the best collection of hyperparameters, you can define a new model, set the values of each hyperparameter, and match the model to all available data. Scikit-optimize employs a Sequential model-based optimization algorithm to quickly identify optimal solutions to hyperparameter search issues.

After tuning the XGB hyperparameters, the model is qualified for classification and classifies malware and benign files with an accuracy of 99.5 %

Overview of the method

Air exposure is the main source of respiratory and cardiovascular diseases in our daily lives. When the world's population expands, so does the consumption of automobiles. As a consequence, mercury emissions from diesel cars cause severe heart and lung conditions. In this step, we suggest a hybrid model approach that uses data mining and machine learning technology to classify and forecast diseases. The CLIQUE and XGBoosting algorithms were used to accurately predict diseases.

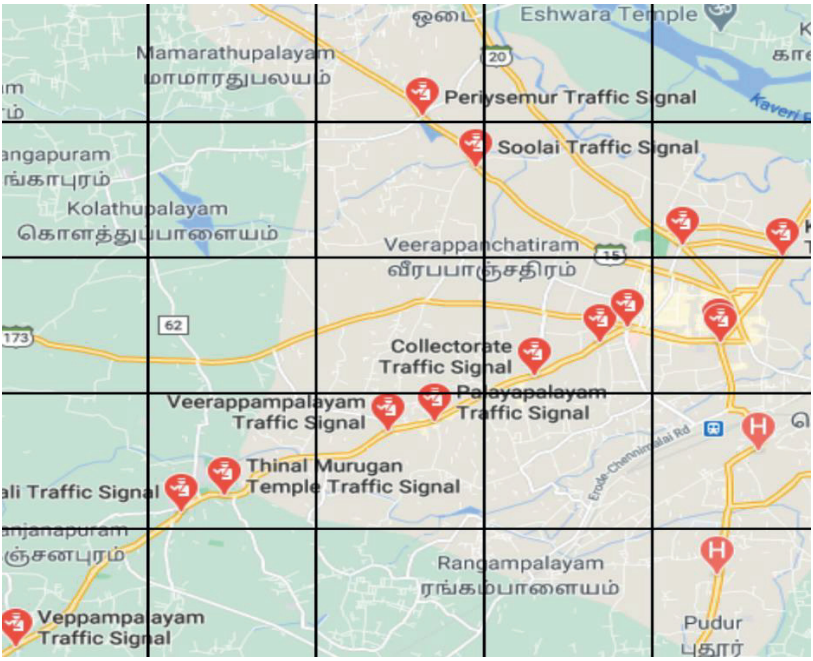

Figure 1. Geo-Spatial region

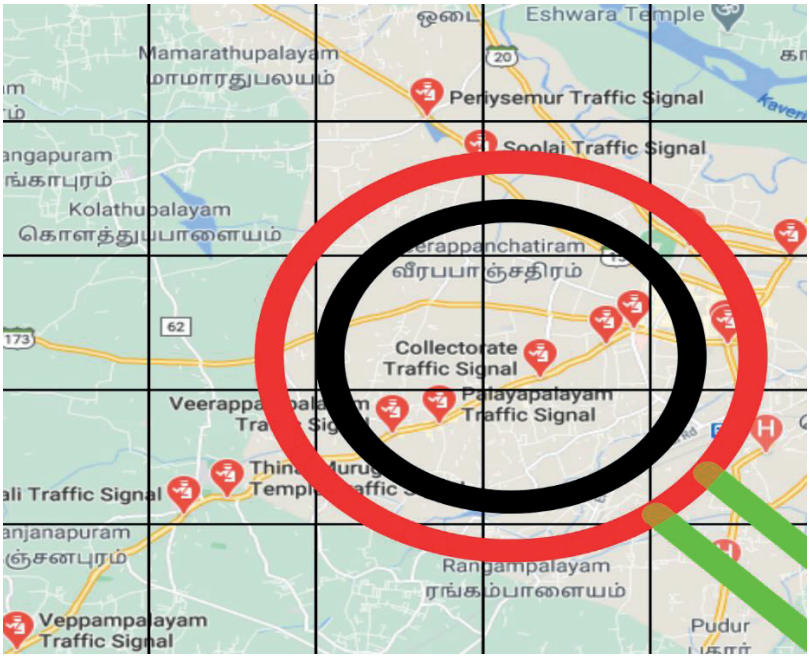

Figure 2. Clustering of region using CLIQUE algorithm

To start, geospatial data was clustered using a grid partitioning algorithm, a data mining technique. We use the CLustering In QUEst algorithm in our proposed work, which is a subspace clustering algorithm used to cluster geo-spatial regions in order to obtain all air pollutant datasets from the atmosphere. In this scenario, for example, we need air pollutant datasets near traffic signals in the erode region. The field is clustered using the grid clustering algorithm, as seen in Figure 1. If we choose a particular location, Signals in and around Palayapalayam, for example, are clustered by our algorithm using the CLIQUE subspace clustering method, as seen in Figure 2.

Our proposed grid partitioning algorithm clusters the input region in an efficient manner. It enhances the speed of clustering and accuracy. The acquired air pollutant features are then applied for feature selection process. The required air pollutant features like CO, Ozone, SO_2, NO_2 and Particulate Matters ($PM_{2.5}$, PM_{10}) are then selected in the feature selection process. Each and every selected air pollutant datasets are then calculated against Air Quality Index. Then, the AQI value is the input for eXtreme Gradient Boosting decision tree algorithm.

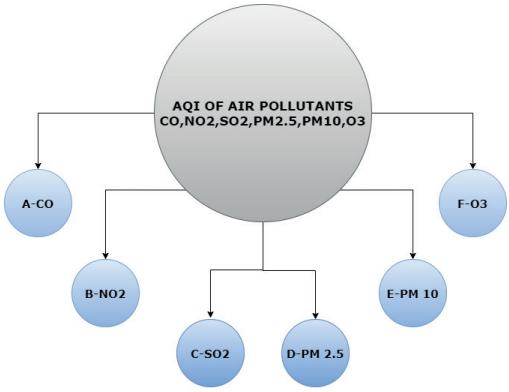

Figure 3. eXtreme Gradient Boosting Algorithm Decision Tree

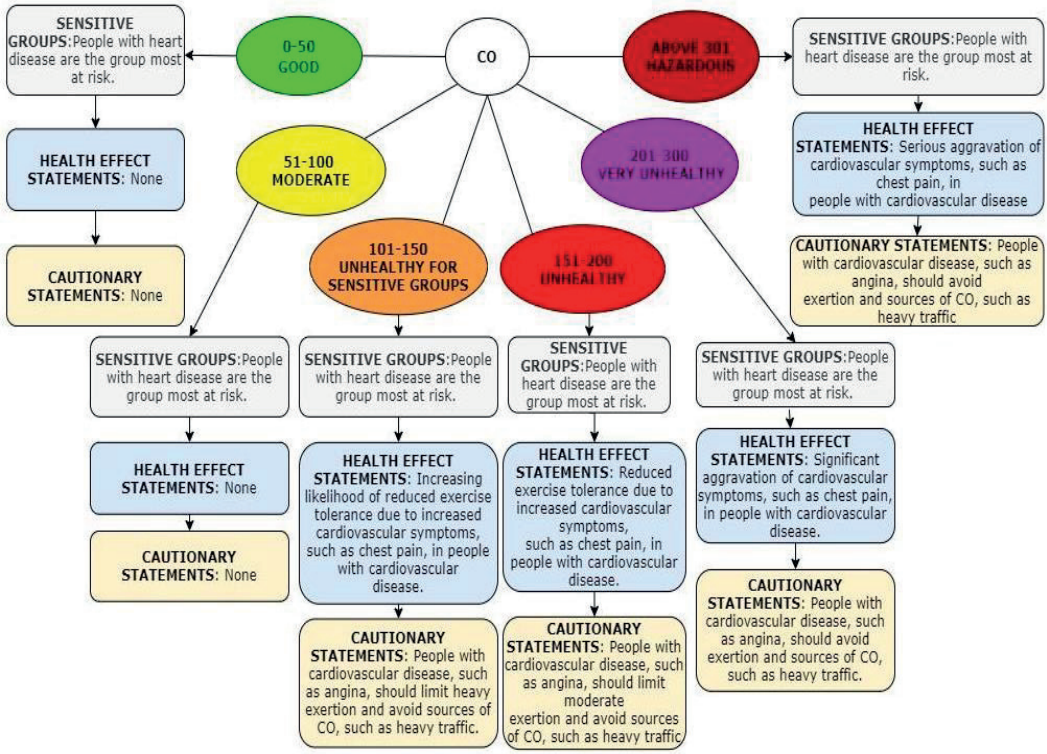

Figure 4. Classification for Carbon Monoxide A-(CO)

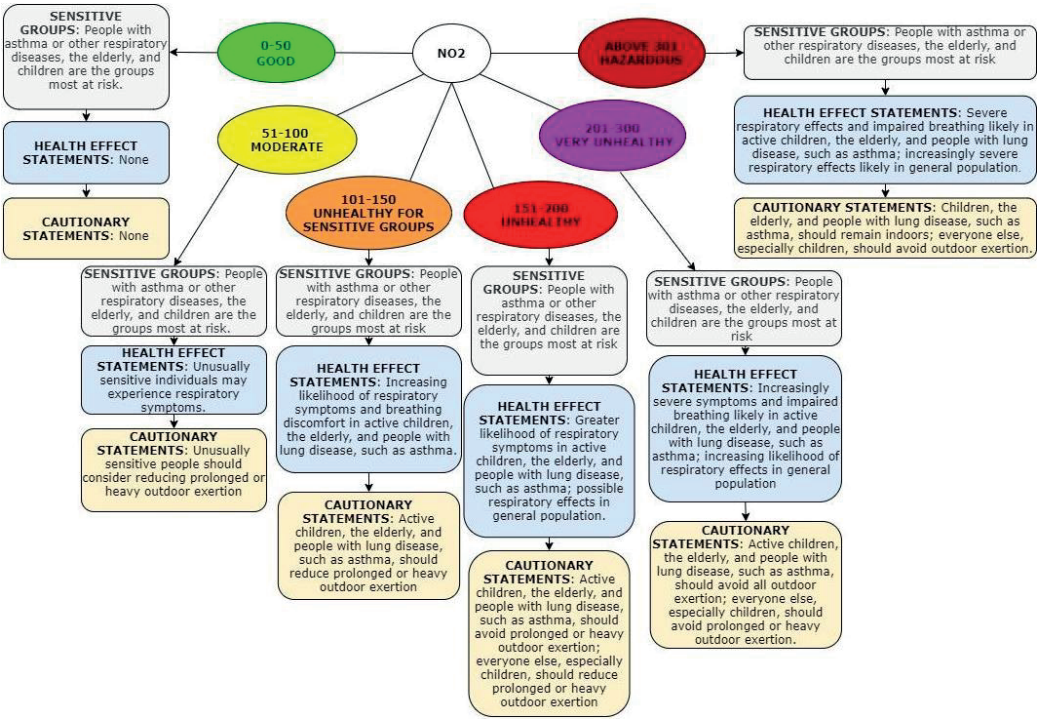

Figure 5. Classification for Nitrogen dioxide B-(NO_2)

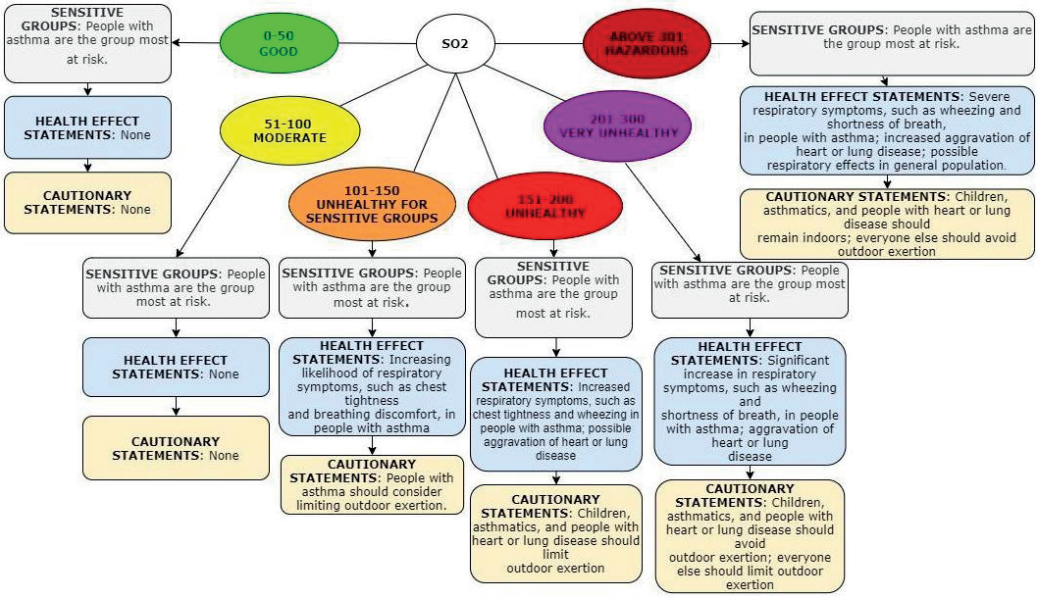

Figure 6. Classification for Sulphur dioxide C-(SO_2)

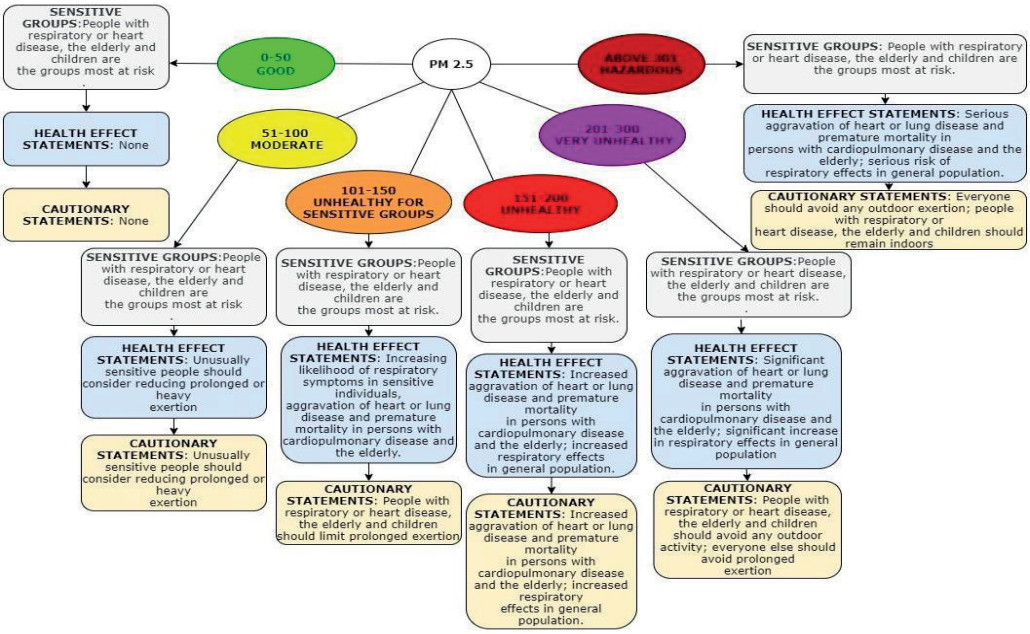

Figure 7. Classification for Particulate Matter 2.5 ($PM_{2.5}$)

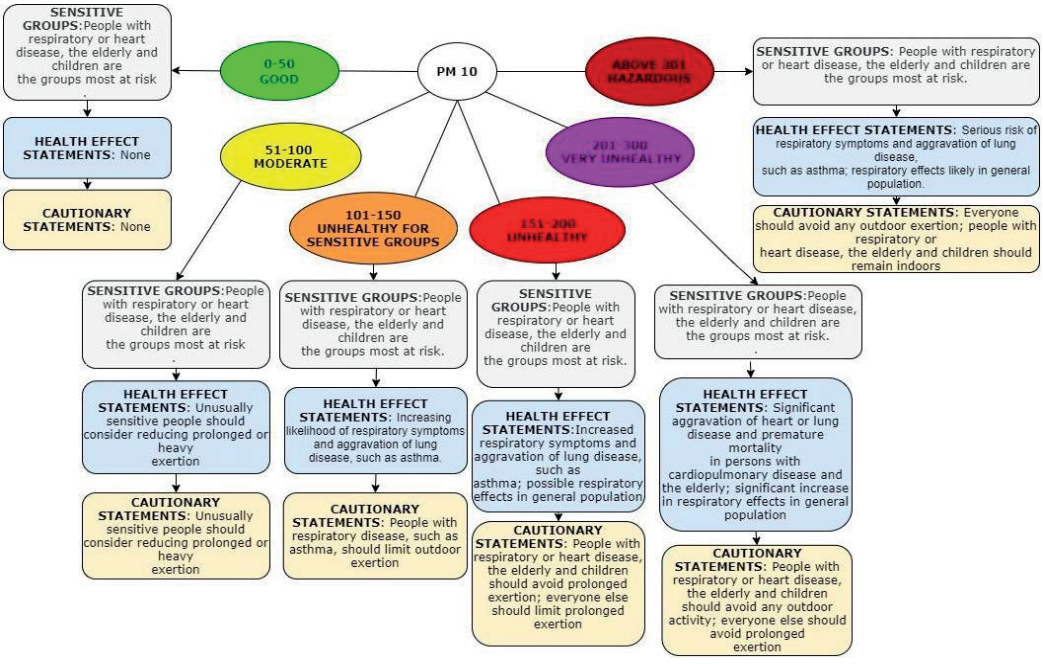

Figure 8. Classification for Particulate Matter 10 (PM_{10})

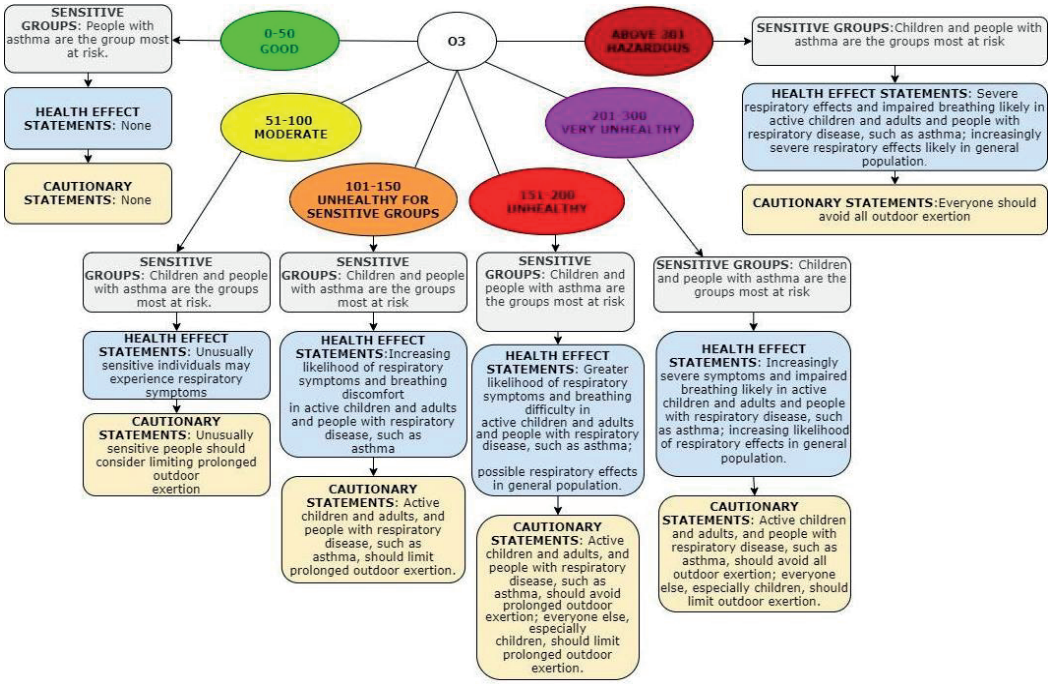

Figure 9. Classification for Ozone (O_3)

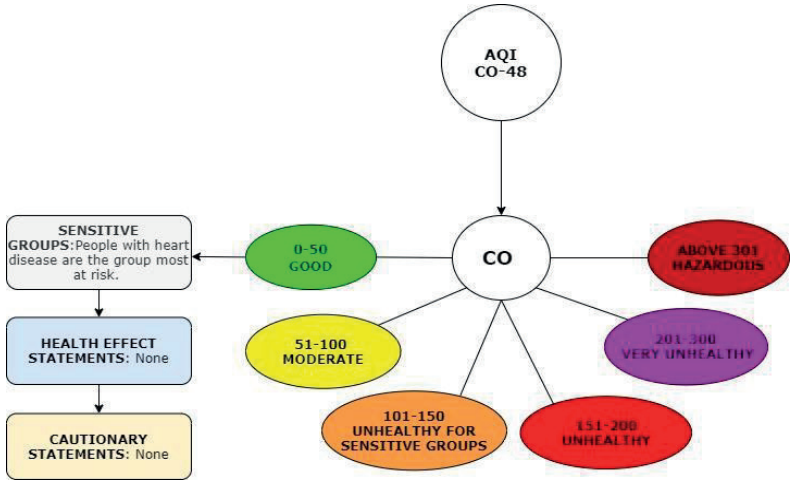

Figure 10. Example classification using eXtreme Gradient Boosting

The higher the AQI amount, the higher the level of air pollution and, as a result, the higher the health danger. The AQI value measured from the air pollutant databases is listed for AQI values. The condition is deemed good when the AQI is between 0 and 50. When the AQI value varies between 51 and 100, the condition is Moderate. When the AQI varies between 101 and 150, the condition is Satisfactory. When the AQI value varies from 151-200, the status is Unhealthy. When the AQI value varies between 201-300, the condition is Quite Good. When the AQI value

exceeds 300, the condition is declared hazardous. The classification is based on AQI ratios, and it is then further categorised for disease prediction. The resulting AQI amounts are listed for diseases in order to learn more about the health problem.

EXAMPLE

If we consider AQI of Carbon Monoxide gas as 48.So the input of the decision tree is taken as AQI-48.So the input of the decision tree is taken as AQI-48. It checks for the gas as well as AQI category for 48.It chooses the category from 0-50 and the AQI level is stated as GOOD. From this category, we can predict the groups which are sensitive as people with heart disease are the group most at risk. From this category, we can predict the groups which are sensitive as People with heart disease are the group most at risk, statements for health conditions as None because this level will not affect humans and also cautionary statements as None hence there is no health affects for humans.

The overall process flow diagram for this proposed work is shown in the Figure.9

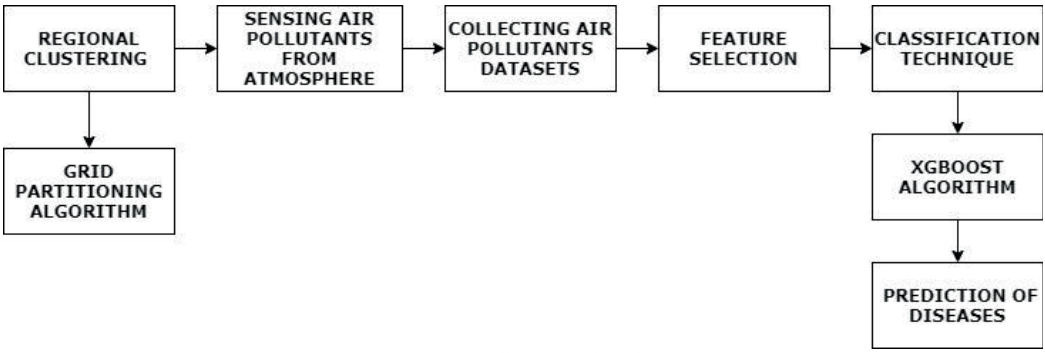

Figure 11. Overall process flow diagram

Results and discussion

Our proposed approach employs a mixture of data mining and machine learning algorithms for effective disease identification, assisting in the alerting of citizens to risk statements provided by air pollution released by motor vehicles. Grid partitioning is an elegant technique for clustering data points that is also recognised for its superior efficiency. The eXtreme Gradient Boosting algorithm which is a well-known for its parallel processing and is a non-greedy tree pruning for decision trees that reduces computational expense and time in decision trees. As a result, these two benefits of algorithms have been merged to conduct an effective procedure for disease prediction triggered by atmospheric air contaminants. Quality measures such as accuracy, precision, recall, and F-score have been used to test the proposed work. The average air pollutant datasets for PM2.5,PM10, NO2, CO, SO2, and O3 for a specific location are shown in Table.2. It is the dataset that reflects the possibility of diseases by taking into account the Air Quality Index (AQI), which is used to warn and alert the public regarding the likelihood of everyday emission levels. A considerable number of people are at risk of serious health problems when the AQI rises. An average human consumes about 11,000 litres of air every day. As a result, the air emissions released from motor vehicles cause health problems for anyone who breathe them in, which may even result in death. Figure.9 depicts a graph of AQI amounts for total air contaminants over the course of a day..

Table 2. Average air pollutant datasets

PLACE	DATE	$PM_{2.5}$	PM_{10}	NO_2	CO	SO_2	O_3	AQI	STATUS
Erode	03-04-2020	81.4	124.5	20.5	0.12	15.24	127.09	184	SATISFACTORY
Erode	04-04-2020	78.32	129.06	26	0.14	26.96	117.44	197	SATISFACTORY
Erode	05-04-2020	88.76	135.32	30.85	0.11	33.59	111.81	198	SATISFACTORY
Erode	06-04-2020	64.18	104.09	28.07	0.09	19	138.18	188	SATISFACTORY
Erode	07-04-2020	108.06	167.62	47.05	0.08	16.05	70.74	225	POOR
Erode	08-04-2020	100.75	172.04	53.94	0.11	14.05	59.2	251	POOR
Erode	09-04-2020	106.25	171.56	43.09	0.13	15.45	66.9	228	POOR
Erode	10-04-2020	83.79	141.83	47.47	0.3	13.35	77.54	223	POOR

Erode	11-04-2020	42.71	80.24	17.35	0.49	9.53	30.68	87	MODERATE
Erode	12-04-2020	54.73	94.12	12.79	0.58	8.21	30.21	89	MODERATE
Erode	13-04-2020	50.91	99.84	16.33	0.64	10.34	26.24	97	MODERATE
Erode	14-04-2020	38.5	106.7	16.82	0.58	11.02	26.62	100	MODERATE
Erode	15-04-2020	7.16	26.39	5.22	0.59	6.62	14.29	46	GOOD
Erode	16-04-2020	7.97	33.2	6.48	0.61	6.01	11.52	40	GOOD
Erode	17-04-2020	6.48	23.83	3.54	0.47	5.97	11.63	33	GOOD
Erode	18-04-2020	7.2	34.11	5.73	0.5	7.01	18.9	49	GOOD
Erode	19-04-2020	8.27	27.27	5.86	0.53	6.69	7.51	32	GOOD
Erode	20-04-2020	139.38	230.27	140.17	1.24	42.26	20.87	304	VERY POOR
Erode	21-04-2020	126.47	187.83	106.1	1.43	15.29	26.24	312	VERY POOR
Erode	22-04-2020	127.94	196.3	92.41	1.33	15.9	28.51	304	VERY POOR

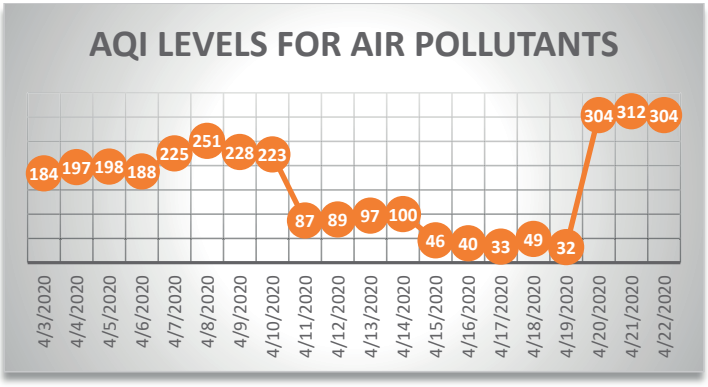

Figure 12. AQI levels for air pollutants

Figure.12 is the graphical representation of Air Quality Index levels for various air pollutants like carbon - monoxide, nitrogen-dioxide, sulphur-dioxide, ozone, particulate matter ($PM_{2.5}$, PM_{10}) for various time periods which is on daily basis.

The three different algorithms were evaluated for different performance metrics.Figure.13 shows the accuracy rate as 98.6% of a hybrid approach which was well greater than other two approaches such as support vector machine has 93.85% and random forest has 94.28%.

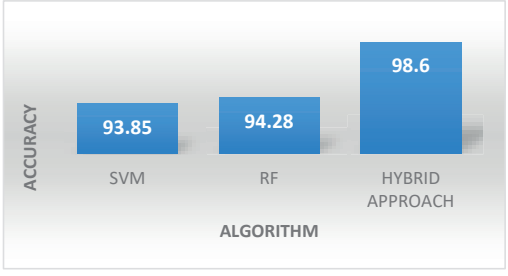

Figure 13. Comparison of algorithms against Accuracy

Figure.14 shows the precision rate of hybrid approach as 98.7% which was more precise than support vector machines has 94.8%and random forest has 94.52%.

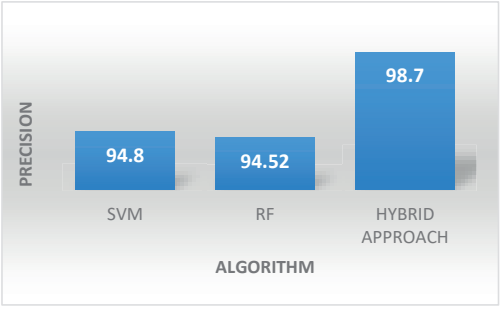

Figure 14. Comparison of algorithms against Precision

Figure.15 shows the recall rate of hybrid approach as 98.95% which was more precise than support vector machines has 96.4% and random forest has 96.75%.

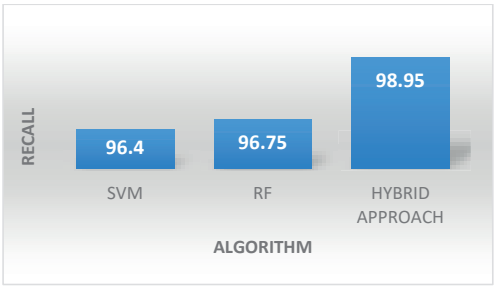

Figure 15. Comparison of algorithm against Recall

Figure.15 shows the recall rate of hybrid approach as 99% which was more precise than support vector machines has 97.23% and random forest has 97.88%.

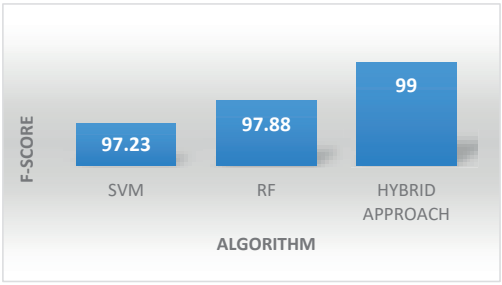

Figure 16. Comparison of algorithm against F-Score

Thus the overall efficiency of our proposed hybrid approach was 98% in comparison with other single techniques.

CONCLUSION

The fundamental aim of this paper is to predict the diseases The fundamental aim of this paper is to predict the diseases caused due to air pollutants emitted from the motor vehicles by an efficient approach of using hybrid algorithms. Here combination of two techniques were used such as data mining and machine learning. In this paper, two efficient algorithms were proposed such as grid partitioning clustering algorithm and eXtreme Gradient Boosting. This hybrid algorithm have been chosen on basis of its performance and accuracy. The poor performance and accuracy in the existing techniques have the difficulty of disease forecasting. Our proposed hybrid technique has performance and accuracy much greater than any other single technique for disease forecasting. Through this method we can attain an accurate disease prediction results using data mining and machine learning models. The grid partitioning clustering algorithm and XG Boosting algorithm are used for efficient prediction of diseases. Hence by this disease prediction method we can alert the people who are residing in nearby cities by preventing them from serious health effects and sometimes death. For the following algorithms such as the Vector support, the Random Forest and the Hybrid solution, the output measurements are compared. An overall accuracy of our proposed hybrid approach was 98 % which proves an efficient diseases prediction in real-time environment.

References

1. Agarwal, A., Kaushik, A., Kumar, S., & Mishra, R.K, (2020). "Comparative study on air quality status in Indian and Chinese cities before and during the COVID-19 lockdown period". Air Quality, Atmosphere & Health. doi:10.1007/s11869-020-00881-z
2. Sarkar, M., Das, A., &Mukhopadhyay, S, (2020). "Assessing the immediate impact of COVID-19 lockdown on the air quality of kolkata and Howrah, West Bengal, India". Environment, Development and Sustainability. doi:10.1007/s10668-020-00985-7
3. Sanchez, K.A., Foster, M., Nieuwenhuijsen, M.J., May, A.D., Ramani, T., Zietsman, J., &Khreis, H. (2020). "Urban policy interventions to reduce traffic emissions and traffic related air pollution: Protocol for a systematic evidence map". Environment International, 142, 105826, https://doi.org/10.1016/j.envint.2020.105826
4. Markandeya, Verma, P.K., Mishra, V., Singh, N.K., Shukla, S.P., & Mohan, D, (2020). "Spatio-temporal assessment of ambient air quality, their health effects and improvement during COVID – 19 lockdown in one of the most polluted cities of India". Environmental Science and Pollution Research. Doi:10.1007/s11356-020-11248-3
5. El Fazziki, A., Benslimane, D., Sadiq, A., Ouarzazi, J., &Sadgal, M. (2017). "An Agent Based Traffic Regulation System for the Roadside Air Quality Control", IEEE Access, 5, 13192–13201. doi:10.1109/access.2017.2725984
6. Bigazzi, A. Y., & Rouleau, M. (2017). "Can traffic management strategies improve urban air quality? A review of the evidence". Journal of Transport & Health, 7, 111–124. doi:10.1016/j.jth.2017.08.001
7. D. Kim, S. Cho, L. Tamil, D. J. Song and S. Seo, (2020). "Predicting Asthma Attacks: Effects of Indoor PM Concentrations on Peak Expiratory Flow Rates of Asthmatic Children", in IEEE Access, vol. 8,pp. 8791-8797,doi: 10.1109/ACCESS.2019.2960551
8. J. An and W. Chung,(2018). "Wavelength-Division Multiplexing Optical Transmission for EMI-Free Indoor Fine Particulate Matter Monitoring", in IEEE Access, vol. 6, pp. 74885-74894, doi: 10.1109/ACCESS.2018.2882576
9. X. Xia and L. Yao,(2019), "Spatio-Temporal Differences in Health Effect of Ambient PM2.5 Pollution on Acute Respiratory Infection Between Children and Adults", in IEEE Access, vol. 7, pp. 25718-25726, doi: 10.1109/ACCESS.2019.2900539
10. P. S. G. De MattosNeto et al., (2021). "Neural-Based Ensembles for Particulate Matter Forecasting", in IEEE Access, vol.9, pp.14470-14490, doi: 10.1109/ACCESS.2021.3050437.

ISSN print: 1224-5984
ISSN online: 2248-3942

Rom Biotechnol Lett. 2022; 27(1): 3282-3291
doi: 10.25083/rbl/27.1/3282-3291

Received for publication, December, 19, 2021
Accepted, January, 15, 2022

Original paper

An Efficient Agrobacterium-mediated Genetic Transformation Using cry1F gene in Castor (Ricinus communis L.) for protection Against lepidopteran Insects

ROHAN V. KANSARA[1], SANJAY JHA[2], VANRAJSINH H. SOLANKI[1], SUMANKUMAR JHA[3], VISHAL S. SRIVASHTAV[1], VIVEK V. MEHTA[4], HIREN K. PATEL[5], CHAITANYA S. MOGAL[1]

[1] Department of Plant Molecular Biology and Biotechnology, Navsari Agricultural University, Navsari-396450, Gujarat, India.
[2] Department of Plant Molecular Biology and Biotechnology, ASPEE Shakilam Agricultural Biotech Institute, Navsari Agricultural University, Athwa Farm, Surat-395007, Gujarat, India.
[3] Department of Forest Biology and Tree Improvement, College of Forestry, Navsari Agricultural University, Navsari-396450, Gujarat, India.
[4] Regional Horticulture Research Station, ASPEE college of Horticulture and Forestry, Navsari Agricultural University, Navsari-396450, Gujarat, India.
[5] School of Sciences, P.P. Savani University, Surat-394135, Gujarat, India.

Abstract

Castor (*Ricinus communis* L.) is an essential non-edible, pharmaceutical, and industrial oilseed as well as vulnerable to foliage feeders like *Spodoptera litura* which resulted in a loss of production. This report focuses on the development of an optimized protocol for the transformation of castor shoot apices by *Agrobacterium tumefaciens* strain *LBA4404* containing plasmid construct *pBIN1F* harboring neomycin phosphotransferase (*nptII),* as selectable marker gene and *Bacillus thuringiensis var. aizawai (Bt) cry1F* gene controlled by cauliflower mosaic virus 35S promoter. Several parameters like O.D., concentration of kanamycin and acetosyringone were optimized and produced a significant difference in the transformation efficiency. Co-cultivation time and seedling age were factors, with overall transformation efficiency of 2.0% in 15 days-old seedlings and co-cultivated for 3 days. The surviving and actively developing shoot apices were validated for gene integration by molecular analysis after being preliminarily screened on kanamycin. Furthermore, PCR, qRT-PCR and insect bioassay were used to confirm the putative primary transformants. When bioassayed against newly hatched *Spodoptera litura* hatchlings, these putative transgenics with *cry1F* gene caused significant (≤93%) insect mortality. *Cry1F* gene expressing transgenic plants had adequate defence against *Spodoptera litura* when exposed to castor.

Keywords *Ricinus communis*, *Agrobacterium*-mediated transformation, *Cry1F* gene, Shoot apex, *Spodoptera litura,* qRT-PCR

To cite this article: KANSARA RV, SANJAY JHA, SOLANKI VH, SUMANKUMAR JHA, SRIVASHTAV VS, MEHTA VV, PATEL HK, MOGAL CS. An Efficient *Agrobacterium*-mediated Genetic Transformation Using *cry1F* gene in Castor (*Ricinus communis* L.) for *p*rotection Against *lepidopteran* Insects. *Rom Biotechnol Lett*. 2022; 27(1): 3282-3291. DOI: 10.25083/rbl/27.1/3282-3291.

✉ *Corresponding author: SANJAY JHA, Department of Plant Molecular Biology and Biotechnology, ASPEE Shakilam Agricultural Biotech Institute, Navsari Agricultural University, Athwa Farm, Surat-395007, Gujarat, India.
Mobile: +91-7600059128; Office Tel: +91 2637 282143; Fax +91 2637 282145
E-mail: sanjayjha874@gmail.com

Introduction

The most significant commercial oilseed crop is castor (*Ricinus communis* L.). Because of the seed's strong oil content (48%-60%), notable oil output (500-1,000L of oil/acre), and this plant's unusual capacity to manufacture oils with exorbitant amounts (80%-90%) of hydroxylated, monosaturated fatty acid, i.e. Ricinoleic acid, it is an excellent candidate for the production of high value, industrial oil feedstocks (BRIGHAM [1]; NAIK & al [2]). Castor oil has unique properties that make it a cost-effective source of raw materials for ultrapure biodiesel, short-chain aviation fuels, fuel lubrication additives, and regular biopolymer processing (GOODRUM & GELLER [3]; PINZI AND PILAR DORADO [4]). India, China, Brazil, and Thailand are the top castor-producing nations, while the United States and Japan are the top importers (M. SUJATHA & al [5]). In 2019, India's provisional castor oil exports to major countries totaled around 0.5 million tonnes (SOLVENT EXTRACTORS' ASSOCIATION OF INDIA [6]). India is a major producer of castor seeds, producing around 1.082 million tonnes in 2018–19, with Gujarat leading the way with 0.889 million tonnes (SOLVENT EXTRACTORS' ASSOCIATION OF INDIA 2019 [6]).

Globally, the cultivation of castor is constrained by the improved cultivars' vulnerability to insect attack. Reliable sources of resistance to major insect pests are rather limited in the available germplasm of this monotypic genus (M. SUJATHA, M. SAILAJA [7]). About 100 species of insect pests are recorded on castor at differing phenological stages of the crop among which castor semi looper (*Achoea janata*), capsule borer (*Conogethes puncitiferalis*), *Spodoptera litura*, red hairy caterpillar (*Amsacta albistriga*), jassids (*Empoasca flavescenes*) and whitefly (*Trialeurodes ricini*) cause considerable damage to castor (M. LAKSHMINARAYANA, M.A. RAOOF [8]). *Spodoptera litura* is the most common insect that causes castor defoliation (A.K. SARMA & al [9]). According to the yield loss calculation, seed yield loss will vary from 35% to 50%, based on crop growth stages and pest attack. Castor has the inherent ability to absorb up to 25% leaf damage without substantial seed yield loss, while damage to spikes and capsules results in significant yield loss (V.D. REDDY & al 2011 [10]).

Insect pest tolerance, disease resistance, seed production, oil content, and ricinoleic acid content are the primary breeding targets for rectification in castor. Traditional breeders, on the other hand, are limited by time, space, and the need to maintain genetic fidelity. Cross-pollinating behaviour makes it much more difficult for traditional breeders to keep paternal lines pure. For traditional breeders and biotechnologists, the effective tissue culture protocol is often a call for further development and upliftment of castor farmer's economies (A.S. SINGH & al [11]). The major bottleneck in biotechnological interventions for castor improvement is the lack of regeneration protocol, which is reproducible and applicable to a broad range of genotypes. Difficulties in tissue culture-related regeneration have compelled researchers to adopt meristem-based transformation methods that have revolutionized plant genetic engineering of major agronomic crops, which were considered recalcitrant to i*n vitro* manipulations (M. SUJATHA, M. SAILAJA [7]; I. POTRYKUS [12]). No published report(s) dealing with the genetic transformation of castor plants, successfully deploying agriculturally useful gene(s), exist especially using *cry1F*.

Different genetic transformation methods were used to confer insect pest resistance to transgenic castors, including *Agrobacterium*-mediated (M. SUJATHA, M. SAILAJA [7]; B. MALATHI & al [13]; A.M. KUMAR & al [14]); Direct gene (M. SAILAJA al [15]); containing the Bt genes *cry1Ab* (B. MALATHI & al [13]), *cry1EC* (M. SUJATHA & al [16]), chimeric *cry1AcF* *Agrobacterium*-mediated genetic manipulation protocols have also been successfully optimised and applied to industrially relevant crops such as *Cajanus cajan* (M.J. PAREKH & al [17]), *Ocimum gratissimumi* (S. KHAN & al [18]), *Gossypium hirsutum* (V.H. SOLANKI & al [19]; V. KHANDELWAL & al [20]), *Trachyspermum ammi* (M. NIAZIAN & al [21]), *Oryza sativa* (V. SRIVASHTAV & al [22]) and *Camellia sinensis* (H.R. SINGH & al [23]) deploying agriculturally useful gene(s) for biotic and abiotic stresses.

As a parental line and cross hybrid, castor plant variety SKP-84 (SardarKrushinagar Pistillate-84), Fusarium wilt resistant, has strong general combiner for seed yield per plot and for one or more characters [D. DUBE & al [24]) as well as yield contributing characters (A.V. PANERA & al [25]). This multiple character inheritances may be used to establish potential breeding viewpoints for variety production. Using the meristem proliferation method evolved in our laboratory (R.V. KANSARA & al [26]) to defend against foliage feeder *Spodoptera litura* by insect bioassay, the current study was conducted to optimize conditions and to develop an efficient for *Agrobacterium*-mediated transformation protocol of castor.

Materials and methods

Plant materials

Fusarium wilt resistant Variety SKP-84, which had been used as parent line for some high yielding hybrids like GCH 7 (Gujarat Castor Hybrid-7), was procured from the Castor-Mustard Research Station, Sardarkrushinagar Dantiwada Agricultural University, Gujarat, India.

Agrobacterium strain and the binary vector

Agrobacterium tumefaciens strain LBA4404 was used for the experiments. The binary vector pBIN1F harboring the construct neomycin phosphotransferase (nptII), which is a kanamycin resistance gene, acts as a selectable marker and cry1F gene (Bacillus thuringiensis var. aizawai), which confers resistance to lepidopteran insects (selectively damages midgut). The chimeric genes were under the control of the CaMV35S promoter and OCS terminator. The Agrobacterium strain harboring given construct (Fig. 1) was provided by Dr. P. AnandKumar, Director, National Institute for Plant Biotechnology, (NIPB), Indian Council of Agricultural Research (ICAR), New Delhi, India for the genetic transformation experiment purpose.

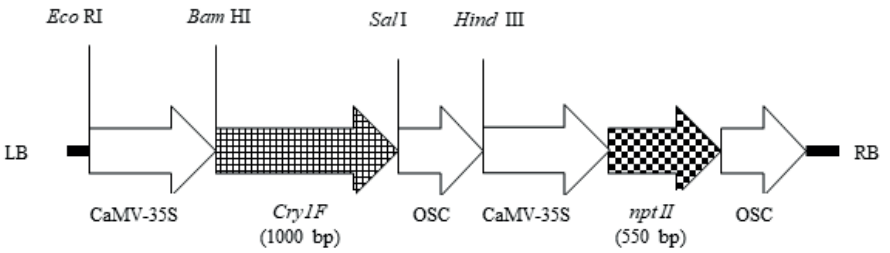

Figure 1. The T-DNA construct of binary vector pBIN1F harboring *cry1F* gene and selectable marker *nptII*

In vitro regeneration process for preparation of shoot apex

In vitro studies were conducted based on our previous successfully optimized in vitro plant regeneration protocol for fusarium wilt-resistant castor (Ricinus communis L.) parental line SKP-84 through the apical meristem (R.V. KANSARA & al [26]) in the Department of Plant Molecular Biology and Biotechnology at Navsari Agricultural University, Navsari, Gujarat, India. Mature seeds were decoated, rinsed (in running tap water), and surface sterilized with 0.1% (w/v) aqueous mercuric chloride solution for 4 min, subsequently washed (6 times) with sterile distilled water. Then, the material was blotted dry on sterile filter paper. Subsequently, the seeds were carefully dissected from the dorsal side and incubated on basal MS (T. MURASHIGE, F. SKOOG. [27]) medium MS basal salt medium with 3% (w/v) sucrose, pH 5.8, and solidified with 0.8% agar (Hi-media) for germination. The cultures were maintained at 25±2^{0}C under 16/8 h (light/dark) photoperiod with light provided by cool white fluorescent lamps at an intensity of 50 µmol $m^{-2}s^{-1}$. After that germinated 10, 15, and 18 days old seedlings were selected and the shoot apexes were carefully excised for co-cultivation with A. tumefaciens culture.

Determination of kanamycin threshold level

The castor plant's minimum inhibitory concentration of the selective antibiotic kanamycin was determined in the first phase of the experiment. As a result, the shoot apex was excised from developing seedlings and cultured separately on castor shoot proliferation media (MS medium with 0.25 mg/L BAP+ 0.50 mg/L kin) (R.V. KANSARA & al [26]) with kanamycin concentrations of 0, 25, 50, 75 and 100 mg/L. Both cultures were incubated at 25°C under a 16/8 h photoperiod with cool white fluorescent lamps providing an intensity of 50 µmol $m^{-2}s^{-1}$. To determine the optimal kanamycin concentration on a selective medium, the number of explants that survived and produced several shoots was counted.

Genetic transformation

A. tumefaciens strain LBA4404 culture was maintained on YEB medium (Beef extract 5 g/L, Yeast extract 1 g/L, Peptone 5 g/L, $MgSO_4.7H_2O$ 0.05 g/L, Sucrose 5 g/L, Agar 15 g/L) containing filter-sterilized 50 mg/L kanamycin and 10 mg/L rifampicin, incubated at 28ºC under dark conditions for 3–4 days. Single, isolated colonies from YEB medium plates were inoculated individually in 50 ml YEP medium (Yeast extract 10 g/L, Peptone 10 g/L, NaCl 5 g/L) containing 50 mg/L kanamycin and 10 mg/L rifampicin, incubated at 28ºC in an incubator-shaker at 200 rpm for 20–24 hours. Bacterial cells corresponding to an optical density (OD) of approximately 0.6 at 600 nm were pelleted by centrifugation (at 6000 rpm for 10 min), followed by washing twice with liquid YEP. The meristem explants excised at different days were injected with A. tumefaciens culture harboring the cry1F gene constructs and co-cultivated in dark for different periods. After co-cultivation, explants were rinsed with sterile distilled water 4 times containing 300 mg/L cefotaxime for 15 min and rinsed with sterile distilled water 4 times for 10 min with constant shaking. Cleaned shoot apices were blotted dry using a sterile paper towel and cultured on the selection medium consisting of castor multiplication medium (MS + 0.25 mg/L + 0.5 mg/L Kin) with 300 mg/L cefotaxime and 50 mg/L kanamycin. The Petri dishes were incubated at a temperature of 28ºC under 16-h photoperiod and kanamycin-resistant shoots were sub-cultured every two weeks. Surviving shoot apices were transferred to a half-MS medium containing 0.5 mg/L NAA without kanamycin for rooting of plantlets. For hardening, the rooted plants were moved to vermicompost-filled containers. Figure 2 shows the method for explant preparing, co-cultivation, collection, and recovery of plantlets.

Factors influencing Agrobacterium mediated gene transformation

Various factors influence transformation efficiency viz. Seedling age (10, 15 and 18 days), bacterial growth phase (OD 0.2, 0.4, 0.6, 0.8 and 1.0), co-cultivation duration (3, 5 and 7 days) and acetosyringone concentration (50, 100, 200, 300 and 400 µM) were investigated. Four replicates of thirty explants were used in each experiment. Any of the tests were carried out three times. On the basis of surviving shoots on a selective medium expressing the marker genes and positive by polymerase chain reaction, all of the above parameters were assessed and optimized.

DNA extraction and polymerase chain reaction (PCR)

Total genomic DNA was isolated from young leaves of independent putative transformed and untransformed (control)

plants using the CTAB method (J.J. DOYLE [28]) and screening was done by PCR using the nptII and cry1F genes specific primers (Bangalore Genei, India) for amplification of 550 bp and 1000 bp fragments (Table 1). The PCR reaction mixture (20 ml) contained 50 ng template DNA, 1x PCR buffer, 2.5 mM $MgCl_2$, 400 µM dNTPs, 0.3 U Taq DNA polymerase, 1 µl of each forward and reverse primer at a final concentration of 0.25 mM. For the positive control, 50 pg of the pBIN1F plasmid DNA was used. DNA from an untransformed castor plant was used for transformation control and reaction mix without DNA as a negative control. The amplification reactions were conducted on thermocycler of Eppendorf from Germany. The PCR reaction profile included 94ºC for 5 min followed by 30 cycles at 94ºC for 1 min, 53ºC (nptII) and 55 ºC (cry1F) for 1 min, 72^{0}C for 1 min 30 seconds with a final extension at 72^{0}C for 5 min. The amplification products were analyzed on 1.2% agarose-ethidium bromide gels by electrophoresis and documented in the gel documentation system.

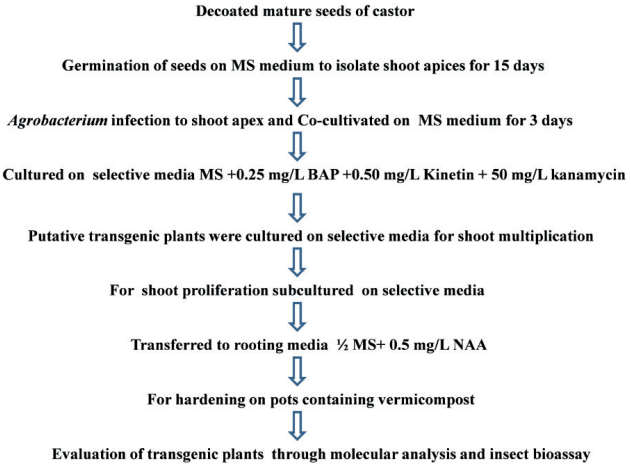

Figure 2. The representation of procedure developed for *Agrobacterium*-mediated genetic transformation of castor plants

Table 1. Details of used primers for amplification of *nptII* and *cry1F* genes

Gene name	Primer	Primer sequence	Amplicon length(bp)
❖ Gene specific for PCR			
nptII	Forward	5'–AAGAACTCGTCAAGAAGGCGATA–3'	550[a]
	Reverse	5'–ATGGGGATTGAACAAGATGGATT– 3'	
cry1F	Forward	5'–ATG GAG AACAACATCCAGAAT– 3'	1000[a]
	Reverse	5'–CAGTTTGTTGGAAGGCAACTC– 3'	
❖ Endogenous gene for qRT-PCR			
β-ACT	Forward	5'–TTCGCAGCAACAAACAT– 3'	371[b]
	Reverse	5'–TAAGCGGTGCCTCGGTAAGAAG– 3'	
❖ Gene specific for qRT-PCR			
cry1F	Forward	5'–GATGAAATCCCACCTCAGGA–3'	247[b]
	Reverse	5'–CGGGTCCTCTAACAACCGTA–3'	

β-ACT: Beta-actin; a: Length of the PCR amplified fragment with DNA template; b: Length of the PCR amplified fragment with cDNA template

Quantification by qRT-PCR

A modified TRIzol™ (Invitrogen, USA) method was used to isolate total RNA from adolescent leaf tissues of putatively transformed, untransformed, and control plants (V. SRIVASHTAV & al [22]). The analysis was conducted using QuantiFast SY BR Green PCR Master Mix in real-time PCR (qRT-PCR) (Qiagen, USA). The endogenous control was beta-actin (β-ACT) (Table 1). qRT-PCR (ABI-7300 Applied Biosystem, USA) reactions was performed with an

initial denaturation at 95°C for 5 minutes followed by 30 cycles of 95°C for 10 seconds and 60°C for 20 seconds. The endogenous control and gene specific qRT-PCR primers were used for cry1F are mentioned in Table 1. Gene-specific primers were designed using Primer-BLAST Software.

Insect bioassays

Control plants and putative transformants were subjected to insect bioassays. Freshly hatched neonate larvae of the Spodoptera litura [Collected from the Castor Research Station, Department of Plant Breeding, Navsari Agricultural University, Navsari, Gujarat, India (Latitude: 200 57' N and Longitude: 720 54' E; Agro-ecological situation-III)] were used in detached leaf bioassays under controlled environmental conditions, and the experiments were replicated three times. Using a fine camel hairbrush, ten larvae were infested on a leaf per petri plate with moist filter paper. The plates were incubated at 26 ± 2°C with relative humidity (RH) of 65%-70% and a 16 h photoperiod of light and 8 h of darkness for 2 days. According to the insect assay conducted by V.H. SOLANKI & al [19], data on percent mortality were computed after two days of feeding.

Statistical analysis

Statistical approaches were used to compare treatment means when optimizing criteria for genetic transformation and Microsoft Excel 2010 software was used to evaluate the results. All graphs were created using the Prism 8.09 programme. The findings are shown as mean ± standard error (SE). The results were subjected to analysis of variance (ANOVA), and the critical difference at 5% was used to compare treatment means (V.G. PANSE & P.V. SUKHATME [29]).

Results and discussion

This experiment describes results dealing with the establishment of a reproducible Agrobacterium-mediated genetic transformation protocol for insect resistance.

Optimization of Antibiotic Concentration

The use of proper concentrations of antibiotics used in the selection medium is essential in transformation experiments, in which the antibiotic serves as the selective agent that allows only transformed cells or plants to survive. Kanamycin has been extensively used as a selective antibiotic in transformation experiments, mainly because several plant transformation vectors include neomycin phosphotransferase II (nptII) gene as a selectable marker (M. NIAZIAN & al [21]; S. MISHRA & al [30]). Only transformed cells can grow in the presence of kanamycin. In our experiment, isolated shoot apices were transferred onto MS medium supplemented with 0.50 mg/L Kin + 0.25 mg/L BAP containing kanamycin at 0.25.50.75 and 100 mg/L after pre-culturing on basal MS medium for 7 days. Ten shoot apices were placed in each Petri plate and replicated four times for each concentration. Over a period of three weeks, the number of elongated shoot apices was counted and recorded each week. The control (without kanamycin) grew very well in MS media. Shoot elongation was significantly decreased on MS media containing kanamycin in a dose-dependent manner. The concentration of kanamycin at and above 50 mg/L was extremely lethal for survival and growth of castor shoot apices killing all the shoots within two weeks of culture with 13.55% of plant survival (Fig. 3a). Hence, a concentration of 50 mg/L kanamycin was decided for selecting putative transgenic apices henceforth in the present study. These results agree with earlier reports on some other medicinal plants like Ocimum gratissimumi (D. AGGARWAL & al [31]), Trachyspermum ammi (S. KHAN & al [18]), Withania somnifera (S. MISHRA & al [30]) and Bacopa monnieri (M. NIAZIAN & al [21]).

Optimization of A. tumefaciens concentration, co-cultivation duration and acetosyringone concentration

Efficient transformation parameters were analyzed using different A. tumefaciens concentrations (Absorbance of 0.2.0.4. 0.6.0.8 and 1.0 at OD600) and duration of co-cultivation (1.2.3.4 and 5 days). In each treatment combination, twenty shoot apices were placed with four replications. The survival percent of transformed plants after co-cultivation and frequency of transformation were recorded and showed that both A. tumefaciens concentrations had a significant effect on transformation frequency. The highest survival of transformed plants number and frequency of positive plants observed at OD600=0.6.

The transfer of T-DNA from A. tumefaciens to plant cells is a complicated process. The highest observed survival percent transformed plant was 48.16% and frequency of transformed plant were 2.2, which occurred at OD600=0.6 and 3 days co-cultivation (Fig. 3b and c). Co-cultivation with A. tumefaciens for 1 day was not long enough to maximize the transfer event. The data show that transformation frequency was always lower in 1-day co-cultivation than 2 days co-cultivation at different A. tumefaciens concentrations. Increasing the A. tumefaciens concentration did not always increase the transformation frequency. This may be because having A. tumefaciens concentration too high can cause A. tumefaciens overgrowth problems and reduction in plant regeneration (S. JIN & al [32]). Therefore, OD600=0.6 for 3 days co-cultivation was selected as the efficient transformation parameters in the present investigation.

In this step, the effects of five concentrations of acetosyringone, including 50, 100, 200, 300 and 400 µM, were evaluated with bacterial culture at O.D.600 to increase the transformation efficiency (Fig. 3d). The results showed the highest transformation frequency 2.18% on the supplementation of 100 µM acetosyringone in the inoculation time (Fig. 3d). Acetosyringone, a phenolic compound, is secreted on the wounding of plant tissues. It is also vir gene inducer and involved in the relocation of T-DNA to plant cells (S.E. STACHEL & al [33]). Earlier, different concentrations of acetosyringone have been reported to enhance Agrobacterium-mediated genetic transformation efficiency in Gossypium hirsutum (KHANDELWAL & al [20]) and Trachyspermum ammi (M. NIAZIAN & al [21]). Thus, the optimal concentration can be varied from plant to plant and affected by other transformation factors.

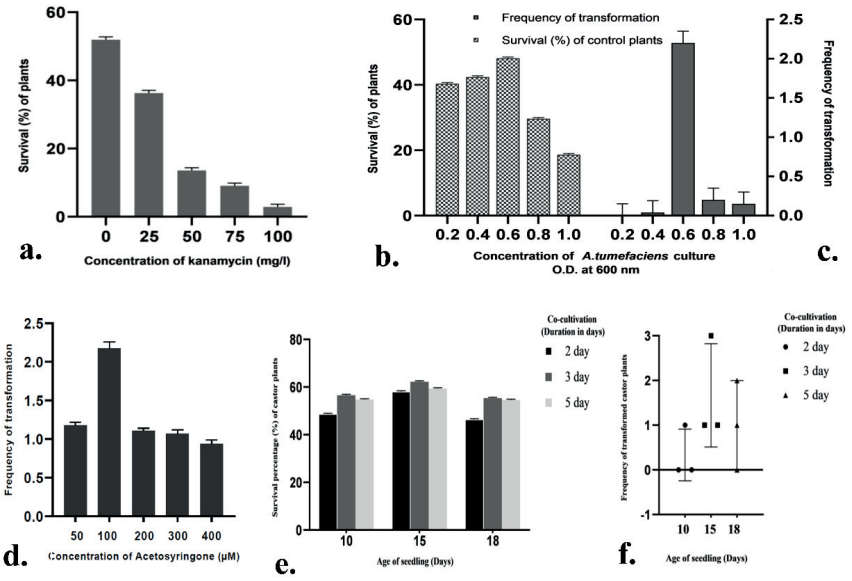

Figure 3. Factors influencing genetic transformation efficiency**. a.** effect of different kanamycin concentrations on the shoot apices of control castor plants (n=4); **b.** effect of *A. tumefaciens* (O.D. at 600nm) culture concentrations on survival percentage; **c**. frequency of transformation of castor plants (n=4) **d.** effect of different concentrations of acetosyringone on the frequency of transformation (n=4) **e.** Effect of age of the explants (days after germination of seeds) and co-cultivation duration with *A. tumefaciens* on survival percentage of the isolated shoot apices **f.** Transformation frequency of PCR positive plants after genetic transformation (n=4)**.** All results were represented as mean ± standard error (SE)

Optimization of seedling age for co-cultivation

The effect of the age of seedlings on survival percentage was found to be significant. The maximum survival percentage was found for fifteen days old seedlings (59.89%) compared to ten days (53.32%) and eighteen days (52.07%) age of seedlings. The effect of co-cultivation duration was found to be significant. Co-cultivation duration for three days gave the maximum survival percentage (58.06%) of the seedlings. Increasing co-cultivation duration above three days drastically reduced the survival percentage. The interaction effect of the age of the seedlings and co-cultivation duration was also found to be significant (Fig. 3e). The survival percentage for three days old seedlings and the co-cultivation duration for fifteen days gave a higher survival percentage (78.33%) (Fig. 3e). A reduction in the survival percentage (52.33%) was observed in the case of eighteen days old seedlings and two days of co-cultivation duration.

Analysis of putative transgenic plants

Age of the seedlings to isolate shoot apices and co-cultivation duration was found to influence the frequency of transformation. Fifteen days age of the seedlings gave a higher frequency of transformation 2.0%, while ten days and eighteen days age of the seedlings gave 0.66% and 0.33% frequency of transformation, respectively (Fig. 3f). Co-cultivation duration for three days on an average gave a maximum frequency of transformation (1.66%) while the co-cultivation period for the two days and five days gave 0.33% and 1% frequency of transformation. No transformants were obtained with ten days of seedling and two days of co-cultivation and in eighteen days of seedling for two days and five days co-cultivation duration. The interaction effect for the age of seedling and co-cultivation duration was also found to be significant. The maximum frequency of transformation (3%) was obtained for fifteen days of the age of seedling and three days of co-cultivation (Fig. 3f). Ten days and eighteen days age of seedling and co-cultivation for three days gave 1% frequency of transformation. A similar frequency of transformation was also obtained in ten days old seedlings and co-cultivation of five days, for fifteen days old seedling with co-cultivation for two days and for eighteen days old the seedling and co-cultivation for three days.

Production of putative transgenic plants

The shoot apices were co-cultivated with A. tumefaciens for 3 days. After co-cultivation, the shoot apices were transferred to MS medium with 50 mg/L kanamycin and 300 mg/L cefotaxime and established multiple shoot regenerative medium (BAP 0.25 mg/L + Kinetin 0.50 mg/L) (Fig. 4 a,b,c and d). Under kanamycin

selection pressure, most of the shoots and leaves appeared to be bleached and some shoots that were initially green bleached out gradually, leaving only a few green shoots (Fig. 4e and f). Even regeneration of bleached plant parts was observed when in vitro regeneration dependent Agrobacterium-mediated transformation approach applied (N. AHMAD, Z. MUKHTAR [34]). At every three weeks' interval, Shoot apices were transferred to fresh media. After four selections, surviving shoots were transferred to MS media without kanamycin to induce rooting. Rooting of the transformed shoot apices occurred when they were transferred from kanamycin selection medium to kanamycin free medium. Further, the hardening of the transformed plants required optimization in the pots. The morphological features of the transgenic plants did not differ from those of non-transgenic plants. Out of 250 explants, A. tumefaciens treated shoot apices placed on kanamycin selection, five (2%) regenerated plants grew (Fig. 5a and b) and were transferred to further culturing while others died.

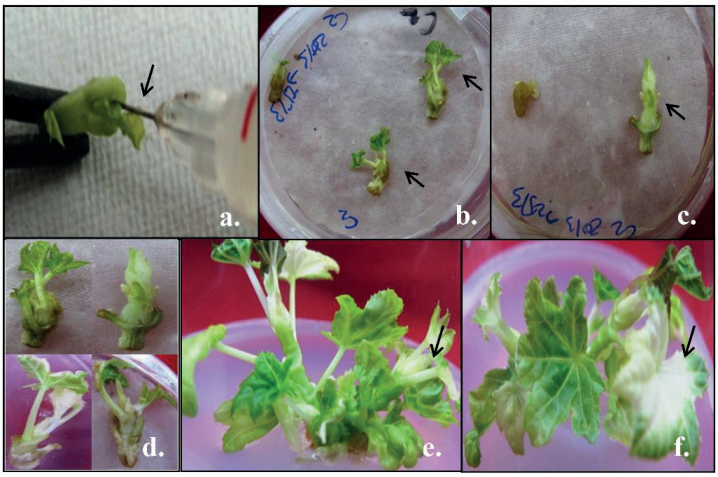

Figure 4. *Agrobacterium* infected shoot apices on selective medium containing kanamycin and cefotaxime. **a.** *Agrobacterium* infection to shoot apex; **b and c.** shoot apices on selective medium containing kanamycin and cefotaxime; **d.** putative transformed castor plants; **e.** multiplication and subculturing on selective MS medium contains 0.25 mg/L BAP + 0.5 mg/L Kin + 50 mg/L kanamycin + 300 mg/L cefotaxime after 3 weeks of inoculation and **f.** bleach color leaves

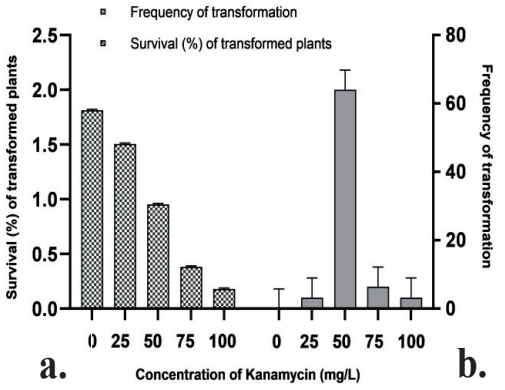

Figure 5. Effect of varying kanamycin concentrations on **a.** survival percentage and **b**. frequency of transformation of *Agrobacterium* mediated genetic transformed castor plants (n=4). All results were represented as mean ± standard error (SE)

Molecular analysis

Genomic DNA was isolated from the putatively transformed plants for screening of genetically transformed plants. The presence of transgenes was confirmed by PCR amplification of the gene for nptII and cry1F (Fig. 6a and b) in the kanamycin-resistant T0 plants. The presence of a band at 550 bp and 1000 bp in transformed plants established the integration of the nptII and cry1F genes, respectively in the castor genome. Amplification of 550 bp and 1000 bp fragments were absent in the non-transformed control PCR plants which showed that PCR was free of contamination (Fig. 6a and b). In addition, this negative control revealed the accuracy of the PCR procedure. The dark and strong band with the same size of 550 bp and 1000 bp of nptII and cry1F were observed in the PCR amplification of plasmid as a positive control.

Quantitative real-time PCR (qRT-PCR) analysis

Total RNA was isolated from putative transgenic plants and wild type (Fig. 6c). The PCR positive transformants were evaluated and further subjected to quantitative real-time PCR (RT-PCR) analysis for the presence of

introduced cry1F gene. The primary positive transformants were selected to detect cry1F gene by RT-PCR. The transformed plants showed amplification of cry1F gene in RT-PCR analysis. The realtime PCR indicated amplification with average Ct value. The real-time PCR runs along with the wild type (positive control), one non-transgenic plant (negative control) and four transgenic samples. The amplified RT-PCR DNA was executed and separated on 1.5% (w/v) agarose gel. The RT-PCR results showed that the β-ACT and cry1F gene were amplified to the required band size of 371 bp and 247 bp, respectively from cDNAs of putative transgenic plants (Fig. 6d and e). The higher expression level was observed in plants T1 (2.8 folds), T3 (2.63 folds), and T4 (2.68 folds) plants while the lowest expression level was observed in T2 (1.93 folds) plant (Fig. 6f).

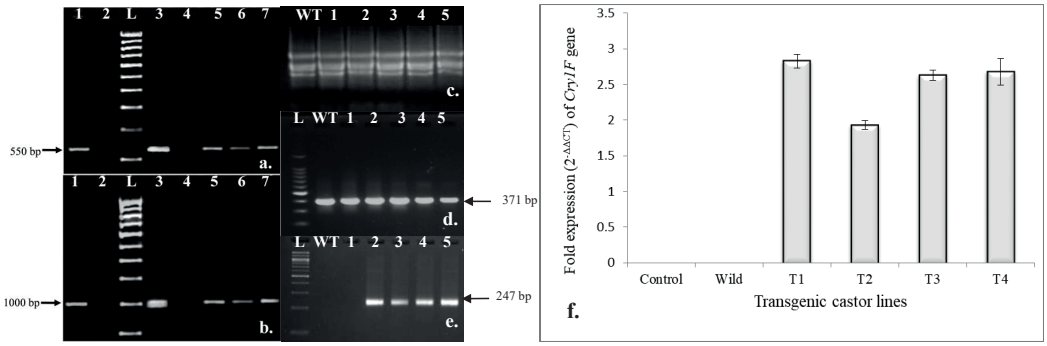

Figure 6. Molecular evaluation of putative transgenic castor plants (T_0 progeny).
a. PCR amplification of specific gene *nptII* and **b.** *cry*1F. Lane 1, 5-7: genomic DNA of transformed plants; Lane 3: positive control pBIN1F plasmid; Lane 2 and 4: negative control (untransformed plants); Lane L: 500 bp DNA marker, purchased from Banglore Genei; **c.** isolated total RNA from castor plants; RT- PCR products showed the amplification of **d.** Beta-actin gene- Internal control and **e.** *cry1*F gene. WT:wild type: Lane 1: untransformed plant; Lane 2-5: transformed plants; Lane L: 100 bp DNA marker, purchased from Banglore Genei **f.** Fold expression levels of *cry*1F gene in different putative transgenic castor plantsby qRT-PCR (T1-T4:Putative transgenic plant leaves; control and wild type)

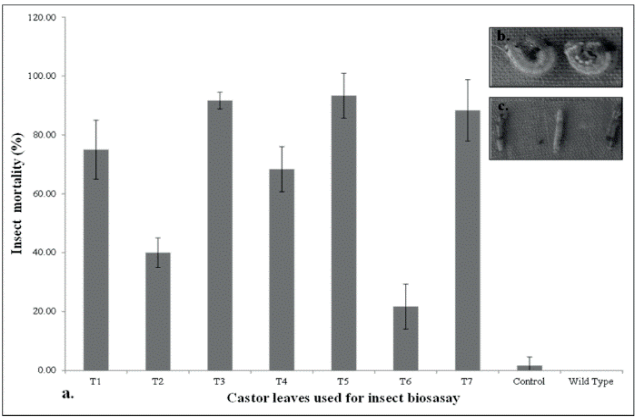

Figure 7. Effect of CRY protein on *Spodoptera litura* larva fed on the **a**. untransformed control castor **b.** putative transgenic castor and **c.** percent mortality of larva on the detached leaves of selected putative transgenic plants of T_0 generation (T1-T7: Putative transgenic plant leaves; control and wild type) (n=3)

Thus, fifteen day age of the seedling, three days of co-cultivation with O.D.600=0.6 of Agrobacterium at 50 mg/L of kanamycin gave a higher frequency of transformation 2.0%. It can be concluded that the transformation efficiency does depend upon genetic transformation factors as well as other parameters such as the age of an explant and plant growth regulators optimized for different in vitro regeneration protocols (R. BARANSKI [35]).

Insect bioassay of transformed castor plants with S. litura under in vitro conditions

To confirm the effect of cry1F gene, the insect bioassay of neonate larvae of Spodoptera litura was performed using the

leaf of T0 putative transgenic castor plants. Different transformants depicted diversification with insect resistance. During our insect bioassay study, it was observed that the larvae found dead after two days of infestation on the transgenic leaf disclosed different levels of insect mortality range from 21.67% to 93.33%, while on control plant was 1.67% (Fig. 7a). Moreover, the larva fed on putative transformed castor plant observed reduced growth of larva growth compared to the normal larval growth on the susceptible untransformed castor plant (Fig. 7b and c). Likewise, transgenic cotton lines were evaluated and showed higher resistance against chewing insect pests (V.H. SOLANKI & al [19]; KHANDELWAL & al [20]); H.A. SIDDIQUI & al [36]. Consequently, it was defined that the cry1F protein produced in the putative transgenic castors was sufficient toxic to Spodoptera litura and confer resistance in the castor plant. Previously, it was already reported the mode of action of Bt cry toxins to an insect that inserts into the cell membrane of the insect midgut, form pores, disturb the osmotic balance, induce swelling and lysis of the cells. Finally, the insect larvae stop feeding and die (J. GONZÁLEZ-CABRERA & al [37]; L. PARDO-LOPEZ & al [38]). Earlier, transgenic castors depicted higher resistance to neonate larvae castor semilooper on transformed plant with integration of the cry1Ab and bar genes through Agrobacterium genetic transformation (B. MALATHI & al [13]). Similarly, bioassay of castor semilooper and S. litura larvae showed varying levels of larval mortality and slow growth in larvae feed on transgenic plants leaf tissues then control plants which were transformed with Bt chimeric gene cry1EC, cry1AcF, and cry1Aa by Agrobacterium-mediated genetic transformation methods in the laboratory (M. SUJATHA & al [16]; A.M. KUMAR & al [14]; T. MUDDANURU & al [39]).

Conclusion

To conclude, this study represents an improved *Agrobacterium*-mediated castor genetic transformation that incorporates the binary Ti vector as well as the function of central point impacting. Using shoot apices as explants in the parental line SKP-84, the established *in vitro* genetic transformation protocol proved viable for the Bt cry gene *cry1F*. In the insect testing facility, these putative transgenics demonstrated resistance to *Spodoptera litura*. Furthermore, the standardized protocol has the potential to facilitate the genetic modification in castor inserting agriculturally useful genes (s) and render a healthier approach for further insect resistance plant development studies through genetic engineering which accelerates its immense economic and industrial significance of castor plants.

Abbreviations

A. tumefaciens – Agrobacterium tumefaciens; Bt – Bacillus thuringiensis; SKP-84 – Sardarkrushinagar pistillate-84; S. litura – Spodoptera litura; GCH 7 – Gujarat castor hybrid-7; nptII – Neomycin phosphotransferase; Bt cry – Bt crystal proteins; CaMV35S – Cauliflower mosaic virus 35S; OCS – Octopine synthase gene; LB – Left border; RB – Right border; YEB – yeast extract beef broth; YEP – yeast extract peptone; MS – Murashige and Skoog medium; BAP – 6-Benzylaminopurine; Kin – kinetin; OD – optical density; CTAB – Hexadecyltrimethylammonium bromide; PCR – polymerase chain reaction; RH – relative humidity; ANOVA – analysis of variance; T-DNA – transfer-DNA; vir gene – virulence gene; T – transgenic; qRT-PCR – quantitative real time PCR

Acknowledgements

Authors are thankful to Castor–Mustard Research Station, Sardarkrushinagar Dantiwada Agricultural University, Gujarat, India for providing seed material to carry out the experiment. We are also thankful to Dr. P. Anandkumar, NIPB-ICAR, New Delhi, India for providing gene construct.

Compliance with ethical standards

This article does not contain any studies involving animals or human participants as objects of research. All authors declare that they have no conflict of interest.

Author contributions

RK, SJ and VHS performed the research work. RK, SJ, VHS, SKJ and VS were contributed to all data collection and transgenic analysis. SJ, RK, SKJ and VHS analyzed data and prepared primary draft of manuscript. SJ supervised the all research activities. RK, VS, HP and VM wrote marked errors and confirmed the final draft of the manuscript. All authors reviewed and approved the final version of the manuscript.

References

1. R.D. BRIGHAM. Castor: Return of an old crop. In: Janick, J. and Simon, J.E. (Eds.), New crops. Wiley, New York, pp 380-383 (1993).
2. S.N. NAIK, D.K. SAXENA, B.R. DOLE, S.K. KHARE. Potential and Perspective of Castor Biorefinery, *In Waste Biorefinery*, Elsevier, pp 623-656 (2018)
3. J.W. GOODRUM., D.P. GELLER. Influence of fatty acid methyl esters from hydroxylated vegetable oils on diesel fuel lubricity, *Bioresou Tech*, 96 (7): 851-855 (2005).
4. S. PINZI, M. PILAR DORADO. Advances in Biodiesel Production: Processes and Technologies chap. 4: pp 69 (2012).
5. M. SUJATHA, P.V. DEVI, T.P. REDDY. Insect pests of castor (*Ricinus communis* L.) and their management strategies. *Pests and pathogens: Management strategies*, 177 (2011).
6. Solvent Extractors' Association of India Online: https://seaofindia.com. (2019).
7. M. SUJATHA, M. SAILAJA. Stable genetic transformation of castor (*Ricinus communis* L.) *via Agrobacterium tumefaciens*-mediated gene transfer using embryo axes from mature seeds, *Plant Cell Rep,* 23(12):803-810 (2005).
8. M. LAKSHMINARAYANA, M.A. RAOOF. Insect pests and diseases of castor and their management, Directorate of Oilseed Research, pp 2-28 (2005).
9. A.K. SARMA, M.P. SINGH, K.I. SINGH. Resistance of local castor genotypes to *Achaea janata* Linn. and *Spodoptera litura* Fabr., *J Appl Zool Re,* 17(2):179-181 (2006).
10. V.D. REDDY, N.P. RAO, K.V. RAO. Insect Pests of Castor (*Ricinus communis* L.) and their Management Strategies, *Pests and Pathogens: Management Strategies,* 177-198 (2011).

11. A.S. SINGH, S. KUMARI, A.R. MODI, B.B. GAJERA, S. NARAYANAN, N. KUMAR. Role of conventional and biotechnological approaches in genetic improvement of castor (*Ricinus communis* L.), *Ind Crops Prod,* 74:55-62 (2015).
12. I. POTRYKUS, Gene transfer to plants: Assessment of published approaches and results, *Ann Rew Plant Physiol Plant Mol Biol*, 42:205-225 (1991).
13. B. MALATHI, S. RAMESH, K.V. RAO, V.D. REDDY. *Agrobacterium*-mediated genetic transformation and production of semilooper resistant transgenic castor (*Ricinus communis* L.), *Euphytica,* 147(3): 441-449 (2006).
14. A.M. KUMAR, R. SREEVATHSA, K.N. REDDY, P.T. GANESH, M. UDAYAKUMAR. Amenability of castor to an *Agrobacterium*-mediated in planta transformation strategy using a *cry1AcF* gene for insect tolerance. *J of Crop Sci and Biotechnol*, 14(2):125-132 (2011).
15. M. SAILAJA, M. TARAKESWARI, M. SUJATHA. Stable genetic transformation of castor (*Ricinus communis* L.) via particle gun-mediated gene transfer using embryo axes from mature seeds. *Plant Cell Rep*, 27:1509-1519 (2008).
16. M. SUJATHA, M. LAKSHMINARAYANA, M. TARAKESWARI, P.K. SINGH, R. TULI. Expression of the *cry1*EC gene in castor (*Ricinus communis* L.) confers field resistance to tobacco caterpillar (*Spodoptera litura* Fabr) and castor semilooper (*Achoea janata* L.). *Plant Cell Rep*, 28(6):935-946 (2009).
17. M.J. PAREKH, M.K. MAHATMA, R.V. KANSARA, D.H. PATEL, S. JHA, D.A. CHAUHAN. *Agrobacterium* mediated genetic transformation of pigeon pea (*Cajanus cajan* L. Millsp) using Embryonic Axes for Resistance to Lepidopteron Insect, *Ind J Agric Biochem*, 27(2):176-179 (2014).
18. S. KHAN, N. FAHIM, P. SINGH, L.U. RAHMAN. *Agrobacterium tumefaciens* mediated genetic transformation of *Ocimum gratissimum*: a medicinally important crop. *Ind Crops Prod*, 71:138-146 (2015).
19. V.H. SOLANKI, V. KHANDELWAL, D.H. PATEL, M.K. MAHATMA. *Agrobacterium* mediated In planta transformation of *Gossypium hirsutum* cv G. Cot. 10. *Indian J of Plant Physiol,* 16:303-308(2011).
20. V. KHANDELWAL, V.H. SOLANKI, R.V. KANSARA. An improved *Agrobacterium*-mediated genetic transformation protocol for Cotton (*Gossypium hirsutum* L.)-An Economical important crop, *Res J Chem Environ,* 20: 11 (2016).
21. M. NIAZIAN, S.A. SADAT-NOORI, M. TOHIDFAR, P. GALUSZKA, S.M.M. MORTAZAVIAN. *Agrobacterium*-mediated genetic transformation of ajowan (*Trachyspermum ammi* (L.) Sprague): an important industrial medicinal plant. *Ind Crops Prod* 132:29-40 (2019).
22. V. SRIVASHTAV, S. JHA, V. PAREKH. Overexpression of *Lmgsh*F from *Listeria monocytogenes* in Indica Rice Confers Salt Stress Tolerance. *Russ J Plant Physl,* 66(6):911-921 (2019).
23. H.R. SINGH, P. HAZARIKA, M. DEKA, S. DAS. Study of *Agrobacterium*-mediated co-transformation of tea for blister blight disease resistance, *J of Plant Biochem Biotechnol,* 29(1):24-35 (2020).
24. D. DUBE, R. BHAKTA, K. BHATI. Studies on combining ability and heterosis for seed yield and yield components in Rabi castor (*Ricinus communis* L.), *The Pharma Innovation,* 7(5):171-175(2018).
25. A.V. PANERA, A.R. PATHAK, R.B. MADARIYA, D.R. MEHTA. Studies on combining ability for seed yield and yield components in castor (*Ricinus communis* L.). *The Pharma Innovation*, 7(7):550-554(2018).
26. R.V. KANSARA, S. JHA, S.K. JHA, M.K. MAHATMA. An efficient protocol for *in vitro* mass propagation of fusarium wilt resistant castor (*Ricinus communis* L.) parental line SKP-84 through apical meristem. *The Bioscan,* 8 (2):403-408(2013).
27. T. MURASHIGE, F. SKOOG. A revised medium for rapid growth and bioassays with tobacco tissue culture, *Physiol Plant,* 15: 473-497(1962).
28. J.J. DOYLE, J.L. DOYLE. Isolation of plant DNA from fresh tissue. Focus 12:13-15(1990).
29. V.G. PANSE, P.V. SUKHATME. Statistical Analysis for Agricultural Workers, ICAR, New Delhi, 50-65 (1985).
30. S. MISHRA, S. BANSAL, R.S. SANGWAN, N.S. SANGWAN. Genotype independent and efficient *Agrobacterium*-mediated genetic transformation of the medicinal plant *Withania somnifera* Dunal, *J of Plant Biochem Biotechnol*, 25(2):191-198(2016).
31. D. AGGARWAL, N. JAISWAL, A. KUMAR, M.S. REDDY. Factors affecting genetic transformation and shoot organogenesis of *Bacopa monnieri* (L.) Wettst. *J of Plant Biochem Biotechnol,* 22(4):382-391(2013).
32. S. JIN, X. ZHANG, Y. NIE, X. GUO, C. HUANG. Factors affecting transformation efficiency of embryogenic callus of upland cotton (*Gossypium hirsutum*) with *Agrobacterium tumefaciens*, *Plant Cell Tissue Organ Cult,* 81 (2):229-237(2005).
33. S.E. STACHEL, E.W. NESTER, P.C. ZAMBRYSKI, A plant cell factor induces *Agrobacterium tumefaciens* vir gene expression. *PNAS* 83(2):379-383 (1986).
34. N. AHMAD, Z. MUKHTAR. Genetic manipulations in crops: challenges and opportunities. *Genomics* 109(5-6):494-505(2017).
35. R. BARANSKI. Genetic transformation of carrot (*Daucus carota*) and other Apiaceae species. *Trans Plant J,* 2 (1):18-38 (2008).
36. H.A. SIDDIQUI, M. ASIF, S. ASAD, R.Z. NAQVI, S. AJAZ, N. UMER, S. MANSOOR. Development and evaluation of double gene transgenic cotton lines expressing Cry toxins for protection against chewing insect pests, *Scientific reports,* 9(1):1-7 (2019).
37. J. GONZÁLEZ-CABRERA, G.P. FARINÓS, S. CACCIA, M. DÍAZ-MENDOZA, P. CASTANERA, M.G. LEONARDI, J. FERRÉ. Toxicity and mode of action of *Bacillus thuringiensis* Cry proteins in the Mediterranean corn borer, *Sesamia nonagrioides* (Lefebvre). *Appl Environ Microbiol*, 72(4):2594-2600(2006).
38. L. PARDO-LOPEZ, M. SOBERON, A. BRAVO. *Bacillus thuringiensis* insecticidal three-domain Cry toxins: mode of action, insect resistance and consequences for crop protection. *FEMS* Microbiol Rev 37(1):3-22 (2013).
39. T. MUDDANURU, A.K. POLUMETLA, L. MADDUKURI, S. MULPURI. Development and evaluation of transgenic castor (*Ricinus communis* L.) expressing the insecticidal protein *Cry1Aa* of *Bacillus thuringiensis* against lepidopteran insect pests. *Crop Protection* 119:113-125(2019).

ISSN print: 1224-5984
ISSN online: 2248-3942

Rom Biotechnol Lett. 2022; 27(1): 3292-3301
doi: 10.25083/rbl/27.1/3292-3301

Received for publication, December, 03, 2021
Accepted, January, 16, 2022

Original paper

Evaluation of the genotoxic activity of wastewater obtained after steam distillation of essential oil of Bulgarian Rosa alba L. – in vivo study

TSVETELINA GERASIMOVA[1], MARGARITA TOPASHKA-ANCHEVA[1], ANA DOBREVA[2], ALMIRA GEORGIEVA[3,4], MILKA MILEVA[3]

[1] Department of Ecosystem Research, Environmental Risk Assessment and Conservation Biology, Institute of Biodiversity and Ecosystem Research, Bulgarian Academy of Sciences, 2 Gagarin Str., Bulgarian Academy of Sciences, Sofia 1113, Bulgaria
[2] Institute for Roses and Aromatic Plants, Agricultural Academy, Kazanlak 6100, 49 Osvobojdenie Blvd, Bulgaria
[3] Department of Virology, The Stephan Angeloff Institute of Microbiology, Bulgarian Academy of Sciences, 23, Acad. G. Bonchev, str., 1113 Sofia, Bulgaria
[4] Institute of Neurobiology, Bulgarian Academy of Sciences, 23, Acad. G. Bonchev, str., 1113 Sofia, Bulgaria

Abstract

The process of essential oil water-steam distillation leaves a water fraction as a rest material of the technological process. This residual fraction represents a serious environmental pollutant. The aim of the present study was to investigate the clastogenic and cytotoxic effects of *R. alba* L. distillation wastewater in laboratory animal's test model *in vivo*. The ICR mice received a single dose (0.01 mL/b. w.) of 20% (v/v) or 11% (v/v) wastewater solution by intraperitoneal administration. The chromosomal aberrations frequency, mitotic index and micronuclei formation in peripheral blood were scored. The results suggested that the distillation wastewater extracts of white oil-bearing rose *R. alba* L. did not induce a considerable amount of chromosome aberrations, but a cell proliferation inhibition in mice bone marrow cells, compared to the negative control group ($p<0.001$). The rodent erythrocyte MN assay showed a slightly increased frequency of micronucleated polychromatic erythrocytes under the present experimental conditions. *Rosa alba* L. wastewater solution applied showed a negligible genotoxic effect, but a slight antiproliferative effect.

Keywords *Rosa alba* L., wastewater products, genotoxicity, *in vivo* mammalian erythrocyte micronucleus test.

To cite this article: GERASIMOVA T, TOPASHKA-ANCHEVA M, DOBREVA A, GEORGIEVA A, MILEVA M. Evaluation of the genotoxic activity of wastewater obtained after steam distillation of essential oil of Bulgarian *Rosa alba* L. – *in vivo* study. *Rom Biotechnol Lett*. 2022; 27(1): 3292-3301. DOI: 10.25083/rbl/27.1/3292-3301.

*Corresponding author: TSVETELINA GERASIMOVA, Department of Ecosystem Research, Environmental Risk Assessment and Conservation Biology, Institute of Biodiversity and Ecosystem Research, Bulgarian Academy of Sciences, 2 Gagarin Str., Bulgarian Academy of Sciences, Sofia 1113, Bulgaria
E-mail: cvetij@yahoo.com

Introduction

Plants in the genus Rosa of the family Rosaceae are among the most valuable oil-bearing plants. From ancient times the rose has been declared the Queen of Flowers, due to its wonderful aroma and beautiful inflorescences. The application of rose essential oils, aqueous and alcoholic extracts from flowers for the treatment and prevention of various diseases dates back to the beginning of human civilization due to their therapeutic efficacy - antidepressant effects, psychological relaxation, improvement of sexual dysfunction, antioxidant, antimicrobial, antifungal, probiotic and antipyretic effects, smooth muscle relaxation, lipid-lowering, antiulcerogenic effects, etc. (Gochev et al., 2010; Shohayeb et al., 2014; Abdel-Hameed et al., 2015; Georgieva et al., 2019). Rose flowers are a rich phytocomplex of ingredients that determine their biological activity (Bakkali et al., 2008).

In Bulgaria, the most popular method for the production of rose oil is a classical method of water-steam distillation, which leaves a water fraction as a rest material of the technological process. They are data existing that only in Bulgaria the essential oil of *Rosa alba* L. is distilled separately from *Rosa damascena* Mill. (Kovacheva et al., 2010; Dobreva et al., 2011). The low yield of essential oil of *Rosa alba* L. leads to the release of bulky waste - (i) spent rose petals as a solid residue, as well as (ii) wastewater - liquid residue (Slavov et al., 2017).

So, the wastewater after rose oil distillation represents a serious environmental problem as pollutants because they are discarded into the drainage system and the rivers (Wedler et al., 2016).

Recently, there is great attention on the valorization of plant materials and reusing the potentially bioactive ingredients of these materials. Many new novel approaches are studied, including the extraction of polysaccharides from the biomass and the introduction of integrated methods for the more complete valorization of the rose waste by-products. Due to insufficient data on their composition and biological activities, most of the methods for rose waste valorization still remain on a laboratory scale (Slavov et al., 2017).

As a by-product of hydrodistillation, wastewater is rich in water-soluble compounds as polyphenols, glycosides, tannins, etc., so they could be used as a good natural inexpensive source of biologically active compounds after more phytochemical, *in vitro*, and *in vivo* studies. These compounds are the subject of a rather scarce but growing number of studies in terms of their genotoxic potential. Sabahi et al. (2020) applied a cytotoxicity assay on HepG2 cells (human liver cancer cell line) exposed to different concentrations of *R. damascena* Mill. polyphenol-enriched fraction of wastewater for 24 and 48 h. A significant toxicity at a concentration of 100 µg/mL and higher was reported in this cell line, but on human lymphocytes a range of concentrations (25-100 µg/mL) did not show any genotoxicity and could be considered as nongenotoxic concentrations. However, this type the results need to be validated in *in vivo* settings (Rothfuss et al., 2011). Different components of *Rosa alba* L. have been subjected to various studies. Naikwade et al. (2009) reported a learning and memory-enhancing activity of *Rosa alba* L. Authors indicated that aqueous extract of *Rosa alba* L. calyces might be useful memory restorative agent when treating cognitive disorders such as Alzheimer's disease. Yon et al. (2018) demonstrated that petal extract of white rose (*Rosa hybrida* L.) containing polyphenols and flavonoids exerted neuroprotective effects via antioxidative and anti-inflammatory activities in glutamate-treated HB1.F3 human neural stem cells and kainic acid-challenged male ICR mice. Therefore, authors suggested that petal extract of *Rosa hybrida* could be a good candidate as an anti-epileptic or neuroprotective agent for clinical trials to attenuate seizure-related brain injury.

In the scientific literature are described various methods and technology for rose waste utilization are sought as well as to reuse these wastewaters and the compounds contained therein with potential beneficial effects. One such study provides evidence that phenolic compounds in water by-product obtained after hydro-distillation of Taif rose (*Rosa damascena Miller var. trigintipetala Dieck*) showed antioxidant activity (Abdel-Hameed et al., 2015). Taif rose water by-product extract did not produce pathological abnormality and had an excellent safety profile in acute, sub-chronic, and chronic toxicity studies in adult male Swiss albino mice. Polyphenol-containing rose oil distillation wastewater from *Rosa damascena* Mill. was also proved to have dose-dependent antiproliferative activity on immortalized human keratinocytes (Wedler et al., 2016).

Since rose petals are known to contain compounds with potential antiproliferative activity (Wedler et al., 2016), it was therefore of interest to investigate *Rosa alba* L. distillation wastewater extracts and their contribution to possible genotoxic and antiproliferative effect. Based on this data consideration, we formulated the objective of the present work - to investigate the clastogenic and cytotoxic effects of *Rosa alba* L. distillation wastewaters through classical cytogenetic methods on a laboratory animals test model.

Materials and methods

Preparation of wastewaters

The wastewaters were collected after the distillation of rose flowers, in the semi-industrial installation of the Institute for Roses and Aromatic Plants, Kazanlak. The process parameters were as follows: raw material 8 - 10 kg; hydro module 1:4; flow rate 16-20 ml/min; duration 150 min. The wastewaters were collected in cool conditions for the next stage of the investigation.

Chemicals

The standard experimental mutagen N-methyl-N'-nitro-N-nitrosoguanidine MNNG (50 µg/mL) (CAS-Nr.: 70-25-7, from Fluka – AG, Switzerland) was used as a positive control. A parallel experiment with 0.9% NaCl solution was used to a negative control.

Total flavonoid and phenolic content assay

The Folin-Ciocalteu method with some modifications was used for the measurement of the total phenolic content. 150 µL of the tested waters were added to 1.25 mL of Folin-Ciocalteu reagent (diluted 1:10) and 1 mL of Na_2CO_3 solution (7.5%). After incubation of 30 min at room temperature, the absorbance was measured at 765 nm against blank. Gallic acid was used as a reference standard for plotting the calibration curve for polyphenols, and quercetin – for flavonoid content respectively. The final results were calculated as gallic acid equivalents per 1 mL wastewater (GAE/1 ml water) and QueE/ml respectively, on the basis of a standard curves.

Animals and treatment

Eight-week old male and female ICR strain albino mice (20.0±1.5g b.w.), were delivered from Slivnitza animal breeding house, Bulgarian Academy of Sciences, Sofia. Animals were transported to the Animal house facility of Institute of biodiversity and ecosystem research and were kept for several days at standard laboratory conditions - temperature 20-22^{0}C, photoperiod 7 am to 7 pm, free access to standard for laboratory animal's food and water.

The experiments were performed in accordance with Bulgaria's Directorate of Health Prevention and Humane Behavior toward Animals. Bulgarian Food Safety Agency (BFSA) published a Certificate number 125 and standpoint 45/2015 for 5 years period for use of animals in experiments for the Stephan Angeloff Institute. The Ethical Committee of The Stephan Angeloff Institute approved the experimental design and protocols of the work with decision from 4.10.2020.

The ICR mice were randomly assigned to four experimental groups (eight male/eight female animals each) and kept in standard cages isolating the control and the treatment groups to avoid cross contamination. All tested substances were given as a single treatment by intraperitoneal (i.p.) injection.

The following experimental groups (n=8, 4♂4♀ each) were defined: Group 1. Animals, injected with 20 % wastewater solution (0.01 mg/mL); Group 2. Animals, injected with 11 % - wastewater solution (0.01 mg/mL). Group 3: MNNG 50 µg/mL (0.01 mg/mL). Group 4: Untreated control group, injected only with 0.9% NaCl (0.01 mg/mL). Throughout the experiment, all animals were observed twice daily after initial i.p. treatment for any clinical signs of toxicity.

Cytogenetic assay

The cytogenetic assay protocol (Preston et al., 1987) was applied for each experimental group starting at the 24th (4♂4♀) or 48th (4♂4♀) after intraperitoneally treatment with the respective solution. To obtain metaphase chromosomes suitable for cytogenetic analysis, one hour before bone marrow cell isolation a mitotic inhibitor colchicine – 0.04 mg /g b.w. was intraperitoneally (i.p.) injected. For scoring of micronuclei, blood smears were prepared prior colchicine treatment. Animals were euthanized by diethyl ether anesthesia, bone marrow cells were flushed from femur and hypotonized in a 0.075 M KCl at 37^{0}C for 15 min. The cell fixation procedure includes a solution of cold methanol: glacial acetic acid (3:1), followed by resuspendation and dripping on precleaned cold wet glass slides and air dried. The slides were stained in 5 % Giemsa solution (Sigma Diagnostic). Up to 50 well-scattered metaphase plates were analyzed from each animal using light microscopy (Olympus CX 31) x 1000. The structural changes in the chromosomes - chromosomal aberrations (CA) were used as an endpoint for genotoxicity. The main types of aberrations – breaks and fragments, were separately scored for each animal in all eight experimental groups. Mitotic indices (MI) were determined by counting the number of dividing cells among 1500 cells per animal (Darzynkiewicz et al., 1987). The frequencies of abnormalities and the mitotic index were determined for each animal and then the mean ± standard error of mean for each group was calculated.

The in vivo mammalian erythrocyte micronucleus test (MN test)

The MN test was performed in accordance with the OECD test guideline No. 474 for the testing of chemicals (OECD, 2016). Samples of peripheral blood were taken once 48 hours after initial treatment from all dose groups to facilitate integration with the other toxicity tests. For each of the eight mice in the group 5µL peripheral blood was collected through the tail vein. The blood was diluted with 45 µL Sörensen's phosphate buffer (pH 6,8) (Mitkovska et al., 2012) and a drop of this solution was smeared on a microscopic slide. Slides were air dried and fixed for 10 min with absolute methanol. Dry slides were independently coded prior to scoring by a single investigator. The smeared preparations were stained with Acridine orange (AO) (Merck) according to Hayashi et al. (1983) with some modifications. The A.O. stock solution was prepared as a 0.1% aqueous solution, available for several weeks at 4°C. A.O., 0.24 mM in 1/15 M Sörensen's phosphate buffer (pH 6.8) which is 1/15 M Na_2HPO_4 and 1/15 M KH_2PO_4, prepared separately and mixed together in a ratio to have pH 6.8 (2 parts of stock solution and 30 parts of the buffer), was used as a working solution. AO (50 µL of a 1mg/mL solution) was dropped on dry blood sample slides and spread by immediately covering the slide with coverslip glass (24x32mm). The cells were allowed to settle for few minutes and the analysis was then performed with a fluorescence microscope at 400x magnification. Observations were made using Axio Scope A1 – Carl Zeiss Fluorescent Microscope with 40X EC Plan-NEOPLUAR objective equipped with FITC 495 nm excitation filter.

The criteria used for the identification of micronuclei (MNi) and to distinguish them from artifacts in the cytoplasm, were described by Schmid (1975). MNi were generally round or oval in shape, with sharp borders and exhibited a strong yellow-green fluorescence. MNi were easily distinguishable in PCE, which emit red fluorescence (Hayashi et al., 1983).

From each slide, at least 2000 polychromatic erythrocytes (PCE) or at least 4000 per animal were screened for the incidence of micronucleated immature

erythrocytes. The proportion of immature among total (immature + mature) erythrocytes is determined for each animal by counting a total of at least 1000 normochromatic erythrocytes (NCE) per slide or 2000 NCE per animal. Only monolayers without overlapping cells were targeted for each slide.

Statistical analysis

Results are expressed as mean value ± standard deviation (SD) for each group and the data were statistically evaluated for their significance by analysis of variance using two-tailed, two-sample Student's t-test. Statistical significance is expressed as $p<0.001$; $p<0.01$; $p<0.05$; $p>0.05$ - (not significant).

Results and discussion

The wastewater of *Rosa alba* L. was examined for its total phenolic composition and total flavonoid content. Our results showed that it contained 7.6 μg GAE/ml polyphenols and 5.2 μg QueE/mL liquid. The low level of polyphenols is probably due to their low water solubility, or higher levels of polyphenolic glycosides that are difficult to detecting.

Polyphenols regulate many cellular, biochemical, and immunological events involved in the initiation and progress of genotoxic processes (Chahar et al., 2011). Dietary polyphenols, including flavonoids, have protective effects against DNA damage induced by different genotoxic agents. They are data existing that they quite often realize their genoprotection action by the mechanisms include (i) reducing oxidative stress; (ii) metal ion chelating; (iii) modulation of enzymes responsible for bioactivation of genotoxic agents and detoxification of their reactive metabolites. The quercetin-like structures containing in the wastewater of *Rosa alba* L. have the same chemical analogs as were reported by Luca et al. (2016), so they are able to exert their genoprotective effect by a similar mechanism.

The paper presents the effect of oil-bearing Bulgarian rose *Rosa alba* L. distillation wastewater introduced intraperitoneally over a well-known *in vivo* test model - ICR mice.

The changes in chromosomal aberrations frequency (CAF), mitotic index (MI) and micronuclei formation (MN) in peripheral blood were studied. Micronuclei are small satellite structures, representing chromosomal fragments lacking centromeres. The frequency of micronuclei is also commonly used as a cytogenetic biomarker. The *in vivo* MN test in peripheral blood erythrocytes is widely used as a short-term assay for the detection of agents able to induce chromosomal aberrations in somatic cells (Hayashi et al., 1990). For short-term studies, polychromatic erythrocytes are taken into account (OECD, 2016). An increase in the frequency of micronuclear polychromatic erythrocytes is an indication of induced chromosomal damage.

In this study, we present data on the presumptive genotoxic and cytotoxic effects of *Rosa alba* L. wastewater in two concentrations – 20% and 11% solution applying the bone marrow test system scheme by Preston et al. (1987) and Darzynkiewicz et al. (1987), as well as the *in vivo* mammalian erythrocyte micronucleus test (OECD, 2016).

Table 1. Clastogenic effect and antiproliferative activity of bone marrow cells in ICR line laboratory mice after *i.p.* supplementation with *R. alba L.* wastewater

			Type of chromosomal aberrations				
Compound and dose	*Time after treatment*	*Number of metaphases scored*	*Breaks*	*fragments*	*Rearrangements* **c/c**	*% of cells with aberrations (mean±SD)*	*Mitotic index (‰) (mean±SD)*
Rosa alba L. wastewaters *20 %*	24 h	*400*	**4**	**4**	**18**	**2.0 ± 1.51**	**16,83 ± 3.18**
	48 h	*400*	**1**	**3**	**19**	**1.0 ± 1.07**	**10.49 ± 1.79**
Rosa alba L. wastewaters *11 %*	24 h	*400*	**2**	**1**	**17**	**0.75 ± 1.03**	**8.91 ± 3.07**
	48 h	*400*	**1**	**2**	**17**	**0.75 ± 1.49**	**13.87 ± 4.10**
MNNG (50μg/mL)	24 h	*400*	**18**	**17**	**4**	**10.75 ± 4.27**	**11.25 ± 3.59**
	48 h	*400*	**21**	**19**	**14**	**13.00 ± 3.38**	**11.21 ± 2.68**
Control 0.9%NaCl	24 h	*350*	**0**	**5**	**11**	**1.14 ± 1.57**	**17.73 ± 2.99**
	48 h	*500*	**0**	**0**	**3**	**0.6 ± 0.3**	**16.88 ± 0.56**

c/c – centromere/centromeric fusion

Chromosomal aberration assay

The data about the percentage of chromosomal aberration frequencies (breaks and fragments) and mitotic indices are presented in Table 1.

Cytogenetic analysis revealed breaks, fragments, translocations, and other chromosomal rearrangements in the bone marrow metaphase plates. Centromere-centromeric fusions predominate. These chromosomal rearrangements

lead to the appearance of biarmed chromosomes without altering the amount of genetic material. Breaks and fragments were presented almost equally in all experimental groups. Chromatid type of aberrations (breaks and fragments) in metaphases may occur in response to single-chain ruptures induced in the early S phase, as well as a result of incomplete or unsuccessful reparation (Pfeiffer et al., 2000).

The percentage of aberrant mitoses in the experimental mice group, treated with 20% solution of *Rosa alba* L. wastewaters, calculated at the 24th hour from the beginning of the experiment was 2.0% ± 1.51 and slightly decreased at 48th h (1.0% ± 1.07), but the means are not significantly different (p>0.05).

The results about the percentage of cells with chromosomal aberrations showed a slight reduction in the percentage of mitoses with aberrations (0.75% ± 1.03 and 0.75% ± 1.49) in the bone marrow mice cells, treated with 11% wastewater at the 24th and 48th h compared to the data in 20% wastewater treated groups, but the difference is not statistically significant (p>0.001). The data of experimental groups, treated with wastewater in both concentrations (20% and 11%), are statistically undistinguishable from those calculated in the 0.9% NaCl control groups (p>0.001) (t_{st}=1.0755 and t_{st}=0.579, respectively) (Fig. 1).

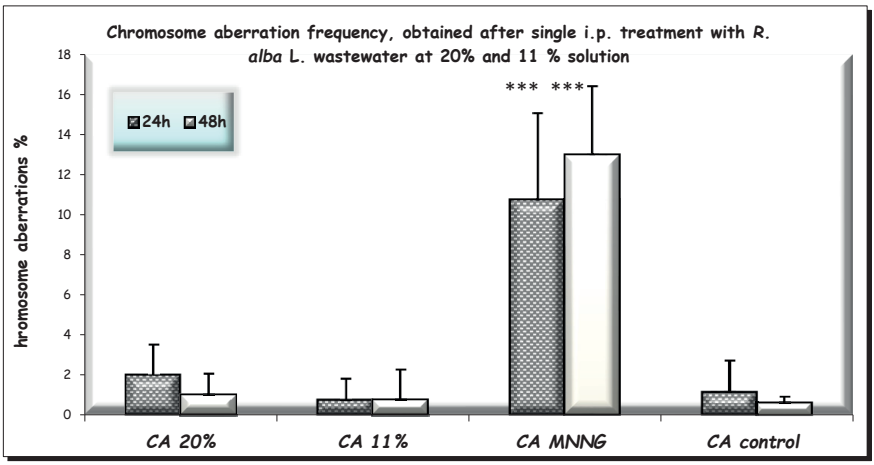

Figure 1. Frequency of chromosomal aberrations (CA) observed after *Rosa alba* L. wastewater treatment (20% and 11 % wastewater solution) in bone marrow of ICR mice. Data are expressed as mean ± SD; ***p<0.001 compared with the positive control MNNG.

Obviously, the number of aberrant metaphases in all experimental groups is dramatically lower in comparison with the relevant values obtained for the positive control group (MNNG 50μg/mL) (10.75% ± 4.27 and 13.00% ± 3.38) (t=5.2915 and t=7.202, respectively) (p<0.001).

The results of our experiments clearly showed that the tested wastewater concentrations from *Rosa alba*'s water-steam distillation does not cause a real clastogenic effect in the bone marrow cells of the experimental mouse line.

These results are consistent with the data of *in vitro* cytotoxicity assay (Sabahi et al., 2020). Authors tested a range of concentrations of *R. damascena* polyphenol-enriched fraction (25–100 μg/mL) and the results did not show any genotoxicity, so these concentrations could be considered as nongenotoxic. The comet assay analysis in the same paper showed that this *R. damascena* polyphenol-enriched wastewater fraction (25–100 μg/mL) protects human lymphocytes against H_2O_2-induced DNA damages significantly. This, according to the authors, is attributable to that the phenolic compounds reduce free radicals' side effects before they induce any DNA damages.

Mitotic index

The mitotic index as a measure of the proliferation status in treated with *Rosa alba* L. wastewater bone marrow cell populations displays a different picture from that described in the experimental chromosomal aberration test assessment (Fig. 2). The results showed a significant decrement in mitotic activity of bone marrow cells at the 48th hour compared to the 24th hour experimental group in 20% wastewater concentrations tested (p<0.001).

On the contrary, MI significantly increases at the 48thh in the lower concentration tested – 11% (p<0.05). This contradictory result is also repeated when we compare the MI data in bone marrow cells of 20% and 11% wastewater treated animal groups at the 24th h from the beginning of the experiment (p<0.001). The means were not statistically distinguishable in 48th h mice group (p>0.05) - at the 48th hour the mitotic activity was not suppressed in the lower *R. alba* L. concentration tested (11% wastewater solution). A longer period of treatment (48 hours) does not provide clear evidence of cytostatic effect, i.e. does not significantly affect the mitotic cycle preparation and progression in stem bone marrow cells population.

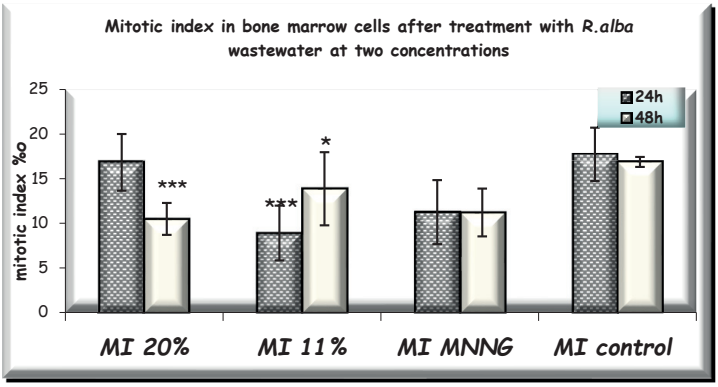

Figure 2. Value of mitotic activity (MI) observed after *Rosa alba* L. wastewater treatment in bone marrow cells. Data are expressed as mean ± SD. *p<0.05; ***p<0.001 compared with the negative control group.

The values of MI as an indication of the degree of cytotoxicity in the treated bone marrow cell population were compared with those in the negative control groups. These data show that acute treatment with *R. alba* L. wastewater for a short period of time (24 hours) leads to a suppression of dividing activity in bone marrow cells only in the experimental group, treated with the lower dose (11% solution of *R. alba* wastewater) (p<0.001).

With regard to the values for the mitotic index in all experimental variants there is no significant difference compared to the values for MI obtained in the positive control (MNNG) (p>0.05), with one exception - 20%/24h *R. alba* L. wastewater (t_{st}=3.523) (p<0.01).

This significant reduction in mitotic activity of bone marrow cells in almost all tested concentrations points that *R. alba* L. wastewater in the concentrations applied significantly influences the replicative capacity of the cells.

Such dose-dependent antiproliferative activity in immortalized human keratinocytes with half maximal inhibitory concentration (IC50) of 9.78 μg/mL was reported by Wedler et al. (2016). Authors pointed that the polyphenol-enriched wastewater fraction from *Rosa damascena* Mill. could be developed as a supportive therapy against hyperproliferation-involved skin diseases. Antiproliferative activity of geraniol in cancer cells has been also reported by Carnesecchi et al. (2002; 2004) using various assays. Sabahi et al. (2020) pointed out that polyphenol-enriched *R. damascena* fraction exerted significant cytotoxicity *in vitro* at a concentration of 100 μg/ml and higher.

Consistent with the above mentioned, this flavonoid content is apparently the reason for the observed reduction in mitotic activity in bone marrow cells. In the wastewater sample of *Rosa alba* L., used in our study, the phenolic composition was 7.6 mg GAE and 5.2 μg QueE/mL total flavonoid content.

Our results obtained for the antiproliferative effects of wastewater are logical due to the certain flavonoids contain, in particular quercetin, which is known for its inhibitory effect on cell division (Delgado et al., 2014; Klimaszewska-Wiśniewska et al., 2017). Klimaszewska-Wiśniewska et al. (2017) found that quercetin induced G_2/M arrest and polyploidy, and also exerted a dose-dependent cytotoxic effect on the tested cells with an IC_{50} value of 74 μM. Authors suggested that "the possible mechanism underlying quercetin-induced mitotic catastrophe involves the perturbation of mitotic microtubules leading to monopolar spindle formation, and, consequently, to the failure of cytokinesis".

Table 2. *In vivo* micronucleus test, performed in ICR line laboratory mice after single *i.p*. supplementation with *R. alba* L. wastewater. The frequencies of micronuclei in peripheral blood erythrocytes are presented as mean ± standard deviation per group.

Compound and dose	*Time after treatment*	*Number of animals*	*Number of PCE scored*	*Total MNPCE*	*MNPCE/4000 PCE (%) Mean ± SD %*	*PCE/(PCE+NCE) (%) Mean ± SD %*
Rosa alba L. wastewater *20%*	48 h	**4♂ 4♀**	**32561**	**48**	**0.15 ± 0.02**	**8.57 ± 0.84**
Rosa alba L. wastewater *11%*	48 h	**4♂ 4♀**	**32373**	**30**	**0.09 ± 0.03**	**9.25 ± 1.66**
MNNG (50μg/mL)	48 h	**4♂ 4♀**	**32681**	**226**	**0.69 ± 0.03**	**8.67 ± 1.50**
Control 0.9%NaCl	48 h	**4♂ 4♀**	**32600**	**20**	**0.06 ± 0.01**	**21.27 ± 2.77**

Total MNPCE – total number of observed MN in at least 4000 PCE per animal; MNPCE – micronucleated polychromatic erythrocytes; PCE - polychromatic erythrocyte; NCE – normochromatic erythrocyte;

Since polyphenols are the major component of wastewaters (Wedler et al., 2016; Sabahi et al., 2020), such investigations are important in the context of further efforts to create appropriate technology for rose wastewater utilization to reduce the disposal of the product with a large volume and valuable composition.

Micronucleus assay

Throughout the test period, no signs of toxicity were detected in any of the animals, treated with the listed substances.

The rodent erythrocyte MN assay, according to the regulatory requirements (The National Toxicology Program, OECD TG, Rothfuss et al., 2011), is usually the first choice among *in vivo* assays for subsequent testing when *in vitro* gentotoxicity tests proved to be positive. In the experimental scheme presented in this paper, a single-dose regimen was applied, thus only MNPCEs were taken into account for determining a positive result. The number of MNPCE was given separately for each treatment group. The results of the micronucleus assay with peripheral blood erythrocytes are summarized in Table 2.

Table 2. *In vivo* micronucleus test, performed in ICR line laboratory mice after single *i.p*. supplementation with *R. alba* L. wastewater. The frequencies of micronuclei in peripheral blood erythrocytes are presented as mean ± standard deviation per group.

Compound and dose	*Time after treatment*	*Number of animals*	*Number of PCE scored*	*Total MNPCE*	*MNPCE/4000 PCE (%) Mean ± SD %*	*PCE/(PCE+NCE) (%) Mean ± SD %*
Rosa alba L. wastewater *20%*	48 h	**4♂ 4♀**	**32561**	**48**	**0.15 ± 0.02**	**8.57 ± 0.84**
Rosa alba L. wastewater *11%*	48 h	**4♂ 4♀**	**32373**	**30**	**0.09 ± 0.03**	**9.25 ± 1.66**
MNNG (50μg/mL)	48 h	**4♂ 4♀**	**32681**	**226**	**0.69 ± 0.03**	**8.67 ± 1.50**
Control 0.9%NaCl	48 h	**4♂ 4♀**	**32600**	**20**	**0.06 ± 0.01**	**21.27 ± 2.77**

Total MNPCE – total number of observed MN in at least 4000 PCE per animal; MNPCE – micronucleated polychromatic erythrocytes; PCE - polychromatic erythrocyte; NCE – normochromatic erythrocyte;

Initially, the ratio of PCE to total erythrocytes (PCE+NCE) was determined for each animal and used as an index of cytotoxicity. These ratios showed significant differences only among the *R. alba* treatment groups (20% and 11%) and the negative control group ($p<0.01$ and $p<0.001$, respectively) (Table 2). In presence of *R. alba* wastewater, the percentage PCE decreased significantly, which may indicate a suppression of bone marrow proliferation probably due to mitotic arrest. The lack of statistical significance between the positive control group (treated with the model alkylating agent MNNG 50μg/mL) and the two wastewater concentrations ($p>0.001$) supports this assumption since MNNG is well known mutagen and is cytotoxic to mammalian cells (O'Brien & Brown, 2006).

The MNPCE frequencies were statistically significant and did yield dose-dependent pattern among the two wastewater treatment groups ($p<0.001$). *R. alba* wastewater at concentration of 20% significantly increased the frequency on MNPCE from 0.06% ± 0.01 (mean value for the positive control group) to 0.15% ± 0.02 ($p<0.001$). A statistically significant increase in the incidence of MNPCE over the control value was also observed following treatment with 11 % *R. alba* wastewater (0.09% MNPCE/4000 PCE, $p<0.05$) (Fig. 3).

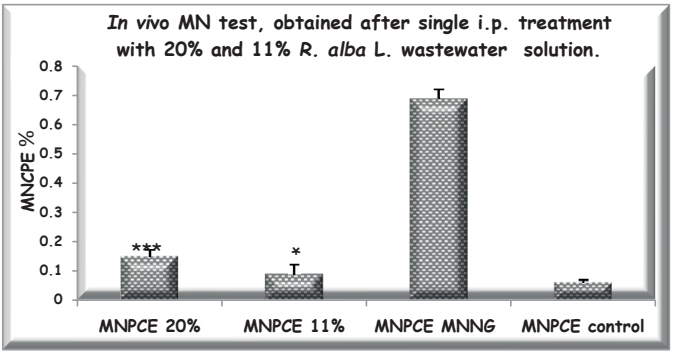

Figure 3. Induction of MN observed after *Rosa alba* L. wastewater treatment in peripheral polychromatic erythrocytes. Data are expressed as mean ± SD. *$p<0.01$ and ***$p<0.001$ compared with the negative control.

These results are consistent with the data of Gateva et al. (2021), who reported that *in vitro* treatment with Rosa alba L. oil in a range of concentrations from 50 to 500 μg/mL enhanced the frequency of micronuclei in dose-related manner. The formation of micronuclei increased above two-fold compared to the negative control in human lymphocyte cultures.

Regarding wastewater, the original results obtained by us are difficult to compare with literature data. This is especially true for the scarce experimental data on genotoxic activity. There are some data for the individual components of wastewater - flavonoids and polyphenols, as well as for the main product of water-steam distillation of R. alba L. - rose oil.

Geraniol is one of monoterpenes, present in high percentage in *Rosa alba* L. waste biomass (Slavov et al., 2017), in hydrosol (Georgieva et al., 2019) as well as in *Rosa alba* L. essential oil (Gateva et al., 2021). It was found to possess well-expressed antioxidant properties. Geraniol was tested for cytotoxicity and genotoxicity by Doppalapudi et al. (2007). The authors observed that geraniol did not induce a significant increase in bone marrow micronucleus of mice treated with 375, 750, and 1500 mg/kg. No statistically significant increases in the frequency of micronucleated PCE were seen at any dose level in either male or female mice at the 24 or 48 h time point, and there was no dose-related increase in the frequency of micronuclei.

Our results demonstrated a slight increase in the frequency of MNPCE in treated with *Rosa alba* L. wastewater animals, which is an indication of induced chromosome damage, which ends up as MN.

Conclusion

Under the conditions employed in this study, our results suggested that the white oil-bearing rose *Rosa alba* L. distillation wastewater extracts at 20% and 11% doses did not induce a considerable amount of CAs. The reported low percentage of breaks and fragments in bone marrow cells of experimental ICR mice can be considered as a sure indicator, predicting the absence of clastogenic wastewater effect (lack of significant chromosome-damaging action). This result was accompanied by cell proliferation inhibition in ICR mice bone marrow following intraperitoneally administration of both wastewater concentrations, compared to the negative control group ($p<0.001$).

As an additional standard battery for genotoxicity - rodent erythrocyte micronucleus assay in peripheral blood was applied *in vivo*. From the results is evident that *Rosa alba* L. wastewater was determined to induce a slightly increased frequency of micronuclei in peripheral blood erythrocytes of male and female ICR mice under the present experimental conditions.

Rosa alba L. wastewater solution in both concentrations applied showed a negligible genotoxic effect, but a slight antiproliferative effect.

Disclosure statement

No potential conflict of interest was reported by the authors.

Acknowledgements

The team expresses heartfelt thanks to the financial support of Project of Bulgarian National Sciences Fund КП-06 H36/17 (granted to Assoc. prof. M. Mileva, PhD)

References

1. ABDEL-HAMEED E, BAZAID S, SABRA A. Total phenolic, *in vitro* antioxidant activity and safety assessment (acute, sub-chronic and chronic toxicity) of industrial taif rose water by-product in mice, *Pharmaceutical Letter*, 2015; 7(2): 251–259.
2. ALMONTE-FLORES DC, PANIAGUA-CASTRO N, ESCALONA-CARDOSO G, ROSALES-CASTRO M. Pharmacological and Genotoxic Properties of Polyphenolic Extracts of *Cedrela odorata* L. and *Juglans regia* L. Barks in Rodents. Evidence-based complementary and alternative medicine. *eCAM*. 2015; 187346. doi.org/10.1155/2015/187346
3. BAKKALI F, AVERBECK S, AVERBECK D, IDAOMAR M. Biological effects of essential oils - a review. *Food and Chem Toxicol*. 2008; 46: 446-475. doi: 10.1016/j.fct.2007.09.106
4. CARNESECCHI S, BRAS-GONCALVES R, BRADAIA A, ZEISEL M, GOSSÉ F, POUPON M-F, RAUL F. Geraniol, a component of plant essential oils, modulates DNA synthesis and potentiates 5-fluorouracil efficacy on human colon tumor xenografts. *Cancer Lett*. 2004; 215(1): 53-59. doi: 10.1016/j.canlet.2004.06.019
5. CARNESECCHI S, LANGLEY K, EXINGER F, GOSSE F, RAUL F. Geraniol, a component of plant essential oils, sensitizes human colonic cancer cells to 5-Fluorouracil treatment, *J. Pharmacol. Exp. Ther*. 2002; 301(2):625-630. doi: 10.1124/jpet.301.2.625
6. CHAHAR MK, SHARMA N, DOBHAL MP, JOSHI YC. Flavonoids: A versatile source of anticancer drugs. *Pharmacogn Rev*.2011; 5(9): 1–12. doi: 10.4103/0973-7847.79093
7. DARZYNKIEWICZ Z. Cytochemical probes of cycling and quiescent cells applicable to flow cytometry. In: *Techniques in Cell Cycle Analysis (Biological Methods) 1987th Edition*, Kindle Edition by Joe W. Gray (Author), Zbigniew Darzynkiewicz, 1987; 272 – 290. ISBN-13: 978-0896030978
8. DELGADO A, FERNANDES I, GONZÁLEZ-MANZANO S, DE FREITAS V, MATEUS N, SANTOS-BUELGA C. Anti-proliferative effects of quercetin and catechin metabolites *Food Funct*. 2014; 5(4): 797-803. doi: 10.1039/c3fo60441a
9. DOBREVA A, KOVATCHEVA N, ASTATKIE T, ZHELJAZKOV VD. Improvement of essential oil yield of oil-bearing (*Rosa damascena* Mill.) due to

surfactant and maceration. *Ind Crop Prod*. 2011; 34:1649–1651. doi:10.1016/j.indcrop.2011.04.017
10. DOPPALAPUDI RS, RICCIO ES, RAUSCH LL, SHIMON JA, LEE P, MORTELMANS K, KAPETANOVIC I, Crowell J, MIRSALIS J. Evaluation of chemopreventive agents for genotoxic activity. *Mutat. Res*. 2007; 629: 148-160. https://doi.org/10.1016/j.mrgentox.2007.02.004
11. GATEVA S, JOVTCHEV G, CHANEV C, GEORGIEVA A, STANKOV A, DOBREVA A, MILEVA M. Assessment of anti-cytotoxic, anti-genotoxic and antioxidant potential of Bulgarian *Rosa alba* L. essential oil. *Caryologia*. 2020; 73(3): 71-88. doi: 10.13128/caryologia-260.
12. GEORGIEVA A, DOBREVA A, TZVETANOVA E, ALEXANDROVA A, MILEVA M. Comparative study of phytochemical profiles and antioxidant properties of hydrosols from Bulgarian *Rosa alba* L. and *Rosa damascena* Mill., *Journal of Essential Oil Bearing Plants*, 2019; 22(5): 1362-1371, DOI: 10.1080/0972060X.2019.1699867
13. GOCHEV V, DOBREVA A, GIROVA T, STOYANOVA A. Antimicrobial activity of essential Oil from *Rosa alba*. *Biotechnology & Biotechnological Equipment*, 2010; 24(1): 512-515. DOI: 10.1080/13102818.2010.10817892
14. HAYASHI M, MORITA T, KODAMA Y, SOFUNI T, ISHIDATE JR.M. The micronucleus assay with mouse peripheral blood reticulocytes using acridine orange-coated slides. *Mutat. Res. Letters*. 1990; 245(4): 245-249. https://doi.org/10.1016/0165-7992(90)90153-B
15. HAYASHI M, SOFUNI T, ISHIDATE M. An application of Acridine Orange fluorescent staining to the micronucleus test. *Mutation Research Letters*. 1983; 120(4): 241-247. doi: 10.1016/0165-7992(83)90096-9
16. KLIMASZEWSKA-WIŚNIEWSKA A, HAŁAS-WIŚNIEWSKA M, IZDEBSKA M, GAGAT, M, GRZANKA A, GRZANKA D. Antiproliferative and antimetastatic action of quercetin on A549 non-small cell lung cancer cells through its effect on the cytoskeleton. *Acta Histochemica.* 2017; 119(2): 99-112. https://doi.org/10.1016/j.acthis.2016.11.003
17. KOVACHEVA N, RUSANOV K, ATANASSOV I. Industrial cultivation of oil bearing rose and rose oil production in Bulgaria during 21st century, directions and challenges. *Biotechnol Biotechnol Eq.* 2010; 24:1793–1798. doi:10.2478/ V10133-010-0032-4
18. LUCA VS, MIRON A, APROTOSOAIE AC. The antigenotoxic potential of dietary flavonoids. *Phytochem Rev*. 2016; 15: 591–625. https://doi.org/10.1007/s11101-016-9457-1
19. MILEVA M, KUSOVSKI V, KRASTEV D, DOBREVA A, GALABOV A. Chemical composition, *in vitro* antiradical and antimicrobial activities of Bulgarian *Rosa alba* L. essential oil against some oral pathogens. *Int. J. Curr. Microbiol. App. Sci*. 2014; 3(7): 11-20. ISSN: 2319-7706
20. MITKOVSKA V, CHASSOVNIKAROVA TS, ATANASOV N, DIMITROV H. Environmental genotoxicity evaluation using a micronucleus test and frequency of chromosome aberration in free-living small rodents. *J. BioSci. Biotech*. 2012; 1(1): 67-71. ISSN: 1314-6246
21. NAIKWADE NS, MULE SN, ADNAIK RS, MAGDUM CS. Memory-enhancing activity of *Rose alba* in mice. *International Journal of Green Pharmacy*. 2009; 3(3): 239-242. ISSN: 0973-8258
22. O'BRIEN V, BROWN R. Signalling cell cycle arrest and cell death through the MMR System, *Carcinogenesis*. 2006; 27(4): 682–692, https://doi.org/10.1093/carcin/bgi298
23. OECD, 2016. OECD test guideline No. 474 for the testing of chemicals https://www.oecd-ilibrary.org/docserver/9789264264762en.pdf?expires=1616068940&id=id&accname=guest&checksum=80F54DA4886040B71182A492D85C19FE
24. PRESTON R, DEAN B, GALLOWAY S, HOLDEN H, MCFEE A, SHELDY M. Mammalian *in vivo* cytogenetic assay analysis of chromosome aberrations in bone marrow cells. *Mutation Research/Genetic Toxicology.* 1987; 189(2): 157–165. https://doi.org/10.1016/0165-1218(87)90021-8
25. PFEIFFER P, GOEDECKE W, OBE G. Mechanisms of DNA double-strand break repair and their potential to induce chromosomal aberrations. Mutagenesis. 2000 Jul;15(4):289-302. doi: 10.1093/mutage/15.4.289. PMID: 10887207.
26. ROTHFUSS A, HONMA M, CZICH A, AARDEMA M, BURLINSON B, GALLOWAY S, HAMADA S, KIRKLAND D, HEFLICH R, HOWE J, NAKAJIMA M, O'DONOVAN M, PLAPPERT-HELBIG U, PRIESTLEY C, RECIO L, SCHULER M, UNO Y, MARTUS H-J. Improvement of *in vivo* genotoxicity assessment: Combination of acute tests and integration into standard toxicity testing. *Mutation Research/Genetic Toxicology and Environmental Mutagenesis*. 2011; 723(2): 108-120. https://doi.org/10.1016/j.mrgentox.2010.12.005
27. SABAHI Z, FARMANI F, MOUSAVINOOR E, MOEIN M. Valorization of waste water of *Rosa damascena* oil distillation process by Ion exchange chromatography. *Sci World J*. 2020; 5409493. doi: 10.1155/2020/5409493. eCollection 2020.
28. SCHMID W. The micronucleus test. *Mutation Research*. 1975; 31: 9–15. https://doi.org/10.1016/0165-1161(75)90058-8
29. SHOHAYEB M, ABDEL-HAMEED S, BAZAID SA, MAGHRABI I. Antibacterial and antifungal activity of *Rosa damascena* Mill. essential oil, different extracts of rose petals. *Global Journal of Pharmacology*. 2014; 8(1): 1–7. DOI: 10.5829/idosi.gjp.2014.8.1.81275
30. SLAVOV A, VASILEVA I, STEFANOV L, STOYANOVA A. Valorization of wastes from the rose oil industry. *Reviews in Environmental Science and Bio/Technology*. 2017; 16(2): 309–325. https://doi.org/10.1007/s11157-017-9430-5

31. WEDLER J, RUSANOV K, ATANASSOV I, BUTTERWECK VA. Polyphenol-enriched fraction of rose oil distillation wastewater inhibits cell proliferation, migration and TNF-α-induced VEGF secretion in human immortalized keratinocytes. *Planta Med.* 2016; 82(11-12): 1000-1008. doi: 10.1055/s-0042-105158

32. YON JM, KIM YB, PARK D. The ethanol fraction of white rose petal extract abrogates excitotoxicity-induced neuronal damage *in vivo* and *in vitro* through inhibition of oxidative stress and proinflammation. *Nutrients.* 2018; 10(10): 1375. doi: 10.3390/ nu10101375.

ISSN print: 1224-5984
ISSN online: 2248-3942

Rom Biotechnol Lett. 2022; 27(1): 3302-3308
doi: 10.25083/rbl/27.1/3302-3308

Received for publication, December, 01, 2021
Accepted, January, 18, 2022

Original paper

In vitro elicitation supports the enrichment of 2H4MB production in callus suspension cultures of D. hamiltonii Wight & Arn

UMASHANKAR KOPPADA, PRADEEP MATAM, GIRIDHAR PARVATAM

Plant Cell Biotechnology Department, Council of Scientific and Industrial Research – Central Food Technological Research Institute, Mysore – 570 020, Karnataka, India

Abstract Influence of elicitation on *in vitro* production of 2-Hydroxy-4-Methoxy Benzaldehyde (2H4MB), a structural isomer of vanillin from callus suspension cultures of *Decalepis hamiltonii* was investigated. *In vitro* culture conditions were optimized to induce callus, suspension culture and biomass followed by metabolite production. Suspension cultures were established using leaf generated friable callus. Maximum content of 2H4MB production 0.079 ± 0.01 mg $100g^{-1}$ DW and biomass 197.5 ± 1.5 gL^{-1} were observed by 4^{th} week of culturing. Elicitation was induced to suspension cultures by using *m*-topolin (*m*T), sodium nitroprusside (SNP), and pectin individually at different concentrations. *m*-topolin (15 µM), pectin (15 µM) and SNP (10 µM) supported 0.31 mg$100g^{-1}$ DW, 0.27 mg$100g^{-1}$ DW and 0.21 mg$100g^{-1}$ of 2H4MB production respectively by 4^{th} week. This data infers that the elicitation improves 2H4MB content in callus suspension cultures of *D. hamiltonii*.

Keywords Biomass, Elicitor, Callus cell suspension cultures, *Meta*-topolin (N6-(meta-hydroxybenzyl) adenine), Sodium nitroprusside (SNP), Pectin

To cite this article: KOPPADA U, MATAM P, PARVATAM G. In vitro elicitation supports the enrichment of 2H4MB production in callus suspension cultures of D. hamiltonii Wight & Arn. *Rom Biotechnol Lett*. 2022; 27(1): 3302-3308. DOI: 10.25083/rbl/27.1/3302-3308.

*Corresponding author: GIRIDHAR PARVATAM, In vitro elicitation supports the enrichment of 2H4MB production in callus suspension cultures of D. hamiltonii Wight & Arn.
E-mail: giridharp@cftri.res.in

Introduction

Secondary metabolites produced by the plants have wide range of application as industrial raw materials, in medicines, food products as enzymes, and flavour etc**.** Flavors originate from the natural sources mostly from plants have high commercial value. Vanillin is one such metabolite obtained from plants which has wide application in flavoring industry. *Vanilla planifolia* and *V. tahitensis* are major natural sources for the production of vanillin flavor. Due to its high demand and inadequate availability of natural vanillin, synthetically manufactured vanillin is brought in to application to meet the demand. But this has not been readily accepted in some countries due to regulatory guidelines thereby natural vanillin is having persistent demand (Vaithanomsat P & al [1]**).** 2-Hydroxy-4-methoxybenzaldehyde (2H4MB) is an isomer of vanillin, has sweet fragrance can be readily used as alternative to synthetic vanillin. 2H4MB is reported to synthesized through phenyl propanoid pathway and present in few plant species such as *Decalepis hamiltonii, Hemidesmus indicus* (Mehmood Z & al [2]), *Mondia whytei* and root bark of *Periploca sepium* (Yamashita Shi J &al [3]). In *Decalepis hamiltonii* tubers 2H4MB constitutes 96% of volatile oil, hence is the major aromatic compound and its flavor extract is recognized as GRAS by United States Food and Drug Authority (Nagarajan S & al [4]. 2H4MB along with other bioactives reported to have many bioactive properties like antioxidant antimicrobial, and hepatoprotective etc. (Pradeep M & al [5]. This endemic plant *D. hamiltonii* familiar as swallow root, for its rich aroma and bioactives has been constantly over exploited from ages for various applications and currently in the state of endanger.

Plant tissue culture is a promising technique in which *in vitro* production of secondary metabolites in plant cell suspension cultures has been reported from various food and medicinal plants (Dias MI & al [6]). In *D.hamiltonii,* tissue culture technique is reported to be extensively used for cultivation of plants using nodal explants (Obul Reddy B & al [7]), (Sharma S & al [8]) shoot tips (Giridhar P & al [9]), and *in vitro* rooting of micro shoots (Reddy BO & al [10]). Similar, efforts were made to enhanced production of flavor metabolites through precursor feeding in cell suspension cultures (Pradeep M & al [11]). Nitric oxide as a bioactive molecule is biosynthesized during plant pathogen interactions and reported to exhibit proxidant as well as antioxidant properties in plants (Delledonne M & al [12]). It induces plant defense genes and accumulation of cyclic acid that leads to expression of systemic acquired resistance (Crawford NM & al [13]). Prior art indicates the presence of NO in the plant kingdom and its connection in growth, development (Beligni MV &al [14]), senescence (Jie TU & al [15]), defense responses (Arun M & al [16]) and *in vitro* regeneration (Tan BC & al [17]). SNP at high concentrations stimulated various secondary metabolites such as catharanthine in *Catharantuse roseus* (Xu J & al [18]), hypericin in *Hypericum perforatum* (Xu MJ & al [19]), phenols and flavonoids in Ginkgo biloba *in vitro* cultures (El-Beltagi HS & al [20]). *Meta*-topolin (N^6-(*meta*-hydroxybenzyl) adenine) is a highly active aromatic, unconventional cytokinin isolated and characterized from poplar leaves (Strnad M & al [21]). Meta-topolin has been shown to promote *in vitro* shoot proliferation and improve quality of shoots in several plant species (Aremu AO & al [22]). The potential of *m*T to induce organogenesis from somatic embryo derived cotyledon explants in Cassava (Chauhan RD & al [23]), *Opuntia stricta* (Souza M & al [24]) and *Corylus colurna* (Gentile A & al [25]) was assessed. It is reported to prevent oxidative stress in sugar cane micropropagation (Souza M & al [26]) and production of flavonoids of *Amburana cearensis* (Vasconcelos JNC & al [27]).

However, there are no reports regarding the influence of elicitation on callus suspension cultures of *D. hamiltonii*. As there is a demand in the market for natural flavor (Giridhar P & al [28]), experiments to obtain flavor metabolites through tissue culture will facilitate effective potentiation. Elicitation is technique which was reported to be most significant approach in enhancement of metabolites (Saini RK& al [29]), (Sridevi V & al [30]). Biotic and abiotic elicitors are reported to increase accumulation of metabolites in plant *in vitro* and *in vivo* (Kim HJ & al [31]), (Perez-Balibrea S & al [32]). Accordingly, in the present study, investigations were carried out to determine potential benefit of m-topolin, sodium nitroprusside (SNP) and pectin for efficient augmentation of flavour metabolites, since no such studies on *D. hamiltonii* and its metabolites are available.

Materials and methods

Chemicals

Murashige and Skoog medium, 2, 4-Dichlorophenoxyacetic acid, (2, 4-D), Kinetin (Kn), m-topolin and Sodium nitroprusside (SNP) of plant tissue culture grade were purchased from Hi-media (Mumbai, India). 2H4MB standards was supplied by Fluka (Switzerland). Pectin from Sigma-Aldrich India. HPLC grade methanol and acetonitrile obtained from Merck (Mumbai, India)

Plant material and culture conditions

D. hamiltonii Wight & Arn., fruits were collected from 12 year old plant grown at Departmental garden in CSIR-Central Food Technological Research Institute, Mysore, India. The seeds were separated from the dried capsule and surface sterilization of seeds was done using 0.1% (w v^{-1}) mercuric chloride (Hi-media, Mumbai) for 5 min followed by washing (4-5 times) with autoclaved distilled water (Saini RK & al [29]). Sterilized seeds were inoculated in the MS media with 0.2 µM gibberellic acid (GA_3), (Murashige T,& Skoog F [33]) containing 3% (w·v^{-1}) sucrose (Hi-media, Mumbai) and 0.8% (w·v^{-1}) of agar (Hi-media, Mumbai) at 25 ± 2 °C under 45 µmol.m^{-2} s^{-1} light for 16 h photoperiod. The leaves of seedling were used as explant for callus induction.

Callus induction and development of suspension cultures

Leaves from 6 weeks old seedling plant were used as explants for callus induction. Leaves from seedling plant were chopped (leaf 1 sq.cm) and inoculated in MS medium containing 9.06 µM 2,4-D (2,4-D, Hi-media, Mumbai), in combination with 2.32 µM Kinetin (Kin, Hi-media, Mumbai), 3% (w/v) sucrose, and 0.8% (w/v) agar for solid

media (not for suspension culture) (Pradeep M & al [11]). The pH of the medium was adjusted to 5.8 and autoclaved at 121 °C for 15 min. Callus cultures were maintained at 25 ± 2 °C in 45 µmol.m^{-2} s^{-1} light for 16 h photoperiod. These calluses were sub-cultured every 4 weeks. The friable callus mass that was obtained after two subcultures was used for preparation of suspension cultures. This callus was transferred to 150 ml conical flasks containing 40 ml liquid medium and grown for 8 weeks on a rotary shaker at 95 rpm at 24 ± 2 °C in 16 h photoperiod.

Elicitor treatment

Preparation of elicitor stock solution

Stock solution of 1M concentration *m*-topolin was prepared by dissolving in 0.5N KOH solution. Similarly, sodium nitroprusside, and pectin stock solutions were prepared in sterile distilled water. These stock solutions were sterilized by filtering through 0.22 µm PVDF membrane filters (Durapore) and were inoculated in known concentration to *in vitro* callus cell suspension cultures of *D. hamiltonii.*

Elicitation in callus suspension cultures

m-topolin, pectin, and SNP were added to callus suspension cultures in different concentrations (10, 15 and 20 µM) for evaluation of callus growth and 2H4MB content. Suspension cultures without elicitor was also maintained in similar conditions as a control. Callus biomass was harvested from the suspension culture medium after every week (1st to 4th week) to record callus biomass accumulation as fresh weight (FW) and content of 2H4MB. All the experiments were performed with three replicates for each concentration treatment and the experiment was conducted twice.

Extraction of metabolites

The 2H4MB content from the callus was extracted as described earlier(Pradeep M & al [11]). Callus from suspension cultures were separated using Whatman no.1 filter paper. The solvent extract thus obtained was evaporated to dryness under vacuum. The cell mass in the filter paper was thoroughly washed with distilled water and dried in an oven at 35^{0}C for 12 h, weighed and powdered with mortar and pestle. The powder thus obtained was extracted with 2 volumes of ethyl acetate and centrifuged at 10,000 rpm for 15 min. The supernatant was concentrated and dried under vacuum. The dried residue was dissolved with a known volume of methanol and the flavour attributing compounds such as 2H4MB were analyzed.

Screening of flavour metabolites by HPLC and MS analysis

The major flavour ascribing metabolites quantification and confirmation from the solvent extracts of *D. hamiltonii* callus was done by HPLC (SPD-20AD, Shimadzu, Kyoto, Japan) and MS(QTof Ultima Waters Corporation, Micro Mass UK) as reported earlier but with slight modification (Gururaj HB & al [34]). The isocratic mobile phase contained Methanol: Acetonitrile: Water: Acetic acid (47:10:42:1). C18 column (250 x 4.6 mm and 5-µm diameter) was used (Sunfire column, Waters Corporation, MA, USA) for the sample separation and analysis. The flow rate was maintained at 1 ml min^{-1} throughout analysis and the detection wavelength was 280 nm. The samples were respectively injected and mean area for three replicate analyses were calculated. Quantitative analysis was done based on the area of standard (Fluka, Switzerland) for which known amount was injected. 2H4MB in the samples were identified based on the retention time for the corresponding standard. The mass spectral data were accompanied by a Mass Lynux 4.0 SP4 data acquisition system. The ionization mode was negative(Pradeep M & al [11]).

Statistical analysis

The experiments were conducted in a completely randomized design with three replicates. Data were subjected to an analysis of variance (ANOVA). To determine the significant difference, Duncan's multiple range test (DMRT) was performed using SPSS software (Version 17).

Results and discussion

Culture establishment

Cell suspension cultures were developed on MS medium (without agar) containing 3% sucrose, with the combination of 2 mgL^{-1} 2,4-D and 0.5 mgL^{-1} Kinetin, wherein the biomass and 2H4MB content is observed to be good (Pradeep M & al [11]). The callus cultures biomass was observed at regular interval, which shows that the growth of the callus in suspension cultures had some physical changes that include color and texture. During the first week to second week the light greenish colored callus cells start changing their color to green, later by 4th week it was friable and dark green with 197.52 ± 1.48 gL^{-1} of biomass and after 8 weeks they turn brown with 184.23 ± 1.84 gL^{-1} of biomass (Fig 2a). Maximum 2H4MB production was recorded by 4th week (0.079 ± 0.01 mg100g^{-1} DW), but showed decline from 6th week (0.003 ± 0.014 mg100 g^{-1} DW) and 8th week (0.002 ± 0.031 mg 100 g^{-1} DW).

Elicitation with m-topolin (mT)

Callus cultured on MS medium supplemented with different concentration of *m*-topolin gave the highest level of 2H4MB among the treatment when compared to control. The results obtained for *D. hamiltonii* callus cultures suggest that their degree of differentiation had a significant influence on the biochemical synthesis of 2H4MB. However, significant accumulation of all the analyzed flavour metabolites 2H4MB was evident with maximum content at 4 weeks and then a depletion in the metabolites content was observed. There was a gradual increase in levels of flavour metabolites from 1st day to the 4th week. The maximum accumulation of 2H4MB was recorded as 0.31 ± 0.01 mg 100 g^{-1} DW in 4 weeks grown culture that supplemented with 15 µM *mT* as a cytokinin inducer (Fig.4). HPLC analysis of ethyl acetate extract of suspension cultures resulted in the detection of 2H4MB with a retention time of 8.5 min at wavelength of 280 nm in standard HPLC chromatogram. Quantitative HPLC determination (Fig. 3) of respective metabolites in samples showed that the contents of 2H4MB were notably higher in *mT* treated suspension cultures. *m*- topolin is reported to be use as an alternative to cytokinin in tissue culture as it has

a great influence on physiological property and in production of quality explant (Aremu AO & al [22]), (Ahmad N & al [35]). It was reported to improve *in vitro* morphogenesis, rhizogenesis and increase biochemical content in differ plants (Chauhan RD & al [23])(Gentile A & al [25], (Ahmad A & al [36]). Meta-topolin induced *in vitro* regeneration and enhanced the secondary metabolites in the leaf tissues (Khanam MN & al [37]). (Aremu AO & al [38]) reported higher phenolic production in 'Williams' banana treated with *mT* when compared to the BA-treated and control (PGR-free) plants. It is reported to prevent oxidative stress in sugar cane micro propagation (Souza M & al [24]) and production of flavonoids in *Amburana cearensis* (Vasconcelos JNC& al [27]).

Elicitation with Pectin

In the present study, pectin treatments to cultures resulted in only moderate change in their biomass with progressive increase from 2nd to 4th week (Fig.5a) in comparison to control. The maximum accumulation of 2H4MB 0.29 ± 0.01 mg $100g^{-1}$ DW was found in 4 weeks of cultured cells supplemented with 15 µM of pectin (Fig. 5b). The addition of pectin has shown a significant influence on cell growth in *Gymnema sylvestre* R. Br (VeerashreeV & al [39]). Pectin involved in activating secondary metabolism in *M. citrifolia* cell suspension cultures (Dornenburg H & al [40]), *Calendula officinalis* (Wiktorowska & al [41]*)*, and *Hypericum adenotrichum* (Yamaner O & al [42]) was known. Pectin's structure is a practically and fundamentally diverse class of galacturonic acid rich polysaccharides which can go through plentiful alteration with an accompanying change in physicochemical properties (Wolf S & al [43]).

Elicitation with Sodium nitroprusside (SNP)

The results obtained for *D. hamiltonii* callus cultures with SNP suggest that their degree of differentiation had a significant influence on the biochemical synthesis of 2H4MB (Fig 6). The maximum accumulation of 2H4MB 0.21 ± 0.01 mg100 g^{-1} DW was recorded in 4 weeks of cultured cells supplemented with 10 µM concentration of SNP and it was found to be significant (Fig.6). In plants, various environmental and hormonal stimuli are transmitted either directly or indirectly by nitric oxide (NO) signalling cascades (Delledonne M & al [12]), (Crawford NM & al [13]). A good number of reports reveal the significance of NO, and the usage of sodium nitroprusside (SNP) that form a transition metal nitroxyl anion (NO-) complexes (Beligni MV & al [14]), (Jie TU &al [15]). SNP in combination with auxin 2,4-D is reported to improve cell division that leads to embryonic cell formation in *Medicago sativa* (Ahmad N & al [35]) and shoot multiplication in vanilla (Tan BC & al [17]).

Conclusion

On the basis of our study augmented production of 2H4MB from callus suspension cultures has been demonstrated. The feeding of mT, SNP and pectin to *D. hamiltonii* callus suspension culture medium supports the augmented accumulation of 2H4MB, with substantial increase in 4.5 folds under m-topolin elicitation, followed by 3.6, 2.4 folds in presence of pectin and sodium nitroprusside, which act as a inducers for the cells to increase the production of 2H4MB. The optimized culture conditions conceivably can be applied for scale-up studies for 2H4MB production.

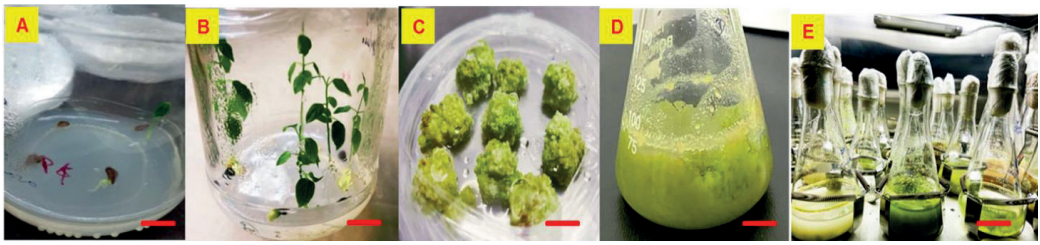

Figure 1. A *In vitro* plants germinated from seeds (bar=10 cm); **B** *In vitro* seedlings of *D. hamiltonii* (bar=10 cm); **C** Callus induction on medium bearing 2,4-D (9.06 µM) & kinetin (2.32 µM) (bar= 5 cm) **D** Callus cell suspension on medium with 9.06 µM 2,4-D and 2.32 µM kinetin after 4 weeks (bar=5 cm); **E** Rotary shaker with suspension cultures (bar=15cm)

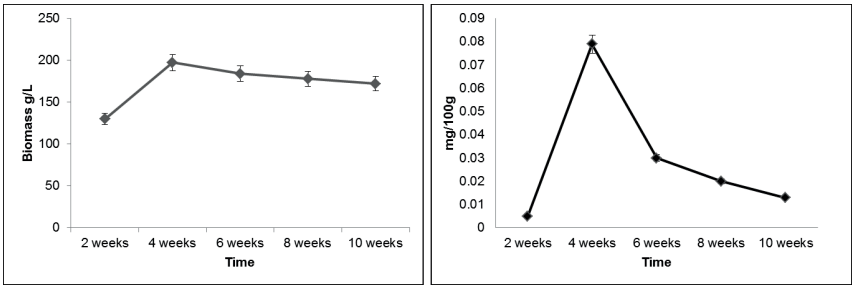

Figure 2. Callus growth and its 2H4MB quantification in suspension cultures. **a)** Callus biomass at different time intervals; **b)** 2H4MB content in callus during its growth.

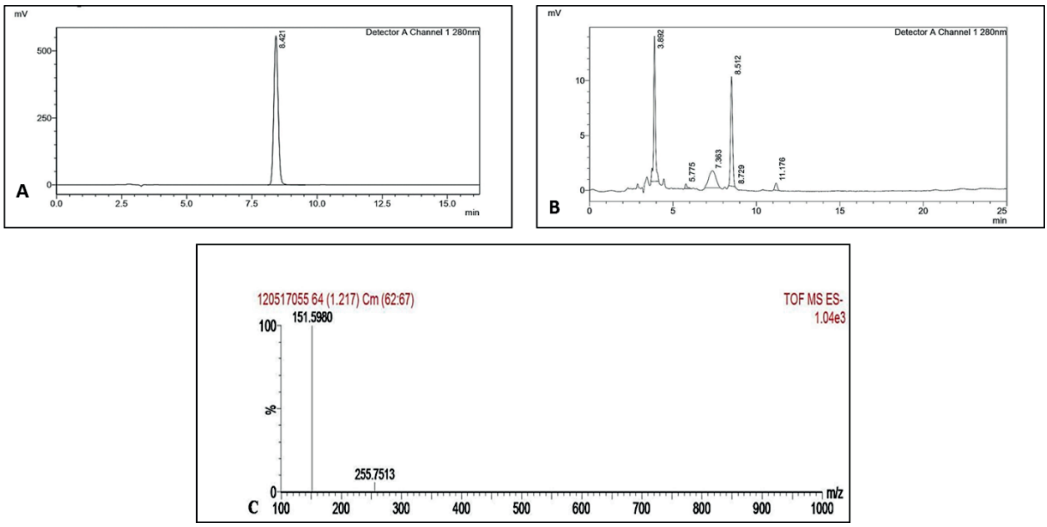

Figure 3. Quantification of 2H4MB using HPLC and confirmation by MS-ESI. **A)** 2H4MB standard; **B**) Chromatogram of Callus elicited with m-topolin ; **C)** MS fragment of 2H4MB Callus elicited with m-topolin

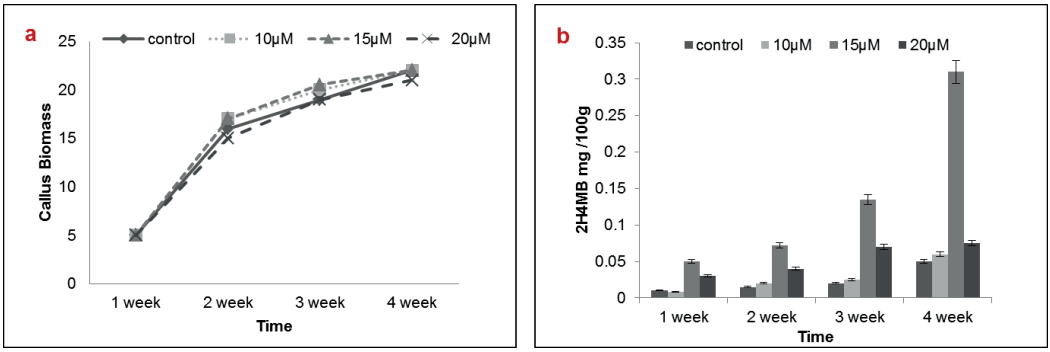

Figure 4. Influence of m topolin on callus suspension cultures. a) Callus biomass (FW); b) 2H4MB content.

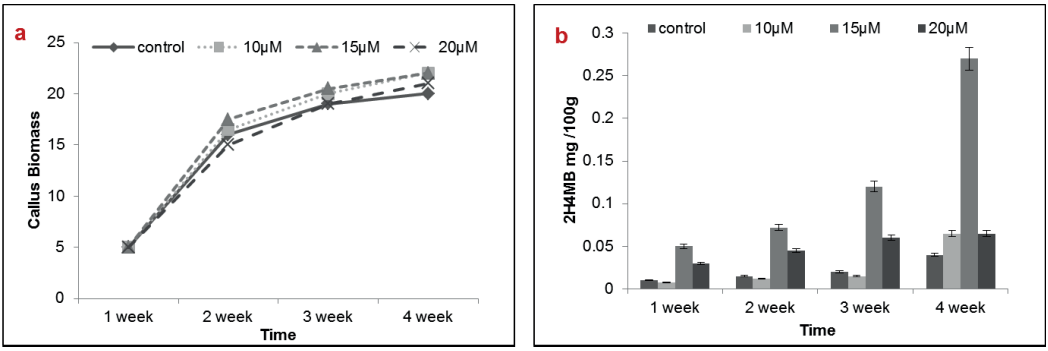

Figure 5. Influence of Pectin on callus suspension cultures. a) Callus biomass (FW); b) 2H4MB content.

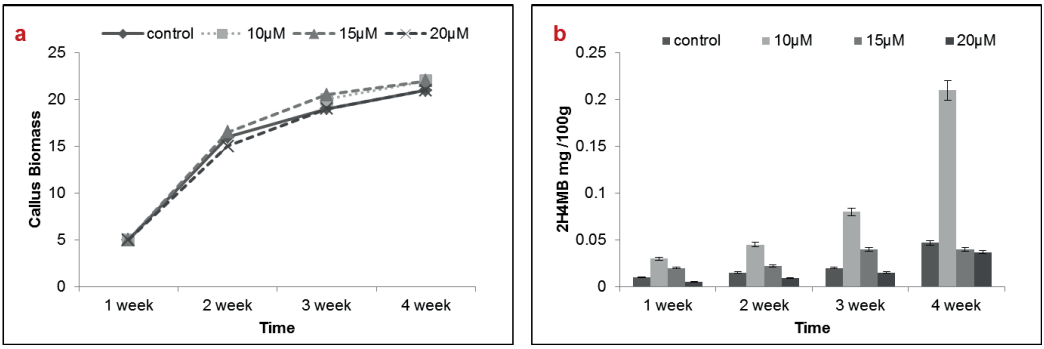

Figure 6. Influence of Sodium nitroprusside on callus suspension cultures. a) Callus biomass (FW); b) 2H4MB content.

Conflicts of Interest

The authors declare that there are no conflicts of interest.

Acknowledgements

The authors are thankful to SERB, New Delhi, India for funding the project (SERB/EMR/2016/001049). All the authors are thankful to Director, CSIR-CFTRI, Mysore for providing infrastructure and necessary facilities.

References

1. Vaithanomsat P, Apiwatanapiwat W. Feasibility study on vanillin production from *Jatropha curcas* stem using steam explosion as a pretreatment. *Inter J Chem Biolo Engr.* 2009; 3:839-842
2. Mehmood Z, Dixit AK, Singh A, et al. Indian Herb *Hemidesmus indicus* - A Potential Source of New Antimicrobial Compounds. 2016; 6:734-738. https://doi.org/10.4212/2161-0444.100042
3. Shi J, Yamashita T, Todo A, et al. Repellent from traditional Chinese medicine, *Periploca sepium* Bunge. *Zeitschrift fur Naturforschung Teil* C: *Biochemie, Biophysik, Biologie, Virologie.* 2007; 62:821-825
4. Nagarajan S, Rao LJM, Gurudutt KN. Chemical composition of the volatiles of *Decalepis hamiltonii* (Wight & Arn). *Flavour Fragance J.* 2001; 16:27–29. https://doi.org/10.1002/1099-1026(200101/02)16:1<27: AID-FFJ937>3.0.CO;2-F
5. Pradeep M, Kiran K, Giridhar P. A Biotechnological Perspective Towards Improvement of *Decalepis hamiltonii*: Potential Applications of Its Tubers and Bioactive Compounds of Nutraceuticals for Value Addition. In: Shahzad A, Sharma S, Siddiqui SA (eds) Biotechnological strategies for the conservation of medicinal and ornamental climbers. *Springer International Publishing, Cham*, 2016; pp 217-238
6. Dias MI, Sousa MJ, Alves RC, Ferreira ICFR. Exploring plant tissue culture to improve the production of phenolic compounds: A review. *Ind. Crops Prod.* 2016; 82:9-22. https://doi.org/10.1016/j.indcrop.2015.12.016
7. Obul Reddy B, Giridhar P, Ravishankar GA. The effect of triacontanol on micropropagation of *Capsicum frutescens* and *Decalepis hamiltonii* W & A. *Plant Cell Tiss Organ Cult.* 2002; 71:253-258. https://doi.org/10.1023/A:1020342127386
8. Sharma S, Shahzad A. Encapsulation technology for short-term storage and conservation of a woody climber, *Decalepis hamiltonii* Wight and Arn. *Plant Cell Tiss Organ Cult* 2012;111 :191-198. https://doi.org/10.1007/s11240-012-0183-0
9. Giridhar P, Gururaj HB, Ravishankar GA. *In vitro* shoot multiplication through shoot tip cultures of *Decalepis hamiltonii* Wight & Arn., a threatened plant endemic to Southern India. *In Vitro Cell. Dev. Biol. Plant.* 2005; 41:77-80. https://doi.org/10.1079/IVP2004600
10. Reddy BO, Giridhar P, Ravishankar GA. *In vitro* rooting of *Decalepis hamiltonii* Wight & Arn., an endangered shrub, by auxins and root-promoting agents. *Curr. Sci*. 2001; 1479-1482
11. Pradeep P, Parvatam G, Shetty NP. Enhanced production of vanillin flavour metabolites by precursor feeding in cell suspension cultures of *Decalepis hamiltonii* Wight & Arn., in shake flask culture. *3 Biotech.* 2017; 7:376. https://doi.org/10.1007/s13205-017-1014-0
12. Delledonne M, Xia Y, Dixon RA, Lamb C. Nitric oxide functions as a signal in plant disease resistance. *Nature*. 1998; 394:585-588. https://doi.org/10.1038/29087
13. Crawford NM, Guo F-Q. New insights into nitric oxide metabolism and regulatory functions. *Trends Plant Sci.* 2005; *10:195-200*
14. Beligni MV, Lamattina L. Nitric oxide counteracts cytotoxic processes mediated by reactive oxygen species in plant tissues. *Planta.* 1999; 208:337-344
15. Jie TU, Wen-Biao S, Lang-Lai XU. Regulation of nitric oxide on the aging process of wheat leaves. *J. Integr. Plant Biol.* 2003; 45:1055-1062
16. Arun M, Naing AH, Jeon SM, et al. Sodium nitroprusside stimulates growth and shoot regeneration in *chrysanthemum*. *Hortic Environ Biotechnol.* 2017; 58:78-84
17. Tan BC, Chin CF, Alderson P. Effects of sodium nitroprusside on shoot multiplication and regeneration of *Vanilla planifolia* Andrews. *In Vitro Cell Dev Biol-*

Plant. 2013; 49:626-630. https://doi.org/10.1007/s11627-013-9526-8
18. Xu J, Yin H, Wang W, et al. Effects of sodium nitroprusside on callus induction and shoot regeneration in micropropagated *Dioscorea opposita*. *Plant Growth Regul.* 2009; 59:279-285
19. Xu M-J, Dong J-F, Zhu M-Y. Nitric oxide mediates the fungal elicitor-induced hypericin production of *Hypericum perforatum* cell suspension cultures through a jasmonic-acid-dependent signal pathway. *Plant Physiol.* 2005;139:991-998
20. El-Beltagi HS, Ahmed OK, Hegazy AE. Protective effect of nitric oxide on high temperature induced oxidative stress in wheat (*Triticum aestivum*) callus culture. *Not Sci Biol.* 2016; 8:192–198
21. Strnad M. The aromatic cytokinins. *Physiol. Plant.* 1997; 101:674-688
22. Aremu AO, Bairu MW, Dolezal K, Finnie JF, Van Staden J. Topolins: a panacea to plant tissue culture challenges. *Plant Cell Tiss Organ Cult.* 2012; 108(1):1-6.
23. Chauhan RD, Taylor NJ. Meta-topolin stimulates de novo shoot organogenesis and plant regeneration in cassava. *Plant Cell Tiss Organ Cult.* 2018; 132:219-224. https://doi.org/10.1007/s11240-017-1315-3
24. Souza M, Barbosa M, Zarate-Salazar J, et al. Use of meta-Topolin, an unconventional cytokinin in the *in vitro* multiplication of *Opuntia stricta* Haw. *Biotecnol. Veg.* 19:85–96
25. Gentile A, Frattarelli A, Nota P, et al. The aromatic cytokinin meta-topolin promotes *in vitro* propagation, shoot quality and micrografting in *Corylus colurna* L. *Plant Cell Tiss Organ Cult.* 2017;128:693–703. https://doi.org/10.1007/s11240-016-1150-y
26. Souza M, Barbosa M, Zarate-Salazar J, et al. Use of meta-Topolin, an unconventional cytokinin in the *in vitro* multiplication of *Opuntia stricta* Haw. *Biotecnol. Veg.* 2019;19:85-96
27. Vasconcelos JNC, Brito AL, Pinheiro AL, et al. Stimulation of 6-benzylaminopurine and meta-topolin-induced *in vitro* shoot organogenesis and production of flavonoids of *Amburana cearensis* (Allemao) A.C. Smith). *Biocatal. Agric. Biotechnol.* 2019; 22:101408. https://doi.org/10.1016/j.bcab.2019.101408
28. Giridhar P, Rajasekaran T, Ravishankar GA. Improvement of growth and root specific flavour compound 2-hydroxy-4-methoxy benzaldehyde of micropropagated plants of *Decalepis hamiltonii* Wight & Arn., under triacontanol treatment. *Sci. Hortic.* 2005; 106:228-236. https://doi.org/10.1016/j.scienta.2005.02.024
29. Saini RK, Harish Prashanth KV, Shetty NP, Giridhar P. Elicitors, SA and MJ enhance carotenoids and tocopherol biosynthesis and expression of antioxidant related genes in *Moringa oleifera* Lam. leaves. *Acta Physiol Plant.* 2014; 36:2695-2704. https://doi.org/10.1007/s11738-014-1640-7
30. Sridevi V, Parvatam G. Impacts of biotic and abiotic stress on major quality attributing metabolites of coffee beans. *J. Environ. Biol.* 2015; 36:377
31. Kim HJ, Chen F, Wang X, Rajapakse NC. Effect of chitosan on the biological properties of sweet basil (*Ocimum basilicum* L.). *J. Agric. Food Chem.* 2005; 53:3696-3701
32. Perez-Balibrea S, Moreno DA, García-Viguera C. Improving the phytochemical composition of broccoli sprouts by elicitation. *Food Chem.* 2011; 129:35-44
33. Murashige T, Skoog F. A Revised Medium for Rapid Growth and Bio Assays with Tobacco Tissue Cultures. *Physiol Plant.* 1962; 15:473-497. https://doi.org/10.1111/j.1399-3054.1962.tb08052.x
34. Gururaj HB, Padma MN, Giridhar P, Ravishankar GA. Functional validation of *Capsicum frutescens* aminotransferase gene involved in vanillylamine biosynthesis using Agrobacterium mediated genetic transformation studies in *Nicotiana tabacum* and *Capsicum frutescens* calli cultures. *Plant Sci.* 2012; 195:96-105. https://doi.org/10.1016/j.plantsci.2012.06.014
35. Ahmad N, Strnad M. Meta-topolin: A Growth Regulator for Plant Biotechnology and Agriculture. Springer *Nature*. 2021
36. Ahmad A, Anis M. Meta-topolin Improves *In Vitro* Morphogenesis, Rhizogenesis and Biochemical Analysis in *Pterocarpus marsupium* Roxb.: A Potential Drug-Yielding Tree. *J Plant Growth Regul.* 2019; 38:1007–1016. https://doi.org/10.1007/s00344-018-09910-9
37. Khanam MN, Javed SB, Anis M, Alatar AA. meta-Topolin induced *in vitro* regeneration and metabolic profiling in *Allamanda cathartica* L. *Ind Crops Prod.* 2020; 145:111944. https://doi.org/10.1016/j.indcrop.2019.111944
38. Aremu AO, Bairu MW, Szucova L, et al. Assessment of the role of meta-topolins on *in vitro* produced phenolics and acclimatization competence of micropropagated 'Williams' banana. *Acta Physiol Plant.* 2012; 34:2265-2273. https://doi.org/10.1007/s11738-012-1027-6
39. Veerashree V, Anuradha CM, Kumar V. Elicitor-enhanced production of gymnemic acid in cell suspension cultures of *Gymnema sylvestre* R. Br. *Plant Cell Tiss Organ Cult.* 2012; 108:27-35. https://doi.org/10.1007/s11240-011-0008-6
40. Dornenburg H, Knorr D. Strategies for the improvement of secondary metabolite production in plant cell cultures. *Enzyme Microb. Technol.* 1995; 17:674-684. https://doi.org/10.1016/0141-0229(94)00108-4
41. Wiktorowska E, Długosz M, Janiszowska W. Significant enhancement of oleanolic acid accumulation by biotic elicitors in cell suspension cultures of *Calendula officinalis* L. *Enzyme Microb. Technol.* 2010; 46:14-20. https://doi.org/10.1016/j.enzmictec.2009.09.002
42. Yamaner O, Erdag B, Gokbulut C Stimulation of the production of hypericins in *in vitro* seedlings of *Hypericum adenotrichum* by some biotic elicitors. *Turk J Bot.* 2013; 37:153-159
43. Wolf S, Greiner S. Growth control by cell wall pectins. *Protoplasma*. 2012; 249:169-175. https://doi.org/10.1007/s00709-011-0371-5.

ISSN print: 1224-5984
ISSN online: 2248-3942

Rom Biotechnol Lett. 2022; 27(1): 3309-3314
doi: 10.25083/rbl/27.1/3309-3314

Received for publication, December, 01, 2019
Accepted, January, 28, 2022

Original paper

The assessment of the soil mineralization processes along the traffic corridors from urban and rural areas in Romania

I. PĂCEŞILĂ[1,2], E. RADU[1], C. C. BÎRSAN[1], M. CONSTANTIN[1,2]

[1] Institute of Biology Bucharest, Spl. Independentei, 296, 060031, Bucharest, Romania
[2] The Research Institute of the University of Bucharest, ICUB, Bucharest, Romania

Abstract The soils of the green areas located near the traffic corridors accumulate different pollutants, especially heavy metals, which have an important impact on the microbial decomposition processes. The extracellular enzymes can be used as an indicator of the metabolic activity of the microorganism communities. Four extracellular enzymes - α and β glucosidase, alkaline phosphatase and alanine aminopeptidase - were assessed in green areas close to the traffic zones in several urban, peri-urban and rural localities in Romania. The data showed that the highest values of enzymatic activities were registered in rural areas. At the same time, the spatial dynamics of the studied enzymes revealed an important variability between the three types of sampled areas, without a clear pattern of their distribution.

Keywords soil mineralisation, extracellular enzymatic activity

To cite this article: PĂCEŞILĂ I, RADU E, BÎRSAN CC, CONSTANTIN M. The assessment of the soil mineralization processes along the traffic corridors from urban and rural areas in Romania. *Rom Biotechnol Lett*. 2022; 27(1): 3309-3314. DOI: 10.25083/rbl/27.1/3309-3314.

✉ *Corresponding author: I. PĂCEŞILĂ, Institute of Biology Bucharest, Spl. Independentei, 296, 060031, Bucharest, Romania.
E-mail: ioan.pacesila@gmail.com

Introduction

The extracellular enzymatic activity it is well acknowledged to play an important role in the mineralization of the detrital organic matter (DOM) and in the nutrient recycling process in soils, contributing to the ecosystems functioning. The extracellular enzymes are released in soils by numerous microorganisms (especially by bacteria and fungi), but also by the roots of some plants. They hydrolyze the large organic polymeric molecules (a major component of DOM) to simpler molecules that can be used by microorganisms or plants as a source of nutrients and energy. Due to their action, these enzymes are involved in the main biogeochemical cycles of the biogenic elements like C, N, S, etc. Thus, the evaluation of the extracellular enzymes activity could conduct to a better understanding of the DOM composition, a major component in the soil formation. The quantitative and qualitative alterations of DOM influence the composition and distribution of microorganism communities and, therefore, the specific of the biochemical processes carried out at the soil level - processes of a great importance for defining the characteristics of different types of soil (IGALAVITHANA & al. [1]; DATTA & al. [2]; ZAHIR & al. [3]; SHERENE [4]).

The intensity of the enzymatic activity in soils varies with the pressure of the environmental - physical, chemical and biological factors, of natural or anthropogenic origin. In the urban and rural inhabited areas, the presence of increasing quantities of heavy metals in soils (Ni, Cd, Cu etc.) is often recognized as a major factor that influences the activity of the extracellular enzymes. Another factor that can impact the decomposition processes in soil is represented by the pollution with fertilizers (especially of organic nature) used in the agricultural treatments. Most frequently, these fertilizers stimulate the enzymatic activity in soil and, thus, modify the rates of the biogeochemical processes at this level (KIM [5]; PETRISOR & LAZAR [6]; IGALAVITHANA et al. [1]).

The composition of the vegetation that covers the soils also influences the extracellular enzymatic processes in respect to the quantity and quality of the detrital organic matter produced. The enzymatic activity in soil is more intense in its upper layer, often related to a higher microbial biomass and detrital organic matter amount of this substrate. In the rhizosphere, the intense activity of many enzymes is sustained by a higher amount of the cellular debris and root excretes released in the environment (DICK & KANDELER [7]).

Regarding the urban and suburban areas, the soil undergoes different biochemical changes due to anthropogenic activities: agriculture, forestry, industrial activities, infrastructure and support activities etc. (MOREL & al. [8]). Thus, the urban soils are characterized by a higher heterogeneity and are frequently contaminated with important quantities of pollutants such as heavy metals and hydrocarbons, which represent a real thread for the human population, as well as for the plant and animal communities.

The purpose of the present study is to analyze and highlight the dynamics of the extracellular enzyme intensity in vegetated soils from territories along different traffic corridors in urban, peri-urban and rural localities in Romania.

Materials and methods

The samples were taken from the first 5 cm below the surface layer of the soil, between April and May 2016, from several urban and rural localities in the NE, E and SE part of Romania. All the 60 sampled points were placed in central or peripheral areas of the localities, in the proximity of trafficked roads, in parks or in the green areas of the blocks of flats. The sample size in different counties followed the density of the air quality monitoring stations in the chosen locations, according to the National Network of the Air Quality Monitoring in Romania (www.calitateaer.ro [9])), in order to asses possible pressures induced by the airborne pollution across the heterogeneity of our study area (ŞTEFĂNUŢ & al. [10]).

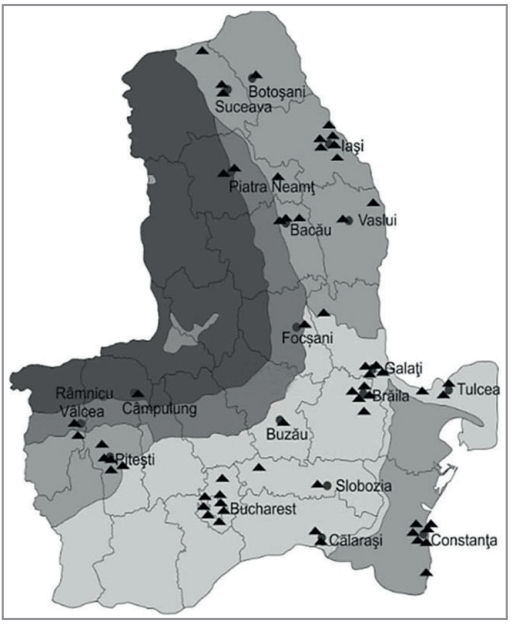

Figure 1. The study area and the sampling stations

The enzymatic activity was assessed using the substrate consumption method (OBST [11]). Four enzymes involved in soil mineralization processes (BANERJE et al. [12]; ZHANG et al. [13]; NIEMI et al. [14]) have been investigated: α glucosidase (α GLC) and β glucosidase (GLC) associated with the C cycle, the alkaline

phosphatase (AP) involved in the P cycle and the alanine aminopeptidase (AMP) active in the N cycle (Tab. 1). The intensity of the enzymatic activity was expressed in units of nmol substrate per gram per hour or per day (24 h). All the processed data used in the cluster multivariate analysis were log transformed.

The statistical analyzes were performed using the PAST program ver. 2.17c (HAMMER & al. [15]) and following PAST Reference manual methodology.

Table 1. The enzymatic activities assessed in the urban, peri-urban and rural localities from the NE, E and SE part of Romania

Enzymatic activity	Substrate	Measurement unit (nmol $g^{-1}h^{-1}$)
α Glucosidase (EC 3.2.1.20)	p - nitrophenyl - α - D - glucopyranoside	p-nitrophenol
β Glucosidase (EC 3.2.1.21)	p - nitrophenyl - β - D - glucopyranoside	p-nitrophenol
Alkaline phosphatase (EC 3.1.3.1)	4 - nitrophenyl - phosphate	p-nitrophenol
Alanine aminopeptidase (EC 3.2.1)	L - alanine - 4 - nitroanilide - hydrochloride	p-nitroanilline

Table 2. The intensity ranges of the assessed enzymatic activities across the study sites

Enzymatic activity	nmol substrate $g^{-1}d^{-1}$
α Glucosidase (α GLC)	469,5 ± 457,5
β Glucosidase (β GLC)	1033,5 ± 997,5
Alkaline phosphatase (ALP)	1100 ± 1037
Alanine aminopeptidase (AMP)	1574 511

Results and discussion

By analyzing **the spatial distribution of the extracellular enzymatic activity** in the considered study areas, the highest intensity was mainly recorded for alanine aminopeptidase and the lowest, for α-amylase, with large variations for each enzyme (Tab.2).

In the rural areas, the enzymatic activity often appeared to be higher than in the urban areas (Fig. 2). The exception was observed for AMP that registered a higher average intensity for the peri-urban area.

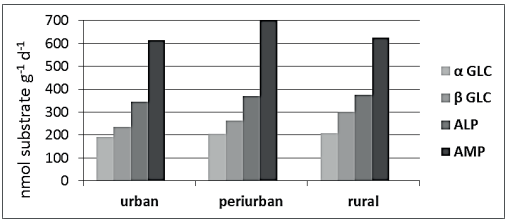

Figure 2. The average activity of the extracellular enzymes studied in the urban, periurban and rural areas

The data suggest the presence of some less favorable conditions for the MOD mineralization processes in the urban, highly trafficked areas. The accumulation of the polluting substances, especially heavy metals from the traffic emissions, can induce a significant impact in the environment on the microorganism communities, mainly decreasing their extracellular enzymatic activity (KHAN et al. [16]). However, this was not a tendency for all the analyzed sites; many of them in the urban area presented a higher extracellular enzymatic activity than in the rural areas. The dynamic of mineralization processes is influenced by many local factors, but the quantity and quality of the substrate are playing a major role (BURNS [17] DICK & KANDELER [7]). In our study, we aimed to sample a high variability of soil quality across the selected locations. On the other hand, some categories of microorganisms are known to develop different mechanisms of resistance to the heavy metals stress (AZARBAD & al [18], HOOSTAL & al. [19]). As well, the rate of absorption of the heavy metals by the vegetal layer modulate their impact on soils (TANGAHU et al. [20]), and subsequently on the bacterial extracellular enzymatic activity.

α GLC, registered the most intense activity in an urban park from Bucharest (751 nmol p-nitrophenol $g^{-1}d^{-1}$, Titan Park) and the lowest in a different type of urban site, in Iaşi, when we sampled the green area located in the proximity of the trafficked N. Iorga street (12 nmol p-nitrofenol $g^{-1}d^{-1}$).

β GLC activity was the most intense in Bosia village from Iaşi county (2031 nmol p-nitrophenol $g^{-1}d^{-1}$), at a sampling site placed near the main road, while its lowest value was assessed in an urban location, in Brăila - Brăila county (32 nmol p-nitrophenol $g^{-1}d^{-1}$), at the green area close to the central Independenţei Square.

AP phosphatase enzymatic activity varied between 2137 nmol p-nitrophenol $g^{-1}d^{-1}$ in Măgurele - Ilfov county (at a station located in the garden of a block of flats located to the outskirts of the city) and 63 nmol p-nitrophenol $g^{-1}d^{-1}$, in Botoşani - Botoşani county (for a sample taken as well from the garden of a block of flats, from M. Eminescu street).

AMP registered its highest value in Iaşi (3085 p-nitrofenol $g^{-1}d^{-1}$), in the rural area from the outskirts of the city, near M. Sadoveanu alley. Its minimum intensity (63 nmol p-nitrophenol $g^{-1}d^{-1}$) was assessed at the same station where AP recorded its minimum intensity, namely in Botoşani, in the garden of a block of flats.

In addition, because the intensity of soil level enzymatic processes can be influenced by soil physico-chemical characteristics (BŁOŃSKA et al [21]), it is also important to consider the types of soil identified in the studied areas. According to the data from the literature (STANILA & DUMITRU [22]) the ones from the category chernisols (predominantly chernozem), cambisols (predominantly distriambosols) and luvisols (predominantly luvosols) are prevalent. From table 3 it can be observed that, in general, *α* and *β* GLC were

more intense in the stations located in regions where chernisols are dominant, while AP and ALP recorded higher values in the regions where cambisols predominate. In general, chernisols are recognized to have a high content of organic matter (VYSLOUŽILOVÁ et al [23]), but the concentration and quality of organic matter may widely vary in the case of all soil types, depending on the specificity of the area (ZARNEA [24]). However, the extracellular enzymatic activity across the sampling sites of different soil types did not show a high variation, suggesting that, most likely, the metabolic activity of the heterotrophic microorganism communities involved in the geochemical circuits at C, N and P, was not significantly influenced by the type of soil present in the sampling area.

.

Table 3. The intensity of enzymatic activity assessed on different soil types

Enzymatic activity average value (nmol substrate h^{-1} mL^{-1})	α GLC	β GLC	ALP	AMP
chernisols	215,16	284,67	355,16	641,25
cambisols	206,53	269,61	351,87	646,46
luvisols	205,98	277,95	351,62	623,12

For a better understanding of the spatial variability of each bacterial extracellular enzymatic activity in soil across the study zones - urban, peri-urban, rural areas, we further performed the cluster analysis following Ward's method (Fig. 3).

Regarding the intensity of the substrate consumption performed by the four studied enzymes, we observed a similarity between α GLC and β GLC activities (Fig. 3). This could be the result of the amount of plant debris in the analyzed soils, the two enzymes being involved in the degradation of the vegetal glucidic substrates such as cellulose and starch. The activities of these two enzymes also showed the smallest spatial variability in the three types of studied areas. At the same time, we should mention that each enzyme revealed a specific dynamic per site type.

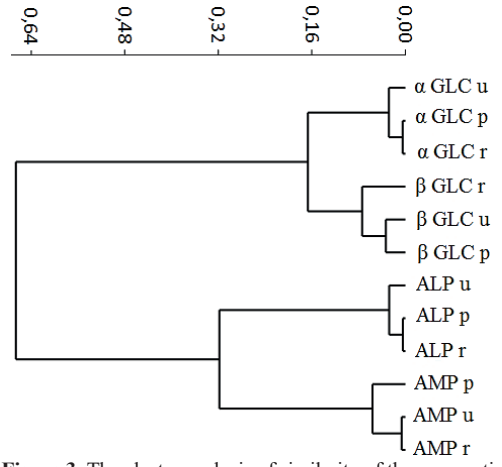

Figure 3. The cluster analysis of similarity of the enzymatic activities evaluated across the tree types of sampled locations (u – urban, p – peri-urban, r – rural) (Ward's method, Coph. Corr.: 0,696)

APL and α GLC enzymatic activity are the most similar in rural and peri-urban locations. Instead, the variability of β GLC enzymatic activities was the lowest between urban and peri-urban areas, and AMP, between the urban and rural sites.

The differences between the intensity of the extracellular enzymatic activities evaluated at different locations could be explained by the variation of the pressures exerted by the natural or anthropic environmental factors (KIM [4], DICK & KANDELER [8]).

The extracellular enzymes are considered to be very sensitive to changes in the ecosystems state, including pollution. Consequently, they can be used as early indicators of soil quality and health (LI & al. [25]) based on their property of quick response to changes in the environment, in comparison to other parameters (RAO & al. [26]). Due to this property, the study of the extracellular enzymatic activity of the bacterial communities can be used to improve the understanding of the dynamic and role of soils in the evolution of different types of ecosystems.

Conclusions

The intensity of the assessed enzymatic activities registered important variations across the sampling stations in the surveyed area, a fact that could be explained by considering the high variability of soil quality between the selected locations. The highest intensity values were recorded in most of the cases for the alanine aminopeptidase and the lowest for the α-glucosidase enzymatic activity. Generally, considering the entire data set, the enzymes analyzed from the rural soil substrate often showed a higher intensity in comparison with the ones analyzed from the urban areas samples. The pollution from

the sites along the trafficked roads or from the central areas of the cities could explain these differences. α GLC and β GLC revealed the highest spatial similarity in terms of their substrate consumption across the sampled sites. Each enzyme presented a specific dynamics in all the three types of studied locations (urban, peri-urban and rural areas).

Acknowledgment

This study was funded within the projects no. RO1567-IBB02/2019, RO1567-IBB04/2019 and RO1567-IBB05/2019 of the Institute of Biology Bucharest, Romanian Academy, IBB and by The Research Institute of the University of Bucharest, ICUB, Bucharest, Romania.

References

1. A.D. IGALAVITHANA, S. E. LEE., Y. H LEE, D. C. TSANG, J. RINKLEBE, E. E. KWON., Y. S. OK, Heavy metal immobilization and microbial community abundance byvegetable waste and pine cone biochar of agricultural soils, *Chemosphere* 174: 593–603 (2017).
2. R. DATTA, S. ANAND, A. MOULICK, D. BARANIYA, S. I. PATHAN, K. REJSEK, V. VARNOVA, M. SHARMA, D. SHARMA, A. KELKAR, How enzymes are adsorbed on soil solid phase and factors limiting its activity: A Review, *Int. Agrophys*, 31: 287–302 (2017).
3. Z. A. ZAHIR, M. A. R. MALIK, M. ARSHAD, Soil enzymes research: review, *Online Journal of Biological Science*, 1(5): 299–307 (2001).
4. T. SHERENE, Role of soil enzymes in nutrient transformation: A review, *Bio Bulletin*, 3(1): 109– 131 (2017).
5. H. KIM, A review of factors that regulate extracellular enzyme activity in wetland soils, *Korean Journal of Microbiology*, 51(2): 97-107 (2019).
6. I. G. PETRISOR, I. LAZAR, Emerging Contaminants–The Problem, Examples and Bioremediation AlternativesPart I, *Romanian Biotechnological Letters*, 11: 2693-2701 (2006).
7. R. DICK, E. KANDELER, Enzymes in Soil, Encyclopedia of Soils in the Environment, *Elsevier, Oxford*, 448-456 (2005).
8. J. L. MOREL, C. CHENU, K. LORENZ, Ecosystem services provided by soils of urban, industrial, traffic mining, and military (SUITMAs), *J. Soils Sediments*, 15:1659-1666 (2015).
9. http://www.calitateaer.ro/public/home-page/?__locale=ro, accessed on February 2016.
10. S. ŞTEFĂNUŢ, A. MANOLE, C.M. ION, M. CONSTANTIN, C. BANCIU, M. ONETE, M. MANU, I. VICOL, M. M. MOLDOVEANU, S. MAICAN, I. COBZARU, G. R. NICOARĂ, I. L. FLORESCU, D. E. MOGÎLDEA, M. D. PURICE, D. C. NICOLAE, D. R. CATANĂ, G. TEODOSIU, A.C. DUMITRACHE, M. G. MARIA, C. VÂTCĂ, M. OANŢĂ, K. ÖLLERER, Developing a novel warning-informative system as a tool for environmental decision-making based on biomonitoring, *Ecological Indicators*, 89: 480-487 (2016).
11. OBST U., Test instructions for measuring the microbial metabolic activity in water sample. Anal Chem, 321:166, 168 (1985).
12. A. BANERJEE, S. SANYAL, S. SEN, Soil phosphatase activity of agricultural land: A possible index of soil fertility, *Agricultural Science Research Journal*, 2: 412–419 (2012)
13. L. ZHANG, W. CHEN, M. BURGER, L. YANG, P. GONG, Z. WU, Changes in soil carbon and enzyme activity as a result of different long-term fertilization regimes in a greenhouse field, *PLOS ONE*, 10(2):e0118371 (2015).
14. R. M. NIEMI., I. HEISKANEN, S. SAARNIO, Weak effects of biocharamendment on soil enzyme activities in mesocosms in bare or *Phleum pratense* soil, *Boreal Environ .Res.*, 20: 324–33 (2015).
15. Ř. HAMMER, D.A.T. HARPER, P.D. RYAN, PAST: Paleontological statistics software package for education and data analysis, *Palaeontologia electronica*, 4(1): p. 9 (2001).
16. S. KHAN, Q. CAO, A. E-L. HESHAM, Y. XIA, J. Z. HE, Soil enzymatic activities and microbial community structure with different application rates of Cd and Pb, *Journal of Environment Sciences*, 19: 834–840 (2007).
17. R. G. BURNS, Enzyme activity in soil: location and a possible role inmicrobial ecology, *Soil Biology & Biochemistry*, 14: 423 – 427 (1982).
18. H. AZARBAD, C. A. VAN GESTEL, M. NIKLIŃSKA, R. LASKOWSKI, W. F. RÖLING, N. M. VAN STRAALEN, Resilience of soil microbial communities to metals and additional Stressors: DNA-based approaches for assessing "Stress-on-Stress" responses, *Int J Mol Sci*, 17 :933 (2016).
19. M. J. HOOSTAL, M. G. BIDART-BOUZAT, J. L. BOUZAT, Local adaptation of microbial communities to heavy metal stress in polluted sediments of Lake Erie, *FEMS Microbiol Ecol*, 65: 156-168 (2008).
20. B. V. TANGAHU, S. ABDULLAH, H. BASRI, M. IDRIS, N. ANUAR, M. MUKHLISIN, A review on heavy metals (As, Pb, and HG) uptake by plants throug phytoremediation, *Int. J. of Chemical Engeneering*, 1-31 (2011).
21. E. BŁOŃSKA, J. LASOTA, M. ZWYDAK, The relationship between soil properties, enzyme activity and land use, *Forest Research Papaper*, 78(1):39–44 (2017).
22. A. L. STĂNILĂ, M. DUMITRU, Soils Zones in Romania and Pedogenetic Processes, *Agriculture and Agricultural Science Procedia*, 10: 135-139 (2016).
23. B. VYSLOUŽILOVÁ, D. ERTLEN, D. SCHWARTZ, L. ŠEFRNA, Chernozem. From concept toclassification: a review, *AUC Geographica*, 51: 85–95 (2016).
24. G. ZARNEA, Tratat de microbiologie generală, Vol. V, *eds. Of Romanian Academy*, *Bucharest*, pp. 583 - 611 (1994).
25. T. LI, L. MENG, U. HERMAN, Z. LU, J. CRITTENDEN, A Survey of Soil Enzyme Activities along Major Roads in Beijing: The Implications for

Traffic Corridor Green Space Management, *Int. J. of Environmental Research and Public Health*, 12: 12475–12488 (2015).

26. RAO C. S., GROVER M., KUNDU S., DESAI S., Soil Enzymes, Encyclopedia of Soil Science, Third Edition 2100-2107. (2017).

ISSN print: 1224-5984
ISSN online: 2248-3942

Rom Biotechnol Lett. 2022; 27(1): 3315-3329
doi: 10.25083/rbl/27.1/3315-3329

Received for publication, February, 01, 2021
Accepted, October, 19, 2021

Original paper

Adipose Tissue-derived Cardiomyocytes for Enhancing Cardiac Remodeling in a Rat Model of Acute Myocardial Infarction

MOHAMED S. KISHTA[1,2], MOHAMED RAGAA MOHAMED[3], HADEER A. AGLAN[1,2], MOHAMED A.M. ALI[3], HANAA H. AHMED[1,2]

[1] Hormones Department, Medicine and Clinical Studies Research Institute, National Research Centre, Giza, Egypt, Affiliation ID: 60014618.

[2] Stem Cell Lab., Center of Excellence for Advanced Sciences, National Research Centre, Giza, Egypt, Affiliation ID: 60014618.

[3] Biochemistry Department, Faculty of Science, Ain Shams University, Cairo, Egypt.

Abstract

This investigation was directed towards addressing the pivotal role of adipose tissue-derived cardiomyocytes seeded onto nanofiber (NF) in repairing the deteriorated cardiac tissue in a model of MI. Molecular analysis for *MEF2C* and *Actn* expression was attained to ensure the differentiation of ADMSCs into cardiomyocytes *in vitro*. The *in vivo* study was conducted on forty adult rats assigned into four groups: (1) control; (2) MI; (3) MI treated with adipose tissue-derived cardiomyocytes; (4) MI treated with adipose tissue-derived cardiomyocytes seeded onto NF. Treatment of MI-challenged rats with adipose tissue-derived cardiomyocytes modulates ST height, heart rate, RR, PR, QTc, QRS intervals and P duration as manifested in the ECG. The biochemical parameters corroborated the ECG outcomes as they displayed significant inhibition in serum LDH and CK-MB enzymes activity as well as significant suppression in cardiac cTnT level paralleled with significant elevations in cardiac Cx43 and Actn levels in the treated groups. Molecular analysis of *GATA4* and *NKX2.5* gene expression levels declared significant downregulation in the treated groups. Photomicrographs of cardiac tissue sections of rats in the treated groups showed great renovation in the cardiac microarchitecture. Conclusively, this study delivers a futuristic approach for treatment of MI by applying differentiated cardiomyocytes systematically.

Keywords Adipose tissue-derived cardiomyocytes, Electro-spun nanofibers, *In vitro*, *In vivo*, Myocardial infarction.

To cite this article: KISHTA MS, MOHAMED MR, AGLAN HA, ALI MAM, AHMED HH. Adipose Tissue-derived Cardiomyocytes for Enhancing Cardiac Remodeling in a Rat Model of Acute Myocardial Infarction. Rom Biotechnol Lett. 2022; 27(1): 3315-3329. DOI: 10.25083/rbl/27.1/3315-3329.

*Corresponding author: HADEER A. AGLAN, Hormones Department, Medical Research Division, National Research Centre, Giza, Egypt, Affiliation ID: 60014618.
Phone: 20233371615; Fax: 20233370931; Postal address: 33 EL Bohouth St. (Former EL Tahrir St.)-Dokki-Giza-Egypt- P.O. 12622
E-mail: ha_dero@yahoo.com

Introduction

Acute myocardial infarction is one of the master causes of human mortality all over the world. It contributes to massive loss of cardiomyocytes, interchanges of unfavorable biological environment and modifying electrical connections by fibrosis scar constitutions. Thus, MI results in shortage of blood supply to the heart, leading to heart spoilage and heart failure (Si et al. 2020). Moreover, perturbation of homeostatic balance produces a series of sequential issues like ventricular stiffness, inflammatory events, necrosis, apoptosis, remodeling that leads to the alteration of heart muscle contractility. Medical and surgical advances such as pharmacotherapies and percutaneous coronary interference can crucially offer their benefaction towards terrible impacts of MI (Yoshizumi et al. 2016). Meanwhile, they display ineffectual towards rejuvenating myocardium and assembling new contractile tissues. As regards to solving this issue, empirically and virtually substantial risk heart transplantation is the unique mandatory medication for MI. Thus, to avoid this difficult therapy, great effort of investigators has led to principles of cell inoculation, a rising therapeutic modality *versus* MI (Liang et al. 2019).

Cell-based regenerative medicine could improve blood supply to the damaged heart, and minimize the area of infarction (Bolli et al. 2013) through secretions of several cytokines such as hepatocyte growth factor (HGF) and vascular endothelial growth factor (VEGF) (Zhao et al. 2015). Direct injection of cells into the heart is problematic, because of a significant loss of living cells in addition to the pro-arrhythmic effects (Song et al. 2010).Tissue engineering using cell sheets has been developed to overcome these disadvantages; the cell sheet could improve the viability of cells (Patila et al. 2015) and prolong secretion of cytokines (Memon et al. 2005). Initially, sheets of skeletal myoblast cells have been reported to enhance cardiac functions in patients with severe heart failure. However, collecting skeletal myoblasts from patients requires invasive procedures, and it takes a long time to obtain a sufficient number of myoblasts. In addition, myoblasts secrete low levels of cytokines and lack capability to differentiate into cardiomyocytes (Miyagawa et al. 2010). Thus, an alternative source of stem cells for cell sheets is required.

To date, mesenchymal stem cells (MSCs) have become the most practiced cell types of clinical trials for the intervention of MI (Lee et al. 2015), due to their safety, multi-differentiation potential, nutritional activity, immunomodulatory properties, and abundant donor sources. MSCs have low immunogenicity due to the low expression of major histocompatibility complex MHC II as well as the lack of expression of MHC I on T-lymphocytes, which act as molecules to present processed antigens, leading to immune tolerance and allowing allogeneic transplantation (Miao et al. 2017).

Adipose tissue-derived mesenchymal stem cells (ADMSCs) cultured with the proper stimulating growth factors can differentiate into several lineages, including cardiomyocytes-like cells, suggesting their potential as a cell source for repairing the damaged cardiac tissues. It has been stated that they secrete numerous cytokines and growth factors to counteract cardiac dysfunction and remodeling after MI (Otsuki et al. 2015). However, the poor survival and low engraftment efficiency of the donor cells in the infarcted myocardium challenged its therapeutic efficacy.

Biomaterials can assist cell survival, integration and communication with a proper microenvironment that closely mimics the native tissue architecture (Liu et al. 2012). Therefore, they might promote the appropriate differentiation and maturation of cardiac progenitor cells (CPCs) for cardiac tissue regeneration. Various types of scaffolds have been explored to accommodate heart tissue cells. To guide the organization, growth, and differentiation of cells, biomaterial scaffolds should possess the ability to provide not only mechanical support for the cells, but also the chemical and biological cues needed for stimulating the specific differentiation of cells (Langer and Tirrell 2004). Thus, it should provide a 'microenvironment' for stem cell responsible trans-differentiation effect both at the anatomical and functional dimensions (Scadden 2006). Electrospun nanofibers (NF) are novel materials characterized by an enormous surface to volume ratio, high porosity, and a structure resembling that of the extracellular matrix, thus facilitating their employment in a broad range of biomedical and tissue engineering applications (Agarwal et al. 2008).

The present approach was tailored to establish the possible contribution of adipose tissue-derived cardiomyocytes seeded onto NF in intensifying cardiac relieve in an experimental model of MI.

Materials and methods

Nanofibrous Scaffold Coated Plates

Nanofibrous scaffold coated plates were purchased from Corning® Lab Ware with Ultra-Web™ (Corning Incorporated, USA). Ultra-Web synthetic surfaces are composed of randomly orientated electro-spun polyamide nanofibers with an average fiber diameter of 280 nm. This creates a culturing substrate that mimics the structural components within the basement membrane or extracellular matrix.

Protocol for Isolation of ADMSCs

Adipose tissue was excised from both the omentum (i.e., abdominal) and inguinal regions of male *Wistar* strain rats (Aird et al. 2015). The excised adipose tissues (1 cm^3) were washed extensively with phosphate buffer solution (PBS, Biowest, France) to remove the contaminating debris and red blood cells, then minced with fine tissue scissors. The fragmented tissues were incubated with 0.1% collagenase (NB4 standard grade from Serva Electrophoresis GmbH, Germany) and kept in a slow shaking water bath at 37°C for 60 min. Thereafter, collagenase was removed by diluting the

samples with PBS. The cell suspension was centrifuged twice at 800 xg for 10 min. The supernatant containing mature adipocytes was removed and the precipitate was passed through 100 µm mesh syringe filter generated from 100% borosilicate glass microfiber (Chen et al. 2014).

The obtained cells were cultured in Dulbecco's modified Eagle's medium (DMEM, Biowest) high glucose containing 30% fetal bovine serum (FBS, Biowest) and 1% penicillin-streptomycin (Biowest) for 10 to 14 days in the culture flask. Then, the flasks were incubated at 37°C in a humidified atmosphere containing 5% CO_2. To exchange the medium, the flasks were washed with PBS in order to remove non-adhered cells and the medium was replaced. This process was performed at least two times/week. Plentiful ADMSCs with confluence of 95 % in the culture plate were harvested using 0.25% trypsin/1 mM EDTA (Biowest) to be re-cultured again as 1stsubculture. This process was repeated till reaching 3rd subculture (Lin et al. 2016).

Identification of ADMSCs

ADMSCs culture flasks were examined under optical inverted microscope in order to determine their morphological feature. The morphology of ADMSCs is one of the hallmarks of MSCs. Flowcytometry technique was accomplished at the 3rd passage of ADMSCs using CD44, CD90 and CD45 cell surface antigens to emphasize whether the isolated ADMSCs preserve their phenotype after expansion in culture (Woodbury et al. 2000). The phycoerythrin (PE)-conjugated CD44 and CD90 antibodies were supplied from Milteny Biotech (Germany) and R&D Systems (UK) respectively. While, the fluorescein isothiocyanate (FITC)-conjugated-CD45 antibody was acquired from Dako Co. (Denmark). The cells were incubated with the antibody against each of the surface antigens for 30 min at 4°C for CD44 as well as CD90 and 10 min at 4°C for CD45 followed by flowcytometry analysis using Beckman Counter Elite XL (USA) equipment. The surface marker antigens represent the second most common trait of MSCs.

Differentiation of ADMSCs into Cardiomyocytes

Differentiation of ADMSCs into cardiomyocytes was induced by adding a cocktail of growth factors for 12 successive days following the method described by Hahn et al. (2008) with slight modification. The differentiation medium consisted of a combination of 2 µl/100 ml bone morphogenetic-2 (BMP-2; R&D Systems, UK), 1 µl/100 ml insulin-like growth factor-1 (IGF-1; Komabiotech, Korea), 5 µl/100 ml fibroblast growth factor-2 (FGF-2; Bio Basic Inc., Canada), 10 µl/100 ml dexamethasone (Sigma, USA) and 146.6 µl/100 ml ascorbic acid (Sigma) in a complete medium composed of antibiotic antimycotic (l ml/100 ml, Biowest), FBS (2 ml /100 ml, Biowest) which was completed to 100 ml DMEM high glucose (Biowest).

Detection of Cardiomyocyte Differentiation by qRT-PCR

After 12 days of ADMSCs culturing in the differentiation media, the cells were harvested using 0.25% trypsin EDTA to be subjected to molecular analysis for both myocyte-specific enhancer factor 2C (*MEF2C*) and alpha sarcomeric actin (*Actn*) to ensure the differentiation of ADMSCs into cardiomyocytes. Total RNA was isolated using an RNA extraction kit (RNeasy; Qiagen, Germany) and 2 µg of total RNA was subjected to reverse transcription using the QuantiTect Reverse Transcription kit (Qiagen) as recommended by the manufacturer manual. Quantitative real-time polymerase chain reaction (qPCR) was performed using the QuantiTect SYBR Green PCR kit (Qiagen) according to the manufacturer's instruction. Specific primer sequence for *MEF2C*, *Actn* and housekeeping gene glyceraldehyde-3-phosphate dehydrogenase (*GAPDH*) were used for qPCR. The primer sequences for detecting *MEF2C* gene were F: 5′-AGCAGGTGCTGACGGGAACAA-3′ and R: 5′-TCACAGTCGCACAGCACGCTC-3′ (Zhang et al. 2012). While, the primer sequences for detecting *Actn* gene were F: 5′-GACCACAGCTGAAC-GTGAGA-3′ and R:5′-CATAGCACGATGGTCGATTG-3′ (Hahn et al. 2008). Furthermore, the primer sequences for detecting *GAPDH* gene were F:5′-GGCTCTCTGCTCCTCCCTGTT-3′ and R: 5′-GCGGGATCTCGCTCCTGGAAG-3′ (Zhang et al. 2012). qPCR was carried out under the following thermal conditions: an initial denaturation step at 94°C for 4 min, followed by 40 cycles of 94°C for 15 s, annealing at 55°C for 20 s, and extension at 72°C for 20 s, and a final extension step of 10 min at 72°C. Each reaction was done in a total volume of 20 µl, consisting of 12.5 µl SYBR@ Premix Ex, 0.5 µl each primer (10 µmol/L), 2 µl cDNA and 4.5 µl ddH_2O. The main equations used were ΔCt = Ct (gene of interest) – Ct (housekeeping gene) followed by $\Delta\Delta Ct = \Delta Ct$ (treated sample) – ΔCt (untreated sample) and the overall formula to calculate the relative fold gene expression level was $2^{-\Delta\Delta Ct}$ which was employed to quantify the relative amount of mRNA expression normalized to GAPDH.

Labeling Cells with Iron Oxide Nanoparticles

The Feridex IV (Berlex Laboratories, USA), a sterile aqueous colloid of dextran-coated super paramagnetic iron oxide nanoparticles (at a concentration of 25 µg/ml) and poly-L-lysine (PLL, Sigma-Aldrich, USA) (at a concentration of 375 ng/ml) were used for labeling of the differentiated cardiomyocytes. Feridex was mixed with PLL (1:10) and the mixture was shaked for 30 min at room temperature before being added to the supplemented medium. The differentiated cardiomyocytes were incubated in the labeled medium for 24 hours before infusion in the experimental animals.

Animal Handling

Forty adult male albino rats of *Wistar* strain weighing 150-180 g were provided from the Animal Care Facility of the National Research Centre, Giza, Egypt and housed in polypropylene cages in an animal holding room of Hormones Department under ambient temperature (25±1°C), a relative humidity (60±5 %), 12-hour light and dark periodicity and *ad libitum* access to tap water and a standard rodent chow consisted of 10 % casein, 4 % salts mixture, 1 % vitamin mixture, 10 % corn oil, 5 % cellulose and completed to 100 g with corn starch (Meladco Co., Cairo, Egypt). The animals were kept under observation for about 14 days before the onset of the experiment for accommodation.

Ethical Statement

Housing and management of animals followed the recommendations and guidelines for the care and use of laboratory animals. The study was carried out in compliance with the code of ethics of the World Medical Association (Helsinki Declaration) for animal experiments and the experimental protocol was approved by the institution Ethical Committee for Medical Research of the National Research Centre, Egypt (Code No:15 016).

Creation of Animal Model of MI

Myocardial infarction (MI) was induced in rats by subcutaneous injection of isoprenaline (Sigma-Aldrich, USA) in a daily dose of 100 mg/kg for 2 consecutive days (van Dijk et al. 2011). The calculated dose of isoprenaline/rat was dissolved in 1 ml of saline.

Experimental Groups

Rats (n=40) were randomly grouped into four equal groups: group (1) negative control [control], group (2) myocardial infarction group [MI], group (3) MI-challenged rats infused intravenously once with adipose tissue derived-cardiomyocytes (3×10^6 cells/rat) [Diff. ADMSCs] and group (4) MI-challenged rats infused intravenously once with adipose tissue derived-cardiomyocytes seeded onto nanofiber (3×10^6 cells/rat) [Diff. ADMSCs on NF] (Yip et al. 2008).

Electrocardiography

After two months of differentiated ADMSCs transplantation, the rats in each group were submitted to electrocardiography (ECG) for validation of MI and for verification of the therapeutic influence of the differentiated ADMSCs. Rats were anesthetized with pentobarbital (25 mg/kg, IP), and placed in a prone position on a board and the electrodes were put subcutaneously in the extended limbs of the rat. ECG amplifier was set to channel I and data were acquired from lead II. V+ needle was inserted to the left leg of the rat, the V- needle was inserted into the right arm of the rat and the ground needle was inserted into the right leg of the rat. Then, the ECG parameters were registered using computerized ECG apparatus (Kent Scientific, USA). Heart rate per minute, was achieved from ECG recordings of average one minute, RR, PR, QTc and QRS intervals also P duration and ST height were calculated from ECG recordings by the computer.

Blood and Tissue Sampling and Homogenization Procedure

Next to taking the ECG recordings, the blood samples were drained from the retro-orbital venous plexus after one night of food deprivation. The blood specimens were allowed to coagulate for 45 min at room temperature to obtain sera. The clear serum samples were isolated by centrifugation at 1800 xg for 15 min at 4 °C using cooling centrifuge and maintained at -20 °C until analysis of LDH and CK-MB enzymes' activities. After collection of the blood samples, the animals were euthanized by cervical dislocation and the heart was rapidly and carefully excised, then partitioned into three portions. The 1st portion was weighed and homogenized in ice-cold medium containing Tris-HCl (50 mmol L^{-1}, pH 7.4) (Hartl and Bister 2013) for biochemical determinations. The 2nd portion was immediately frozen in liquid nitrogen and stored at −80°C prior to extraction for molecular analysis. The 3rd portion was fixed in formalin saline (10%) for histopathological procedure.

The acquired homogenates (10% w/v) from the different studied groups were centrifuged (1800 xg/20 min/4 °C) and the supernatants were obtained and preserved at -20°C pending biochemical assessment (Xu et al. 2012).

Determination of Serum LDH and CK-MB Enzyme Activities

Serum LDH and CK-MB enzyme activities were determined by the spectrophotometric kinetic method according to the manufacturer's protocol provided with the LDH and CK-MB assay kits (Chronolab Systems, Spain).

Assessment of Cardiac Biochemical Variables

Troponin T, Cx43 and Actn levels in cardiac tissue were quantified using ELISA kits, (Glory Science Co., USA) following the manufacturer's manuals.

Molecular Genetic Analysis

Total RNA was isolated from heart tissue using the RNeasy Mini Kit (Qiagen). Approximately 1 µg of total RNA was subjected to reverse transcription using the QuantiTect Reverse Transcription kit (Qiagen) according to the manufacturer's instruction. qPCR was carried out using the QuantiTect SYBR Green PCR kit (Qiagen) following the manufacturer's protocol. Specific primers for *GATA4*, *NKX2.5* and housekeeping gene; *GAPDH* were used for qPCR. The primer sequences for detecting *GATA4* gene were F: 5′-GCCAACCCTGCGAGACACCC-3′ and R: 5′-TCAGCGTTACGGCGCCACAG-3′ while, for detecting *NKX2.5* gene were F: 5′-CCACCTGGCGCTGTGAGACC-3′ and R: 5′-GAAGCGCCGCTCCAGCTCAT-3′. Furthermore, the primer sequences for detecting *GAPDH* gene were F: 5′-GGCTCTCTG-CTCCTCCCTGTT-3′ and R: 5′-GCGGGATCTCGCT-CCTGGAAG-3′ (Hahn et al. 2008). qPCR was performed under the following thermal conditions: an initial denaturation step at 94°C for 4 min, followed by 40 cycles of 94°C for 15 s, annealing at 55°C for 20 s, and extension at 72°C for 20 s, and a final extension step of 10 min at 72°C. Each reaction was done in a total volume of 20 µl, consisting of 12.5 µl SYBR@ Premix Ex, 0.5 µl each primer (10 µmol/L), 2 µlcDNA and 4.5 µl ddH_2O. The main equations used were ΔCt = Ct (gene of interest) – Ct (housekeeping gene) followed by ΔΔCt = ΔCt (treated sample) – ΔCt (untreated sample) and

the overall formula was $2^{-\Delta\Delta C}$ to calculate the relative fold gene expression level.

Hematoxylin and Eosin Staining

After fixation of heart tissue in 10% neutral formalin saline for 24 hours, washing was done in tap water then serial dilutions of alcohol (methyl, ethyl and absolute ethyl) were utilized for dehydration. Specimens were cleared in xylene and embedded in paraffin bee wax at 56 °C in hot air oven for 24 hours. Paraffin bee wax tissue blocks were submitted for sectioning at 4 microns thickness by rotary microtome. After routine de-waxing and hydration, hematoxylin and eosin staining was used and the histopathological alterations of heart tissue were noticed using optical microscope (Bancroft et al. 1996).

Statistical Processing

The results of this study were expressed as mean ± SD. Graph Pad Prism 5 software was used to estimate the statistical analysis. A p value of<0.05 was considered statistically significant using one-way analysis of variance (ANOVA) followed by Tukey's post hoc test.

Results

Identification of ADMSCs

Morphological Feature

ADMSCs exhibited a spindly, fibroblast-like morphology and formed clusters under optical inverted microscope at the 5th day of culturing which represents the traditional phenotypic attitude of MSCs. On the7th day, the cells appeared with evident expansion and proliferation, generating small colonies with several fusocellular, triangular, and polygonal cells. In fact, few cells were triangular or polygonal in shape; however, most of the cells were basically with short or long spindle-shaped appearance. Thereafter, the cells manifested typical morphology with multilayered flat cell bodies having short cell processes connected to adjacent cells on the 14th day with 95% confluence **(Fig. 1)**.

Surface Antigen Profile Analysis

The ADMSCs were also characterized *via* their surface antigen profile using flowcytometry technique. The cells were positive for CD44 by 92.9 % and CD90 by 95.2 % and negative for CD45 by 12.6 % **(Fig. 2)**.

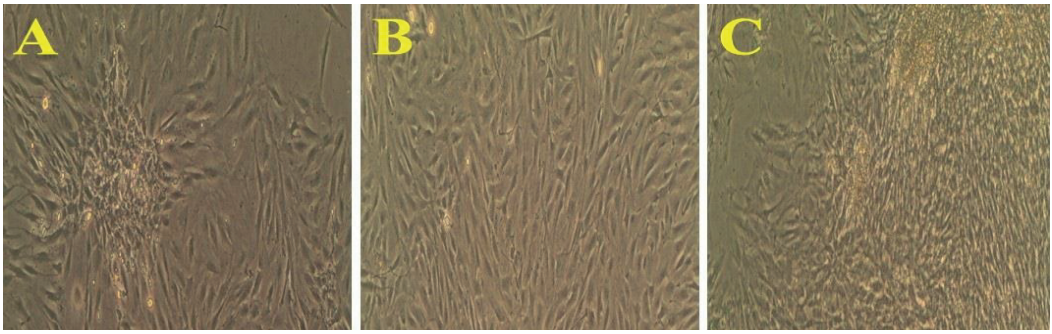

Figure 1. Morphological characteristics of ADMSCs (A) ADMSCs cultured for 5days. (B) ADSCs cultured for 7 days. (C) ADMSCs cultured for 14 days with 95% confluence before 1st subculture.

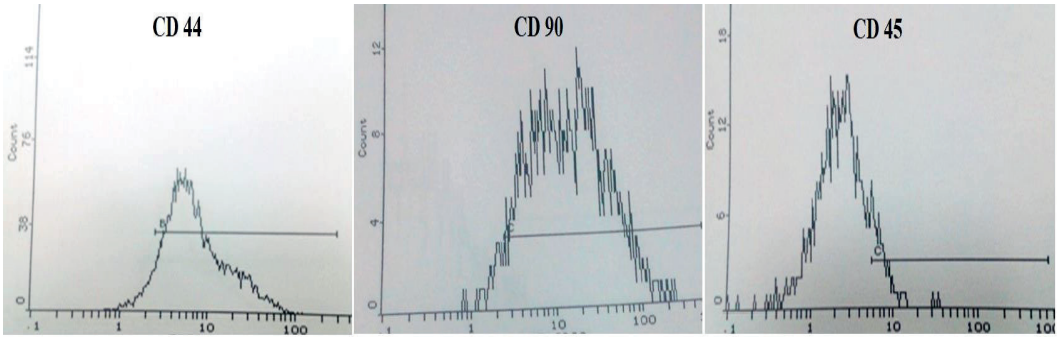

Figure 2. Flowcytometric identification of ADMSCs showing that the cells are positive for CD44 by 92.9 % and CD90 by 95.2 % and negative for CD45 by 12.6 %.

Differentiation of ADMSCs into Cardiomyocytes

Phenotypic characteristics of ADMSCs were examined on six and twelve days from culturing with a cocktail of growth factors to show the stages of differentiation of ADMSCs into cardiomyocytes using inverted light microscope with Euromex camera (Netherlands) **(Fig. 3)**.

Differentiation of ADMSCs into Cardiomyocytes Seeded onto NF

Morphological aspects of the generated cardiomyocytes seeded onto NF under the inverted light microscope were captured by Euromex camera attached to the inverted microscope. Cardiomyocytes cultured on NF in the presence of a cocktail of growth factors on the 3rd day are shown in Fig.(4A). Cardiomyocytes after 7 days of culturing on NF with a cocktail of growth factors are represented in Fig. (4B). Cardiomyocytes after propagation on NF with the involvement of a cocktail of growth factors on the 12th day showing complete confluence are illustrated in Fig. (4C).

Genetic Portrait of the Differentiated Cardiomyocytes

The differentiation of ADMSCs into cardiomyocytes was verified by molecular analysis of *MEF2C* and *Actn* genes expression levels (Fig. 5). Significant ($P < 0.05$) upregulation in the gene expression level of *MEF2C* and *Actn* has been demonstrated in the differentiated ADMSCs *versus* the undifferentiated ADMSCs. Further significant ($P < 0.05$) upregulation in the expression levels of the two genes was noticed in the differentiated ADMSCs seeded onto NF compared to the undifferentiated ADMSCs. *MEF2C* and *Actn* gene expression levels exhibited significant ($P < 0.05$) upregulation when comparing the differentiated ADMSCs seeded onto NF with those lacking NF.

Homing of the Infused Cardiomyocytes

To ensure the accommodation of the transplanted cardiomyocytes into heart tissue of MI-challenged rats, the adipose tissue-derived cardiomyocytes were labeled with iron nano-oxide prior injection into the MI-challenged rats and the rats were left for 2 months. Then, the rats were euthanized and the heart was carefully excised. Cross sections of heart tissue were examined after Prussian blue staining to detect the homing of adipose tissue-derived cardiomyocytes into the heart. The results showed that the stain is absent in the heart tissue section of the MI group. While, it was detected as blue spots upon treatment of MI-challenged rats with the adipose tissue-derived cardiomyocytes without NF or upon treatment with the adipose tissue-derived cardiomyocytes on NF **(Fig. 6)**.

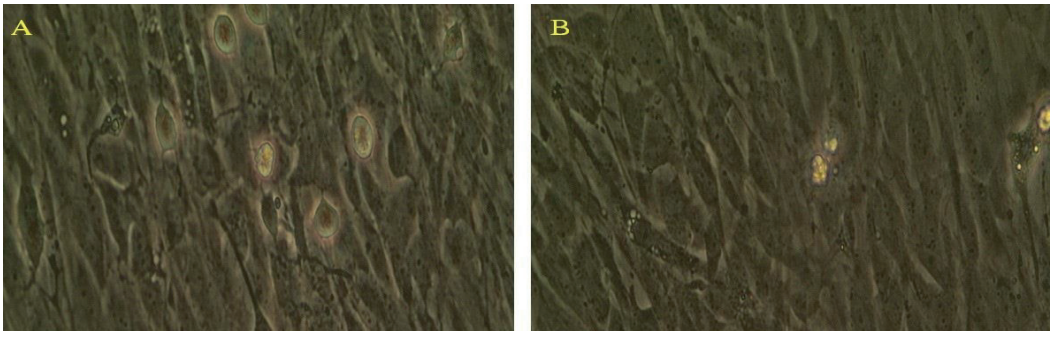

Figure 3. Morphological characterization of cardiomyocytes showing at (A) primary differentiation to cardiomyocytes after 6 days from culturing with growth factors cocktail and (B) colony forming sheets of cardiomyocytes after 12 days.

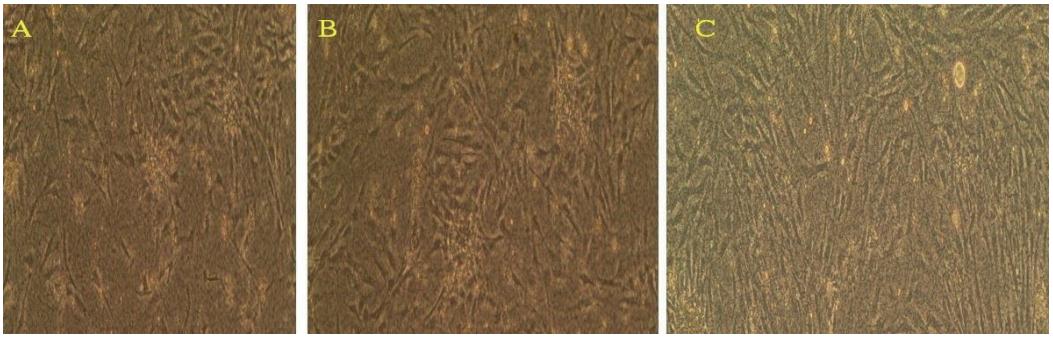

Figure 4. Morphology of cardiomyocytes (A) at the 3rd day of culturing on NF in the presence of growth factors cocktail, (B) at the 7th day of culturing on NF and (C) at the 12th day of culturing on NF displaying complete confluence.

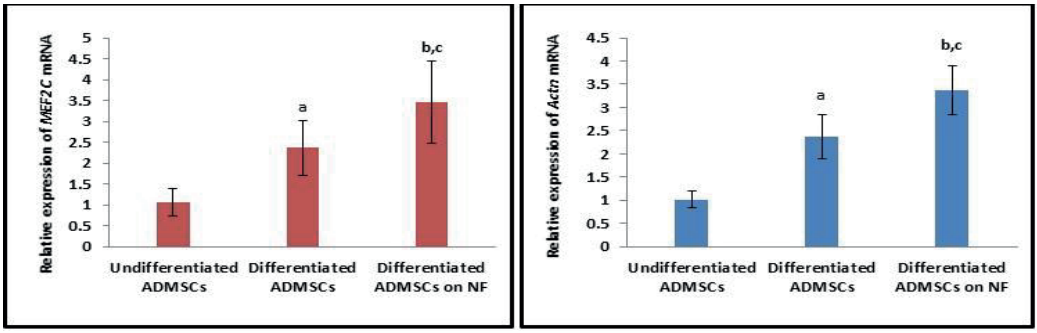

Figure 5. The mRNA expression levels of *MEF2C* and *Actn*.
a: Represent statistically significant value for differentiated ADMSCS VS undifferentiated ADMSCs.
b: Represent statistically significant value for differentiated ADMSCs on NF VS undifferentiated ADMSCs.
c: Represent statistically significant value for differentiated ADMSCs on NF VS differentiated ADMSCs without NF.
All values are expressed as mean ± SD with a statistically significant difference at $P<0.05$.

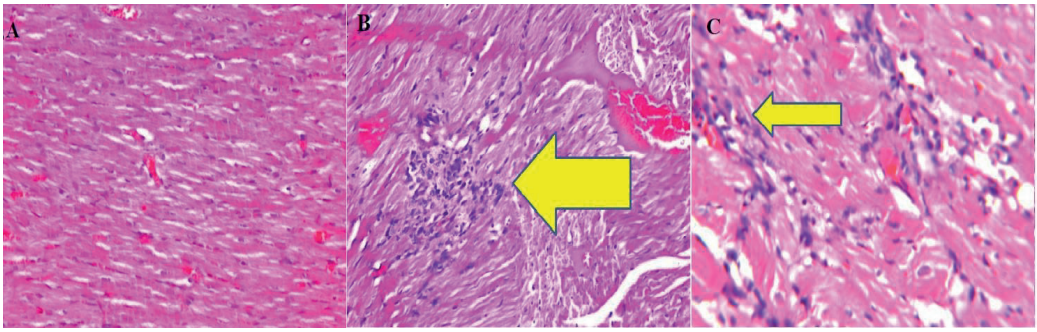

Figure 6. Photomicrophotographs of Prussian blue-stained heart tissue cross sections. (A) MI group, (B) Adipose tissue-derived cardiomyocytes-treated group and (C) Adipose-tissue-derived-cardiomyocytes seeded onto NF-treated group. The yellow arrows showing iron nanooxide blue dots in the treated groups.

Electrocardiogram (ECG) Recordings

Different diagnostic ECG parameters were used to ensure the onset of MI at the beginning of the experiment as well as the efficacy of the treatments after two months. Considered parameters were ST height, heart rate, RR, PR, QTc, QRS intervals and P duration, the ECG measurements of MI-challenged rats showed depressed ST height, heart rate and PR interval with elevated RR, QTc and QRS intervals along with elevation in P duration (Fig. 7). These clear variables are signs for the development of MI. The same elements measured by ECG revealed an improvement after treatment with adipose tissue-derived cardiomyocytes where moderate elevation in ST height, heart rate and PR interval with a moderate decrease in RR, QTc and QRS intervals along with a moderate drop in P duration. The ECG recordings of MI-challenged rats treated with the adipose tissue-derived cardiomyocytes seeded onto NF demonstrated great improvement as indicated by the marked elevation in ST height, heart rate and PR interval with obvious reductions in RR, QTc and QRS intervals along with pronounced drooping in P duration (Fig. 7). Both the decrease and the increase in ECG variables were statistically significant ($P < 0.05$).

Biochemical Findings

The data obtained from the biochemical analyses demonstrated the outcome of treatment with adipose tissue-derived cardiomyocytes and adipose tissue-derived cardiomyocytes seeded onto NF in MI rat model **(Fig. 8)**. The obtained findings clarified that the MI-challenged rats exhibit significant ($p<0.05$) elevation in serum LDH and CK-MB enzyme activities as well as cardiac cTnT level paralleled with significant ($p<0.05$) decline in cardiac Cx43 and Actn levels *versus* their control counterparts. On the opposite side, the treatment of MI-challenged rats with adipose tissue-derived cardiomyocytes or adipose tissue-derived cardiomyocytes seeded onto NF elicited significant ($p<0.05$) inhibition in serum LDH and CK-MB enzyme activities as well as cardiac cTnT level in association with significant ($p<0.05$) enhancement in cardiac Cx43 and Actn levels in comparison with MI-challenged rats. Noteworthy, the MI-challenged rats treated with adipose tissue-derived cardiomyocytes seeded onto NF evoked significant ($p<0.05$) inhibition in serum LDH and CK-MB enzyme activities and cardiac cTnT level along with significant ($p<0.05$) elevation in cardiac Cx43 and AcTn levels *versus* the MI-challenged rats treated with adipose tissue-derived cardiomyocytes.

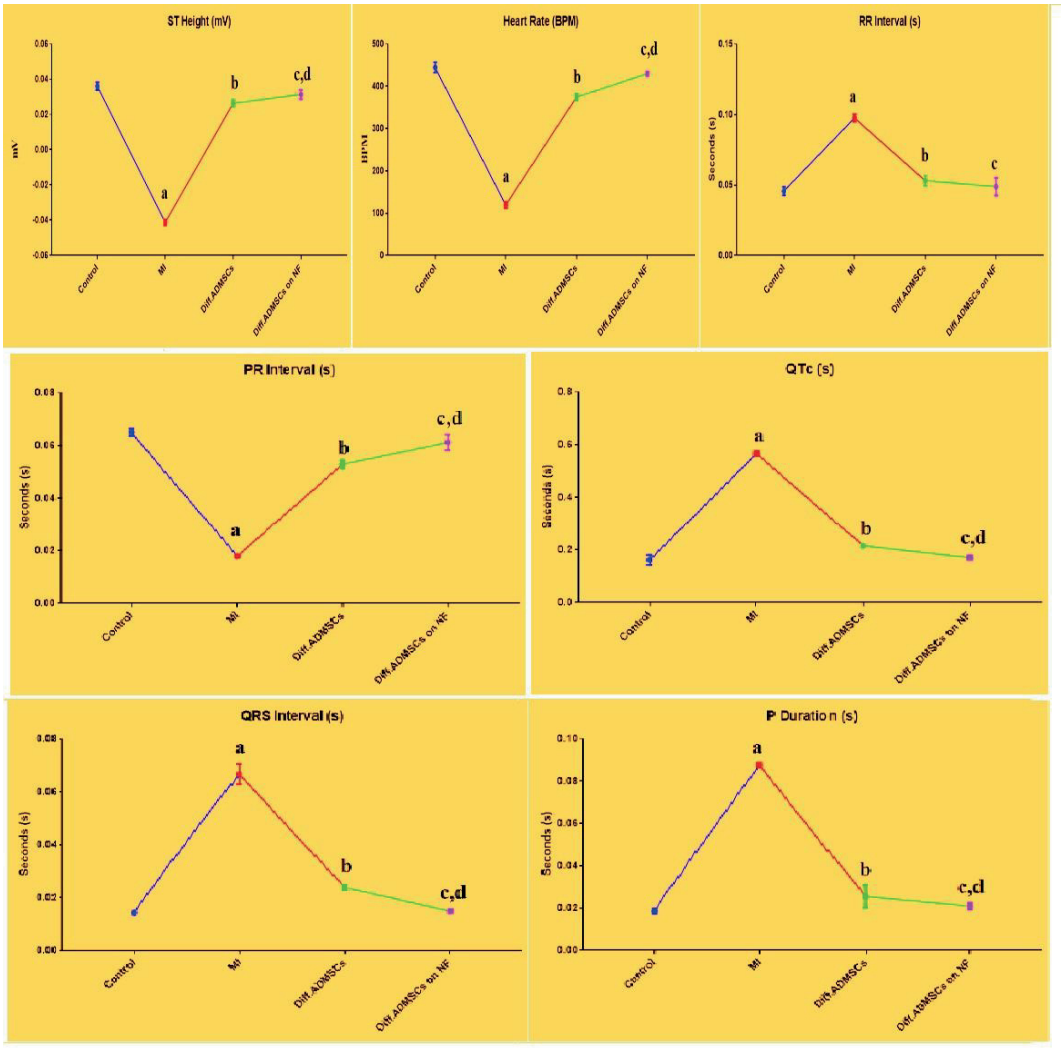

Figure 7. Schematic diagrams for ECG recordings in ST Height, heart Rate, RR, PR, QTc, QRS intervals and P Duration. In each diagram the four groups are represented as control, MI, Diff. ADMSCs and Diff. ADMSCs on NF.
a: Represent statistically significant value for MI VS control.
b: Represent statistically significant value for Diff. ADMSCs VS MI.
c: Represent statistically significant value for Diff. ADMSCs on NF VS MI.
d: Represent statistically significant value for Diff. ADMSCs on NF VS Diff. ADMSCs.

All values are expressed as mean ±SD with statistically significant difference at P<0.05.

Molecular Genetic Outcomes

Figure (9) represented the effect of the infusion with adipose tissue-derived cardiomyocytes and adipose tissue-derived cardiomyocytes seeded onto NF on the gene expression levels of cardiac *GATA4* and *NKX2.5*. The attained data elucidated that the MI-challenged rats display significant ($p<0.05$) upregulation in *GATA4* and *NKX2.5* gene expression levels *versus* the control ones. Significant ($p<0.05$) downregulation in the gene expression levels of *GATA4* and *NKX2.5* has been detected in MI-challenged rats treated with adipose tissue-derived cardiomyocytes or adipose tissue-derived cardiomyocytes seeded onto NF when compared with MI-challenged rats.

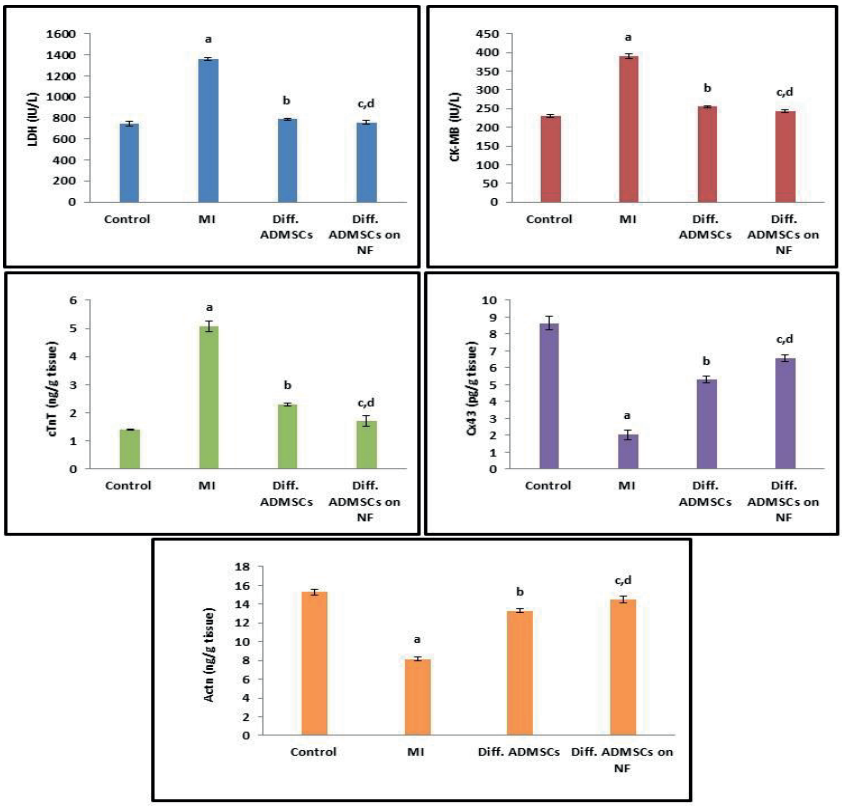

Figure 8. The outcome of treatment with adipose tissue-derived cardiomyocytes and adipose tissue-derived cardiomyocytes seeded onto NF on serum LDH and CK-MB enzyme activities as well as cardiac cTnT, Cx43 and Actn levels in the MI rat model.
a: Represent statistically significant value for MI VS control.
b: Represent statistically significant value for Diff. ADMSCs VS MI.
c: Represent statistically significant value for Diff. ADMSCs on NF VS MI.
d: Represent statistically significant value for Diff. ADMSCs on NF VS Diff. ADMSCs.

All values are expressed as mean ± SD with statistically significant difference at $P < 0.05$.

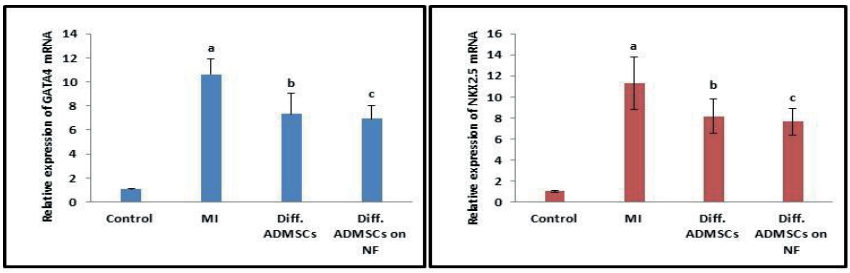

Figure 9. The mRNA expression levels of cardiac *GATA4* and *NKX2.5* in the different studied groups.
a: Represent statistically significant value for MI VS control.
b: Represent statistically significant value for Diff. ADMSCs VS MI.
c: Represent statistically significant value for Diff. ADMSCs on NF VS MI.

All values are expressed as mean ± SD with statistically significant difference at $P < 0.05$.

Histopathological Findings

Transverse cross section of heart tissue obtained from the control rat showed no histopathological alteration and the normal histological structure of the myocardium is noticed **(Fig. 10A)**. While, photomicrograph of heart tissue section of rat in the MI group revealed focal degenerated myocardium with leucocytes inflammatory cell infiltration and myofibroblast proliferation **(Fig. 10B)**. Microscopic investigation of heart tissue section of rat in the group treated with adipose tissue-derived cardiomyocytes disclosed focal area in the myocardium and myofibroblast proliferation with coagulative necrosis in the adjacent area, as well as severe congestion in the myocardial blood vessels **(Fig. 10C)**. Optical micrograph of heart tissue section of rat in the group treated with adipose tissue-derived cardiomyocytes seeded onto NF demonstrated focal area of inflammatory cell infiltration, whilst the intact histomorphological appearance of the heart is seen **(Fig. 10D)**.

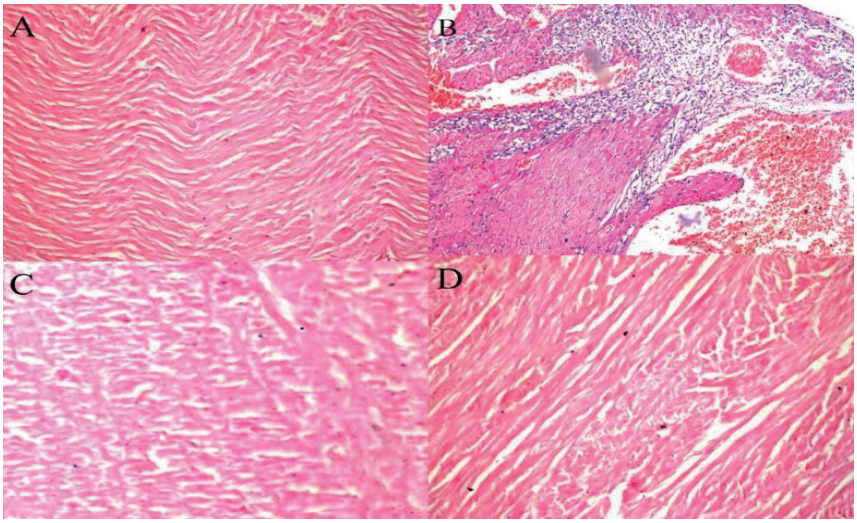

Figure 10. Transverse cross section of the heart tissues of rats in the groups under investigation stained by H&E stain. (A) Control group, (B) MI group, (C) MI treated with adipose tissue-derived cardiomyocytes and (D) MI treated with adipose tissue-derived cardiomyocytes seeded onto NF.

Discussion

The idea of employing stem cells to address cardiac diseases has emerged in the last decade as a leading approach for the regenerative medicine (Karantalis et al. 2012). In 2006, the International Society for Cellular Therapy established the requirements for MSC definition: 1) adherence to plastic in standard culture conditions with a spindly, fibroblast-like morphology; 2) expression of the surface molecules CD73, CD90, and CD44 in the absence of CD34, CD45, CD14, CD11b, CD79a, or CD19; 3) a capacity for differentiation into osteoblasts, adipocytes, and chondroblasts *in vitro*. In the present investigation, the morphological appearance of ADMSCs and the expression of the surface markers (CD44, CD90, CD45) emphasized that the isolated cells are MSCs according to the criteria of the International Society for Cellular therapy (Dominici et al. 2006).

Colony forming units (CFU), could be forced to particular cell lineages through the application of bioactive factors *in vitro* or *in vivo*. The factors that have been shown to induce CFU differentiation into cardiac cells, include dexamethasone and ascorbic acid (Shim et al. 2004), BMP-2 and FGF-2 (Yoon et al. 2005). Additionally, IGF-1 was also used, it is an anabolic growth hormone, that regulates cellular proliferation, differentiation, and senescence, in various tissues (D'Amario et al. 2011). FGF-2 has long been known to stimulate proliferation of cultured mesenchymal cells and it is also involved in regulation of cell survival, migration, and matrix production (Detillieux et al. 2003). BMPs play important roles during various stages of cardiac development, including early cardiogenic differentiation of mesoderm, cardiac tube assembly, looping and jogging, cardiac chamber identity, cardiomyocyte differentiation, and cardiac cushion formation (Van Wijk et al. 2007). It has been cited that, these growth factors exerted anti-apoptotic effects on MSCs which can be implemented by at least 2 mechanisms: 1) FGF-2 prolonged telomerase length and life span of MSCs and it is useful in obtaining a large number of cells with preserved differentiation potential (Bianchi et al. 2003) and 2) FGF and IGF-1 activate PI3-kinase/Akt pathway, which is known to mediate antiapoptotic signaling (Debiais et al. 2004). The differentiation of ADMSCs to

cardiomyocytes was achieved in the current study by using a cocktail of the abovementioned growth factors according the study of Hahn et al. (2008) and the derived cardiomyocytes started to form colonies then connected sheets similar to those demonstrated by Li et al. (2007).

For tissue engineering, using biodegradable scaffolds in combination with stem cell is considered as an alternative strategy that provides a repository for cell delivery leading to enhancement of cell survival (Bokhari et al. 2005; Zhang et al. 2005). In this study, we used nanofiber tissue culture plates as a scaffold material which replicates the extracellular matrix of the heart for the purpose of providing anisotropic support for cardiomyocytes (Davis et al. 2006). Culturing of CFU on NF plate stimulates cells to form a mineralized extracellular matrix (Khan et al. 2015). This explains what happened in our study after culturing ADMSCs-derived cardiomyocytes on NF.

To confirm the molecular changes during the differentiation of ADMSCs into cardiomyocytes by the cocktail of growth factors, we have studied the expression of a panel of specific cardiac genes. Data from qPCR analysis showed that the cardiogenic gene expression levels (*MEF2C* and *Actn*) are upregulated after differentiation of ADMSCs into cardiomyocytes. In cardiogenesis, *MEF2C* and *Actn* are known as key regulators in cardiac development and the recorded upregulation of these genes in the current study agrees with Planat-Bernard et al. (2004). The prominent upregulation of *MEF2C* and *Actn* gene expression levels upon the differentiation of ADMSCs into cardiomyocytes on NF comes in line with the study of Li et al. (2017). These investigators stated that the growing of stem cells on nanofiber intensifies their potentiality to differentiate.

Several paramagnetic contrast agents have been successfully used for *in vivo* cell tracking and labeling of different mammalian cell types (Weissleder et al. 1989). In our study, iron nanooxide was employed to track the differentiated cardiomyocytes to ensure their accommodation in heart tissue. Transverse sections across the heart tissues were examined after Prussian blue staining for the treated groups. It has been shown that the blue spots appear in the group treated with adipose tissue-derived cardiomyocytes and they are more pronounced in the group treated with adipose tissue-derived cardiomyocytes seeded onto NF. These findings emphasize the success of the transplanted cardiomyocytes in sticking to heart tissue.

Concerning the biological experiment of this investigation, the induction of MI in rats was done by isoprenaline, which is considered as a reliable and simple model mimic MI in human (Garson et al. 2015). Large doses of isoprenaline lead to overexcitation of heart beta receptors, increased heart rate, enhancement of cardiac muscle contractility and elevated myocardial oxygen consumption. The excitation of beta receptors, the expansion of peripheral blood vessels and the reduction of their resistance lead to falling of blood pressure, especially diastolic blood pressure resulting in myocardial ischemia (Zhang et al. 2008). Also, the overexcitement of heart beta receptors contributes to the increased local cardiovascular angiotensin, which promotes the overloading of Ca^{2+} inside cardiomyocytes. The overloading of Ca^{2+} in the cardiomyocytes can activate phospholipase causing decomposition of membrane phospholipids; overproduction of free radicals derived from xanthine oxidase leading to lipid peroxidation of the cellular membrane which ultimately leading to cell membrane destruction or even cell death (Hu et al. 2013).

ECG measurements in this study pointed to depressed ST height, heart rate and PR interval with elevated RR, QTc and QRS intervals along with abnormal elevation in P duration. These indices are clear signs of MI as described previously by Hopenfeld et al. (2004). All the parameters recorded by the ECG demonstrated improvement after treatment of MI-challenged rats with adipose tissue-derived cardiomyocytes as the ST height is moderately recovered. In addition, the moderate elevation in heart rate and PR interval paralleled with a moderate decrease in RR, QTc and QRS intervals along with P duration decrement are recorded after treatment with adipose tissue-derived cardiomyocytes. These observations are quite similar to those manifested by kakkar et al. (2006). More success was observed upon treatment of MI-challenged rats with adipose tissue-derived cardiomyocytes seeded onto NF as ECG parameters showed that normal ST height is demonstrated. Also, considerable elevation in heart rate and PR interval with marked decrease in RR, QTc and QRS intervals along with a P duration reduction are registered. The observed signs of recovery obtained from ECG measurements after treatment with adipose tissue-derived cardiomyocytes seeded onto NF concur with the findings of the study of Kijtawornrat et al. (2006).

Various relevant biochemical variables were analyzed in this study to detect the biochemical responses after the treatment of the rat model of MI with the generated cardiomyocytes. The elevated serum activity of lactate dehydrogenase (LDH) and MB fraction of creatine kinase (CK-MB) showed a statistically significant positive correlation with MI in clinical practice (Sivaranjani et al. 2014). In our MI model, these two enzymes demonstrated a significant increase in MI-challenged rats. This observation is in harmony with that demonstrated by Zeng et al. (2018). The overload of calcium caused by isoprenaline to induce MI causes oxidative stress which in turn decreases ATP production that directly affects LDH and CK-MB by a mechanism including the decrease in oxygen supply and the increase in anaerobic glycolysis that lead to the accumulation of lactate and a decrement of pH in the cardiomyocyte resulting in the activation of lysosomal enzymes (Chen and Frangogiannis, 2016). On the other side, these enzymes exhibited a significant decrease in the MI-challenged group treated with adipose tissue-derived cardiomyocytes. Further inhibition in the activity of these enzymes has been detected in the group treated with adipose tissue-derived cardiomyocytes seeded onto NF. The study of Lv et al. (2016) proved that the implantation of MSCs differentiated into cardiomyocytes to infarcted rat improves cardiac functions; this finding is validated in our study by the significant inhibition of serum LDH and CK-MB enzymes activity upon treatment of MI-challenged rats with the generated cardiomyocytes.

Upon onset of MI by isoprenaline in the current study, cardiac cTnT showed significant elevation while cardiac Cx43 and Actn displayed significant reduction as compared

to controls. These results match those observed in infarcted cardiac tissue as reported in the previous studies (Fan 2019). It has been concluded that the formation of highly reactive hydroxyl radicals as a result of oxidation stress yielded from isoprenaline administration induces an alteration and disintegration of proteins such as cTnT, Cx43 and Actn (Huang et al. 1999). Huang et al. (1999) stated that acute ischemic changes in Cx43 phosphorylation are followed by Cx43 loss due to degradation. On the opposite hand, cardiac cTnT displayed significant reduction and cardiac Cx43 as well as Actn showed significant elevation after treatment of MI-challenged rats with the adipose tissue-derived cardiomyocytes or adipose tissue-derived cardiomyocytes seeded onto NF, indicating an obvious sign of cardiac functions improvement as illustrated by the study of Khan et al. (2015). Noteworthy, the influence of treatment with adipose tissue-derived cardiomyocytes seeded onto NF on these cardiac specific biomarkers was more prominent than adipose tissue-derived cardiomyocytes, indicating more advancement in cardiac functions (Wu et al. 2017). It has been demonstrated that the treatment of MSCs with the specific growth factors yielded a great expression of cardiac specific genes, including Cx43 and a preferable gap junction formation (Hahn et al. 2008). The cytoprotective effects of MSCs are suggested to be mediated not only by paracrine actions, but also by direct cell-to-cell communication *via* gap junctions and the treatment with growth factors could potentiate their gap junction-mediated cytotherapeutic action (Krysko et al. 2005).

GATA4 and *NKX2.5* are the early differentiation indices in cardiac cells; they ensure electrical and metabolic coupling between cardiomyocytes and coordinate their contractility. In this study, the gene expression levels of *GATA4* and *NKX2.5* were first upregulated in MI-challenged rats while they showed down regulation after treatment with adipose tissue-derived cardiomyocytes or adipose tissue-derived cardiomyocytes seeded into NF. The noticed upregulation in the gene expression levels of *GATA4* and *NKX2.5* in MI-challenged rats could be allied to the cardiomyocyte hypertrophy resulted from isoprenaline (Sachdeva et al. 2012). While, the observed downregulation in the gene expression levels of *GATA4* and *NKX2.5* in the treated groups with the generated cardiomyocytes could be attributed to the reduction in cardiomyocyte hypertrophy through their paracrine, regenerative and cytoprotective actions (Hahn et al. 2008).

The histomorphological investigation of heart tissue sections in the present approach indicated that isoprenaline injection evokes focal degeneration of the myocardium with leucocytes inflammatory cell infiltration as well as myofibrobalsts proliferation. These histopathological alterations match those observed in the infarcted heart tissue (Talman and Ruskoaho, 2016). The group of rats treated with adipose tissue-derived cardiomyocytes manifested myofibrobalsts proliferation with coagulative necrosis in the adjacent area, as well as sever congestion in the myocardial blood vessels, suggesting that the transplanted cardiomyocytes successfully survived among the myocardial cells and contributed to the healing of cardiac tissue (Wang et al. 2006). The group of rats treated with adipose tissue-derived cardiomyocytes seeded onto NF demonstrated focal area of inflammatory cells infiltration and the connections between the myocardial cells have been clearly defined, whereas certain cells were able to self-assemble to form vessel-like structures, resulting in increased blood circulation within the myocardium. Of note, the recovered myocardial tissues were promoted in the transplanted cardiomyocytes. These observations are in parallel with those noticed in other studies (Li et al. 2017; Gómez-Heras et al. 2019) as the differentiated cardiomyocytes were attracted to the inflammatory-reparative area and they infiltrated the infarcted tissue of the heart (Mazo et al. 2012).

In conclusion, the present investigation provides documents for the successful generation of cardiomyocytes from ADMSCs. Also, this study offers clear pre-clinical evidences for the favorable employment of implantation of the differentiated cardiomyocytes in the recovery from MI. The differentiated cardiomyocytes succeeded in the accommodation within the myocardial infarcted site and proved eminent efficacy in cardiac renovation with heightened cardiac functions, particularly in case of the differentiated cardiomyocytes seeded onto NF. These outcomes were profoundly validated by ECG recordings, cardiogenic biomarkers ratings and histomorphological examination of cardiac tissue. The current approach establishes a new avenue for therapeutic strategy of cardiac remodeling after acute MI.

Acknowledgment

The authors express sincere appreciation to Prof. Adel Bakeer Kholoussy, Professor of Pathology, Faculty of Veterinary Medicine, Cairo University for his kind cooperation in conducting histological examination in this study.

Funding

This work was financially supported by the National Research Centre, Egypt (Thesis fund No. 7/5/1).

References

1. Agarwal S, Wendorff JH, Greiner A. Use of electrospinning technique for biomedical applications. *Polymer* 2008; 49: 5603-5621. doi:10.1016/j.polymer. 2008.09.014
2. Aird AL, Nevitt CD, Christian K, Williams SK, et al. Adipose-derived stromal vascular fraction cells isolated from old animals exhibit reduced capacity to support the formation of microvascular networks. *Exp Gerontol.* 2015; 63: 18-26. doi:10.1016/j.exger.2015.01.044
3. Apple FS. Tissue specificity of cardiac troponin I, cardiac troponin T and creatine kinase-MB. *Clin Chim Acta*. 1999; 284: 151-159. doi:10.1016/s0009-8981(99)00077-7

4. Banchroft JD, Stevens A, Turner DR. Theory and practice of histological techniques. Churchill Livingstone, Philadelphia, 4th Ed/ 1996.
5. Bianchi G, Banfi A, Mastrogiacomo M, Notaro R, et al. *Ex vivo* enrichment of mesenchymal cell progenitors by fibroblast growth factor 2. *Exp Cell Res*. 2003; 287: 98-105. doi:10.1016/s0014-4827(03)00138-1
6. Bokhari MA, Akay G, Zhang S, Birch MA. The enhancement of osteoblast growth and differentiation *in vitro* on a peptide hydrogel-polyHIPE polymer hybrid material. *Biomaterials* 2005; 26: 5198-5208. doi:10.1016/j.biomaterials.2005.01.040
7. Bolli R, Tang XL, Sanganalmath SK, Rimoldi O, et al. Intracoronary delivery of autologous cardiac stem cells improves cardiac function in a porcine model of chronic ischemic cardiomyopathy. *Circulation* 2013; 128: 122-131. doi:10.1161/CIRCULATIONAHA. 112.001075
8. Chen B, Frangogiannis NG. Macrophages in the remodeling failing heart. *Circ Res*. 2016; 119: 776–778. doi:10.1161/CIRCRESAHA.116.309624
9. Chen HH, Lin KC, Wallace CG, Chen YT, et al. Additional benefit of combined therapy with melatonin and apoptotic adipose-derived mesenchymal stem cell against sepsis-induced kidney injury. *J Pineal Res.* 2014; 57: 16-32. doi:10.1111/jpi.12140
10. D'Amario D, Cabral-Da-Silva MC, Zheng H, Fiorini C, et al. Insulin-like growth factor-1 receptor identifies a pool of human cardiac stem cells with superior therapeutic potential for myocardial regeneration. *Circ Res.* 2011; 108: 1467-1481. doi:10.1161/CIRC RESAHA.111.240648
11. Davis ME, Hsieh PC, Takahashi T, Song Q, et al. Local myocardial insulin-like growth factor 1 (IGF-1) delivery with biotinylated peptide nanofibers improves cell therapy for myocardial infarction. *Proceedings of the National Academy of Sciences of the United States of America*, 2006; 103: 8155-8160. doi: 10.1073/pnas.0602877103
12. Debiais F, Lefevre G, Lemonnier J, Le Mee S, et al. Fibroblast growth factor-2 induces osteoblast survival through a phosphatidylinositol 3-kinase-dependent,-β-catenin-independent signaling pathway. *Exp Cell Res*. 2004; 297: 235-246. doi:10.1016/j.yexcr.2004.03.032
13. Detillieux KA, Sheikh F, Kardami E, Cattini PA. Biological activities of fibroblast growth factor-2 in the adult myocardium. *Cardiovasc Res*. 2003; 57: 8-19. doi:10.1016/S0008-6363(02)00708-3
14. Dominici MLBK, Le Blanc K, Mueller I, Slaper-Cortenbach I, et al. Minimal criteria for defining multipotent mesenchymal stromal cells. The International Society for Cellular Therapy position statement. *Cytotherapy* 2006; 8: 315-317. doi:10.1080/1465324 0600855905
15. Fan Y. Cardioprotective effect of rhapontigenin in isoproterenol-induced myocardial infarction in a rat model. *Pharmacology* 2019; 103: 291-302. doi:10.1159/000496800
16. Garson C, Kelly-Laubscher R, Gwanyanya A, Blackhurst D. Lack of cardioprotection by single-dose magnesium prophylaxis on isoprenaline-induced myocardial infarction in adult Wistar rats. *Cardiovas J Afr*. 2015; 26: 242. doi:10.5830/CVJA-2015-055
17. Gómez-Heras SG, Carlota L, Larrea JL, Vega-Clemente L, et al. Main histological parameters to be evaluated in an experimental model of myocardial infarct treated by stem cells on pigs. *Peer J.* 2019; 7: e7160. https://doi:10.7717/peerj.7160
18. Hahn JY, Cho HJ, Kang HJ, Kim TS, et al. Pre-treatment of mesenchymal stem cells with a combination of growth factors enhances gap junction formation, cytoprotective effect on cardiomyocytes, and therapeutic efficacy for myocardial infarction. *J Am Coll Cardiol*. 2008; 51: 933-943. doi: 10.1016/j.jacc.2007.11.040
19. Hartl M, Bister K. Analyzing myc in cell transformation and evolution. In: The Myc gene methods and protocol, Springer, 2013.
20. Hopenfeld B, Stinstra JG, MacLeod RS. Mechanism for ST depression associated with contiguous subendocardial ischemia. *J Cardiovasc Electrophysiol*. 2004; 15: 1200-1206. doi: 10.1046/j.1540-8167.2004.04072.x
21. Hu WS, Lin YM, Ho TJ, Chen RJ, et al. Genistein suppresses the isoproterenol-treated H9c2 cardiomyoblast cell apoptosis associated with P-38, Erk1/2, JNK, and NFkappaB signaling protein activation. *Am J Chin Med*. 2013; 41: 1125-1136. doi: 10.1142/S0192415X13500766
22. Huang XD, Sandusky GE, Zipes DP. Heterogeneous loss of connexin43 protein in ischemic dog hearts. *J Cardiovasc Electrophysiol*. 1999; 10: 79-91. doi: 10.1111/j.1540-8167.1999.tb00645.x
23. Kakkar R, Ye B, Stoller DA, Smelley M, et al. Spontaneous Coronary Vasospasm in KATP Mutant Mice Arises From a Smooth Muscle–Extrinsic Process. *Circ Res.* 2006; 98: 682-689. doi: 10.1161/01.RES.0000207498.40005.e7
24. Karantalis V, Balkan W, Schulman IH, Hatzistergos KE, et al. Cell-based therapy for prevention and reversal of myocardial remodeling. *Am J Physiol Heart Circ Physiol.* 2012; 303: H256-270. doi: 10.1152/ajpheart.00221.2012.
25. Khan M, Xu Y, Hua S, Johnson J, et al. Correction: evaluation of changes in morphology and function of human induced pluripotent stem cell derived cardiomyocytes (HiPSC-CMs) cultured on an aligned-nanofiber cardiac patch. *PloS One* 2015; 10: e0141176. doi: 10.1371/journal.pone.0141176. eCollection 2015
26. Kijtawornrat A, Nishijima Y, Roche BM, Keene BW, et al. Use of a failing rabbit heart as a model to predict torsadogenicity. *Toxicol Sci*. 2006; 93, 205-212. doi:10.1093/ toxsci/kfl025.
27. Krysko DV, Leybaert L, Vandenabeele P, D'Herde K. Gap junctions and the propagation of cell survival and

cell death signals. *Apoptosis*, 2005; 10: 459-469. doi: 10.1007/s10495-005-1875-2.
28. Langer R, Tirrell DA. Designing materials for biology and medicine. *Nature*, 2004; 428: 487-492. doi:10.1038/ nature02388
29. Lee S, Choi E, Cha MJ, Hwang KC. Cell adhesion and long-term survival of transplanted mesenchymal stem cells: a prerequisite for cell therapy. *Oxid Med Cell Longev.* 2015; 2015: 632902. doi: 10.1155/2015/ 632902
30. Li J, Minami I, Shiozaki M, Yu L, et al. Human Pluripotent Stem Cell-Derived Cardiac Tissue-like Constructs for Repairing the Infarcted Myocardium. *Stem Cell Reports*, 2017; 9: 1546-1559. doi: 10.1016/j.stemcr.2017.09.007
31. Li X, Yu X, Lin Q, Deng C, et al. Bone marrow mesenchymal stem cells differentiate into functional cardiac phenotypes by cardiac microenvironment. *J Mol Cell Cardiol.* 2007; 42: 295-303. doi: 10.1016/j.yjmcc.2006.07.002
32. Liang W, Chen J, Li L, Li M, et al. Conductive hydrogen sulfide-releasing hydrogel encapsulating ADSCs for myocardial infarction treatment. *ACS Appl Mater Interfaces*. 2019; 11: 14619-14629. doi:10.1021/ acsami.9b01886
33. Lin KC, Yip HK, Shao PL, Wu SC, et al. Combination of adipose-derived mesenchymal stem cells (ADMSC) and ADMSC-derived exosomes for protecting kidney from acute ischemia–reperfusion injury. *Int J Cardiol.* 2016; 216: 173-185. doi:10.1016/ j.ijcard.2016.04.061.
34. Liu Z, Wang H, Wang Y, Lin Q, et al. The influence of chitosan hydrogel on stem cell engraftment, survival and homing in the ischemic myocardial microenvironment. *Biomaterials* 2012; 33: 3093-3106. doi:10.1016/ j.biomaterials.2011.12.044
35. Lv Y, Liu B, Wang HP, Zhang L. Intramyocardial implantation of differentiated rat bone marrow mesenchymal stem cells enhanced by TGF-β1 improves cardiac function in heart failure rats. *Braz J Med Biol Res.* 2016; 49(6): e5273. doi:10.1590/1414-431X20165273
36. Mazo M, Cemborain A, Gavira JJ, Abizanda G, et al. Adipose stromal vascular fraction improves cardiac function in chronic myocardial infarction through differentiation and paracrine activity. *Cell Transplant.* 2012; 21: 1023-1037. doi: 10.3727/096368911 X623862
37. Memon IA, Sawa Y, Fukushima N, Matsumiya G, et al. Repair of impaired myocardium by means of implantation of engineered autologous myoblast sheets. *J Thorac Cardiovasc Surg.* 2005; 130: 1333-1341. doi:10.1016/j.jtcvs.2005.07.023
38. Miao C, Lei M, Hu W, Han S, et al. A brief review: the therapeutic potential of bone marrow mesenchymal stem cells in myocardial infarction. *Stem Cell Res Ther.* 2017; 8: 242. doi:10.1186/ s13287-017-0697-9
39. Miyagawa S, Saito A, Sakaguchi T, Yoshikawa Y, et al. Impaired myocardium regeneration with skeletal cell sheets--a preclinical trial for tissue-engineered regeneration therapy. *Transplantation*, 2010; 90: 364-372. doi:10.1097/ TP.0b013e3181e6f201
40. Otsuki Y, Nakamura Y, Harada S, Yamamoto Y, et al. Adipose stem cell sheets improved cardiac function in the rat myocardial infarction, but did not alter cardiac contractile responses to β-adrenergic stimulation. *Biomed Res.* 2015; 36: 11-19. doi:10.2220/ biomedres.36.11
41. Patila T, Miyagawa S, Imanishi Y, Fukushima S, et al. Comparison of arrhythmogenicity and proinflammatory activity induced by intramyocardial or epicardial myoblast sheet delivery in a rat model of ischemic heart failure. *PLoS One* 2015; 10: e0123963. doi:10.1371/journal.pone.0123963
42. Planat-Benard V, Menard C, Andre M, Puceat M, et al. Spontaneous cardiomyocyte differentiation from adipose tissue stroma cells. *Circ Res.* 2004; 94: 223-229. doi:10.1161/ 01.RES.0000109792.43271.47
43. Sachdeva M, Liu Q, Cao J, Lu Z, et al. Negative regulation of miR-145 by C/EBP-β through the Akt pathway in cancer cells. *Nucleic Acids Res.* 2012; 40: 6683-6692. doi:10.1093/nar/gks324
44. Scadden DT. The stem-cell niche as an entity of action. *Nature*, 2006; 441: 1075-1079. doi:10.1038/ nature04957
45. Shim WS, Jiang S, Wong P, Tan J, et al. *Ex vivo* differentiation of human adult bone marrow stem cells into cardiomyocyte-like cells. *Biochem Biophys Res Commun.* 2004; 324: 481-488. doi: 10.1016/ j.bbrc.2004.09.087
46. Si R, Gao C, Guo R, Lin C, et al. Human mesenchymal stem cells encapsulated-coacervated photoluminescent nanodots layered bioactive chitosan/collagen hydrogel matrices to indorse cardiac healing after acute myocardial infarction. *J Photochem Photobiol B*. 2020; 206: 111789. doi:10.1016/ j.jphotobiol.2020.111789
47. Sivaranjani N, Venkataraman DD, Elango G, Rao SV, et al. Evaluation of cardiac specific Troponin T as a specific and sensitive biomarker over Creatine Kinase-MB in Acute Myocardial Infarction patients-A correlation analysis study. *Int J Biomed Res.* 2014; 5: 121-123. doi: 10.7439/ijbr.v5i2.501
48. Song H, Cha MJ, Song BW, Kim IK, et al. Reactive oxygen species inhibit adhesion of mesenchymal stem cells implanted into ischemic myocardium *via* interference of focal adhesion complex. *Stem Cells* 2010; 28: 555-563. doi: 10.1002/stem.302
49. Talman V, Ruskoaho H. Cardiac fibrosis in myocardial infarction-from repair and remodeling to regeneration. *Cell Tissue Res.* 2016; 365: 563-581. doi: 10.1007/s00441-016-2431-9
50. van Dijk A, Naaijkens BA, Jurgens WJ, Nalliah K, et al. Reduction of infarct size by intravenous injection of uncultured adipose derived stromal cells in a rat model is dependent on the time point of application. *Stem Cell Res.* 2011; 7: 219-229. doi:10.1016/ j.scr.2011.06.003

51. van Wijk B, Moorman AF, van den Hoff MJ. Role of bone morphogenetic proteins in cardiac differentiation. *Cardiovasc Res.* 2007; 74: 244-255. doi: 10.1016/j.cardiores.2006.11.022
52. Wang T, Xu Z, Jiang W, Ma A. Cell-to-cell contact induces mesenchymal stem cell to differentiate into cardiomyocyte and smooth muscle cell. *Int J Cardiol.* 2006; 109: 74-81. doi:10.1016/j.ijcard.2005.05.072
53. Weissleder R, Stark DD, Engelstad BL, Bacon BR, et al. Superparamagnetic iron oxide: pharmacokinetics and toxicity. *Am J Roentgenol*. 1989; 152: 167-173. doi: 10.2214/ajr.152.1.167
54. Woodbury D, Schwarz EJ, Prockop DJ, Black IB. Adult rat and human bone marrow stromal cells differentiate into neurons. *J Neurosci Res.* 2000; 61: 364-370. doi:10.1002/1097-4547(20000815)61:4<364: AID-JNR2>3.0.CO;2-C
55. Wu Z, Chen G, Zhang J, Hua Y, et al. Treatment of Myocardial Infarction with Gene-modified Mesenchymal Stem Cells in a Small Molecular Hydrogel. *Scientific Rep.* 2017; 7: 15826. doi:10.1038/s41598-017-15870-z
56. Xu H, Deng YH, Wang KQ, Chen DW. Preparation and characterization of stable pH-sensitive vesicles composed of α-tocopherol hemisuccinate. *AAPS PharmSciTech*. 2012; 13: 1377-1385. doi:10.1208/ s12249-012-9863-7
57. Yip HK, Chang LT, Wu CJ, Sheu JJ, et al. Autologous bone marrow-derived mononuclear cell therapy prevents the damage of viable myocardium and improves rat heart function following acute anterior myocardial infarction. *Circ J.* 2008; 72: 1336-1345. doi:10.1253/circj.72.1336
58. Yoon J, Min BG, Kim YH, Shim WJ, et al. Differentiation, engraftment and functional effects of pre-treated mesenchymal stem cells in a rat myocardial infarct model. *Acta Cardiol*. 2005; 60: 277-284. doi: 10.2143/AC.60.3.2005005
59. Yoshizumi T, Zhu Y, Jiang H, D'Amore A, et al. Timing effect of intramyocardial hydrogel injection for positively impacting left ventricular remodeling after myocardial infarction. *Biomaterials* 2016; 83: 182-193. doi: 10.1016/j.biomaterials.2015.12.002
60. Zeng Q, He H, Wang XB, Zhou YQ, et al. Electroacupuncture Preconditioning Improves Myocardial Infarction Injury *via* Enhancing AMPK-Dependent Autophagy in Rats. *Biomed Res Int.* 2018; 2018: 1238175. doi:10.1155/2018/1238175
61. Zhang LL, Liu JJ, Liu F, Liu WH, et al. MiR-499 induces cardiac differentiation of rat mesenchymal stem cells through wnt/β-catenin signaling pathway. *Biochem Biophys Res Commun.* 2012; 420: 875-881. doi: 10.1016/j.bbrc.2012.03.092
62. Zhang S, Zhao X, Spirio L. Ma PX, Elisseeff J (Eds.), PuraMatrix: self-assembling peptide nanofiber scaffolds, Scaffolding in Tissue Engineering, Taylor and Francis, 2005, 217-38.
63. Zhang X, Wei M, Zhu W, Han B. Combined transplantation of endothelial progenitor cells and mesenchymal stem cells into a rat model of isoproterenol-induced myocardial injury. *Arch Cardiovasc Dis.* 2008; 101: 333-342. doi: 10.1016/j.acvd.2008.05.002
64. Zhao T, Zhao W, Meng W, Liu C, et al. VEGF-C/VEGFR-3 pathway promotes myocyte hypertrophy and survival in the infarcted myocardium. *Am J Transl Res.* 2015; 7: 697.